Stony Brook University

The Tropical Atlantic Response to Abrupt Climate Change during Interstadial 12

A Thesis Presented

by

Jennifer Eve Hertzberg

to

The Graduate School

in Partial Fulfillment of the

Requirements

for the Degree of

Master of Science

in

Marine and Atmospheric Science

Stony Brook University

August 2010

Stony Brook University

The Graduate School

Jennifer Eve Hertzberg

We, the thesis committee for the above candidate for the

Master of Science degree, hereby recommend

acceptance of this thesis.

David Black – Thesis Advisor
Assistant Professor, Marine and Atmospheric Science

Henry Bokuniewicz
Professor, Marine and Atmospheric Science

Sultan Hameed
Professor, Marine and Atmospheric Science

This thesis is accepted by the Graduate School

Lawrence Martin
Dean of the Graduate School

Abstract of the Thesis

The Tropical Atlantic Response to Abrupt Climate Change during Interstadial 12

by

Jennifer Eve Hertzberg

Master of Science

in

Marine and Atmospheric Science

Stony Brook University

2010

The critical gaps in our understanding of the Earth's climate system lie in the patterns and forcing mechanisms of climate variability on decadal to submillennial time scales. Equally important and also not clearly understood is the response of low-latitude climate variability to abrupt climate change - most studies of abrupt change come from high-latitude sites. Dansgaard-Oeschger events such as Interstadial 12 are excellent examples of abrupt climate change, and provide an ideal opportunity to examine how the tropics and submillennial-scale variability respond to rapid changes in the global climate system. The Cariaco Basin's (Venezuela) high sedimentation rates, abundant microfossils, and excellent preservation make the site a superb location for high-resolution tropical Atlantic climate reconstructions. This study will present subdecadally resolved data for the critical intervals spanning the abrupt onset of Interstadial 12 (45,810 – 44,668 yBP), and the transition back to stadial conditions (43,895 – 42,831 yBP). Continuous sampling of a Calypso-style piston core at 1 mm intervals and dated with a novel sediment element concentration-based approach resulted in an average sample resolution of ~2 years, making this the highest-resolved record of an interstadial event to date.

Foraminiferal census data were collected on samples for the onset and transition out of Interstadial 12, and were interpreted in the context of modern ecological preferences and the forcing mechanisms responsible for apparent patterns. The interpretation of the abundance records for the onset of Interstadial 12 is complicated by the combined and competing effects of rising sea level on Ekman-induced upwelling within the Cariaco Basin and migrating Intertropical Convergence Zone (ITCZ)-associated variations in trade wind location and fluvial nutrient delivery to the basin. However, the results suggest a northerly shift in the average annual position of the ITCZ by 600 – 700 km in as little as a few centuries, with most of the shift occurring in less than 75 years. The foraminiferal abundance records for the latter part of the interstadial suggest a southerly shift in the average annual position of the ITCZ that acted to enhance upwelling and productivity within the Cariaco Basin. Sea level eventually reached a

critical point in the transition back to stadial conditions that led to upwelling of nutrient-depleted waters and a decline in productivity within the basin. The most probable potential forcing mechanism of a north/south migration of the ITCZ during the interstadial/stadial periods of the last glacial period is likely related to the surface expression of variation in Atlantic meridional overturning circulation.

Spectral and wavelet analyses of the *Globigerina bulloides* absolute abundance records for the onset and termination of Interstadial 12 were performed to isolate dominant periodicities in the data and identify possible forcing mechanisms and related linkages. The results reveal significant variability ranging from interannual to multicentennial scale, some of which are likely related to equatorial Atlantic Ocean dynamics, important air-sea interactions, and potential teleconnections. The influence of North Atlantic Oscillation-type climate variability may have extended further south during the cold stadials of the last glacial period. Atlantic Multidecadal Oscillation (AMO)-type climate variability is only evident in the warmest interval of Interstadial 12, suggesting that AMO-type variability may only operate during warm climate periods, something that has significant implications for modern and near-future climate variability.

Table of Contents

List of Tables

List of Figures

List of Abbreviations

Al..... Aluminum
AMO .. Atlantic Multidecadal Oscillation
^{10}Be Beryllium-10
^{14}C Carbon-14
C.....Celsius
Ca .....Calcium
cm.....Centimeter
cmbsf.....Centimeters below seafloor
CO_2.....Carbon dioxide
Cr..... Chromium
D-O .....Dansgaard-Oeschger
δ^{18}O .....Delta Oxygen-18
ENSO .....El Niño-Southern Oscillation
Fe.....Iron
g..... Gram
GISP2.....Greenland Ice Sheet Project 2
ITCZ..... Intertropical Convergence Zone
K.....Potassium
km ..... Kilometer
ky..... Thousand years
kya.....Thousand years ago
kyBP.....Thousand years before present
L ..... Lightness (sediment reflectivity)
m .....Meter
Mg.....Magnesium
MIS ..... Marine Isotope Stage
µm .....Micrometer
mm ..... Millimeter
mmol .....Millimole
mol .....Mole
N..... North
NAO.....North Atlantic Oscillation
NO_3 ..... Nitrate
ODP.....Ocean Drilling Program
pCO_2...Partial pressure of carbon dioxide
R/V.....Research vessel
SO_4 ..... Sulfate
SOI ..... Southern Oscillation Index
SST..... Sea surface temperature
^{230}Th Thorium-230
Ti .....Titanium
W..... West
XRF.....X-ray fluorescence
yBP..... Years before present

Acknowledgments

This thesis would not have been possible if it were not for the help and guidance I received along the way. The road I took to obtain my degree was certainly not the most direct, but many people really helped to keep me going.

First and foremost, I would like to acknowledge my advisor, Dave. From helping me identify forams to answering any questions I had, he was always there to help and supported all of my decisions, and for that I am very grateful. I also appreciate the many hours he spent reading, editing, and commenting on this thesis, which has greatly improved because of it.

Many thanks are also due to my committee members, Henry and Sultan. Both of them provided invaluable help and assistance along the way, and this thesis has greatly benefited from their revisions and comments.

I am very grateful to my officemate Michael Slattery for reading and commenting on the very rough drafts of this thesis. I also appreciate the many hours he spent listening to me ramble on about my research, classwork, and life. Many thanks are also due to my officemate Morgan Gelinas for keeping me thoroughly entertained and caffeinated.

I would also like to thank the members of the Paleoceanography and Paleoclimatology Lab for their assistance in processing samples. Special thanks to Jennifer Wurtzel for her MATLAB expertise, and for making long days in the lab entertaining.

During my time at Stony Brook, I have become friends with some of the most amazing people. They not only kept me sane, but provided me with hours of fun, entertainment, and when needed, a shoulder to cry on. I owe a great deal of gratitude to Carly Harrington, Anna Webb, Jesse Hornstein, Liz Brown, Stephanie Talmage, and Joy Smith. It would take an entire thesis just to name everyone, so I apologize to those I did not mention, but you know who you are.

Lastly, I would not be where I am today if it were not for my family. I owe immense thanks to my parents for giving me the freedom and means to pursue my dreams. They may never understand what forams are, by they have stood by me through everything, and continue to support every decision I make. I am also grateful to my sisters Emily and Debbie, and my brother Dan for their continued love and support.

This work was funded by National Science Foundation Grant OCE-0705627 and NOAA Grant NA09OAR4310110 to Dr. David Black.

I. Introduction

1.1 Thesis Objectives

The goal of this project is to better understand the nature of interannual- to centennial-scale climate variability in the tropical Atlantic during both a period of abrupt climate change and for an interval when boundary conditions (e.g. sea-level, continental ice volume, pCO_2, global sea surface temperature) were very different from today. A time known as Interstadial 12 was chosen for this study as it was a time of abrupt warming in the high-latitude Northern Hemisphere from the glacial conditions of Marine Isotope Stage 3. At the onset of Interstadial 12, sea level rose between 20 and 30 m (Siddall et al., 2003, 2008; Rohling et al., 2008), or to a level of 60 – 70 m below present levels. A sea surface temperature (SST) reconstruction from the Bermuda Rise estimated an increase from 17.5°C to 20.5°C at the onset of Interstadial 12 (Sachs and Lehman, 1999). Atmospheric CO_2 concentrations, estimated by measuring the CO_2 concentration in air bubbles entrapped in ice cores, yield values of ~250 parts per million for interstadial events (as measured in Greenland ice cores) (Stauffer et al., 1998). Interstadial 12 is one of the warmest interstadial events, as seen from the Greenland Ice Sheet Project 2 (GISP2) $\delta^{18}O$ record (Figure 1.1), and exhibits a classic saw-tooth pattern, with abrupt warming followed by gradual cooling. Interstadial 12 begins with Heinrich Event 5, and it is also the starting interstadial for one of the longer-term Bond cycles (Bond et al., 1993). While not a perfect analogy for potential future climate change because the starting conditions are not the same, examining climate variability

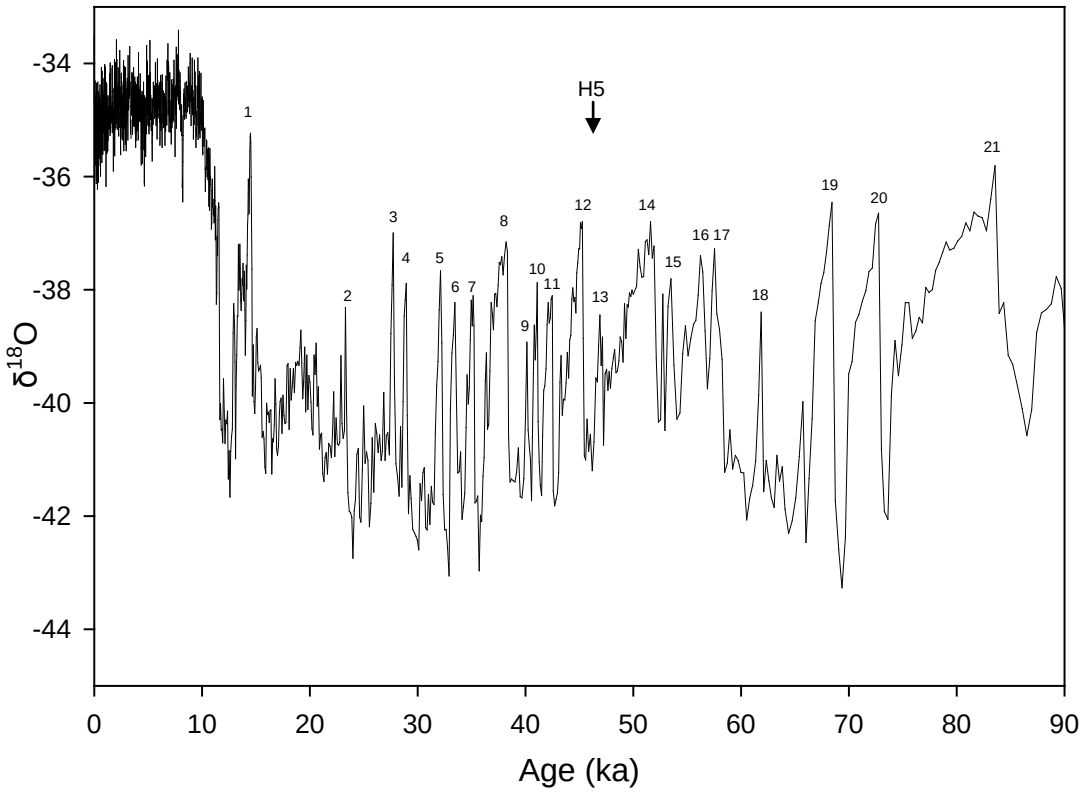

Figure 1.1: Greenland Ice Sheet Project 2 (GISP2) $\delta^{18}O$ record for the past 90,000 years, interpreted as a proxy for air temperature. Isotopically heavier values are indicative of warmer temperatures, while lighter values indicate cooler temperatures. Interstadials are numbered above the graph. H5 indicates Heinrich Event 5. (Data from Stuiver and Grootes, 2000)

during Interstadial 12 will provide the opportunity to help us understand how the climate system responds to a similar direction of change.

To accomplish the goals of this study, I made use of a long piston core collected from the Cariaco Basin in 2003 that contains perhaps the best available sedimentary record of subdecadal- to millennial- scale climate variability in the tropical Atlantic. Like ice cores, the varved sediments accumulating in the Cariaco Basin can be used to study climate on multiple time scales. Prior studies have successfully characterized the interannual- to decadal-scale variability of the Cariaco Basin through the Holocene (Black et al., 1999, 2004; Haug et al., 2001); however, there are no records to date that characterize the nature of variability on these time scales in the tropical Atlantic for periods much older than the Younger Dryas. High sedimentation rates in the Cariaco Basin result in the rapid burial of well-preserved sediments, which makes the basin a premier marine archive of long, continuous records of tropical Atlantic climate variability. The modern climatology of the regions surrounding the Cariaco Basin is largely driven by the seasonal migration of the Intertropical Convergence Zone (ITCZ) and associated variations in trade wind intensity. The varying latitudinal position of the ITCZ drives precipitation variability around the tropical Atlantic and local upwelling variability. The sediment deposited on the floor of the Cariaco Basin records a history of trade wind-induced upwelling and fluvial discharge from northern South America, both processes controlled by the ITCZ's strength and position. This study makes use of these accumulating sediments, and examines how their characteristics and composition change through time. More specifically, the varying abundances of select foraminiferal species are used to create a high-resolution record of tropical Atlantic climate change over a

3,000 year time span during Interstadial 12. This study is the first time a record capable of resolving subdecadal-scale variability has been created for an interstadial event in the tropical Atlantic.

1.2 Interannual to Multi-Centennial Climate Variability

Climate variability occurs on a number of different time scales, from glacial-interglacial cycles occurring on multi-millennial scales, to cycles such as the El Niño-Southern Oscillation (ENSO) that recur every 2-7 years. Variations in the Earth's orbital properties is the primary forcing mechanism of climate variability on glacial-interglacial time scales, and the climatic response to this type of forcing is fairly well understood (Hays et al., 1976; Imbrie et al., 1993). Scientists know much less about climate variability that occurs on shorter, interannual to millennial time scales, due mainly to the lack of long records capable of resolving short-term climate variability. Gaining a better understanding of the patterns and forcing mechanisms of climate variability on sub-millennial time scales will help fill critical voids in our current knowledge of the Earth's climate system.

The El Niño-Southern Oscillation is perhaps the largest single source of interannual climate variability on a global scale (Philander, 1990; Mann and Park, 1994; Chiang, 2009). El Niño (the oceanic component of ENSO) is characterized by warming of surface waters in the tropical eastern Pacific Ocean, while the Southern Oscillation (the atmospheric component of ENSO) is characterized by the continual rise and fall of the sea level pressure difference between the Indonesian Low and the South Pacific High (Philander, 1983). During an El Niño, there is an intensive warming of the upper ocean

in the tropical eastern Pacific lasting for more than 5 months (Philander, 1999; Wang et al., 1999). El Niño is responsible for an eastward shift of convective thunderstorm activity from Indonesia to the central Pacific, wetter than normal conditions along the West coast of tropical South America and at subtropical latitudes of North America and South America (Viles and Goudie, 2003). La Niña, the cold phase of ENSO, tends to produce the opposite trends. NINO3, which refers to the SST anomaly in the NINO3 region (90°W-150°, 5°S-5°N) of the eastern equatorial pacific, is a commonly used index of El Niño (Cane, 2005). The Southern Oscillation Index (SOI) is the normalized sea level pressure difference between Darwin, Australia, and Tahiti (Cane, 2005). When the pressure difference between the two is larger than average, the SOI is positive; when it is smaller than average, the index is negative. El Niño events occur when the SOI is large and negative. This coupled oceanic-atmospheric climate phenomenon occurs every 2 – 7 years (Cane, 2005).

While ENSO dominates subdecadal-scale climate variability, there are multiple decadal-scale processes impacting climate, including the North Atlantic Oscillation (NAO) and the Pacific Decadal Oscillation. The NAO is the dominant mode of atmospheric variability in the North Atlantic region (Visbeck et al., 2003). Like the SOI, the NAO has both positive and negative oscillatory phases. During its positive phase, the NAO shows a stronger than usual subtropical high pressure center around the Azores and a deeper than normal Icelandic low. As a result of the pressure difference, sea levels are higher under the low pressure and lower under the high pressure, and temperatures are colder than normal in the northwest Atlantic and milder in the northeast Atlantic (Hurrell et al., 2003). While in the positive phase, the NAO is associated with stronger than

average surface westerlies across the middle latitudes of the Atlantic onto Europe (Hurrell et al., 2003). Storm tracks are also displaced to the northeast Atlantic region, creating wetter and consequently dryer conditions towards the south of this region in west-central Europe (Visbeck et al., 2003). In its negative phase, the NAO is characterized by a weaker subtropical high and a weaker Icelandic low. The reduced pressure gradient results in higher sea levels in the central Atlantic, lower sea levels in the Arctic, and weaker than average westerlies (Hurrell et al., 2003). The NAO has shown variability in its frequency and intensity over time. A quasi-decadal, 6 to 10 year pattern of variability of the NAO has been more pronounced over the latter half of the twentieth century, while a quasi-biennial pattern dominated the early instrumental record (Houghton et al., 2001).

Numerous studies have found interannual to multicentennial scale variability related to thermohaline circulation/meridional overturning circulation in the North Atlantic. On interannual to decadal scales, changes in North Atlantic circulation appear to be related to the NAO (Delworth and Greatbatch, 2000; Eden and Willebrand, 2001). For periods of a positive NAO, there is an immediate decrease of the heat transport near the subpolar front and an enhancement of heat transport south of 40°N as a response of a change in wind stress (Eden and Willebrand, 2001). After several years, the oceanic response enhances the heat transport throughout the North Atlantic, warming the subpolar North Atlantic (Eden and Willebrand, 2001). Vellinga and Wu (2004) performed a modeling study that implied internal thermohaline circulation variability at interannual and centennial time scales, with the centennial mode being dominant. The study revealed a large-scale air-sea interaction in the Atlantic sector with a centennial time scale

(Vellinga and Wu, 2004). Anomalous northward oceanic heat transport associated with a strong phase of the Atlantic thermohaline circulation generates a cross-equatorial SST gradient, causing the ITCZ to move to a more northerly position with increased strength (Vellinga and Wu, 2004). Sea surface temperature anomalies associated with centennial thermohaline circulation fluctuations have an interhemispheric pattern: when the thermohaline circulation is stronger, SST over most of the Northern Hemisphere becomes warmer as a result of enhanced northward heat transport, while over a large part of the Southern Hemisphere SST cools slightly (Vellinga and Wu, 2004). The enhanced rainfall resulting from the anomalous ITCZ imposes a freshwater flux and produces a salinity anomaly in the tropical North Atlantic that slowly propagates toward the subpolar North Atlantic with a lag of 5 – 6 decades (Vellinga and Wu, 2004). The accumulated low-salinity water lowers upper-ocean density, which causes the thermohaline circulation to slow down and the oscillation to enter the opposite phase (Vellinga and Wu, 2004). Park and Latif (2008) also performed a modeling study and discovered that multicentennial variability in meridional overturning circulation appears to be driven in the Southern Ocean, at a period between 300 and 400 years. They also noted an apparent link between the multicentennial variability and the extent of sea ice cover in the Southern Ocean (Park and Latif, 2008).

Variability in solar output also plays an important part in modulating climate on decadal to centennial scales. The most well known of these cycles is the 11 year sunspot cycle, also known as the Schwabe cycle, due to process of emerging, evolving, and disappearing sunspots and their groups (Beer et al., 2000). The Hale cycle has a period of 22 years and is related to a reversal in the Sun's magnetic field with each Schwabe

cycle (Beer et al., 2000). Variations in the amplitude and period of the 11 year sunspot cycle occur on an ~80 year cycle, known as the Gleissberg cycle (Peristykh and Damon, 2003). Lastly, a ~206 year cycle (the Devries cycle) is prevalent in records of cosmogenic nuclide production including both ^{14}C and ^{10}Be, and is thought to reflect solar variability (Stuiver and Braziunas, 1993). Periods of higher solar activity correspond to times of lower cosmogenic nuclide production, thus their abundance in proxy records is used to reconstruct past solar variability. A ~208 year cycle has been noted in studies of Central American lakes (Curtis et al., 1996; Hodell et al., 2001), and a ~200 year cycle was noted in a study of Cariaco Basin (Venezuela) foraminifera (Peterson et al., 1991), all of which were linked to the ~206 year solar cycle.

1.3 Tropical Atlantic Climate Variability

Ice core records have provided us with an understanding of the timing and magnitude of multi-decadal to millennial-scale climate change, but these records represent conditions for a limited number of geographic locations, and are not necessarily representative of the broader global climate system. Glacial to interglacial and higher frequency climate change has been attributed to high latitude processes, particularly changes in deep water production in the North Atlantic and sea-ice cover (Rahmstorf, 1994; Broecker, 1994; Gildor and Tziperman, 2000). The role that the tropical oceans play in global climate change on multidecadal to millennial time scales is less clear.

In the modern climate system, the tropics are the largest source of interannual to decadal variability, e.g. ENSO, and a number of recent studies have suggested that low-latitude tropical ocean dynamics might have played a more important role in forcing past

climate change than previously thought (Cane, 1998; Clement and Cane, 1999; Clement et al., 2001; Pierrehumbert, 2000). The tropics have the potential to alter the oceanic balance of heat and fresh water, and play a major role as a source of water vapor to the atmosphere (Broecker, 1997; Peterson et al., 2000a).

Interannual to decadal variability are the timescales likely associated with anthropogenic climate change; thus, it is important to understand natural tropical Atlantic climate variability on sub-millennial scales during past times of abrupt climate change. While the influence of ENSO dominates the tropical Pacific, the tropical Atlantic appears to respond to multiple competing influences on interannual to decadal time scales (Sutton et al., 2000). Some of these influences originate in regions remote from the tropical Atlantic, while others arise from local processes (Sutton et al., 2000). The leading mode of tropical Atlantic interannual- to decadal-scale climate variability is the meridional mode, characterized by the latitudinal displacement of the ITCZ and associated trade wind variations (Chang et al., 1997). The meridional SST gradient drives the cross-equatorial flow by creating a surface pressure gradient (Hastenrath and Greischar, 1993), which then drives a cross-equatorial boundary layer flow. This changes the latitudinal position of maximum surface wind convergence, and therefore the ITCZ (Chiang, 2004). Weaker than normal trade winds in the northern subtropics are associated with positive SST anomalies beneath them, and vice versa (Enfield and Mayer, 1997). Colder than normal SSTs in the South Atlantic correspond to weaker than normal trades in the North Atlantic and a smaller than normal southward displacement of the ITCZ during the boreal spring (Marshall et al., 2001). Thus, mechanisms that change the meridional SST gradient are key drivers of tropical Atlantic climate variability. This variability is also strongly

tied to the North Atlantic variability, especially on decadal time scales via the NAO (Marshall et al., 2001). By understanding the role the tropics play in climate variability and the influence exerted on the tropics by other regions, we gain a deeper understanding of the mechanisms of past global climate change. In addition, we can create more accurate models of future climate change if we understand the mechanisms driving past climate change on similar scales.

Recent observational and model analyses suggest that the meridional mode is largely externally driven, most prominently by ENSO and the NAO (Chiang et al., 2000, 2002; Sutton et al., 2000). These external sources drive the anomalous subtropical trade winds, which then create the meridional SST gradient across the equator, and this pattern dissipates once the forcing disappears (Chiang et al., 2004). Not only do numerous forcing mechanisms drive tropical Atlantic climate variability, but the position of the Atlantic ITCZ itself is extremely sensitive to small SST gradients. Chiang et al. (2002) found that the extreme SST variations in the northern tropical Atlantic regions associated with the present-day meridional mode are only about 1°C at most, and yet they are able to displace the position of maximum ITCZ convection thousands of kilometers.

Tropical Atlantic climate is influenced by changes in tropical Pacific convection associated with ENSO and anomalies in Walker Circulation; the north tropical Atlantic warms significantly in response to El Niño, while the south tropical Atlantic response is much weaker (Chiang et al., 2002). Enfield and Mayer (1997) analyzed instrumental SST data and found tropical Atlantic SST variability is correlated with Pacific ENSO variability in several regions, with the most major effect seen in the North Atlantic area of the northeast trade winds west of 40°W along 10°N - 20°N. In this region, 50 – 80%

of the anomalous SST variability is associated with the Pacific ENSO. As ENSO warm phases culminate around December – January in the equatorial Pacific, the Caribbean region experiences a decrease in wind speed, resulting in reduced heat loss in the surface mixed layer due to evaporation and entrainment (Enfield and Mayer, 1997). Following this, a positive anomaly of SST tendency persists for several months, culminating in tropical North Atlantic warming in the late spring and early summer (4 – 5 months after the mature phases of Pacific warm events) (Enfield and Mayer, 1997). Associated with these events is a northward shift in the latitude of the ITCZ with consequent warming immediately north of the mean ITCZ and weak cooling to the south (Enfield and Mayer, 1997). Klein et al (1999) argue that the El Niño warming signal is communicated to the tropical Atlantic via a reduction in surface latent heat flux associated with reduced trade winds.

The leading mode of variability over the mid-latitudes in the Atlantic is the NAO, and there exists a strong link between tropical Atlantic climate variability and the NAO (Marshall et al., 2001). Changes in trade winds, governed by fluctuations in the strength and location of the Azores High, impact SST beneath them through associated surface heat exchange and entrainment at the bottom of the ocean mixed layer (Marshall et al., 2001). The leading pattern of SST variability in the North Atlantic is a direct response of the ocean to the anomalous air-sea fluxes derived by the NAO (Marshall et al., 2001). The SST variability in the North Atlantic and inter-hemispheric SST gradients in the Atlantic share common SST anomalies between the equator and ~30°N (Marshall et al., 2001). Consistent with the NAO impacting the northern subtropical Atlantic, the interannual variability of SST in the tropical Atlantic is strongest in March – May,

lagging the most active NAO season (January – March) by 1 – 2 months (Marshall et al., 2001). Marshall et al. (2001) argue that the NAO could be remotely forced from the tropics. The Hadley Circulation is known to be sensitive to meridional SST gradients in the tropics and could act as an atmospheric 'bridge' to the mid-latitudes, thus modulating mid-latitude NAO variability (Marshall et al., 2001).

Thus, in the tropical Atlantic, there does not appear to be a single dominant mechanism controlling variability. The tropical Atlantic atmosphere is responsive to changes in SST, particularly the cross-equatorial SST gradient. The NAO and ENSO are primary sources of external forcing leading to variability, though their effects may be regionally enhanced (Marshall et al., 2001). Sea surface temperature anomalies north of the equator are subject to remote influence from NAO and ENSO. In response to these anomalies, northward cross-equatorial winds shift the position of the ITCZ, act to reduce the northeasterly mean trade winds in the north, and enhance the southeasterly trades in the south (Marshall et al., 2001). The resulting anomalous heat flux tends to reinforce the initial north-south SST difference, which in turn strengthens the cross-equatorial wind anomalies (Marshall et al., 2001).

The Atlantic Multidecadal Oscillation (AMO) is another subcentennial-scale climate phenomenon that is highly correlated with tropical Atlantic climate patterns. The AMO is a near-global scale mode of observed multidecadal climate variability with alternating warm and cool phases over large parts of the Northern Hemisphere (Knight et al., 2006). Many prominent examples of regional multidecadal climate variability have been related to the AMO, such as North Eastern Brazilian and African Sahel rainfall, Atlantic hurricanes and North American and European summer climate (Knight et al.,

2006). These climate phenomena have been linked to multidecadal variations in Atlantic SST driven by the AMO (Knight et al., 2006), which has a period of ~70 years (Dima and Lohmann, 2007).

Variations in the SST gradient between the north and south tropical Atlantic strongly modulate decadal variations of North East Brazil wet season precipitation (Hastenrath and Greischar, 1993). The warm AMO phase is associated with a northward displacement of precipitation over the tropical Atlantic Ocean, along with a northward cross-equatorial wind anomaly (Knight et al., 2006). These changes imply a shift in the mean ITCZ to the north of its climatological March-April-May position, and hence a reduction in North East Brazil rainfall (Knight et al., 2006). As the cycle of the AMO proceeds, the temperature pattern eventually reverses, forcing an anomalous southerly ITCZ located closer to North East Brazil, thus bringing additional rainfall to the region (Knight et al., 2006). African Sahel rainfall also exhibits distinct multidecadal variability related to the AMO, but is related to an anomalous June-July-August position of the ITCZ, as these are the months when most of the annual rainfall to the region occurs (Knight et al., 2006). A warm AMO phase forces a northward displacement of the mean June-July-August climatological ITCZ and brings increased precipitation to the Sahel (Knight et al., 2006). In the opposite phase, the ITCZ is displaced southward, away from the Sahel, resulting in below average rainfall (Knight et al., 2006). Multidecadal variations in observed major hurricane activity from 1944 to 2000 have also been associated with the AMO (Goldenberg et al., 2001). The influence has been attributed to changes in tropical atmospheric circulation which alter the tropospheric vertical shear in the main hurricane development region, with high shear reducing storm formation

(Goldenberg et al., 2001). In its warm phase, the AMO is linked to greater hurricane activity resulting from increases in North Atlantic SST and reduced vertical wind shear. (Goldenberg et al., 2001).

Table 1.1 summarizes the periodicities of modern climate phenomena that may be relevant to this study.

1.4 Abrupt Climate Change during the Last Glacial Period

Another gap in our understanding of low-latitude climate variability is its response to abrupt climate change. Over the last few decades numerous studies have indicated that the Earth's climate system underwent a series of abrupt oscillations and reorganizations throughout the last glacial period (Dansgaard et al., 1982, 1993; Bond et al., 1993). First recognized in Greenland ice cores, these millennial-scale, abrupt climate events are characterized by shifts between warm and cold states punctuating the climate record for the last glacial period between ~15,000 and 80,000 years ago. There are twenty-five of these distinctive interstadial warming events (Dansgaard et al., 1993) which are now commonly referred to as Dansgaard-Oeschger events, or D-O events. Dansgard-Oeschger events are alternations between warm interstadials and cold stadials, recurring every ~1,500 years (Alley et al., 2001). Interstadial warming occurred abruptly to near-interglacial conditions in a matter of decades, with temperatures changes of ~8 to ~15°C over Greenland during some events (Huber at al., 2006), while cooling occurred much more gradually, giving these events a saw tooth shape in climate records. The saw tooth shape is not unique to D-O events, but is a pattern seen frequently in climate records. The timing and amplitude of these climate events were first identified in some

Climate Oscillation	**Modern Periodicity**	**Reference**
Atlantic Multidecadal Oscillation (AMO)	~70 years	Dima and Lohmann, 2007
Atlantic Niño	3 - 5 years	Chang et al., 2006
El Niño-Southern Oscillation (ENSO)	2 - 7 years	Cane, 2005
North Atlantic Oscillation (NAO)	6 - 10 years	Houghton, 2001

Table 1.1: Table summarizing periodicities of relevant modern climate phenomena.

of the earliest ice core isotopic studies, and are best defined in the Greenland ice core $\delta^{18}O$ record (Figure 1.1) (Dansgaard et al., 1982).

Dansgaard-Oeschger related events are not restricted to Greenland – multiple proxies have shown that many locations in the Northern Hemisphere became warmer and more humid during interstadials, and colder and more arid during stadials (Figure 1.2) (see review paper by Voelker et al., 2002 for an extensive list of references). Bond et al. (1993) were the first to show that the oceans bear the imprint of D-O events, based on a record of sea surface temperatures from the high latitude North Atlantic. Exceptions to these conditions are seen in sea surface temperatures in the Northwest Pacific and the Bay of Bengal (Northeast Indian Ocean), which reveal opposite trends (Kiefer et al., 2001; Kudrass et al., 2001). Contrasting tends are also observed in the productivity of the tropical North Atlantic, with the southern Caribbean increasing in productivity during interstadials and the coastal region off Northwest Africa decreasing in productivity during interstadials (Peterson et al., 2000a; Kiefer, 1998). While the majority of the Northern Hemisphere experiences warm and humid interstadials, the Southern Hemisphere actually cooled during these time periods, as seen from Antarctic ice core $\delta^{18}O$ records (Jouzel et al., 1987). In addition, sea surface temperatures in the Southern Ocean decreased during warm Greenland interstadials (Barker et al., 2009; Kiefer et al., 2001; Roberts et al., 1997), and ice rafted debris was deposited in the Southern Ocean during major interstadials (Kanfoush et al., 2000).

Related to some of the coldest stadial events, and preceding some of the warmest interstadials were six distinctive massive iceberg surges from Northern Hemisphere ice sheets into the North Atlantic, known as Heinrich events. Heinrich events are

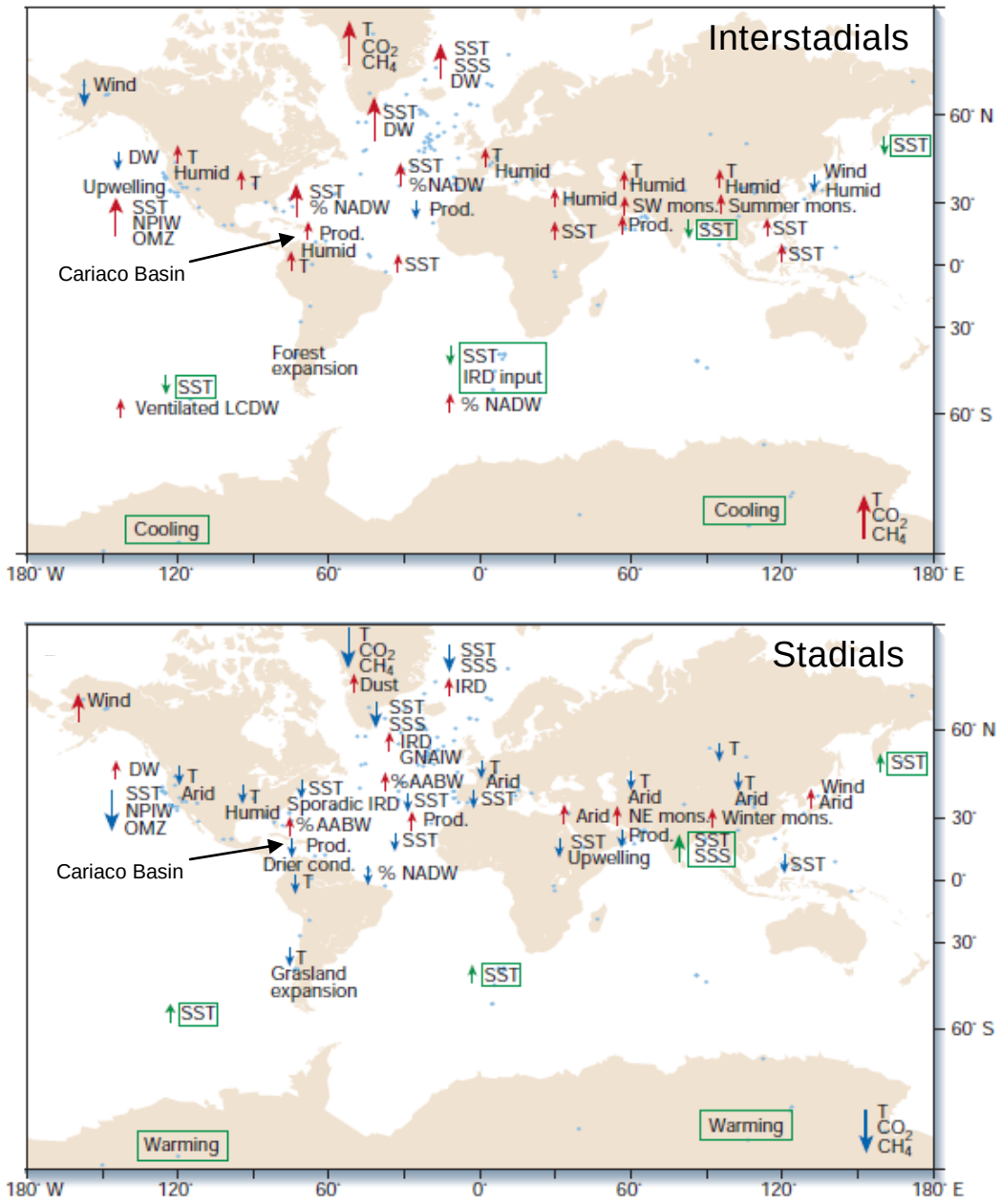

Figure 1.2: Generalized climate features during interstadials (top) and stadials (bottom) based on detailed information from 183 sites summarized in Voelker et al., 2002. Red arrows (blue arrows) indicate trends, that is, warmer (colder), more (less), or increased (lowered). Green text and arrows indicate trends opposite to general climate conditions (e.g. cooling during interstadial, warming during stadial). Abbreviations: T, temperature; SST, sea surface temperature; SSS, sea surface salinity; mons., monsoon; prod., productivity; cond., conditions; IRD, ice-rafted debris; OMZ, oxygen minimum zone. Water masses are labeled as follows: DW, Deep Water; NADW, North Atlantic Deep Water; AABW, Antarctic Bottom Water; NPIW, North Pacific Intermediate Water; LCDW, Lower Circumpolar Deep Water; GNAIW, Glacial North Atlantic Intermediate Water. (Data compiled from sites after Voelker et al., 2002)

documented as thick layers of ice rafted debris (coarse-grained, land-derived materials) in marine sediments in the North Atlantic (Heinrich, 1988; Hemming, 2004). Heinrich events coincide with cold conditions in the North Atlantic and warming in Antarctica (Blunier and Brook, 2001). A sea level increase of 20 – 30 m accompanied Heinrich stadials, while non-Heinrich stadials showed little to no change in sea level (Shackleton, 2000; Siddall et al., 2003). Dansgaard-Oeschger and Heinrich events are related, and are bundled into long-term cooling cycles termed Bond cycles (Figure 1.3) (Bond et al., 1993). Bond et al. (1993) were the first to note these cycles while correlating the Summit ice core (GRIP) $\delta^{18}O$ record to their sea surface temperature reconstruction for the high latitude North Atlantic. Bond cycles begin with an abrupt shift to a markedly warm interstadial, then 2 – 3 interstadials of decreased warming and duration. They culminate in an enormous discharge of icebergs into the North Atlantic during the coldest stadial of the cycle (a Heinrich event), followed by an abrupt shift to the next warmest interstadial (Bond et al., 1993).

A variety of theories have been put forth to explain the abrupt climate swings and events characteristic of the last glacial period, however, none are successful at explaining all of the variability exhibited in climate records. The currently favored paradigm explaining D-O events involves feedback loops associated with a freshening of the North Atlantic via meltwater from Heinrich event iceberg discharges. This freshening affects heat transport from the tropics into the high latitude North Atlantic by stratifying surface waters in regions of deep water formation and weakening or shutting down vertical advection, thus disrupting Atlantic meridional overturning circulation (Rahmstorf, 1995;

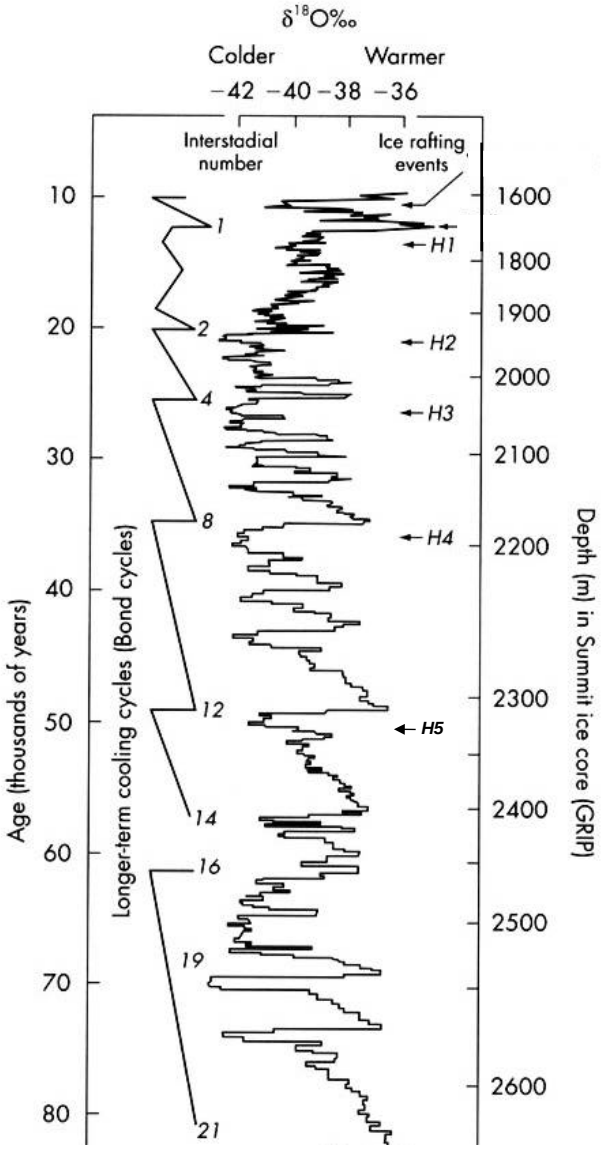

Figure 1.3: Correlation of Greenland Summit ice core (GRIP) $\delta^{18}O$ record and Heinrich events (noted from Deep Sea Drilling Program site 609, numbered to the right of the $\delta^{18}O$ record) to longer-term cooling cycles known as Bond cycles. Interstadials beginning each Bond cycle are shown, and are numbered to the right of the Bond cycles. (After Bond, 1993)

Boyle, 2000). Once freshwater inputs cease and/or salinity levels are restored, the system can resume and heat can once again be transported north (Schmidt et al., 2006).

Dansgaard-Oeschger events are recorded in Cariaco Basin sediments, although the signal is likely not directly temperature-related as it is in Greenland. Still, D-O events are excellent examples of abrupt climate change, and thus provide the opportunity to examine how the tropics and sub-millennial scale variability respond to rapid changes in global climate.

II. Study Area

2.1 Geographic Setting

The Cariaco Basin, situated on the northern shelf of Venezuela, is an ideal location to study past climate change on multiple time scales and has served as the setting for numerous paleoclimate studies of the tropical Atlantic (e.g. Peterson et al., 1991, 2000a; Hughen et al., 1996; Black et al., 1999, 2007; Tedesco and Thunell, 2003a; Peterson and Haug, 2006). There is no better marine archive for long, continuous, high-resolution records of tropical Atlantic climate variability than the Cariaco Basin. High resolution climate reconstructions are possible because of the basin's predominantly anoxic conditions and high sedimentation rates (30 to >100 cm/ky (Peterson et al., 2000b)). Presently, the Cariaco Basin is one of the largest anoxic basins in the world, second only to the Black Sea (Richards, 1975).

The Cariaco Basin is an east-west trending pull-apart basin that is 160 km long and 50 km wide (Lidz et al., 1969; Schubert, 1982). The basin is divided into two major sub-basins, each reaching a maximum depth of ~1400 m, separated by a central saddle at ~900 m water depth (Figure 2.1) (Richards, 1975; Schubert, 1982). In addition, there are two smaller, minor depressions east of the central saddle, the Araya Basin (550 m water depth) and the Margarita Basin (412 m water depth) (Richards, 1975). Connections to the Caribbean Sea occur via two shallow passages, the Centinela Channel in the northwest and the Tortuga Channel in the northeast, with water depths of 146 m and 135 m, respectively (Alvera-Azcárate et al., 2009). Thus, surface waters within the basin can

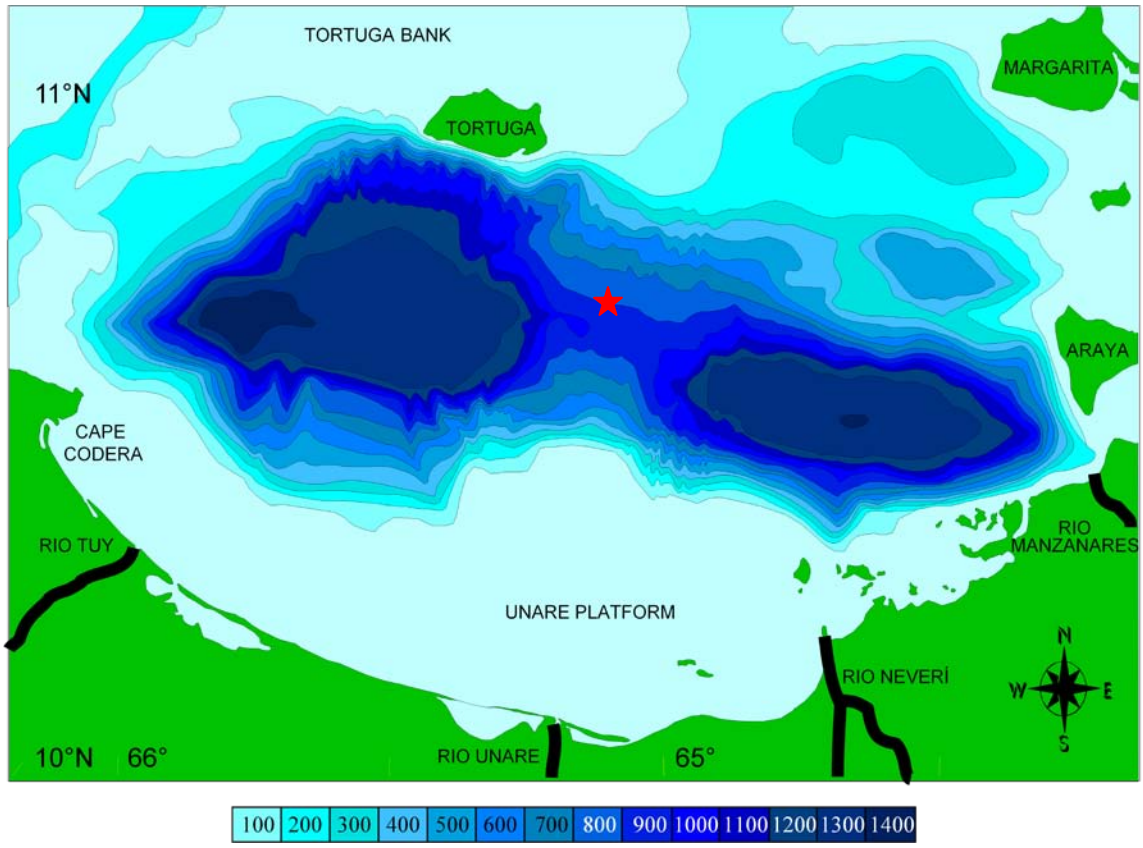

Figure 2.1: Cariaco Basin location and bathymetry, and location of sediment core MD03-2622 (red star). Local rivers surrounding the Cariaco Basin (thick black lines) and depth isobaths (meters, by color) are noted.

exchange freely with Caribbean surface waters while waters below the sill depth are poorly ventilated.

2.2 Regional Climatology

Located at 10°N, the Cariaco Basin sits at the northern extent of the annual latitudinal range of the Intertropical Convergence Zone (ITCZ) (Haug et al., 2001). The ITCZ shifts its position seasonally (Figure 2.2), and is most often associated with the zone of the highest sea surface temperatures (SSTs) and lowest sea-level pressures. The ITCZ is an area of low atmospheric pressure formed from the convergence of the northeast and southeast trade winds. As the winds converge, warm moist air is forced upward and cools and condenses; there is a resultant band of cloud formation and heavy precipitation that is associated with the ITCZ.

Between January and March, the ITCZ is located in a position just south of the equator over the South American landmass. Strong easterly trade winds blowing along the northern coast of Venezuela result in intense Ekman-induced upwelling of cool, nutrient-rich waters in the Cariaco Basin, which fuels the high primary productivity observed in the basin during these months (Scranton et al., 2006). The intense upwelling during this period is in sharp contrast to the diminishing trade winds and weakened upwelling over the basin during the Venezuelan rainy season, beginning in June or July.

During the boreal summer the ITCZ is almost directly over the Cariaco Basin, leading to the rainy season for the areas surrounding the Cariaco Basin, a period also known as the South American Summer Monsoon. Throughout these months, rain falls in the regions that drain directly into the Cariaco Basin (Hastenrath and Greischar, 1993)

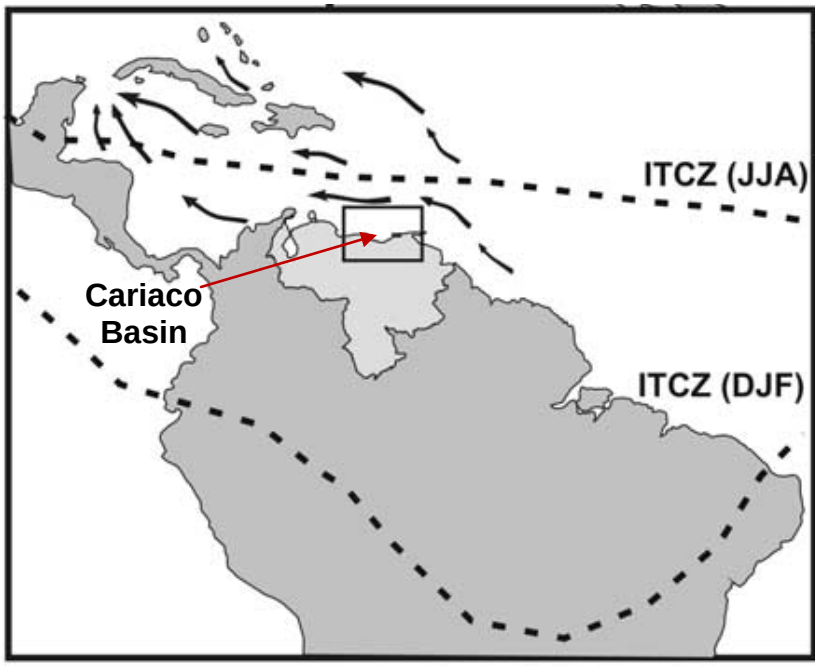

Figure 2.2: Yearly migration of the Intertropical Convergence Zone (ITCZ) over northern South America. Modern latitudinal limits are denoted as dotted lines. Black arrows show the main surface circulation pattern in the Caribbean. Boreal summer months (June, July, August (JJA)) and winter months (December, January, February (DJF)) are noted. Red arrow indicates the location of the Cariaco Basin. (After González et al., 2008)

resulting in the delivery and accumulation of terrigenous material in the basin (Peterson et al., 2000a). Secondary upwelling peaks have also been observed in July–August each year, and last only a month. Astor et al. (2003) suggested that the mid-summer upwelling is related to the initiation of the southward turn in the trade wind.

2.3 Modern Water Column Characteristics and Hydrography

The hydrography and water column characteristics of the Cariaco Basin differ greatly depending on water depth (Astor et al., 2003). The presence of only two shallow sills that allow surface waters to exchange freely with Caribbean Sea water also act as a barrier to horizontal advection and ventilation of water below the sill depths. Thus, the properties of the upper water column are generally similar to those of the open Caribbean Sea (Richards, 1975). However, they show marked temporal variation (Astor et al., 2003). Upwelling in the basin can be defined as the upward displacement of isotherms, whereas upwelling relaxation is noted by the apparent downward migration of isotherms (Astor et al., 2003). Based on these definitions, upwelling generally starts in November or December and subsides sometime after March of the following year, as seen by the migration of the 21°C isotherm (Astor et al., 2003).

In addition to restricted horizontal exchange below sill depth, vertical mixing in the Cariaco Basin is also inhibited by the presence of a strong pycnocline that starts at the surface and extends to the sill depth (Astor et al., 2003). Below 200 m water depth, vertical temperature gradients are small and do not show evidence of a seasonal cycle due to the lack of ventilation and strong pycnocline (Astor et al., 2003). In the upper water column, dissolved oxygen concentrations follow a distinct seasonal cycle, with the

highest values observed in the upper 20 m in spring (Astor et al., 2003). Oxygen is supplied only by air-sea gas exchange and photosynthesis in the upper water column, and it is used by bacterial respiration processes at all depths. The limited oxygen supply, combined with a strong pycnocline, high seasonal productivity, and restricted horizontal exchange, results in anoxia below 250-320 m water depth (Astor et al., 2003). This lack of oxygen leads to sediment almost entirely devoid of benthic organisms, and thus a lack of bioturbation, leading to preservation of a nearly undisturbed sediment record.

2.4 Seasonal Biology

The seasonal biology of the Cariaco Basin is driven largely by the influence the regional climatology has on the water column. During the upwelling season, when primary productivity reaches its yearly maximum, the phytoplankton community is dominated mainly by diatoms (Ferraz-Reyes, 1983). Primary productivity is lower during the rainy, nonupwelling season, and a more diverse phytoplankton community develops, mostly composed of dinoflagellates and cyanobacteria (Ferraz-Reyes, 1983). Coastal assemblages are relatively better developed during this season as they benefit from the fluvial discharge of fresh water and nutrients (Ferraz-Reyes, 1983).

Like the phytoplankton community, the planktonic foraminiferal community is also driven by the seasonal changes in the position of the ITCZ over the Cariaco Basin. The spatial and temporal distributions of the foraminifera species are related to various environmental parameters such as temperature, salinity, light, nutrients, and food supply (Tedesco and Thunell, 2003b). Tedesco and Thunell (2003b) used sediment trap data

from the Cariaco Basin for the period January, 1997 to December, 1999 to quantify the seasonal variations in the planktonic foraminiferal flux and assemblage composition.

Nine species/varities of planktonic foraminifera constitute >85% of the assemblage: *Orbulina universa*, *Globigerinoides ruber* (pink and white varities), *Globigerina bulloides*, *Globigerina quinqueloba*, *Neogloboquadrina dutertrei*, *Globorotalia crassaformis*, *Globorotalia menardii*, and *Globigerinita glutinata* (Tedesco and Thunell, 2003b). While these species are present year round, their flux and contribution to the population vary both seasonally and interannually. Immediately following the peak primary productivity of the late winter-spring upwelling season, the total flux of planktonic foraminifera increases from less than 100 shells m^{-2} day^{-1} to 4000 – 8000 shells m^{-2} day^{-1} (Tedesco and Thunell, 2003b). The peak annual flux of all nine species occurs during spring upwelling.

Globigerina bulloides is the dominant species during the upwelling season, with fluxes reaching ~4000 shells m^{-2} day^{-1} and comprising between 50 – 75% of the total flux during this period (Tedesco and Thunell, 2003b). The abundance of *G. bulloides* is controlled primarily by variations in surface-water productivity (Thunell and Reynolds, 1984; Reynolds and Thunell, 1985), hence its maximum flux and population contribution occur during the upwelling season. *Globigerina quinqueloba* is also common in regions with high production such as coastal upwelling zones (Thiede, 1975). While this species contributes only about 7% to the total annual flux in the Cariaco Basin, it accounts for 20 – 25% of the upwelling assemblage (Tedesco and Thunell, 2003b). *Globorotalia crassaformis* is a deeper-dwelling species and is found mainly in low-oxygenated subsurface waters (Kemle-Von Mücke and Oberhänsli, 1999). It constitutes 10 – 20% of

the total annual foraminiferal flux, and the highest flux and percentage (20 – 40%) occurs during the latter part of the upwelling season (Tedesco and Thunell, 2003b). At this point in the upwelling season, percentages of *G. bulloides* and *G. quinqueloba* are decreasing (Tedesco and Thunell, 2003b), and levels of dissolved oxygen concentrations in subsurface waters are also decreasing (Muller-Karger et al., 2001).

Globigerinoides ruber inhabits the surface mixed layer (Deuser, 1987) and is most abundance in subtropical to tropical oligotrophic waters (Miró, 1971). The species has pink and white morphotypes, living between 0 – 45 m and 25 – 65 m water depth, respectively (Bé, 1982). In the Cariaco Basin, both varieties experience maximum fluxes during upwelling, however, they only reach values up to about 350 shells m^{-2} day^{-1} (Tedesco and Thunell, 2003b). Combined, both varieties account for less than 10% of the total annual flux, but constitute 20 – 30% of the total assemblage when the percentage of *G. bulloides* is at a minimum and SSTs are beginning to decrease just prior to upwelling (Tedesco and Thunell, 2003b).

Neogloboquadrina dutertrei thrives in a well-stratified photic zone, and lives within the thermocline close to the chlorophyll maximum, a zone of high production and maximum food supply (Fairbanks et al., 1982). Chlorophyll values are highest during spring upwelling, when the chlorophyll maximum shoals to about 0 – 25 m (Muller-Karger et al., 2001), and this period coincides with the peak flux of *N. dutertrei* (Tedesco and Thunell, 2003b). *Globigerinita glutinata*, which is most abundant in the upper 50 m of the water column (Kemle-Von Mücke and Oberhänsli, 1999), has peak fluxes of 500 – 1000 shells m^{-2} day^{-1} during the upwelling season (Tedesco and Thunell, 2003b). *Orbulina universa*, a spinose, photic zone inhabiting species, has maximum fluxes of 200

– 400 shells m^{-2} day^{-1} during spring upwelling (Tedesco and Thunell, 2003b). During this period it contributes less than 10% to the total upwelling assemblage, and up to about 6% of the total annual flux (Tedesco and Thunell, 2003b).

2.5 Sediment Provenance and Characteristics

Trade wind-induced upwelling and fluvial discharge from northern South America, both processes controlled by the Intertropical Convergence Zone's (ITCZ) strength and position, are recorded in detail in the sediments of the Cariaco Basin. The lamination of sediments in the Cariaco Basin reflects the pronounced local wet and dry seasons, which create seasonal sedimentation patterns (Hughen et al., 1996; Haug et al., 2001). Dark colored, terrigenous grain-rich layers are deposited during the rainy boreal summer and fall, while lighter colored biogenic-rich layers are deposited during the winter and spring upwelling seasons. Thus an annual deposition layer is composed of one dark and one light band. It is also possible, however, for there to be a secondary peak in production that typically occurs in October that could produce a false band. The distinct seasonal variations in sedimentation, coupled with the basin's anoxic waters, results in the preservation of undisturbed, varved sediments that create a premier archive of past climate change.

Local rivers that have the potential to deliver terrigenous material to the Cariaco Basin include the Tuy, Unare, Manzanares, and Neverí rivers (Figure 2.1). It has been shown that fluvial inputs are primarily from these local rivers, rather than from the larger, but distant plumes of the Orinoco and Amazon Rivers (Martinez et al., 2007; Lorenzoni et al., 2009; Martinez et al., 2010). In terms of sediment discharge, the Tuy is the most

important, followed by the Unare, Neverí, and Manzanares (Martinez et al., 2010). Terrigenous material content is higher in the southern Unare platform, which covers the area from Cape Codera to the Araya Peninsula (Figure 2.1), while lower terrigenous content found east and north indicates a reduced fluvial influence of those areas (Martinez et al., 2010). Thus terrigenous material dominates close to the drainage basins of the local rivers, while calcium carbonate increases as the marine biogenic component becomes increasingly important away from the coast (Martinez et al., 2010). Terrigenous input to the Cariaco Basin varies temporally, with terrigenous concentrations increasing during rainy seasons and decreasing in the dry seasons (Martinez et al., 2007), which closely follows the seasonal shift of the ITCZ.

Another property of Cariaco Basin sediment that reflects the seasonal alternation between river runoff and upwelling are variations in the elemental abundances of iron and titanium (Peterson et al., 2000a; Peterson and Haug, 2006). The possibility that variations in iron abundances are diagenetically controlled is dismissed because sediment titanium variations, which are redox-insensitive (Yarincik et al., 2000a), generally show identical downcore patterns in Cariaco Basin sediment cores to those of iron (Peterson et al., 2000a; Haug et al., 2001, 2003). Instead, iron and titanium variations in the Cariaco Basin are interpreted to reflect changes in terrigenous sediment input (Peterson et al., 2000a; Peterson and Haug, 2006), whereby the terrigenous component is reflected in the strong correlation between detritally associated elements such as Al, Ti, and Fe (Martinez et al., 2010). During the rainy season when the ITCZ is at a more northern position over the Cariaco Basin, terrigenous inputs are at a yearly maximum, and are recorded as a peak in the abundances of iron and titanium in sediment cores (Martinez et al., 2007).

While variations in Ti/Al, Fe/Al, K/Al, and Cr/Al document seasonal changes in terrigenous sources, the seasonality is strongest for Ti/Al and Fe/Al, suggesting a larger contribution during the rainy season of material with high Fe/Al and Ti/Al, with respect to the dry season (Martinez et al., 2007).

Eolian deposition to the Cariaco Basin represents another important source of terrigenous material. Like fluvial input, eolian sedimentation in the basin is also highest during the rainy season (Elmore et al., 2009). During the boreal summer months, when the ITCZ is located near 10°N, the Sahel region is especially arid, allowing for the Saharan air layer to transport dust toward the tropical Atlantic Ocean and the Caribbean, including the Cariaco Basin (Zabel et al., 2003). During the winter months, however, the northeast trade winds carry a smaller dust plume into South America, and away from the Cariaco Basin (Zabel et al., 2003). Elmore et al. (2009) showed that the eolian component of sedimentation makes up roughly 10% of the total terrigenous sedimentation to the Cariaco Basin.

The long-term lithostratigraphy of the sediments deposited on the floor of the Cariaco Basin reflects a history of oscillations between oxic and anoxic water columns, characteristic of interglacial and glacial periods, respectively (Yarincik et al., 2000b). The basin is currently anoxic below ~300 m water depth, the onset of which occurred at ~12.6 kya, and has resulted in the deposition of laminated sediments over this time period (Peterson et al., 1991; Hughen et al., 1996).

Glacial periods are characterized by sea level lowstands and restricted water circulation within the Cariaco Basin. The influx of seawater from the open Caribbean Sea is primarily from the mixed zone, which is depleted in nutrients but rich in dissolved

oxygen (Yarincik et al., 2000a). This combination limits primary production and results in a decreased flux of particulate organic matter to the seafloor of the basin, facilitating oxic conditions in the water column (Peterson et al., 1991; Haug et al., 1998). During these periods, sediment deposited are not laminated and often bioturbated (Peterson et al., 2000b).

At the onset of interglacial periods, melting ice sheets result in a rise of sea level and an influx of nutrient-rich subthermocline waters into the Cariaco Basin that are seasonally upwelled and lead to high levels of primary production (Yarincik et al., 2000a). High primary production results in an oxygen demand that cannot be met by the rate of oxygen replenishment, leading to anoxic conditions (Peterson et al., 1991, 2000b; Haug et al., 1998). During periods of high surface production and anoxia, the sediments deposited are rich in preserved total organic carbon (Haug et al., 1998; Peterson et al., 1991), are unbioturbated, and contain a higher frequency of distinctly laminated intervals (Peterson et al., 1991; Hughen et al., 1996).

III. Prior Studies in the Cariaco Basin

3.1 Studies of Sediment Properties

A large number of studies have utilized sediment from the Cariaco Basin to examine past changes in both regional and global climate change. Heezen et al. (1958, 1959) were the first to report the characteristics of Cariaco Basin sediments using twelve piston cores. Kipp and Towner (1975) published foraminiferal records that were the first to show that the basin's rapidly accumulating sediments preserved climate signals.

More recently, numerous studies have created high-resolution climate records showing that Cariaco Basin sediments provide evidence of abrupt climate events in the Holocene, over the deglaciation, and during the last glacial period that can be linked to climate change in the high-latitude North Atlantic and to other tropical and extratropical regions (e.g. Hughen et al., 1996; Black et al., 1999; Peterson et al., 2000a). Two such studies made use of the sediment reflectivity (Hughen et al., 1996; Peterson et al., 2000a), a proxy thought largely to be controlled by organic carbon contents and changing productivity. An annual deposition layer consists of a lighter colored, plankton-rich layer deposited during the upwelling season, followed by a darker colored, terrigenous grain-rich layer deposited during the rainy season (Hughen et al., 1996). These distinctly colored layers record the seasonal migration of the Intertropical Convergence Zone (ITCZ) over the Cariaco Basin. The lighter colored laminae are more reflective, thus the reflectivity records an alternating pattern of increased productivity followed by increased fluvial input. Hughen et al. (1996) used this principle of grey scale reflectance and

laminae thickness as a paleoproductivity proxy in the Cariaco Basin for the last deglaciation. They found that darker laminae are consistent with period of increased rainfall and lighter laminae are deposited during upwelling conditions. When the reflectance record was compared to the Greenland Summit ice core (GRIP) $\delta^{18}O$ record, the two records exhibited striking similarities, suggesting a common forcing mechanism. Hughen et al. (1996) hypothesized that a shift in North Atlantic thermohaline circulation and the resulting changes in North Atlantic SST could influence tropical Atlantic trade wind strength and eventually Cariaco Basin productivity.

Peterson et al. (2000a) also used sediment color reflectance to demonstrate that the tight linkage of the tropics to the high-latitude ice core records could be extended back at least 90,000 years. The reflectance profile from Ocean Drilling Program (ODP) site 1002 was compared to the Greenland Ice Sheet Project 2 (GISP2) $\delta^{18}O$ record, exhibiting a remarkable resemblance. Peaks in productivity inferred from the sediment reflectance data occurred almost synchronously with the warm interstadial events seen in the Greenland $\delta^{18}O$ record. In addition to using the reflectance as a paleoproductivity proxy, Peterson et al. (2000a) obtained high-resolution elemental (iron, titanium, and calcium) measurements using x-ray fluorescence (XRF). High iron and titanium intensities are closely associated with the darker, terrigenous grain-rich sediment laminae, thus their abundances can be used as a proxy for fluvial input. Using the down-core variations in iron and titanium from ODP site 1002, they hypothesized that millennial-scale productivity pulses recorded in the Cariaco Basin during the last glacial are the result of an increased supply of river-borne nutrients to the region (Peterson et al., 2000a). These periods of high productivity, as seen from increased organic carbon input

inferred from the sediment reflectance data, are synchronous with periods of increased terrigenous delivery to the Cariaco Basin, and occur during warm interstadial events of the last glacial. These conclusions are based on coincident variations between the oscillating dark laminated and light non-laminated sediment from the Cariaco Basin record and the air temperature variations over Greenland as inferred by the $\delta^{18}O$ record from the GISP2 ice core (Peterson et al., 2000a).

It was also suggested that the pulses of increased terrigenous input to the Cariaco Basin are the result of increased rainfall and enhanced runoff from the watersheds of rivers emptying into the basin. The data imply a northward shift of the ITCZ during the warm interstadial events of the last glacial period (Peterson et al., 2000a). This productivity pattern contrasts with the modern dynamics of the Cariaco Basin. Today, higher productivity occurs when the ITCZ is to the south, and is driven by upwelling. In contrast, Peterson et al. (2000a) noted increased productivity associated with northward shifts of the ITCZ during interstadials and the resultant fluvially-derived nutrient input to the basin. Since sea level was lower throughout the last glacial period, fluvial inputs were more direct and volumetrically more important. In addition to the local implications to the Cariaco Basin, this increased precipitation could have affected the salinity balance of the Atlantic and weakened thermohaline heat transport to the high northern latitudes, thus supporting the idea that tropical feedbacks played an important role in modulating global climate during the last glacial period (Peterson et al., 2000a).

In a similar fashion to Peterson et al. (2000a), Haug et al. (2001) also used iron and titanium concentrations from the Cariaco Basin sediment core taken at ODP site 1002 to reconstruct the migration of the ITCZ through the deglaciation and into the

Holocene. They noted low concentrations of both elements in sediments deposited during the Younger Dryas cold period between 12.6 and 11.5 kya (Haug et al., 2001). Concentrations increased during the Pre-boreal period (11.5 to 10.5 kya) and were highest during the Holocene thermal maximum (10.5 to 5.4 kya), with a subsequent long-term decrease (Haug et al., 2001). From this data, they infer that the longer term changes in sediment composition are controlled by the latitude of the ITCZ, and the high iron and titanium concentrations associated with the Holocene thermal maximum indicate a more northerly mean annual position for the ITCZ relative to the later Holocene (Haug et al., 2001). This southward migration of the ITCZ through the Holocene has also been used to explain the collapse of the Mayan civilization due to extensive multiyear droughts that occurred during an already extended regional dry period (Haug et al., 2003).

Peterson and Haug (2006) looked further into the these rapid shifts in the ITCZ and precipitation recorded by Cariaco Basin sediments to attempt to see if the records reflect a forcing mechanism originating in the high latitude Atlantic or to forcing potentially sourced in the tropics. Unfortunately, they were unable to determine whether the observed shifts in the ITCZ position reflect a response to forcing originating in the high latitude Atlantic or forcing potentially driven by El Niño-Southern Oscillation-type variability emanating from the tropical Pacific (Peterson and Haug, 2006). Thus, the need exists to create more high resolution records of climate variability from the tropics during these periods of rapid climate change.

3.2 Foraminiferal Census Studies

Studies of Cariaco Basin sediment recovered from cores have also focused on the varying abundances of planktic foraminifera species present in the sediment (Overpeck et al., 1989; Peterson et al., 1991; Black et al., 1999). Most of these studies have focused on the abundance record of the planktic foraminifera species *Globigerina bulloides* as a proxy record of upwelling in the Cariaco Basin. Sediment trap studies indicate that *G. bulloides* dominates the water column assemblage during the upwelling season (Tedesco and Thunell, 2000b), thus the abundance record of the species is an indirect proxy of trade wind strength and position.

Overpeck et al. (1989) used the inverse seasonal relationship between *G. bulloides* and *Globogerinoides ruber* relative abundances to reconstruct the late Quaternary climate history of the Cariaco Basin. They noted abrupt changes in the *G. bulloides* abundance record at 13 - 12.6 kya, 11 kya, and 10 kya, providing evidence for abrupt changes in trade wind strength (Overpeck et al., 1989). In addition, a global circulation model was used to determine that an increase in trade wind intensity could affect the foraminiferal population. Overpeck et al. (1989) hypothesized that the inferred increase in trade wind intensity could be a result of a melt-water induced glacial cooling in the Gulf of Mexico.

Peterson et al. (1991) performed a foraminiferal census study on a sediment core from the Cariaco Basin, focusing on six species and varieties: *G. bulloides, G. ruber* (pink and white varieties), *Neogloboquadrina dutertrei, Globorotalia menardii,* and *Globigerinita glutinata*. They found results consistent with the study done by Overpeck et al. (1989), with a similar up-core transition from a *G. ruber* dominated assemblage to a

G. bulloides dominated assemblage at 12.6 kya. Also noted at this transition was the presence of laminated sediment and biogenic opal that they inferred to indicate the initiation of strong upwelling as the basin established connections to the open Caribbean Sea during the deglaciation (Peterson et al., 1991).

On much shorter and more recent time scales, Black et al. (1999) showed that the correlation between the tropical Atlantic and high-latitude conditions is evident at the subdecadal level by analyzing the past eight centuries of sediments in the Cariaco Basin. They found a strong correlation between sea surface temperatures (SSTs) in the high latitude North Atlantic, trade wind intensity, and foraminiferal abundances in Cariaco Basin sediments. During periods when SSTs in the North Atlantic are colder than average, the trade winds are more intense over the Cariaco Basin, as inferred from increases in *G. bulloides* abundances over these periods (Black et al., 1999). Hastenrath and Greischar (1993) used instrumental data to show that cooler North Atlantic SSTs result in increased surface pressure over the North Atlantic and a southward shift of the ITCZ, leading to a weakening of the southeast trade winds and an intensification of the northeast trade winds. This is one possible explanation for the observed trends in the *G. bulloides* data (Black et al., 1999).

Black et al. (1999) also performed spectral analysis on the *G. bulloides* time series, revealing concentrations of variance centered at periods of 140 to 500 years, 12.5 to 13.0 years, 8.7 to 9.0 years, 6.8 to 7.0 years, and 6.1 to 6.3 years. The results suggest that a century-scale mode of variability appears to be an important natural aspect of Atlantic variability (Black et al., 1999). In fact, the most important mode of modern variability may be centennial rather than interdecadal in nature and they hypothesize that

this may be related to long-term variations in the couple ocean-atmosphere system, solar forcing, or a combination of these two (Black et al., 1999). The results also confirm the importance of a decadal mode of Atlantic variability, as seen by significant spectral power in the 12.5 – 13.0 year band, believed to be driven by coupled tropical ocean-atmosphere dynamics (Black et al., 1999).

3.3 Geochemical Studies

Many studies have made use of the isotopic composition of the calcium carbonate shells of foraminifera accumulating in the Cariaco Basin to reconstruct climate and hydrographic conditions on multiple time scales (e.g. Lin et al., 1997; Lea et al., 2003; Tedesco and Thunell, 2003a; Black et al., 2004; McConnell et al., 2007). Lin et al. (1997) demonstrated the value of using the $\delta^{18}O$ of multiple species of planktonic foraminifera for surface reconstructions in the Cariaco Basin due to the differing depth zones at which these species live. Tedesco and Thunell (2003a) employed this multi-species $\delta^{18}O$ strategy to reconstruct circum-Caribbean aridity fluctuations which they attributed to variations in the location of the ITCZ and associated variations in precipitation and trade wind intensity. Black et al. (2004) created a $\delta^{18}O$ record for the past 2000 years from the Cariaco Basin from two species of planktic foraminifera, *G. ruber* and *G. bulloides.* They found that variations in the $\delta^{18}O$ record correlate to tropical SSTs over the period of continuous instrumental overlap, but salinity fluctuations may have played a more significant role in the $\delta^{18}O$ variations in the earlier part of the record when the instrumental record is discontinuous (Black et al., 2004). In addition, millennial- and submillennial-scale $\delta^{18}O$ variability over the past 2000 years may be

controlled by upwelling-induced temperature changes and precipitation pattern-related salinity fluctuations (Black et al., 2004).

The Mg/Ca ratio of planktonic foraminifera tests has also been used as a proxy to gain insight into paleo-SSTs. Lea et al. (2003) created a record of SSTs from the Cariaco Basin for the past 25,000 years using Mg/Ca. They showed that tropical Atlantic SST records over the last glacial termination were nearly synchronous with the GISP2 air temperature proxy record (Lea et al., 2003). Black et al. (2007) created a record of tropical Atlantic SST for the past 800 years using Mg/Ca derived from Cariaco Basin foraminifera, which showed a great deal of variability over the time span, with some warming during the Medieval Warm period, significant cooling during the Little Ice Age, and abrupt warming in the twentieth century. These temperature swings represent wider conditions in the Caribbean and western tropical Atlantic, and are not necessarily related to local upwelling variability (Black et al., 2007). McConnell et al. (2004, 2007) used both the $\delta^{18}O$ and the Mg/Ca ratio of two species of planktonic foraminifera from the Cariaco Basin to examine tropical climate variability during Marine Isotope Stage 3 (MIS 3). They found that the lowest oxygen isotope values (~0.25‰) occur during interstadials while the highest values reaching 0.85‰ occur during stadial period (McConnell et al., 2006, 2007). The Mg/Ca results across several of the stadial/interstadial oscillations tend to co-vary with the $\delta^{18}O$ data, with mean Mg/Ca values ranging from a minimum of ~3.0 mmol/mol during stadial period just prior to and immediately after Interstadials 7 and 12, to a maximum of ~4.9 mmol/mol during Interstadial 12 (McConnell et al., 2006, 2007). They also note that there is a double peak

in both the $\delta^{18}O$ and Mg/Ca records across Interstadial 12, with the Mg/Ca record leading by about 400 years (McConnell et al., 2006, 2007).

McConnell et al. (2008) estimated pCO_2 values during MIS 3 (~30 – 55 kyBP) by measuring planktonic foraminiferal shell weights on foraminifera from the Cariaco Basin. Shell weight variability is driven, in part, by changes in the surface water carbonate ion concentration, and when combined with estimates of past seawater temperature and salinity, can yield information on past changes in atmospheric carbon dioxide. McConnell et al. (2008) found that calculated pCO_2 values during interstadial events are higher than those estimated for stadial events despite higher primary productivity, and attributed these higher values to decreased pH and alkalinity due to increased river input and enhanced calcite production.

IV. Materials and Methods

4.1 Materials

In May of 2003, five Calypso piston cores were collected from the Cariaco Basin aboard the R/V *Marion Dufresne* (Laj, 2004) as part of the Paléoclimatologie Isotopes CAlypso pour les Séries Sédimentaires Océaniques (PICASSO) campaign of the International Marine Past Global Change Study (IMAGES) XI program. One of the cores, MD03-2622 (10°42.69' N; 65°10.15' W; 877 m water depth), that contains the sediment that was used in this study, was recovered from the western side of the central saddle (Figure 2.1), and has a length of 48.3 m. The coring location was in close proximity to the Ocean Drilling Program (ODP) Site 1002, which allows for more direct comparison between the two study sites. The core recovered a complete and continuous sequence that spans back through Termination II into Marine Isotope Stage (MIS) 6 (~130 kyBP). The sedimentation rate calculated from the entire core averages 35 cm per thousand years, and the core shows virtually no evidence of disturbance from the coring procedure. An abundance of aragonitic pteropods in the recovered sediments indicated excellent preservation and little to no dissolution. This study focuses on Interstadial 12 (~42,500 – 45,810 yBP). The Interstadial 12 section in the core is visibly laminated and devoid of benthic microfauna (Figure 4.1), indicating deposition under anoxic conditions. The Interstadial 12 section in the ODP Site 1002 record also contains laminated sediments, as do other interstadial events recorded in the core, suggesting

Figure 4.1: Split core photograph of MD03-2622 (section XIV, representing 2010 – 2030 cm below sea floor). Evident in photograph are visible laminations and a lack of sediment disturbance due to bioturbation. Thicker light layers are sections of microturbidite deposition.

an oscillation between oxic and anoxic conditions in the Basin during stadial and interstadial events, respectively (Peterson et al., 2000a).

Interstadial 12 was identified in MD03-2622 based on correlations between sediment reflectance and the Greenland Ice Sheet Project 2 (GISP2) $\delta^{18}O_{ice}$ record (Figure 4.2). Sediment reflectance is a proxy for organic carbon input, and was measured onboard the R/V *Marion Dufresne* using a spectrophotometer at 2 cm intervals. Sediments from Interstadial 12 were sampled at consecutive 1 mm intervals on the working half of the core. Rulers were placed on either side of the core half, 1 mm intervals were marked, and the 1 mm section was scraped off using a glass slide. In total, 1,500 samples were taken over the interval of 19.0 to 20.5 m from MD03-2622. The samples were then freeze-dried to preserve the organics and to make further sample processing much easier (as opposed to oven drying). The next step in processing the samples was washing them. Approximately two-thirds by weight of each freeze-dried sample was rehydrated and disaggregated in a beaker with deionized water, and then poured into a 63 μm sieve. The sample was then wet-sieved through the 63 μm sieve with deionized water. Once completely cleaned, the > 63 μm fraction was removed from the sieve, put in a beaker, and dried in an oven at 50°C. The fine fraction (< 63 μm), which was collected while wet sieveing the sample, was left to settle out of the deionized water, and eventually evaporated off under heat lamps. Once dried, the coarse fraction was weighed and separated into a 63 μm – 150 μm fraction and a > 150 μm fraction using a 150 μm sieve. The > 150 μm fraction contains the majority of foraminifera tests, and this was the fraction used to collect the foraminiferal census data.

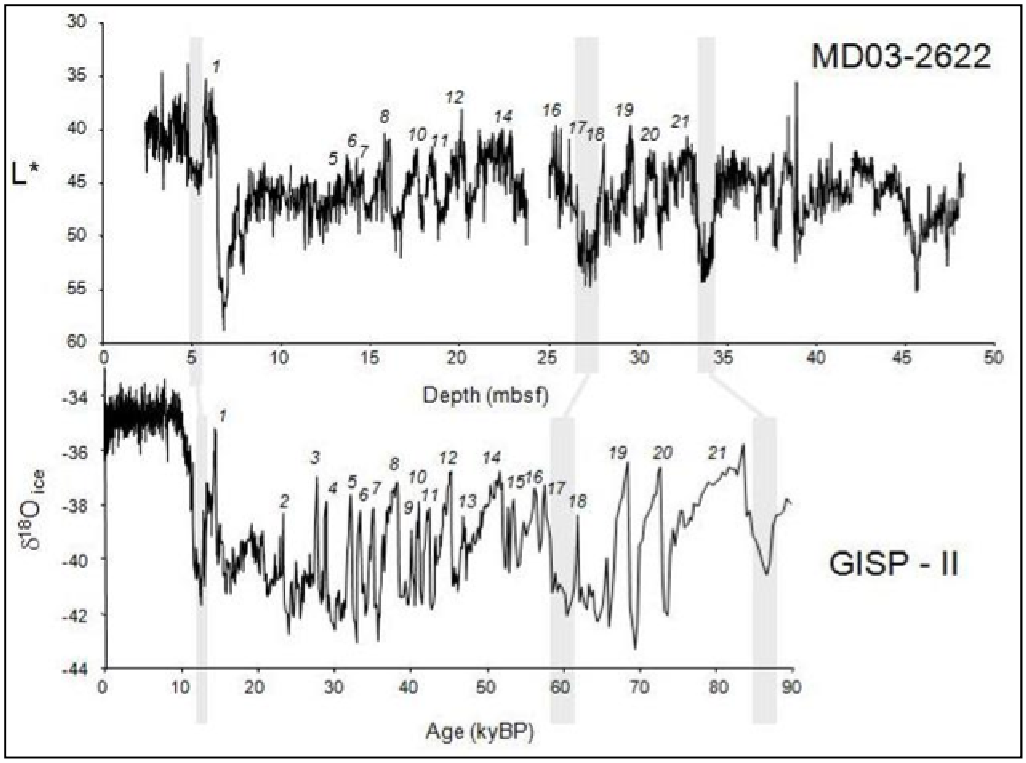

Figure 4.2: Comparison of the Greenland Ice Sheet Project 2 (GISP – II) $\delta^{18}O$ values to the shipboard sediment 'lightness' (reflectance, L*) values measured at 2 cm intervals for the *R/V Marion Dufresne* core MD03-2622.

4.2 Foraminiferal Census

For each sample, the > 150 μm fraction was split using a Sepor microsplitter, when needed, until a suitable aliquot of at least 300 foraminifera was reached. A minimum of 300 individuals per split is preferred because it has been shown to minimize counting errors (Imbrie and Kipp, 1971). This subsample was then placed on a gridded tray, and using a standard stereo microscope, the abundances of various planktonic foraminifera species were counted and recorded. Species individually recorded included *Globigerina bulloides*, *Neogloboquadrina dutertrei*, *Orbulina universa*, *Globigerinella aequilateralis*, *Globorotalia crassaformis*, *Globorotalia menardii*, *Globigerinoides ruber* (pink and white morphotypes), *Globigerinoides sacculifer*, *Globigerina rubescens*, *Globorotalia truncatulinoides*, *Pulleniatina obliquiloculata*, *Globigerina quinqueloba*, and *Neogloboquadrina pachyderma*. These are the most abundant foraminiferal species in the Cariaco Basin sediment record, and most have been used successfully in prior studies as indicators of climate variability (Overpeck et al., 1989; Peterson et al., 1991; Black et al, 1999). In addition, most of these species make up the modern foraminiferal assemblage of the Cariaco Basin, so we know a good deal about their preferred habitat (Tedesco and Thunell, 2003b). All other species of foraminifera present in the sample were grouped into an 'others' category. Foraminiferal faunal counts were performed on the intervals of 1900.0 – 1954.0 cm and 1996.0 – 2050.0 cm, which cover the critical intervals spanning the onset and termination of Interstadial 12. These intervals were chosen to focus on as they represent two periods when we see different patterns of climate change as seen in the GISP2 $\delta^{18}O$ record (a proxy for air temperature) (Figure 4.2). The onset of Interstadial 12 is a period of rapid warming, while the termination of

Interstadial 12 is an interval of gradual cooling, allowing us to compare cycles of natural climate variability under different conditions. Replicate counts were performed every ~10 samples to ensure reproducibility in the data collection. Original values were reproduced in the replicate counts 99 -100% of the time. Relative and absolute abundances were then calculated from the foraminiferal census data (data can be found in Appendices 2 and 3, respectively) to examine changes in the contribution of each species to the total assemblage, and the controls on the abundances of each individual species. The relative abundance is expressed as a percentage value of the total counted foraminiferal population, while the absolute abundance represents the number of foraminifera normalized to per gram of dry sediment.

Foraminiferal census data can yield a great deal of information about past water column characteristics and climate, while doing so in a non-destructive way, thus making it an important oceanographic proxy for paleoenvironmental reconstructions. The foraminiferal assemblage and the relative abundance of each species serves as indicators of particular environmental conditions, such as sea surface temperature, salinity, and productivity. Correct interpretation of records created from census data requires an understanding of the modern ecology and conditions controlling the foraminiferal distribution. Modern sediment trap data (Tedesco and Thunell, 2000b) is used to determine the preferred depth habitats, nutrient availability, and ideal temperatures and salinities for growth of these foraminifera species, making it possible to draw conclusions about past climate variables.

4.3 Age Model

In order to create the most accurate record of annual- to decadal- scale tropical Atlantic climate variability, an age model was created in order to put the down-core variations in foraminiferal abundances into temporal context. An initial age model for the Interstadial 12 section was created by visually matching tie points between the MD03-2622 reflectance data and the dated GISP2 $\delta^{18}O$ chronology, and interpolating between them (Figure 4.2). The problems associated with creating an age model in this fashion have to do with the error of visually matching two graphs and the inherent error in interpolating between tie points. In addition, since one of the major goals of this project is to look at the relation between climate variability in the tropical Atlantic and high northern latitudes, it is important to be as independent as possible from the GISP2 chronology. This allows for potential exploration of leads and lags between the two locations that would have been impossible if the two chronologies were tied directly together.

Two prior studies that have made use of core MD03-2622 (González et al., 2008; González and Dupont, 2009) created chronologies by linking similar features of the sediment reflectance profile with that of the nearby ODP Site 1002D, which has an extremely high-resolution age model for the past 60 kya based on more than 350 accelerator mass spectrometer ^{14}C data on planktic foraminifera (Hughen et al., 2004; Hughen et al., 2006). While this may appear to be the best way to create an age model for the Interstadial 12 portion of MD03-2622, González and Dupont (2009) note that their chronology has limitations prior to 40 kya, when some of the stadials recorded in the Cariaco Basin appear to be shifted relative to the GISP2 record. This occurs because the

ODP Site 1002D chronology is tied to that of the ^{230}Th-dated Hulu Cave stalagmites (Hughen et al., 2006; Wang et al., 2001), which differs from NGRIP and GISP2 chronologies (González and Dupont, 2009).

To overcome some of these challenges, a quasi-independent age model for the Interstadial 12 section of MD02-2622 was created by examining downcore variations in iron and titanium throughout the section. As stated earlier in Chapter 2, Cariaco Basin sediment exhibit a distinct annual peak in iron and titanium abundance associated with increased delivery of terrigenous sediment during the rainy season in the surrounding regions when the ITCZ is directly overhead (Peterson et al., 2000a; Peterson and Haug, 2006). It is this observation that served as the foundation for the age model created for the Interstadial 12 portion of core MD03-2622.

Elemental abundances of aluminum, silicon, sulfur, chlorine, potassium, calcium, titanium, vanadium, manganese, iron, and rhodium were measured for the core using scanning x-ray fluorescence (XRF) at continuous 100 μm intervals by Dr. Gerald Haug at ETH Zurich. Peaks in the abundances of iron and titanium through the 19.0 to 20.5 m interval of the core representing Interstadial 12 were counted. The following procedure was performed twice, once for the iron spectrum and once for the titanium spectrum. Looking at 10 mm intervals at a time, two values were determined. A minimum number of peaks containing the most distinct peaks for the 10 mm interval were counted. Then, a maximum number of peaks containing all of the peaks (above some minimum threshold) for the same 10 mm interval were counted. The minimum and maximum values for the 10 mm interval were then averaged as a way to take into account that there may be more distinct peaks or even double peaks during some years, or weak and even no peaks during

other years. Evident in the split core photographs of MD03-2622 (e.g. Figure 4.1; See Appendix 1) are layers of microturbidite deposition. Microturbidites within the Interstadial 12 interval of MD03-2622 were identified from the photographs along a horizontal axis drawn through the center of the core (Table 4.1). This mid-point in the core was chosen as this is likely the axis along which elemental abundances were determined. Peaks were not counted for the width of microturbidites in the intervals that were noted as containing them (Table 4.1). Thus, this average value is the amount of years contained in that 10 mm interval of the sediment core.

A starting date for the beginning of Interstadial 12 was made by visually aligning the MD03-2622 reflectance data to the dated GISP2 $\delta^{18}O$ chronology (Figure 4.2). The average amount of years contained in each 10 mm interval was then added to consecutive dates beginning with the starting date previously determined. The age models for both the iron and titanium abundance data were then plotted against the initial age model created from the GISP2 $\delta^{18}O$ chronology (Figure 4.3 and figure 4.4). Error for each measurement was calculated separately as the difference between the minimum and maximum year values for each 10 mm interval. The error bars on each point represent the cumulative error as the sum of the error for that point and each prior individual point.

The age model created using the iron abundance data most closely follows the GISP2 age model. At the top of the section of interest, the difference between the iron and GISP2 age models is 32 years, whereas the difference for the titanium model is 275 years. While the titanium age model is further off from the GISP2 age model, the GISP2 age model is within the titanium age model's error the majority of time. One possible explanation for this discrepancy is that the titanium spectrum showed less variation in

Photo ID	Turbidite Range in Photo (cm)	Turbidite Range in Core (cm below sea floor)	Total (mm)
Section XIII			
DSCN2287	No turbidites	No turbidites	0
DSCN2288	124.6 - 124.9	1924.6 - 1924.9	3
	126.3 - 126.5	1926.3 - 1926.5	2
	127.6 - 128.1	1927.6 - 1928.1	5
	137.9 - 138.1	1937.9 - 1938.1	2
DSCN2289	145.7 - 146.1	1945.7 - 1946.1	4
	147.7 - 148.0	1947.7 - 1948.0	3
Section XIV			
DSCN2291	8.8 - 9.3	1958.8 - 1959.3	5
	13.1 - 13.2	1963.1 - 1963.2	1
DSCN2292	24.7 - 24.8	1974.7 - 1974.8	1
	27.9 - 28.1	1977.9 - 1978.1	2
	32.7 - 33.2	1982.7 - 1983.2	5
	33.8 - 34.3	1983.8 - 1984.3	5
	39.4 - 39.8	1989.4 - 1989.8	4
DSCN2293	41.8 - 42.0	1991.8 - 1992.0	2
	43.4 - 43.7	1993.4 - 1993.7	3
	58.8 - 59.1	2008.8 - 2009.1	3
DSCN2294	61.5 - 61.9	2011.5 - 2011.9	4
	65.7 - 66.0 cm	2015.7 - 2016.0	3
	69.3 - 69.7 cm	2019.3 - 2019.7	4
	73.3 - 73.7 cm	2023.3 - 2023.7	4
DSCN2295	No turbidites	No turbidites	0
			Total = 65

Table 4.1: Sections of the Interstadial 12 portion of MD03-2622 that have been identified as microturbidites. See Appendix 1 for photographs with marked sections.

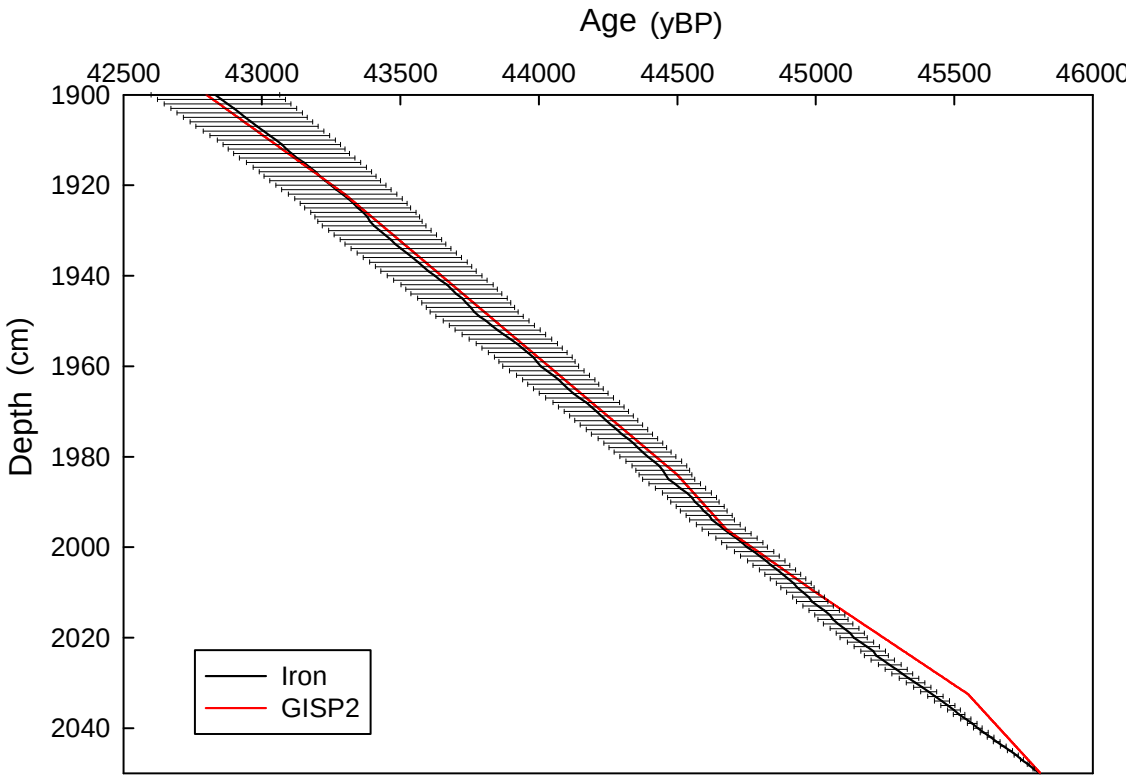

Figure 4.3: Age versus depth plots for the iron abundance- (black line) and Greenland Ice Sheet Project 2 (GISP2)- (red line) based age models. Error bars on the iron- based age model were calculated as the difference between the minimum and maximum year values for each 10 mm interval, and are the cumulative sum of the error for each point and all prior individual points.

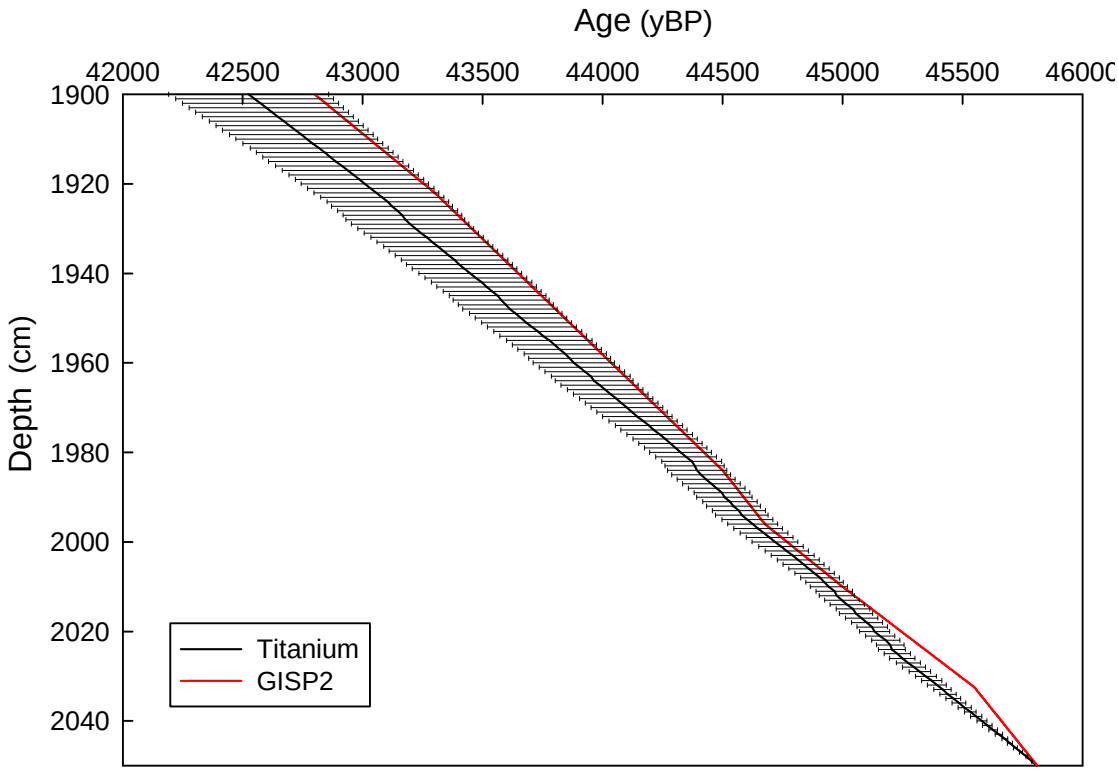

Figure 4.4: Age versus depth plots for the titanium abundance- (black line) and Greenland Ice Sheet Project 2 (GISP2)- (red line) based age models. Error bars on the titanium- based age model were calculated as the difference between the minimum and maximum year values for each 10 mm interval, and are the cumulative sum of the error for each point and all prior individual points.

abundance peaks in each 10 mm interval, thus making it more difficult to distinguish between minimum and maximum peaks. It is unlikely that redox variations can account for the discrepancy between the iron and titanium age models since sediment deposition during Interstadial 12 occurred under anoxic conditions (Peterson et al., 2000a). The slight discrepancy that does exist between the iron and GISP2 age models can be explained by the fact that counting element abundance peaks might not be the most accurate method of creating an age model. Given that the iron age model is nearly identical to GISP2 age model, this also validates the GISP2 age model. This is the first time that an age model has been created in this fashion, and the method appears to be successful. The age model based on the iron abundances was used for the remainder of this study.

4.4. Spectral and Wavelet Analyses

Spectral analysis is a way to isolate dominant periodicities in time series data. In paleoclimate reconstructions, spectral analysis is used to identify significant modes of variability that might be related to possible forcing mechanisms. Prior studies that have performed spectral analysis on foraminiferal abundance data from the Cariaco Basin have focused on the last ~10 ky due to the difficulty in generating high resolution data for older time periods. Peterson et al. (1991) performed spectral analysis on a *G. bulloides* time series from the Cariaco Basin for the last ~10 ky, and at a much higher resolution, Black et al. (1999) did the same for the past 825 years. Spectral analysis was performed on the *G. bulloides* time series using Singular Spectrum Analysis – MultiTaper Method

Toolkit (Ghil et al., 2002; software available from www.atmos.ucla.edu/tcd/ssa/). Prior to performing the analysis, the data was interpolated and detrended using MATLAB. Like spectral analysis, wavelet analysis is a method used to identify significant periods of variability in data sets. However, wavelet analysis is unique in that it looks at the evolution of the periodicities through the time series. Wavelet analyses (Torrence and Compo, 1998; program available from ion.researchsystems.com/IONScript/wavelet/**)** were performed on the *G. bulloides* absolute abundance records for both the onset and termination of Interstadial 12.

V. The Onset of Interstadial 12 – Results & Discussion

5.1 Introduction

The critical gaps in our understanding of the Earth's climate system lie in the patterns and forcing mechanisms of climate variability on decadal to multicentennial time scales. Equally important, and also not clearly understood, is the response of low-latitude climate variability to abrupt climate change as most studies of abrupt climate change come from high-latitude sites. Dansgaard-Oeschger events such as Interstadial 12 are excellent examples of abrupt climate change, and provide a unique opportunity to examine how the tropics and submillennial-scale variability respond to rapid changes in global climate. In addition, more accurate models of future climate change can be created if we understand the mechanisms driving past climate change on similar scales. While not a perfect analogy for potential anthropogenic future climate change as the boundary conditions are not identical, examining climate variability during Interstadial 12 will provide the opportunity to help us understand how the climate system responds to a similar direction of change – in this case, abrupt warming. This chapter focuses on the transition into Interstadial 12 from full stadial conditions.

5.2 Foraminiferal Census Results

Foraminiferal census data were collected on 540 samples representing the onset of Interstadial 12. The relative abundance of each species is expressed as a percentage value of the total counted foraminiferal population, while the absolute abundance

represents the number of foraminifera normalized to per gram of dry sediment. An important issue to note in regards to relative abundances of foraminifera is the "closed sum problem." Relative abundance is calculated as a percentage value of the total counted foraminiferal population, thus it is possible that major variations in one species will change the relative abundance of another species, while that species itself is not actually changing in abundance. As a result, it is important to compare both the absolute abundances and relative abundances of the foraminiferal species to see if one species may be driving the record of another species.

5.2.1 *Globigerina bulloides*

The *G. bulloides* absolute abundance data (Figure 5.1, upper panel) for the onset of Interstadial 12 begin with two periods of increase and decrease, from 45,810 – 45,665 yBP and 45,665 – 45,470 yBP, with maxima at 45,779 yBP and 45,592 yBP, respectively. The former begins with 392 *G. bulloides*/g, comes to a maximum of 1,525 *G. bulloides*/g, and declines to 386 *G. bulloides*/g, while the latter starts with 386 *G. bulloides*/g, increases to 1261 *G. bulloides*/g, and decreases to a minimum of 203 *G. bulloides*/g. Between 45,470 – 45,121 yBP, the absolute abundance plateaus and ranges from 55 *G. bulloides*/g to 614 *G. bulloides*/g with an average of 330 *G. bulloides*/g during this interval. At 45,121 yBP, the absolute abundance of *G. bulloides* steadily increases until 44,853 yBP when a maximum value of 1839 *G. bulloides*/g is reached, which is also the maximum for the onset of Interstadial 12. Values then decline and plateau between 44,846 – 44,751 yBP with *G. bulloides* absolute abundances centered around 719 *G. bulloides*/g. After an abrupt decline to 72 *G. bulloides*/g at 44,743 yBP, absolute abundances increase slightly to 391 *G. bulloides*/g at 44,668 yBP.

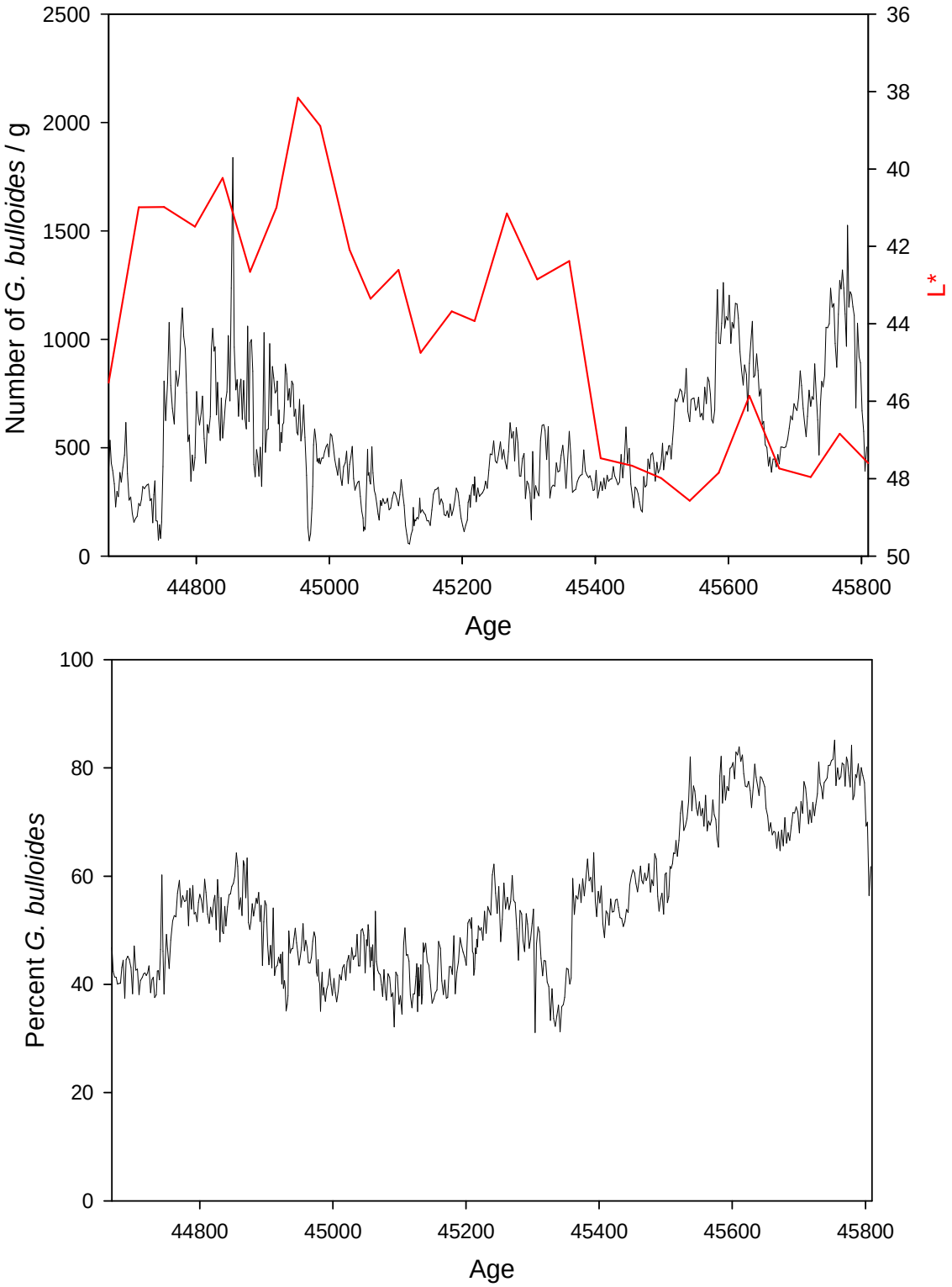

Figure 5.1: *Globigerina bulloides* absolute abundance (upper panel, reflectivity plotted in red) and relative abundance (lower panel) for the onset of Interstadial 12 (45,810 – 44,668 yBP). The relative abundance is expressed as a percentage value of the total counted foraminiferal population, while the absolute abundance represents the number of *G. bulloides* normalized to per gram of dry sediment.

Globigerina bulloides makes up between 69 – 85% (Figure 5.1, lower panel) of the foraminiferal assemblage during the first quarter of the Interstadial 12 onset until 45,522 yBP, when values decline to 31% at 45,341 yBP. This value represents the minimum contribution of *G. bulloides* to the total assemblage throughout the onset of Interstadial 12. The relative abundance of *G. bulloides* then fluctuates throughout the remainder of the onset between 31 and 64%, with an average of 46%. Overall, *G. bulloides* makes up a significantly higher proportion of the foraminiferal assemblage during the first quarter of the transition into Interstadial 12, after which the species contributes to roughly half of the total foraminiferal population.

5.2.2 *Neogloboquadrina dutertrei*

The absolute abundances of *N. dutertrei* do not vary significantly for the first 440 years of the record (Figure 5.2, upper panel) from 45,810 – 45,370 yBP. During this period, the absolute abundance of *N. dutertrei* ranges from 9 *N. dutertrei*/g to 80 *N. dutertrei*/g, and averages around 31 *N. dutertrei*/g. At 45,370 yBP, values increase abruptly by over 200%, reaching 718 *N. dutertrei*/g in 29 years. This value, occurring at 45,341 yBP, is the maximum absolute abundance for *N. dutertrei* for the onset of Interstadial 12. Absolute abundances remain high (over 300 *N. dutertrei*/g) for 41 years until 45,317 yBP, when they begin to decline until 45,120 yBP and a value of 11 *N. dutertrei*/g is reached. *Neogloboquadrina dutertrei* absolute abundances then steadily rise to 345 *N. dutertrei*/g at 44,824 yBP, before declining again.

Neogloboquadrina dutertrei contributes a small fraction (< 8%) of the total foraminiferal population from 45,810 – 45,370 yBP (Figure 5.2, lower panel). The relative abundance of *N. dutertrei* then increases abruptly and contributes to just over

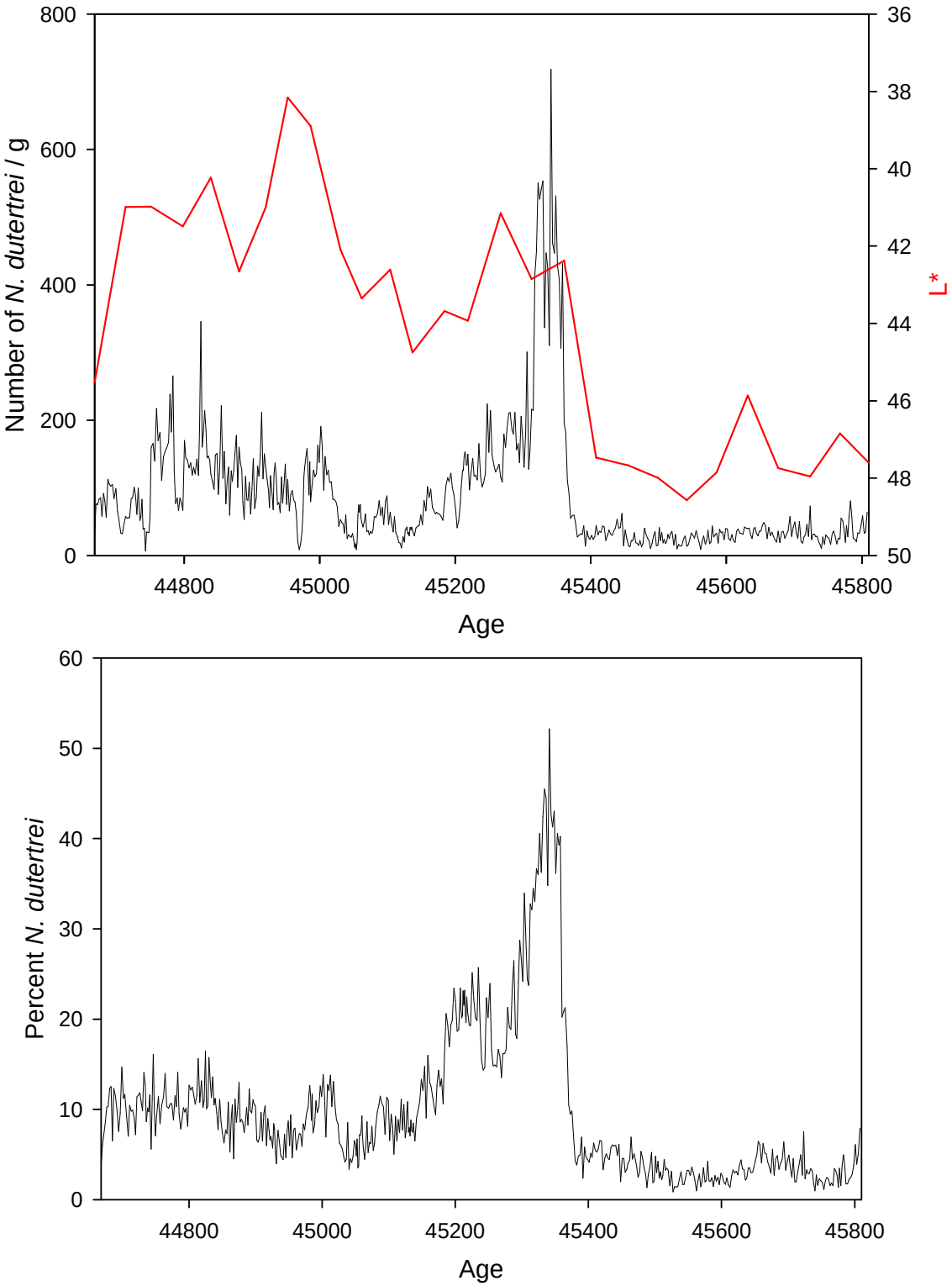

Figure 5.2: *Neogloboquadrina dutertrei* absolute abundance (upper panel, reflectivity plotted in red) and relative abundance (lower panel) for the onset of Interstadial 12 (45,810 – 44,668 yBP). The relative abundance is expressed as a percentage value of the total counted foraminiferal population, while the absolute abundance represents the number of *N. dutertrei* normalized to per gram of dry sediment.

50% of the total foraminiferal assemblage when it reaches its maximum in absolute abundance at 45,341 yBP. The percentage of *N. dutertrei* subsequently declines to 15% at 45,262 yBP before increasing to 22%, where values remain around this level until 45,184 yBP. The relative abundance of *N. dutertrei* then declines and remains around 10% for the remainder of the onset of Interstadial 12.

5.2.3 *Obulina universa*

Orbulina universa's absolute abundance record (Figure 5.3, upper panel) displays high variability for the first 440 years of the onset of Interstadial 12, from 45,810 – 45,370 yBP. Throughout this period, the absolute abundance of *O. universa* ranges from 3 *O. universa*/g to almost 50 *O. universa*/g, averaging around 17 *O. universa*/g. The absolute abundance of *O. universa* reaches a maximum during this period of 49 *O. universa*/g at 45,585 yBP. At 45,370 yBP, the record shows a distinct shift from high to low variability. Throughout the remainder of the onset of Interstadial 12, the absolute abundance of *O. universa* ranges from 0 *O. universa*/g to 13 *O. universa*/g, with an average of approximately 3 *O. universa*/g.

Much like *O. universa*'s absolute abundance record, the relative abundance record (Figure 5.3, lower panel) also displays a distinct shift in variability at 45,370 yBP. Prior to this shift, *O. universa* contributes between 0.3 and 5% to the total foraminiferal population, averaging 2%. The maximum contribution of 5% occurs at 45,449 yBP. After 45,370 yBP, the relative abundance of *O. universa* ranges from 0 to 2%, with an average of 0.4%.

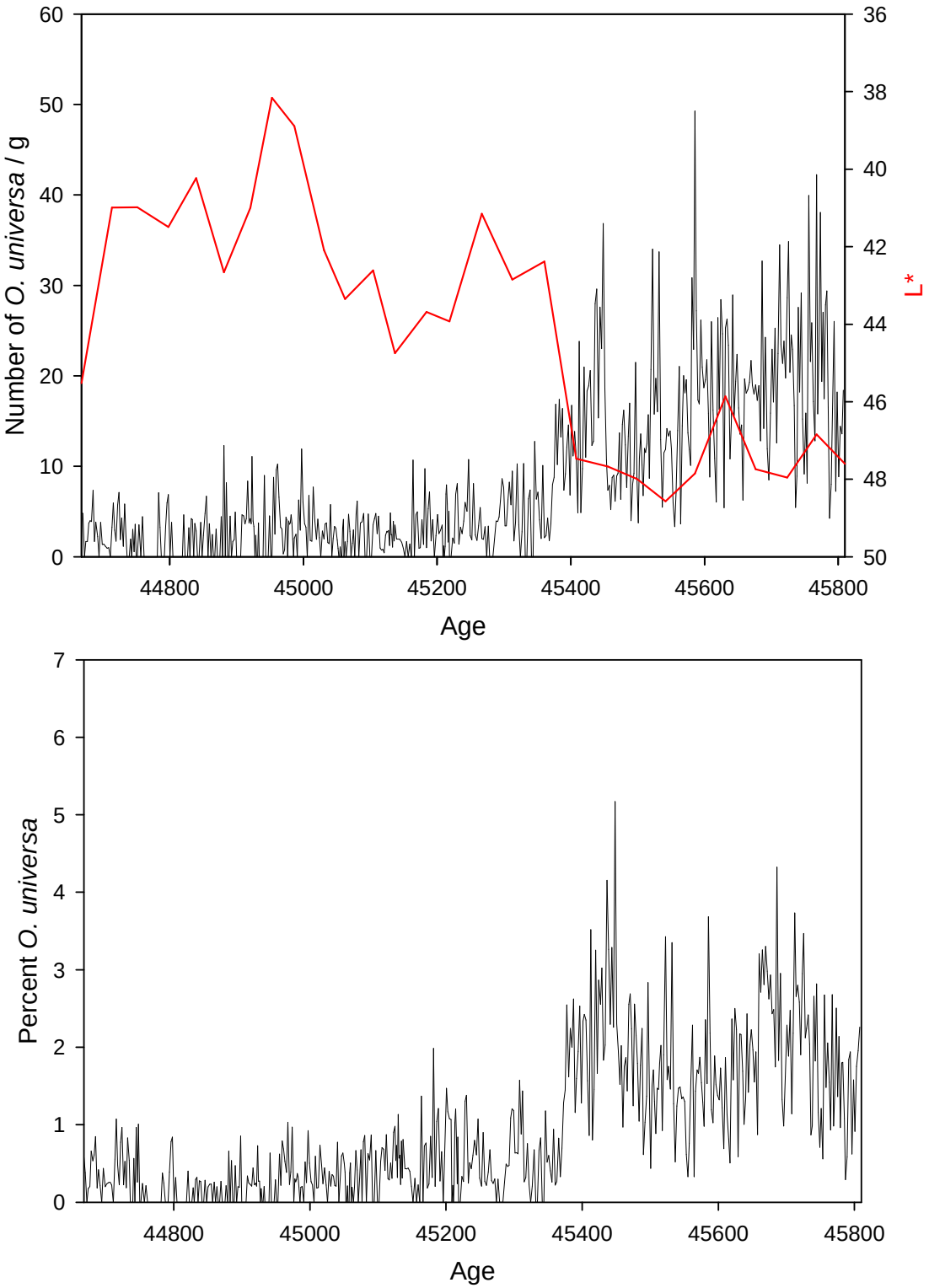

Figure 5.3: *Orbulina universa* absolute abundance (upper panel, reflectivity plotted in red) and relative abundance (lower panel) for the onset of Interstadial 12 (45,810 – 44,668 yBP). The relative abundance is expressed as a percentage value of the total counted foraminiferal population, while the absolute abundance represents the number of *O. universa* normalized to per gram of dry sediment.

5.2.4 *Globigerinella aequilateralis*

The highest peak in the absolute abundance of *G. aequilateralis* (Figure 5.4, upper panel) occurs just into the record of the onset of Interstadial 12 at 45,783 yBP, with a value of 47 *G. aequilateralis*/g. There is a slight shift in variability that occurs at 45,184 yBP. The lower variability after this point is punctuated by a period of slightly higher variability between 45,007 and 44,818 yBP.

The relative abundance of *G. aequilateralis* (Figure 5.4, lower panel) also displays a shift in variability occurring at 45,184 yBP. *Globigerinella aequilateralis* on average contributes to 1.3% of the total foraminiferal population prior to this point, and an average of 0.4% after. The highest relative abundance of *G. aequilateralis,* almost 4%, occurs at 45,401 yBP.

5.2.5 *Globorotalia crassaformis*

Due to an identification error, data for *G. crassaformis* were collected every centimeter until 45,104 yBP, after which data were collected every millimeter. The maximum peak in the absolute abundance of *G. crassaformis* (Figure 5.5, upper panel) for the onset of Interstadial 12 is 13 *G. crassaformis*/g, and occurs at 44,854 yBP.

The maximum contribution of *G. crassaformis* to the total foraminiferal population (Figure 5.5, lower panel), almost 1.5%, occurs at 45,085 yBP. The average relative abundance of *G. crassaformis* throughout the onset of Interstadial 12 is almost 0.2%.

5.2.6 *Globorotalia menardii*

Globorotalia menardii is more prevalent in the absolute abundance record for the onset of Interstadial 12 (Figure 5.6, upper panel) prior to 45,405 yBP, after which its

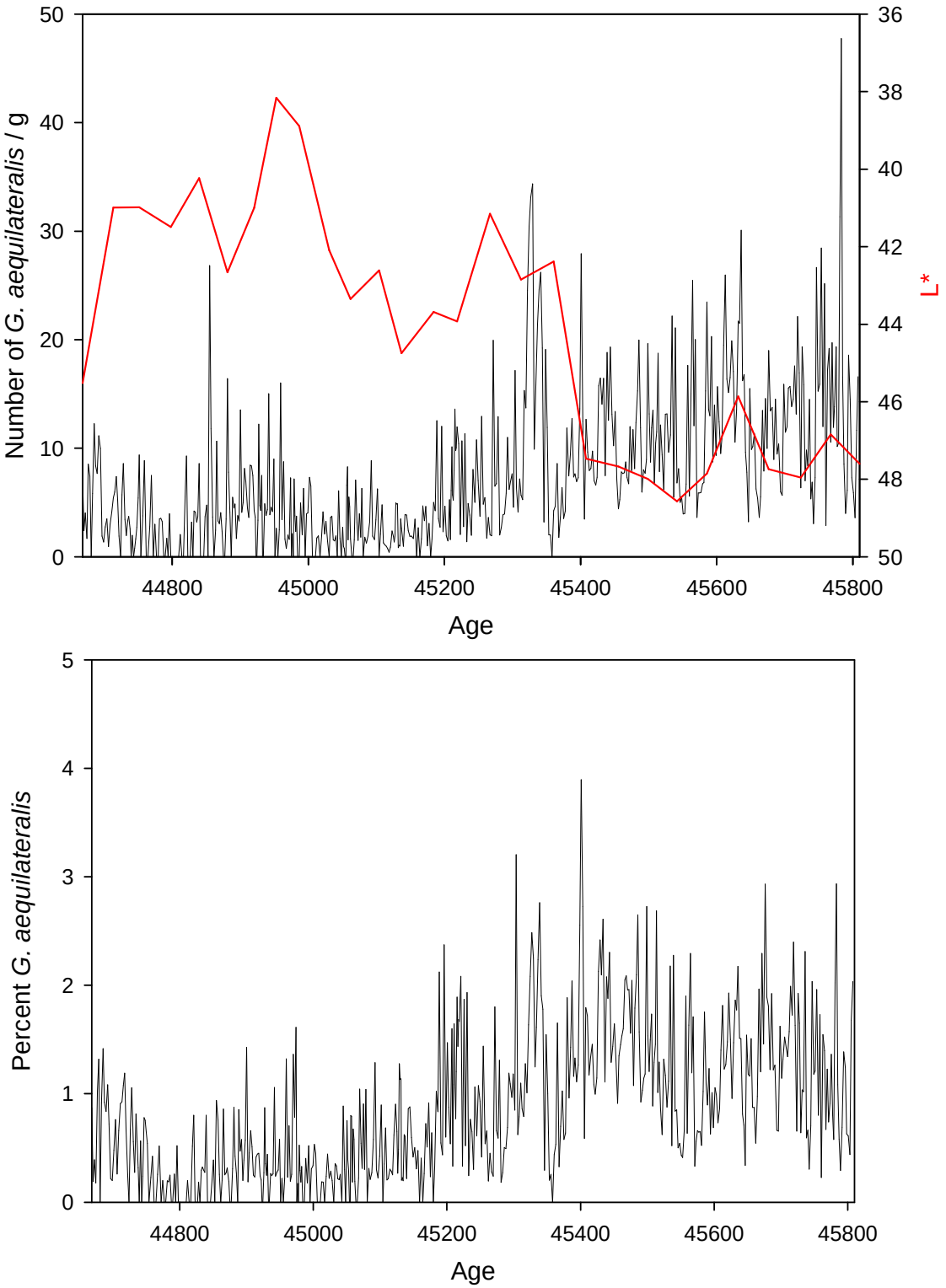

Figure 5.4: *Globigerinella aequilateralis* absolute abundance (upper panel, reflectivity plotted in red) and relative abundance (lower panel) for the onset of Interstadial 12 (45,810 – 44,668 yBP). The relative abundance is expressed as a percentage value of the total counted foraminiferal population, while the absolute abundance represents the number of *G. aequilateralis* normalized to per gram of dry sediment.

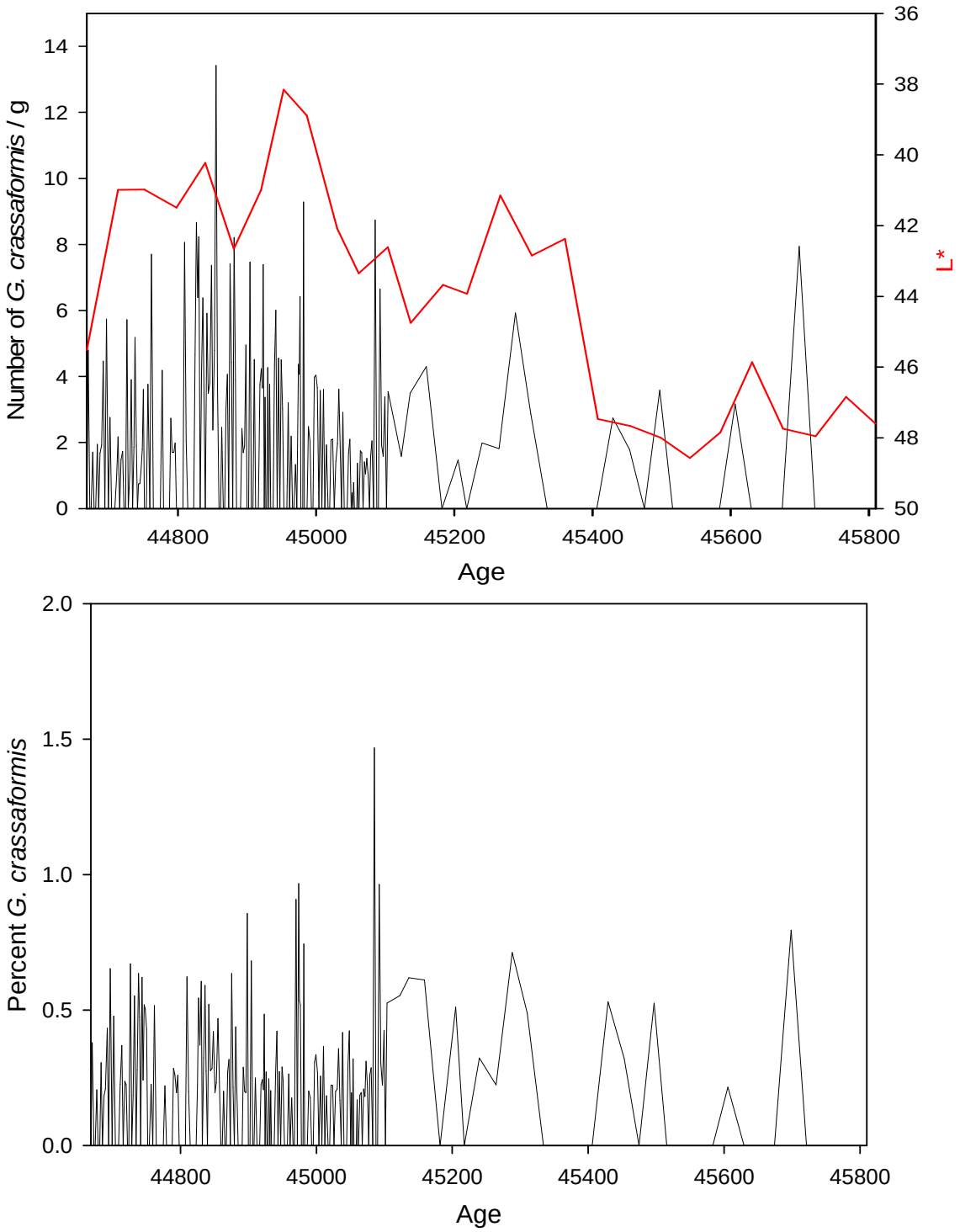

Figure 5.5: *Globorotalia crassaformis* absolute abundance (upper panel, reflectivity plotted in red) and relative abundance (lower panel) for the onset of Interstadial 12 (45,810 – 44,668 yBP). The relative abundance is expressed as a percentage value of the total counted foraminiferal population, while the absolute abundance represents the number of *G. crassaformis* normalized to per gram of dry sediment.

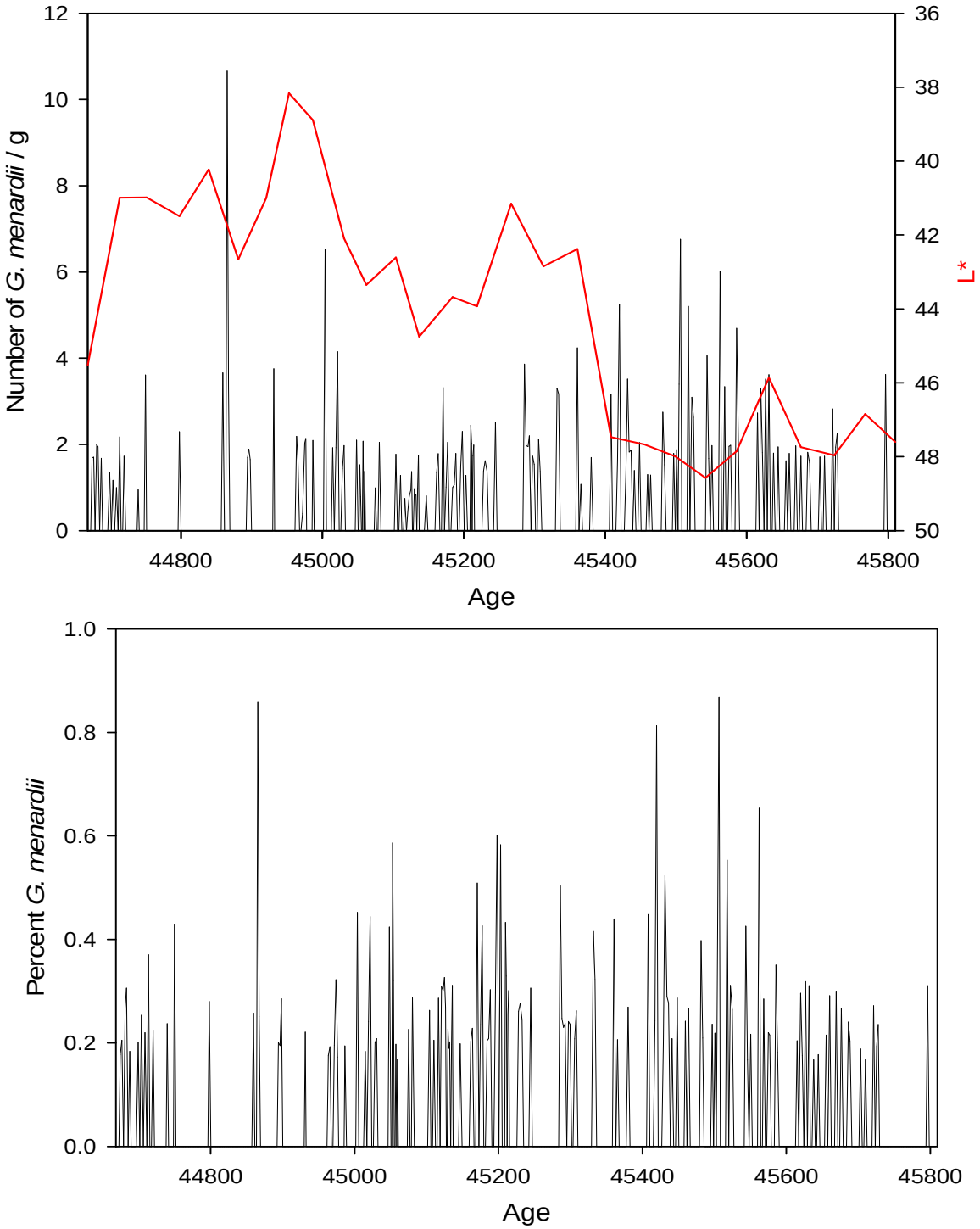

Figure 5.6: *Globorotalia menardii* absolute abundance (upper panel, reflectivity plotted in red) and relative abundance (lower panel) for the onset of Interstadial 12 (45,810 – 44,668 yBP). The relative abundance is expressed as a percentage value of the total counted foraminiferal population, while the absolute abundance represents the number of *G. menardii* normalized to per gram of dry sediment.

appearance is more sporadic. However, the maximum absolute abundance of *G. menardii*, just over 10 *G. menardii*/g, occurs at 44,866 yBP.

Globorotalia menardii contributes very little to the total foraminiferal population, accounting for <0.9% throughout the onset of Interstadial 12 (Figure 5.6, lower panel).

5.2.7 *Globigerinoides ruber* (white morphotype)

The absolute abundance record of the white morphotype of *G. ruber* (Figure 5.7, upper panel) for the onset of Interstadial 12 declines steadily over the first half of the record. After a peak of just over 100 white *G. ruber*/g at 45,791 yBP, the absolute abundance declines to approximately 3 white *G. ruber*/g in 45,216 yBP. After this point, the absolute abundances of white *G. ruber* remain low and never exceed 26 white *G. ruber*/g for the remainder of the record.

At the onset of Interstadial 12, white *G. ruber* contributes a maximum of almost 10% to the total foraminiferal population at 45,805 yBP (Figure 5.7, lower panel). The relative abundance then decreases to around 4% before increasing again to almost 8% at 45,701 yBP. Values decline again to around 3%, and remain at this level for around 250 years before increasing again to almost 8% at 45,431 yBP. The contribution of white *G. ruber* then declines before coming to a minima plateau beginning at 45,115 yBP. During this time, the relative abundance of white *G. ruber* remains < 2% for the remainder of the record, averaging around 0.6%.

5.2.8 *Globigerinoides ruber* (pink morphotype)

The absolute abundances of pink *G. ruber* (Figure 5.8, upper panel) remain low at the beginning of the record (around 25 pink *G. ruber*/g) until 45,610 yBP, when they increase abruptly to almost 170 pink *G. ruber*/g at 45,590 yBP. Values then decline

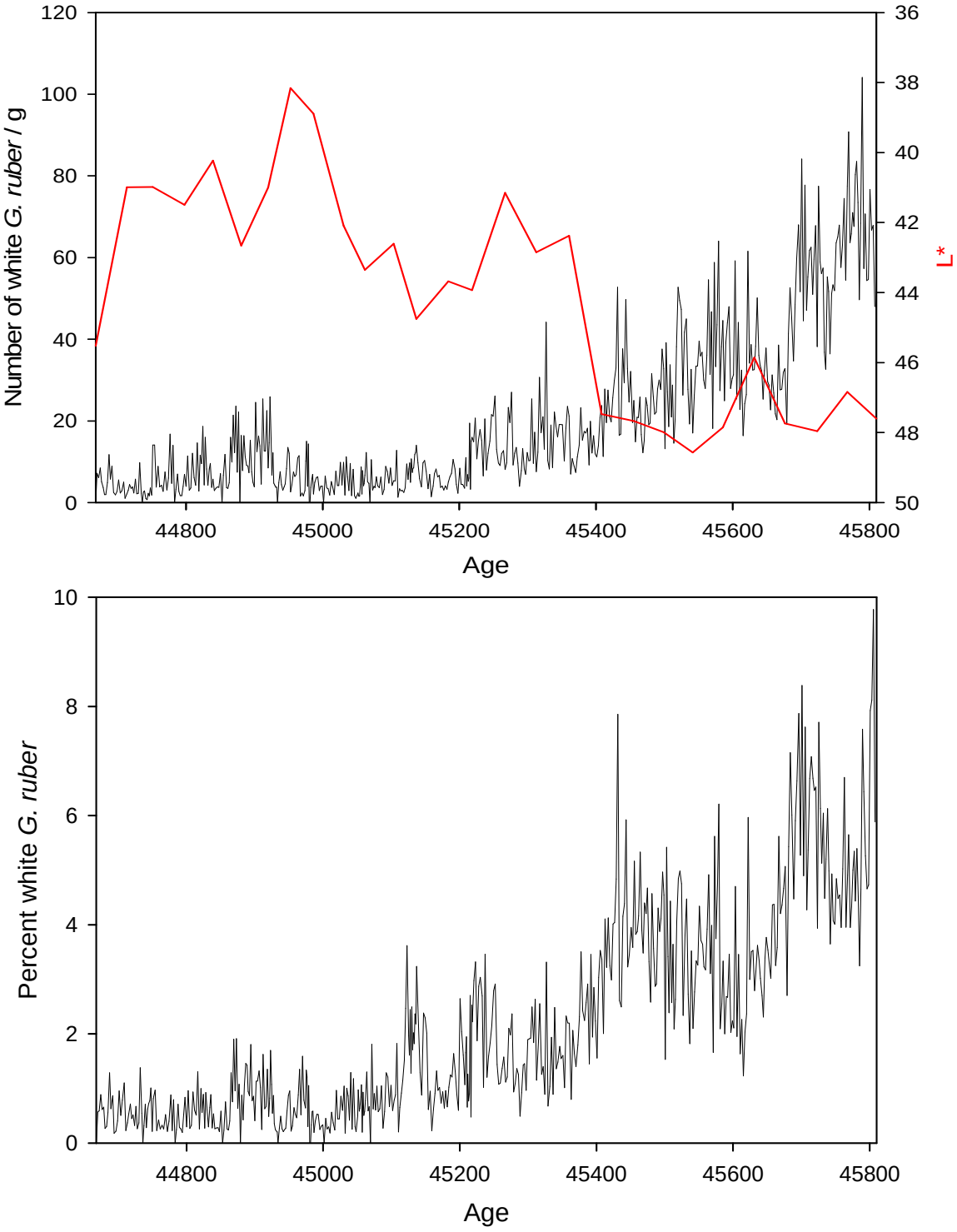

Figure 5.7: White *Globigerinoides ruber* absolute abundance (upper panel, reflectivity plotted in red) and relative abundance (lower panel) for the onset of Interstadial 12 (45,810 – 44,668 yBP). The relative abundance is expressed as a percentage value of the total counted foraminiferal population, while the absolute abundance represents the number of white *G. ruber* normalized to per gram of dry sediment.

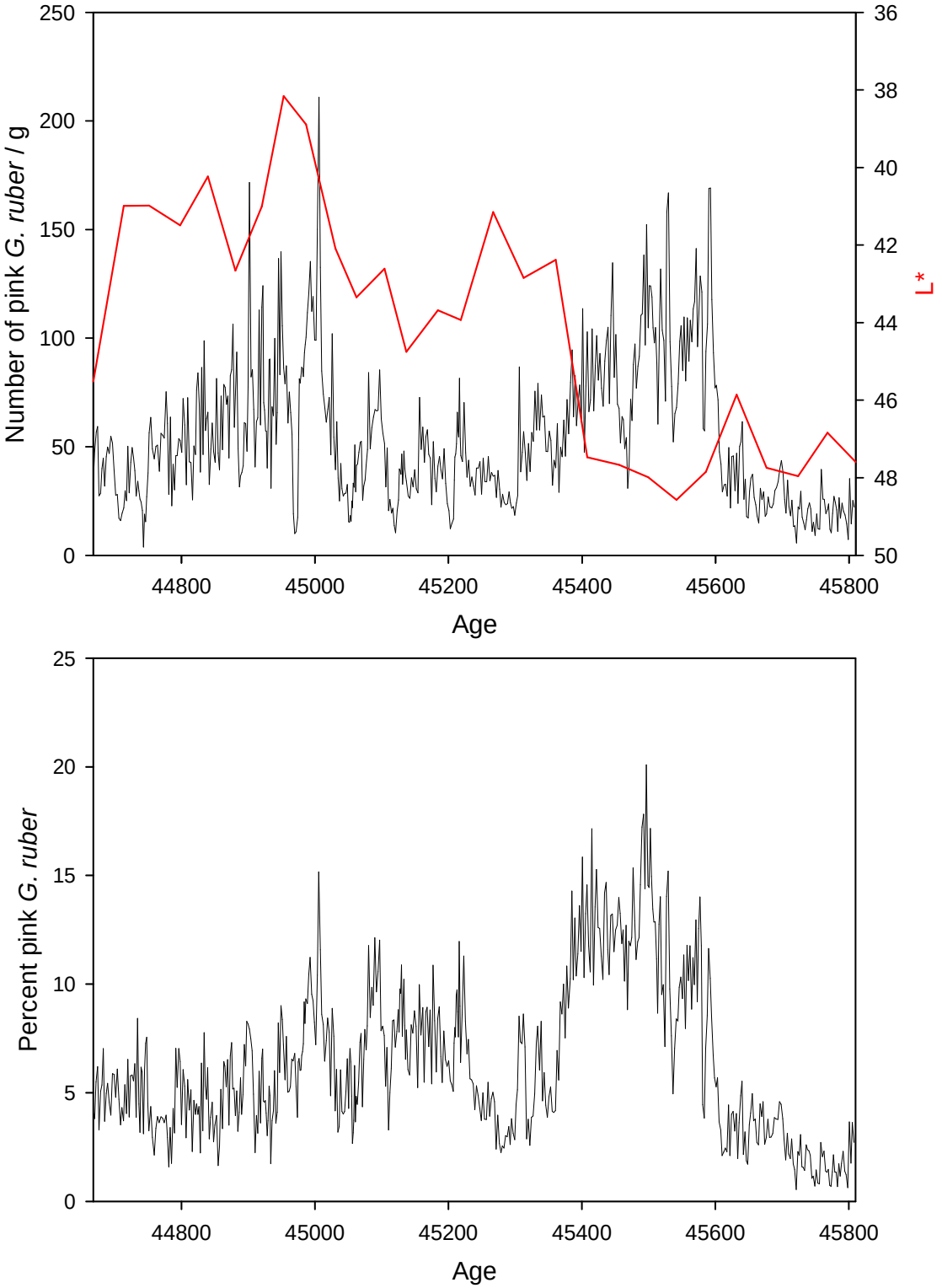

Figure 5.8: Pink *Globigerinoides ruber* absolute abundance (upper panel, reflectivity plotted in red) and relative abundance (lower panel) for the onset of Interstadial 12 (45,810 – 44,668 yBP). The relative abundance is expressed as a percentage value of the total counted foraminiferal population, while the absolute abundance represents the number of pink *G. ruber* normalized to per gram of dry sediment.

gradually until 45,299 yBP, when they reach just over 20 pink *G. ruber*/g. Pink *G. ruber* absolute abundances then go through three cycles of increase and decrease (from ~10 pink *G. ruber*/g - ~80 pink *G. ruber*/g) between 45,299 yBP and 45,050 yBP. Values then increase abruptly to a maximum for the onset of Interstadial 12 of just over 210 pink *G. ruber*/g at 45,006 yBP. After this maximum, absolute abundances of pink *G. ruber* then decline abruptly to 10 pink *G. ruber*/g at 44,972 yBP before increasing again to 170 pink *G. ruber*/g at 44,901 yBP. Subsequently, values decline throughout the remainder of the record.

The relative abundance of pink *G. ruber* (Figure 5.8, lower panel) increases from <1% to over 20% from 45,810 to 45,496 yBP. Values then decline and remain around 7% for the remainder of the record.

5.2.9 *Globigerinoides sacculifer*

There are three distinct periods of variability in the absolute abundance record of *G. sacculifer* (Figure 5.9, upper panel) for the onset of Interstadial 12. The first period is highly variable with large increases and decreases ranging from 4 *G. sacculifer*/g to just over 40 *G. sacculifer*/g. This period ends at 45,371 yBP. After this, there is another period of high variability, but values are lower and range from 0 *G. sacculifer*/g to almost 30 *G. sacculifer*/g. After 45,203 yBP and for the remainder of the record, the absolute abundances of *G. sacculifer* show little variability and range from 0 *G. sacculifer*/g to 14 *G. sacculifer*/g.

Like the absolute abundance record, the relative abundance record of *G. sacculifer* (Figure 5.9, lower panel) shows three periods of differing variability. During the first period, the contribution of *G. sacculifer* to the total foraminiferal population

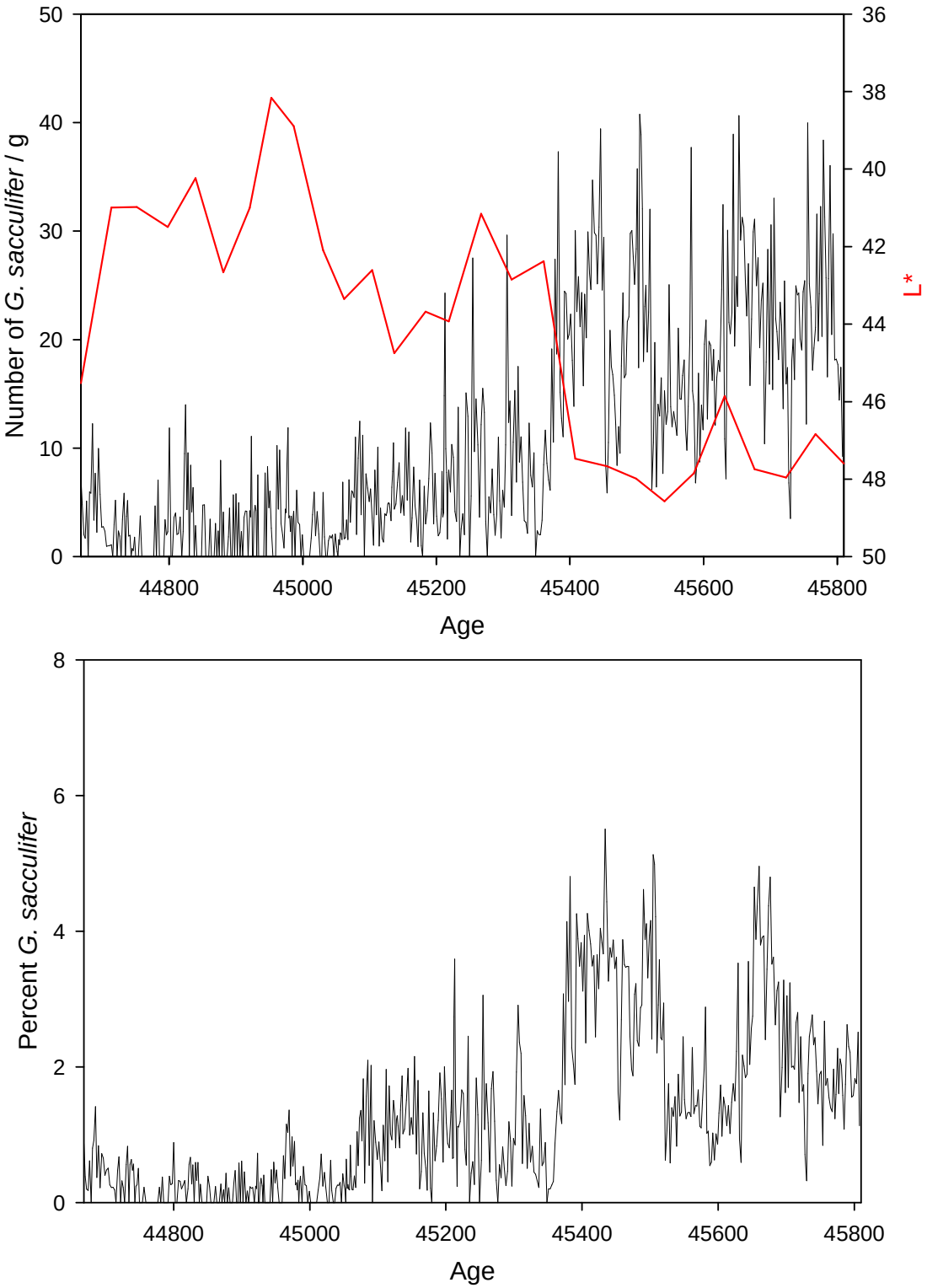

Figure 5.9: *Globigerinoides sacculifer* absolute abundance (upper panel, reflectivity plotted in red) and relative abundance (lower panel) for the onset of Interstadial 12 (45,810 – 44,668 yBP). The relative abundance is expressed as a percentage value of the total counted foraminiferal population, while the absolute abundance represents the number of *G. sacculifer* normalized to per gram of dry sediment.

ranges from <1%, to its maximum contribution of 5.5%, which occurs at 45,433 yBP. The relative abundance of *G. sacculifer* during the second period ranges from 0% to 3.5%, while values remain mostly <1% for the third period.

5.2.10 *Globigerina rubescens*

Globigerina rubescens does not appear often throughout the onset of Interstadial 12, but is more prevalent in the first half of the record (Figure 5.10, upper panel). Absolute abundances remain below 8 *G. rubescens*/g when *G. rubescens* does appear in the record.

Globigerina rubescens accounts for <0.8% of the total foraminiferal population when it is present in the record for the onset of Interstadial 12 (Figure 5.10, lower panel).

5.2.11 *Globorotalia truncatulinoides*

The absolute abundances of *G. truncatulinoides* (Figure 5.11, upper panel) remain quite low or 0 *G. truncatulinoides*/g through the first third of the onset of Interstadial 12, averaging to <1 *G. truncatulinoides*/g. Values remain at this level until 45,410 yBP, when they steadily rise over 190 years until a peak in the absolute abundance is reached at 45,221 yBP of just over 20 *G. truncatulinoides*/g. The absolute abundances of *G. truncatulinoides* then decline until 45,040 yBP, when they become more variable. Values range from 0 *G. truncatulinoides*/g to 17 *G. truncatulinoides*/g until the end of the onset of Interstadial 12, with an average of 3 *G. truncatulinoides*/g.

Globorotalia truncatulinoides makes up <1% of the total foraminiferal population for most the onset of Interstadial 12, with the exception of an abrupt rise and fall to just over 4% at 45,221 yBP (Figure 5.11, lower panel).

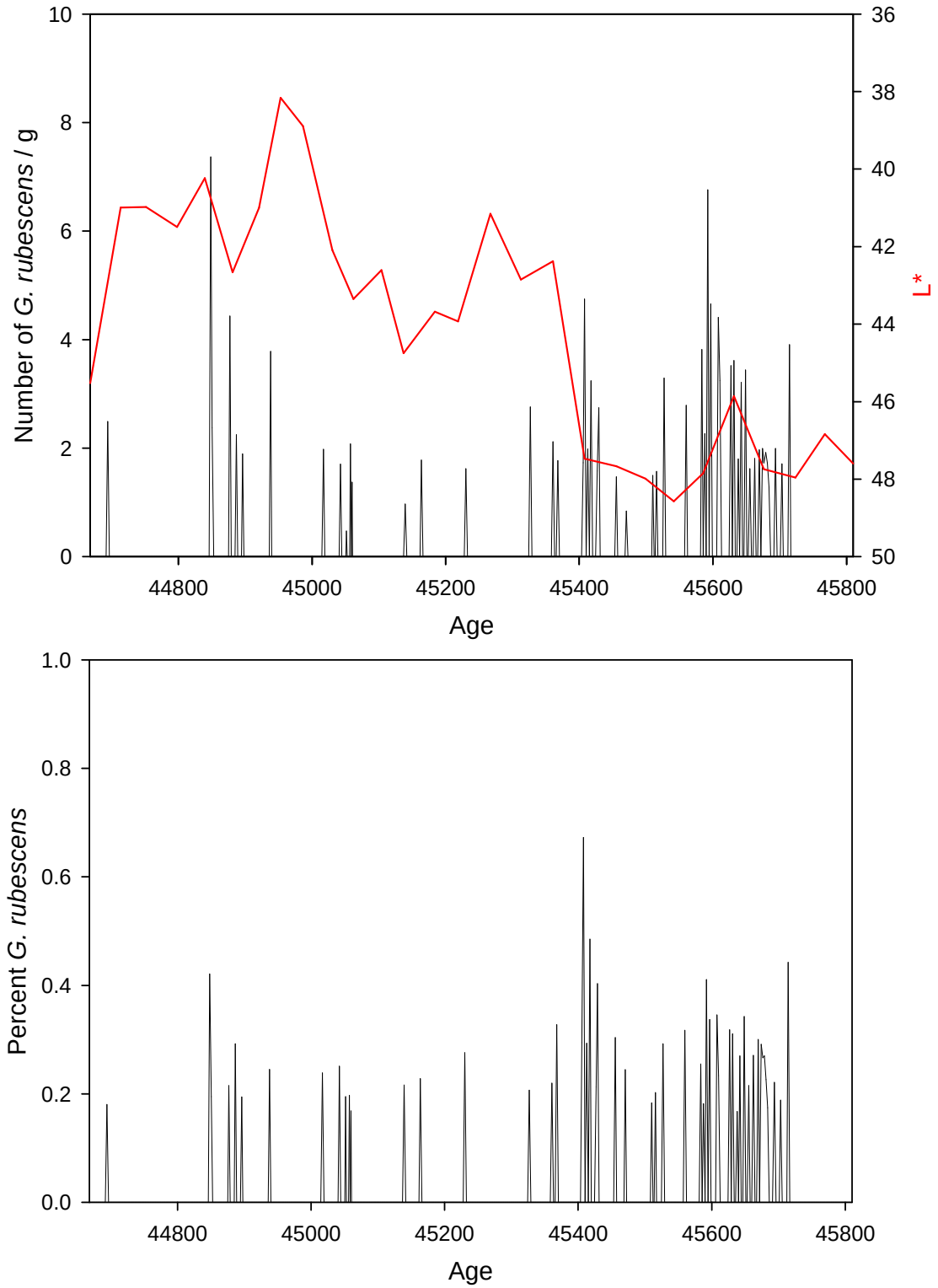

Figure 5.10: *Globigerina rubescens* absolute abundance (upper panel, reflectivity plotted in red) and relative abundance (lower panel) for the onset of Interstadial 12 (45,810 – 44,668 yBP). The relative abundance is expressed as a percentage value of the total counted foraminiferal population, while the absolute abundance represents the number of *G. rubescens* normalized to per gram of dry sediment.

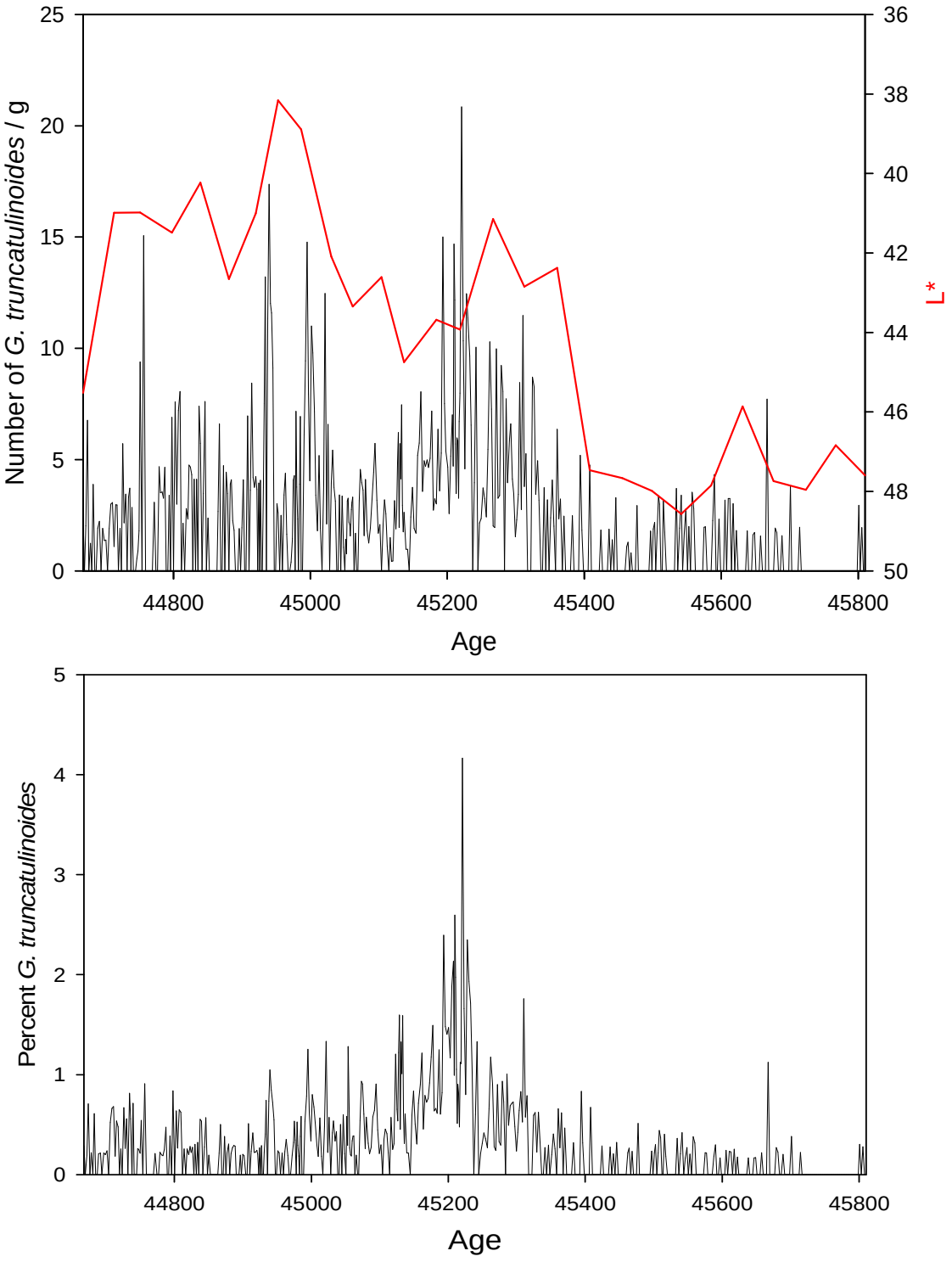

Figure 5.11: *Globorotalia truncatulinoides* absolute abundance (upper panel, reflectivity plotted in red) and relative abundance (lower panel) for the onset of Interstadial 12 (45,810 – 44,668 yBP). The relative abundance is expressed as a percentage value of the total counted foraminiferal population, while the absolute abundance represents the number of *G. truncatulinoides* normalized to per gram of dry sediment.

5.2.12 *Globigerina quinqueloba*

Globigerina quinqueloba is not present in the absolute abundance record for the onset of Interstadial 12 (Figure 5.12, upper panel) until 45,443 yBP. When it appears at this point, absolute abundances remain low, <13 *G. quinqueloba*/g. At 45,304 yBP, values increase abruptly to almost 150 *G. quinqueloba*/g at 45,276 yBP and then decline abruptly to less than 1 *G. quinqueloba*/g. Absolute abundances increase again at 45,108 yBP, and the values remain variable for the duration of the record, ranging from 2 *G. quinqueloba*/g to 113 *G. quinqueloba*/g

As *G. quinqueloba* is not present in the record until 45,443 yBP, it does not contribute to the total foraminiferal population before this point (Figure 5.12, lower panel). At its peak in absolute abundance, *G. quinqueloba* contributes 14% to the total foraminiferal population at 45,276 yBP. After declining abruptly to 0%, values vary for the remainder of the record, from <1% to almost 8%, with an average of 3%.

5.2.13 *Neogloboquadrina pachyderma*

The *N. pachyderma* absolute abundance record (Figure 5.13, upper panel) begins at the species' maximum value for the onset of Interstadial 12 of 92 *N. pachyderma*/g at 45,810 yBP. Values decline abruptly to around 4 *N. pachyderma*/g at 45,730 yBP. Throughout the rest of the record, the absolute abundances of *N. pachyderma* remain very low or non-existent, averaging 4 *N. pachyderma*/g and never reaching above 23 *N. pachyderma*/g.

The relative abundance of *N. pachyderma* (Figure 5.13, lower panel) drops abruptly from just over 11% to <1% between 45,810 and 45,797 yBP. After this point,

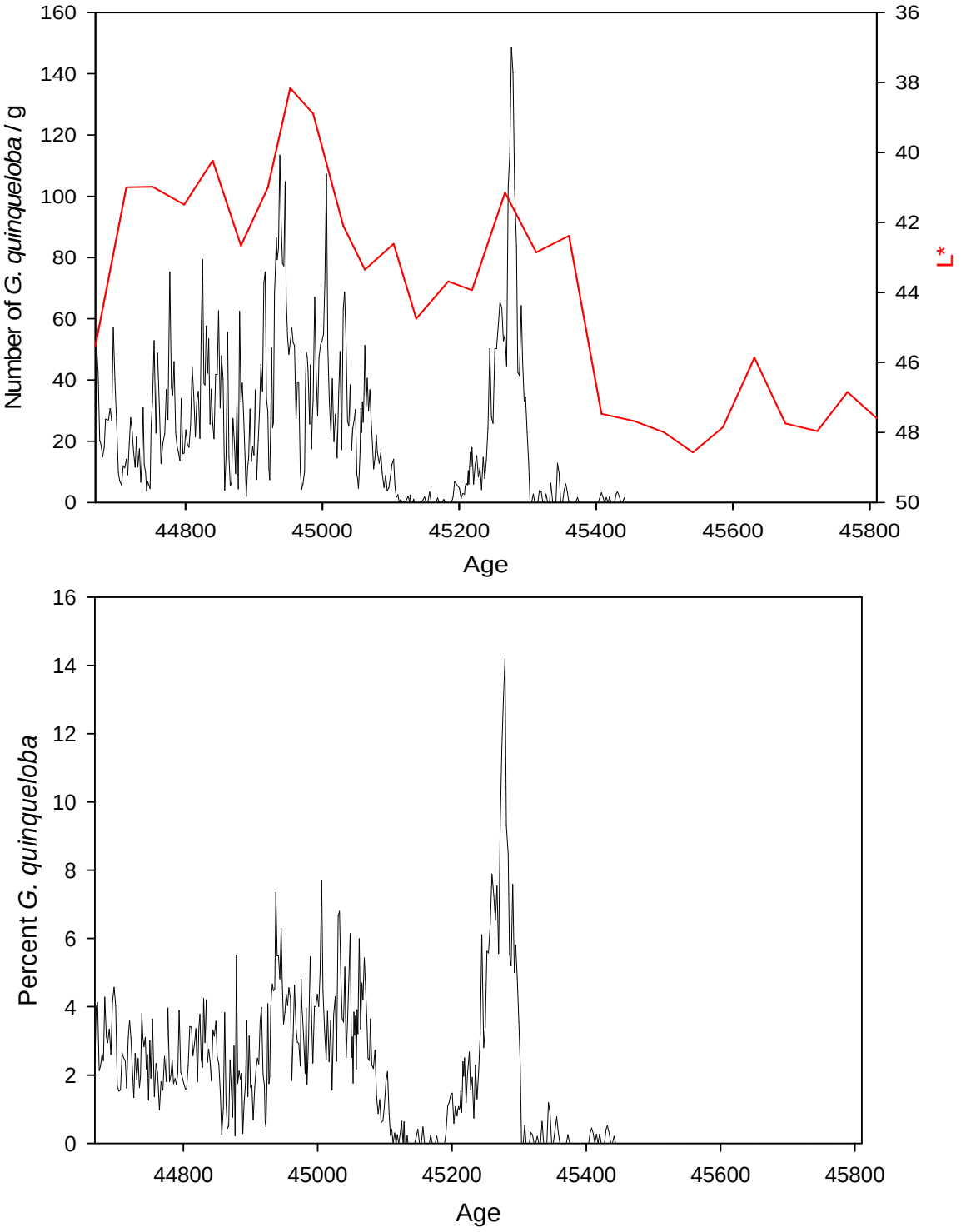

Figure 5.12: *Globigerina quinqueloba* absolute abundance (upper panel, reflectivity plotted in red) and relative abundance (lower panel) for the onset of Interstadial 12 (45,810 – 44,668 yBP). The relative abundance is expressed as a percentage value of the total counted foraminiferal population, while the absolute abundance represents the number of *G. quinqueloba* normalized to per gram of dry sediment.

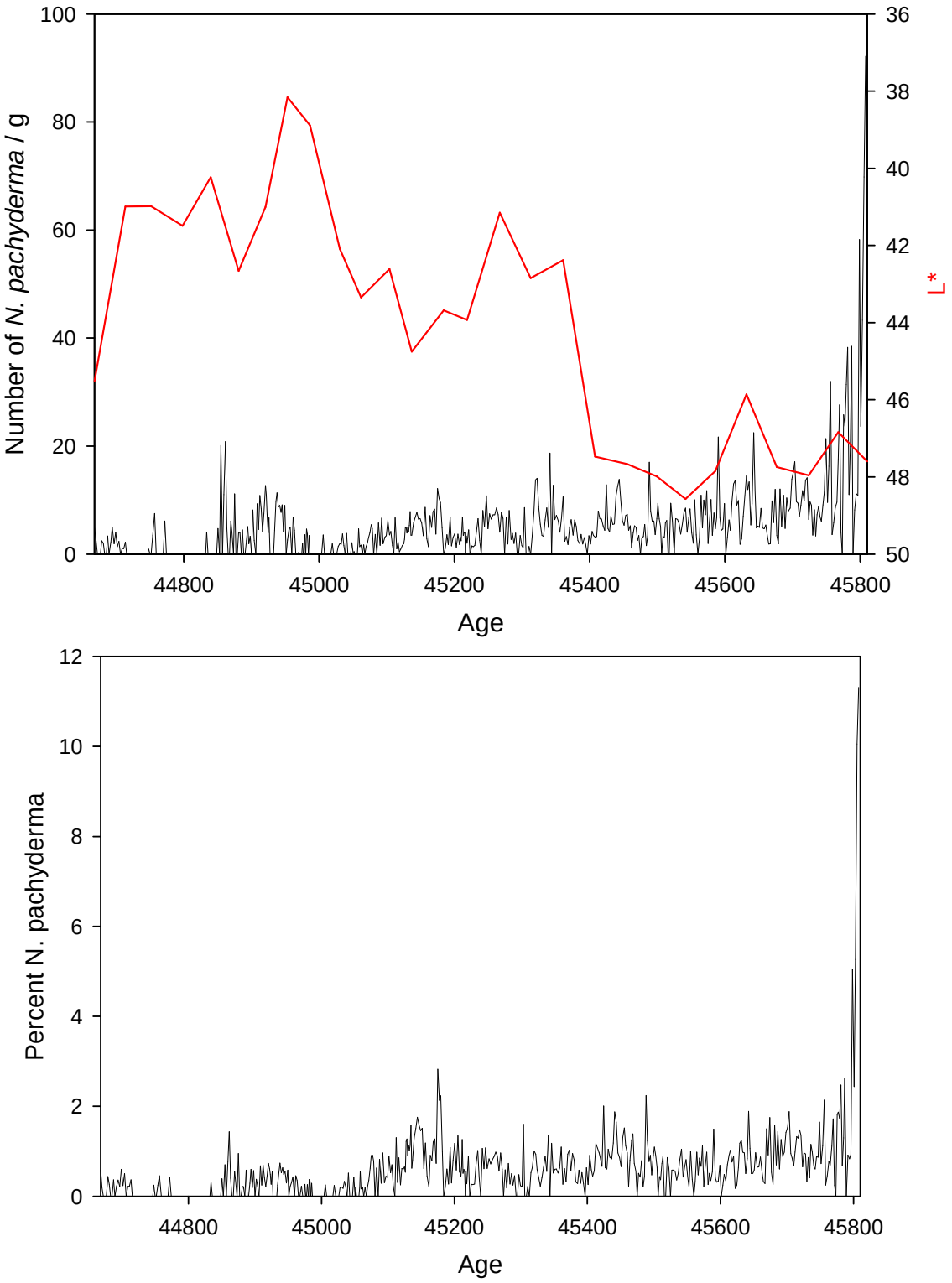

Figure 5.13: *Neogloboquadrina pachyderma* absolute abundance (upper panel, reflectivity plotted in red) and relative abundance (lower panel) for the onset of Interstadial 12 (45,810 – 44,668 yBP). The relative abundance is expressed as percentage value of the total counted foraminiferal population, while the absolute abundance represents the number of *N. pachyderma* normalized to per gram of dry sediment.

N. pachyderma accounts for <2% of the total foraminiferal population for the remainder of the record.

5.2.14 *Pulleniatina obliquiloculata*

The absolute abundances of *P. obliquiloculata* (Figure 5.14, upper panel) are low or at 0 *P. obliquiloculata*/g for the first third of the record, until 45,442 yBP. At this point, values increase and peak to around 9 *P. obliquiloculata*/g between 45,363 and 45,274 yBP. Absolute abundances of *P. obliquiloculata* then decline before coming to an abrupt maximum of 15 *P. obliquiloculata*/g at 44,980 yBP. Values remain variable for the remainder of the onset of Interstadial 12, but never become greater than 8 *P. obliquiloculata*/g.

For the first third of the onset of Interstadial 12, *P. obliquiloculata* does not contribute to the total foraminiferal population often (Figure 5.14, lower panel). A maximum contribution of 1.3% occurs at 45,309 yBP.

5.3 Discussion

The onset of Interstadial 12 was characterized by a number of global changes in both atmospheric and oceanic properties. Over Greenland, a quantitative temperature estimate made by Landais et al. (2004) shows an abrupt increase in surface temperature of 12 ± 2.5 °C. A sea surface temperature (SST) reconstruction from the Bermuda Rise estimated an increase from 17.5 °C to 20.5 °C at the onset of Interstadial 12 (Sachs and Lehman, 1999). In addition, sea level likely rose between 20 and 30 m during the transition into Interstadial 12, a level equivalent to 60 – 70 m below present levels (Siddall et al., 2003, 2008; Rohling et al., 2008).

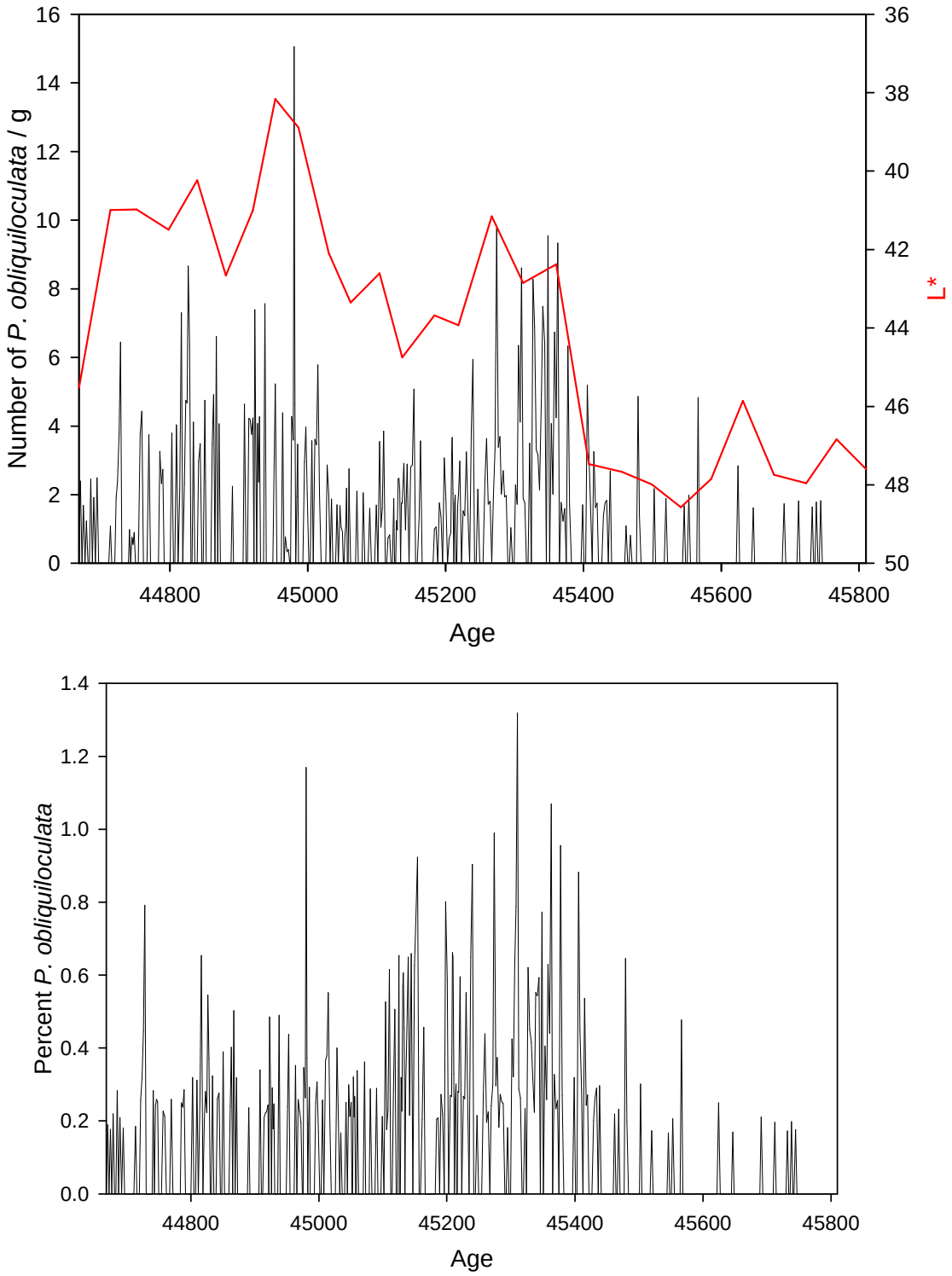

Figure 5.14: *Pulleniatina obliquiloculata* absolute abundance (upper panel, reflectivity plotted in red) and relative abundance (lower panel) for the onset of Interstadial 12 (45,810 – 44,668 yBP). The relative abundance is expressed as percentage value of the total counted foraminiferal population, while the absolute abundance represents the number of P. *obliquiloculata* normalized to per gram of dry sediment.

To correctly identify changes in the foraminiferal population and abundances related to the onset of Interstadial 12 it is important to define the period in which Interstadial 12 actually begins in MD03-2622. The onset of Interstadial 12 is noted in the Greenland Ice Sheet Project – 2 (GISP2) ice core by an abrupt increase in the $\delta^{18}O$ record (Figure5.15), which is interpreted as a proxy for air temperature over Greenland. Isotopically-heavier $\delta^{18}O$ values measured from the ice are indicative of warmer temperatures, thus the onset of Interstadial 12 is defined by abrupt warming. Peterson et al. (2000) noted striking similarities between the GISP2 $\delta^{18}O$ record and a record of sediment reflectance from the Cariaco Basin. Sediment reflectance is a proxy thought largely to be controlled by organic carbon content and changing surface productivity. Periods of abrupt shifts to low sediment reflectance (darker sediment) occur coincidently with periods of abrupt increase in the $\delta^{18}O$ record, thus Interstadial 12 can be marked in the Cariaco Basin sediment record by an abrupt shift in the sediment reflectance record. The MD03-2622 sediment reflectance record also exhibits an abrupt shift to low sediment reflectance coincident with the GISP2 $\delta^{18}O$ record (Figure 4.2). If we use this parameter set by Peterson et al. (2000) to define the onset of Interstadial 12 in MD03-2622, sediment reflectance begins an abrupt shift to low sediment reflectance at 45,408 yBP (Figure 5.15). The height of Interstadial 12, marked by the lowest sediment reflectance value, occurs at 44,953 yBP. An interesting implication of this is the comparison of the sediment reflectivity to the GISP2 $\delta^{18}O$ record (Figure 5.15), to determine if changes in Greenland lead, lag, or are synchronous with changes occurring in the tropics. One issue with making this type of comparison is the fact that the age model created for the Interstadial 12 portion of MD03-2622 is tied at one point to the GISP2 $\delta^{18}O$ record.

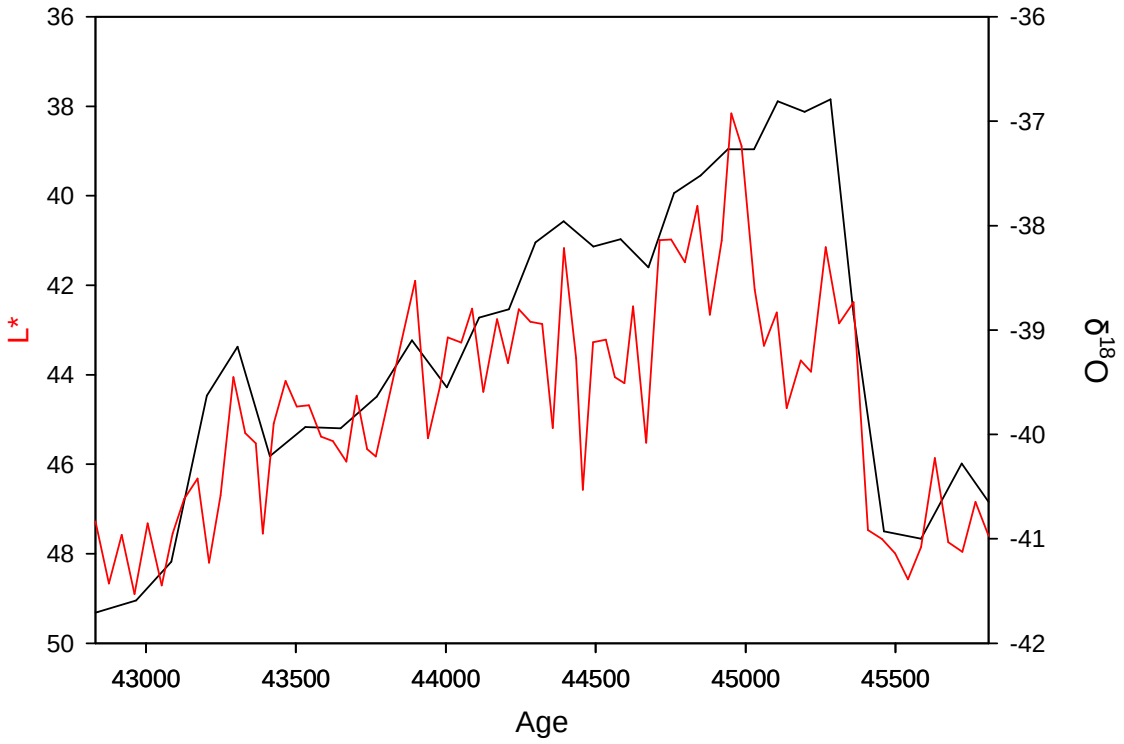

Figure 5.15: Greenland Ice Sheet Project 2 (GISP2) $\delta^{18}O$ record (black line) and MD03-2622 sediment reflectance record (L*, red line) plotted for Interstadial 12.

Given that this tie point is prior to the abrupt shifts in both the sediment reflectivity and $\delta^{18}O$ records, we may be able to speculate on the timing of the events. However, another issue is the resolution at which data were obtained for both records, thus offsets in synchronicity could be due partly, or entirely, to a lack of data points. These issues aside, a comparison of the two records (Figure 5.15) shows the abrupt shift in the GISP2 $\delta^{18}O$ record indicating the onset of Interstadial 12 leading the abrupt shift in the MD03-2622 sediment reflectance record by 52 years. Thus, it seems likely that changes occurring over Greenland are forcing changes in the low latitudes. The teleconnection is almost certainly atmospheric as ocean circulation response time is multidecadal, at best, while the atmosphere can respond on subdecadal time scales. The lag time between the two records may represent the propagation time for changes occurring in the high latitudes to affect the low latitudes.

The remainder of this discussion will focus on variations in the abundances of key species of foraminifera during the onset of Interstadial 12, and the potential climatological forcing mechanisms that may be driving their signals. As some species do not make up a significant fraction of the total foraminiferal population, it is difficult to infer what is driving their abundance variations, and as such, are mostly excluded from discussion.

5.3.1 The *Globigerina bulloides* Record and Supporting Species *Neogloboquadrina dutertrei*, *Globigerinoides ruber* (white), and *Orbulina universa*

Globigerina bulloides is typically a transitional-to-polar species that appears in upwelling environments at all latitudes (Prell and Curry, 1981). The species is found mainly in and above the thermocline in the surface mixed layer (Fairbanks et al., 1982).

As evident by the occurrence of *G. bulloides* in both subpolar and tropical regions, Reynolds and Thunell (1985) suggested that the distribution and abundance of this species is directly related to food availability and surface water productivity rather than temperature. Sediment trap studies within the Cariaco Basin indicate that *G. bulloides* dominates the foraminiferal assemblage during the upwelling season, and thus the abundance record of the species is an indirect proxy of trade wind strength and position (Tedesco and Thunell, 2003b). Prior studies have successfully used the abundance of *G. bulloides* in sediment cores as an upwelling indicator in the Cariaco Basin (Overpeck et al., 1989; Peterson et al., 1991; Black et al., 1999). However, interpreting the Interstadial 12 onset *G. bulloides* abundance record is not straightforward due to the combined and competing effects of rising sea level on Ekman-induced upwelling within the Cariaco Basin and migrating ITCZ-associated variations in trade wind location and fluvial nutrient delivery to the basin.

The relationship between *G. bulloides* abundance and sediment reflectivity does not behave as expected (i.e., strongly correlated, Figure 5.1, upper panel), and thus interpreting this species' abundance fluctuations strictly as a productivity or upwelling indicator should be treated with caution. Peterson et al. (1991) suggested the Cariaco Basin upwelling zone was displaced northward, outside of the basin 12,600 yBP as a result of significantly lower sea level, exposure of the Unare Platform to the south, and resulting effects on Ekman dynamics within the basin under low-stand conditions. Sea level 12,600 yBP is thought to be 90-95 m below present (Fairbanks, 1989), comparable to conditions at the beginning of Interstadial 12 (Siddall et al., 2003, 2008; Rohling et al., 2008). Upwelling definitely occurred within the Basin during the Younger Dryas

(Hughen et al., 1996), a time when sea level was comparable to that of the 20-30 m rise (60-70 m below present, Fairbanks, 1989) associated with the onset of Interstadial 12. Therefore one might expect a correlation between *G. bulloides* abundance and other productivity proxies as high-latitude temperatures rose abruptly, and there is a broad correlation between *G. bulloides* abundance and sediment reflectivity between 45,450 and 44,688 yBP (Figure 5.1, upper panel). Evidence for diminished productivity prior to Interstadial 12 comes from a study done by González et al. (2008), who noted low dinoflagellate cyst accumulation in the Cariaco basin at this time. They attributed the low stadial productivity to restricted inflow of Subtropical Underwater due to lowered sea levels, as it is this water that normally gets upwelled during the spring upwelling season to sustain phytoplankton growth (González et al., 2008). Sea level influences on local upwelling variability can explain some of the disconnect between sediment reflectivity and *G. bulloides* abundance. However, upwelling variability alone is not an entirely satisfactory explanation as *G. bulloides* relative percent data decrease across the onset the interstadial, suggesting other influences on productivity in the basin at this time.

Another possible control on *G. bulloides* abundance is fluvial nutrient delivery to the basin through the onset of Interstadial 12, an influence directly related to the region's climatology. Peak *G. bulloides* abundance just after the height of the interstadial could be related to high iron abundances at this time (Figure 5.16). Iron is an essential nutrient for phytoplankton growth, and iron addition experiments have shown that chlorophyll levels increase with increased iron (Martin and Fitzwater, 1988). Iron is an element required for the synthesis of pigment in phytoplankton, and is also required for the synthesis of several photosynthetic electron transport proteins and for the reduction of

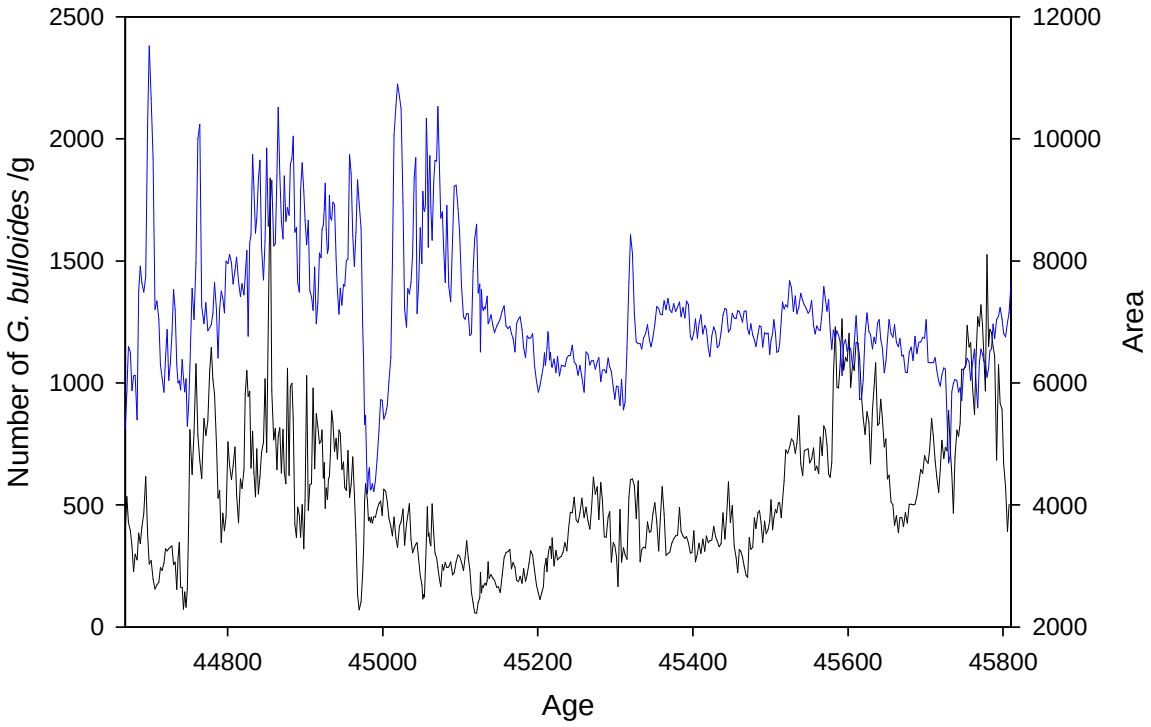

Figure 5.16: *Globigerina bulloides* absolute abundance data (black line) and iron abundance data (blue line) for the onset of Interstadial 12 (45,810 – 44,668 yBP).

CO_2, SO_4, and NO_3 during the photosynthetic production of organic compounds (Martin and Fitzwater, 1988). Thus, variations in iron input to the Cariaco Basin during Interstadial 12 fueled productivity. Indeed, high iron abundances during Interstadial 12 have been suggested as a driving mechanism behind surface productivity in the Cariaco Basin during this time, most likely a result of enhanced regional precipitation in and around the Cariaco Basin associated with a more northerly ITCZ average annual position during the interstadial (Peterson et al., 2000a). This productivity mechanism might also explain why *G. bulloides* relative percent data decrease during the interstadial onset. Despite the cautionary upwelling indicator interpretation, it may be that *G. bulloides* prefers high productivity conditions driven by upwelling rather than those induced by fluvial nutrient input.

Census data from several other foraminifer species provide additional evidence of an increase in fluvial input to the basin during the onset of Interstadial 12. *Neogloboquadrina dutertrei* prefers a well-stratified photic zone, where it dwells in the thermocline, close to the chlorophyll maximum (Fairbanks et al., 1982). In the modern Cariaco Basin, the depth and concentration of the subsurface chlorophyll maximum varies seasonally, with the highest chlorophyll values occurring during spring upwelling (Muller-Karger et al., 2001). During this time, the chlorophyll maximum shoals to around 0-25 m and the highest flux of *N. dutertrei* occurs (Tedesco and Thunell, 2003b). The absolute abundance record of *N. dutertrei* for the onset of Interstadial 12 displays a shift to extremely high values just after the abrupt transition into the interstadial. It is likely that an ecological threshold was reached that contributed to *N. dutertrei* flourishing at this point. Beyond this maximum, absolute abundances of *N. dutertrei* decline, and the

relative percentage of *N. dutertrei* remains at levels comparable to modern values (Tedesco and Thunell, 2003b).

Given what we know about the preferred habitat of *N. dutertrei*, its abundance pattern suggests an increasingly stratified water column, most likely on a seasonal basis that resulted from a climatically-sudden increase in boreal summer/fall precipitation as the ITCZ migrated north. Abundance and relative percent data for *N. dutertrei* display nearly identical patterns, suggesting that variations in this species' abundance plays a role in driving the relative percent of other species in the assemblage. While *G. bulloides* relative percent gradually decreases over the interstadial onset, *N. dutertrei* relative percent increases on average over the interval, albeit with the anomalous large event noted above.

Another species that supports increased fluvial input to the basin across the interstadial onset is *G. ruber* (white). The white morphotype of *G. ruber* is a tropical to subtropical species that inhabits the surface mixed layer between 0 and 45 m water depth (Deuser, 1987; Bé, 1982), and is most abundant in oligotrophic waters (Fairbanks et al., 1982). It tolerates temperatures in the range of 14 to 32°C (Bijma et al., 1990), and reaches maximum abundances in regions where salinity are relatively high (Kemle-von Mücke and Oberhänsli, 1999). The gradual decline in white *G. ruber* at the transition into Interstadial 12 is likely related to a combination of reduced salinity as regional precipitation and fluvial flow to the basin increased, and the resultant change from more oligotrophic waters to less oligotrophic waters with increased productivity.

Census data from a fourth foraminifer species reinforces the notion of increased productivity during the onset of Interstadial 12. *Orbulina universa* is a spinose, photic

zone inhabiting species that is widely distributed from the tropics to subpolar regions (Bé and Tolderlund, 1971). The species also bears algal symbionts and can flourish when food is limited and turbidity is low. The absolute abundance of *O. universa* drops significantly at the abrupt transition into Interstadial 12. As surface productivity increased going into Interstadial 12, species that flourish in nutrient rich conditions could outcompete those that do well when food is limited. Thus, the decline of *O. universa* at the onset of Interstadial 12 likely represents a transition to highly productive waters in the Cariaco Basin during the interstadial.

Spectral analysis has been used previously in foraminiferal census studies in the Cariaco Basin as a way to identify significant modes of Atlantic variability that might point to possible forcing mechanisms. Black et al. (1999) performed spectral analysis on a Cariaco Basin *G. bulloides* abundance record for the last 800 years, and noted spectral power in a 12.5- to 13-year band associated with the so-called Atlantic Thermal Dipole. In a similar fashion, spectral analysis was performed on the *G. bulloides* abundance record for the onset of Interstadial 12 to try to identify possible forcing mechanisms related to the observed variability. The onset of Interstadial 12 was divided into two sections for spectral analysis: the period from 45,462 to 45,810 yBP and the period from 44,668 to 45,462 yBP. These intervals are the period of time just prior to the abrupt onset into Interstadial 12, and the period of time spanning the abrupt onset into the interstadial, respectively. Dividing the *G. bulloides* data into two intervals enabled a direct comparison of stadial (cold) versus interstadial (warm) conditions. By comparing the results of the spectral analysis to known periodicities of modern climate phenomena,

inferences can be made about climate variability during Interstadial 12, assuming these phenomena, if they existed, operated on the same periodicities in the past.

For the interval of 45,462 to 45,810 yBP, the spectral analysis results revealed concentrations of variance in subdecadal to decadal modes (8.5 to 9.0 years and 14.8 years) and a multicentennial mode (130 to 500 years) (Figure 5.17). Given the length of this internal (348 years), it is difficult to make any significant inferences about the multicentennial mode of variability because it is not represented sufficiently in the time series. For the interval of 44,668 to 45,462 yBP, the results revealed concentrations of variance in interannual (4.8 years and 7.6 to 7.9 years), decadal to interdecadal (9.3 to 9.6 years and 24 to 27 years), multidecadal (76 to 90 years), and multicentennial modes (200 to 500 years) (Figure 5.18). Like the prior interval, given the length of this interval of the time series (794 years), it is difficult to make any significant inferences about the multicentennial mode. The main difference between the two intervals is that the latter, warmer interval displays significant interannual, interdecadal, and multidecadal variability that is absent in the earlier colder interval. The results of the Black et al. (1999) study for the past 800 years revealed concentrations of variance centered at periods of 6.1 to 6.3, 6.8 to 7.0 years, 8.7 to 9.0 years, 12.5 to 13.0 years, and 140 to 500 years. The main difference between the modern record and the full record for the onset of Interstadial 12 is a pronounced multidecadal mode in the Interstadial 12 record.

The 8.5 to 9.0 period of variability in the earlier interval for the onset of Interstadial 12 compares well to the periodicity of the North Atlantic Oscillation (NAO). In the modern climate system the NAO is weakly correlated, at best, to the tropical

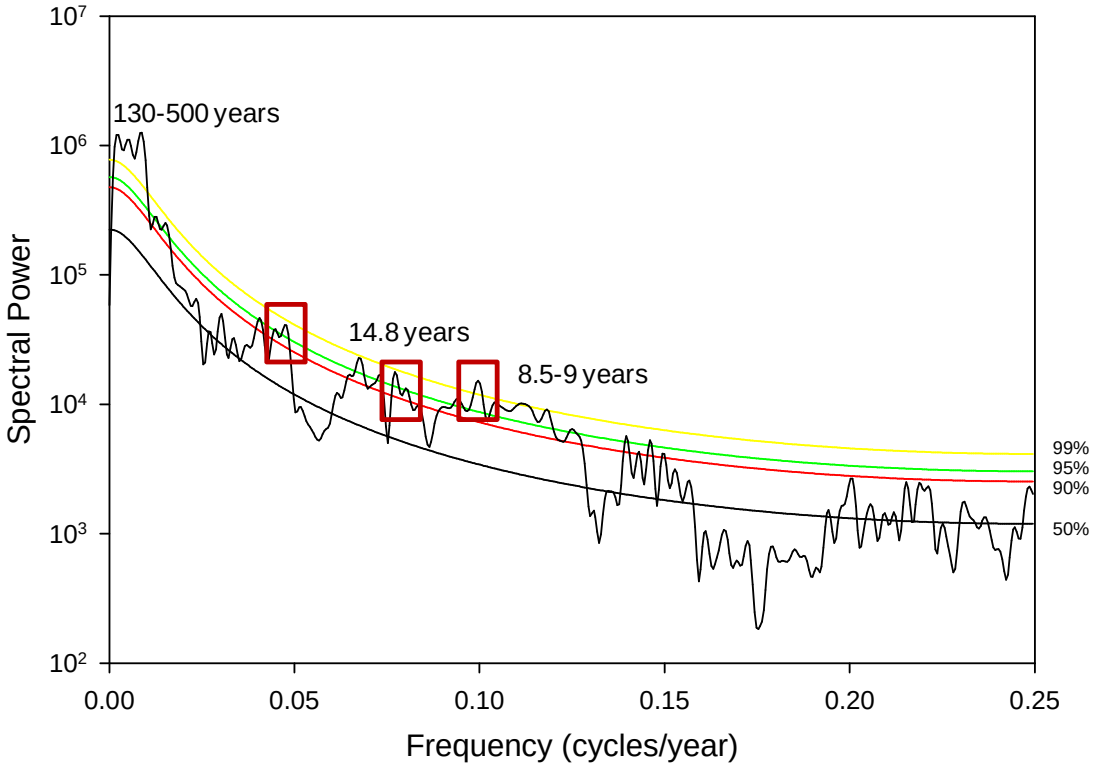

Figure 5.17: Spectral analysis results for the *Globigerina bulloides* absolute abundance time series for the earlier interval of the onset of Interstadial 12 (45,462 to 45,810 yBP). Frequencies are converted to periodicities for peaks above the 99% confidence level. Peaks outlined in red are harmonics.

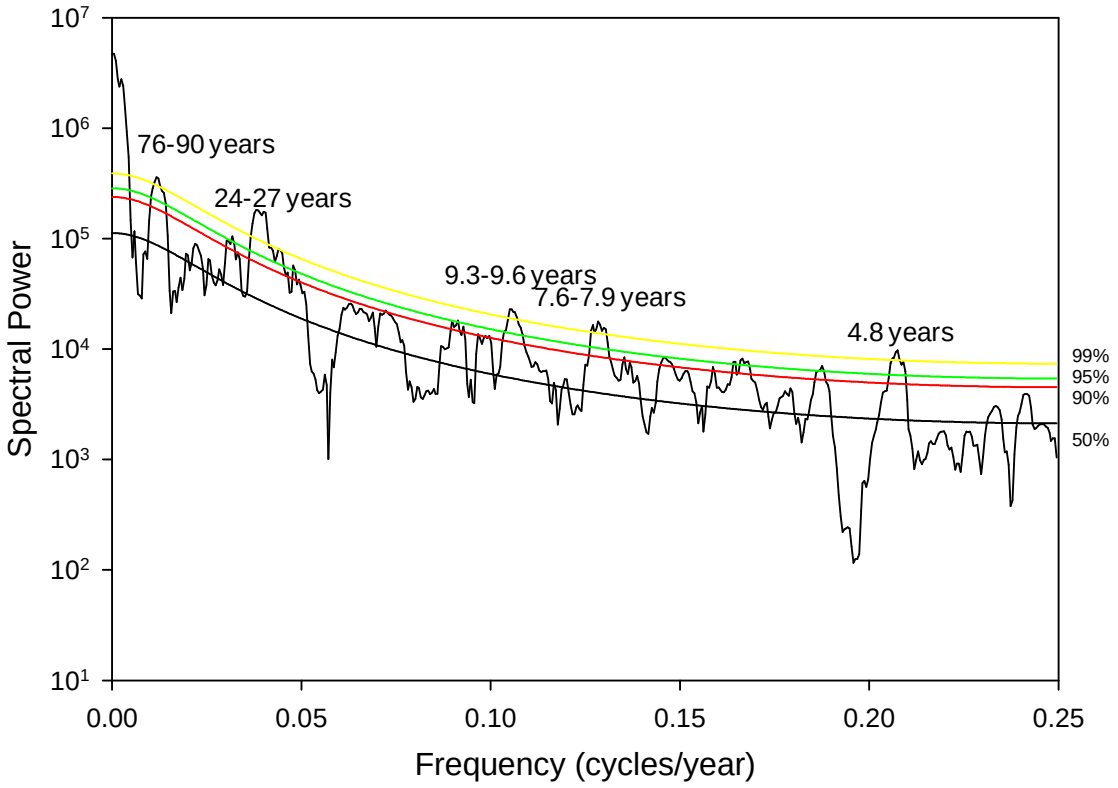

Figure 5.18: Spectral analysis results for the *Globigerina bulloides* absolute abundance time series for the latter interval of the onset of Interstadial 12 (44,668 to 45,462 yBP). Frequencies are converted to periodicities for peaks above the 99% confidence level.

Atlantic. Given that the period prior to the abrupt onset into Interstadial 12 was a cold stadial interval, it is possible that the influence of the NAO was exerted further south than its modern latitudinal extent. The NAO is associated with the strengths of the Icelandic low pressure system and the Azores high pressure system (Hurrell et al., 2003). If the ITCZ had taken a more southerly average annual position during the stadial period prior to Interstadial 12, major atmospheric circulation cells and the latitudinal influence of the NAO may have shifted south in response. Thus, while the influence of the NAO in the modern climate system is weakly correlated to the tropical Atlantic, it is possible the correlation was stronger during cold stadials of the last glacial period in response to a more southerly average annual position of the ITCZ.

While it would be convenient to attribute the interannual variability observed during abrupt onset into Interstadial 12 to the El Niño-Southern Oscillation (ENSO), the presence of ENSO in paleoclimate records prior to more than a few thousand years ago (e.g. Hughen et al., 1999; Tudhope et al., 2001) is a much debated subject. A lesser known interannual phenomenon similar to, but weaker than the Pacific ENSO also occurs in the Atlantic, known as the Atlantic Niño. Warm events of the Atlantic Niño reach their maximum strength in the latter half of the year, with manifestations focused primarily near the equator (Latif and Grotzner, 2000; Wang, 2002). During a warm phase, trade winds in the equatorial western Atlantic are weak and SST is high in the equatorial eastern Atlantic (Wang, 2005). Ascending motion associated with the Gulf of Mexico/Caribbean Sea-Amazon heat source extends eastward and weakens the Atlantic Walker circulation (Wang, 2005). This decreases surface equatorial easterly wind in the western Atlantic, which in turn further increases SST in the equatorial eastern Atlantic

(Wang, 2005). The reverse occurs during a cold phase. The Atlantic Niño is mostly independent of the Pacific ENSO variability, with a shorter characteristic time scale, and is not related to the tropical Atlantic response to the Pacific ENSO (Wang, 2005). Thus, the positive ocean-atmosphere interaction associated with the Pacific Walker circulation, which is responsible for ENSO, seems to also be operating in the Atlantic (Wang, 2005). It has also been observed that the Atlantic Hadley circulation strengthens during the warm phase of the Atlantic Niño (Wang, 2005). It is more likely that the interannual variability in the *G. bulloides* time series from Interstadial 12 is related to the Atlantic Niño as the impacts are more direct and occurs more frequently than ENSO. However, the Atlantic Niño has an observed period range of 3-5 years (Chang et al., 2006), which is right at the edge of the Nyquist frequency for my samples (2-year resolution), thus it is not possible to make interpretations about Atlantic Niño variability based solely on the spectral analysis results presented here.

The multidecadal variability in the *G. bulloides* time series for the latter interval of the onset of Interstadial 12 may be due to the influence of the Atlantic Multidecadal Oscillation (AMO), or something similar to the modern AMO, on the Cariaco Basin during the transition in Interstadial 12. The AMO, which has a period of ~70 years, is highly correlated with tropical Atlantic climate patterns, such as rainfall in North Eastern Brazil and the African Sahel regions, and Atlantic hurricanes (Knight et al., 2006). Warm phases of the AMO force a northward displacement of the ITCZ, brining increased precipitation to the Sahel and reduced rainfall to North Eastern Brazil (Knight et al., 2006). Also in the warm phase, the AMO has been attributed to increased hurricane activity in the Atlantic resulting from increases in North Atlantic SST and reduced

vertical wind shear (Goldenberg et al., 2001). Given that the multidecadal period of variability is not present during the earlier interval for the onset of Interstadial 12, it is possible that climate variability related to the AMO may only operate during warm climate intervals, something that has significant implications for modern and near-future climate variability.

Wavelet analysis was also performed on the *G. bulloides* time series to see how significant periods of climate variability evolved throughout the onset of Interstadial 12. The results revealed significant multidecadal variability just after the abrupt transition into the interstadial (Figure 5.19). Climate variability on these scales is lacking from the record during the cool interval prior to the abrupt onset of Interstadial 12, and also throughout the abrupt transition into the interstadial. This may provide additional evidence that AMO-type variability may only operate during warm climate periods.

The observed decadal and interdecadal modes of variability during the onset of Interstadial 12 (for both the earlier and latter intervals) are periods which have no modern analogs, thus it is difficult to infer what climate phenomena they may be related to. The periodicities also do not show up in other high resolution climate reconstructions. As Interstadial 12 occurred under boundary conditions that are different from modern boundary conditions, it may be that there was climate variability occurring during Interstadial 12 that we do not see in the modern climate system. Another possible explanation is that there are climate phenomena occurring on these periodicities in the modern climate system, but they have not yet been identified.

The results discussed above provide additional support for a switch to a more northerly average annual position of the ITCZ at the abrupt onset of Interstadial 12. The

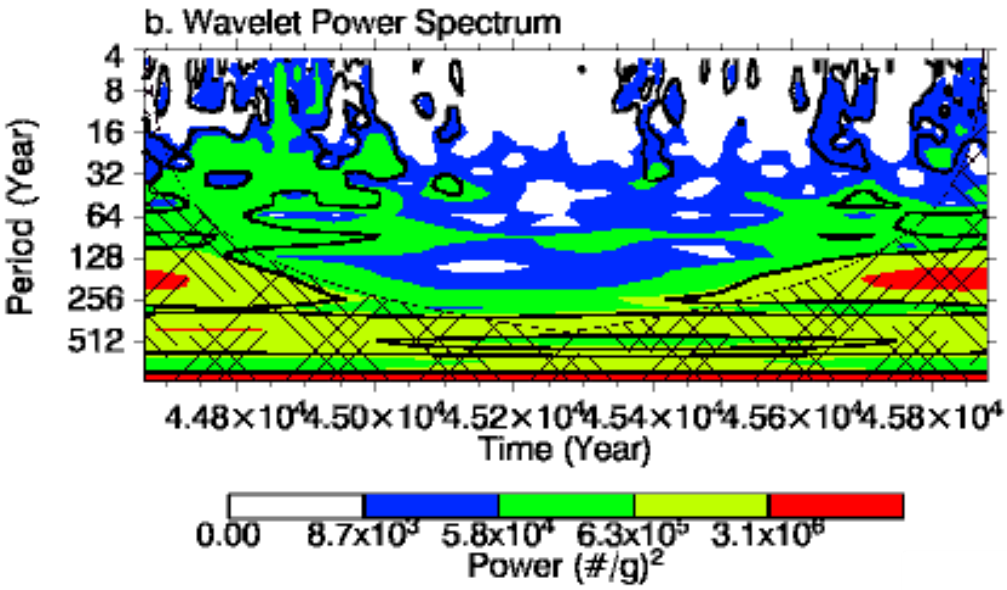

Figure 5.19: Wavelet analysis results for the *Globigerina bulloides* absolute abundance time series for the onset of Interstadial 12 (44,668 to 45,810 yBP). Power outlined in black represents variability significant above the 99% confidence level. Variability under the black dotted line that is hatch marked is below the cone of influence, meaning no inferences can be made about the periods of variability in this region based on the length of the time series.

foraminiferal census results indicate wetter conditions over the Cariaco Basin and surrounding regions. Coincident with this, it would be expected that central South America experienced much drier conditions as the ITCZ would have been located further north over the South American landmass. Wetter conditions would also be expected over Northwest Africa as the ITCZ would also be pulled further north over the African landmass. A study by Burns et al. (2003) compared $\delta^{18}O$ records of stalagmites collected from caves in China and Yemen. Both records display a rapid shift to more negative $\delta^{18}O$ at the onset of Interstadial 12, indicative of increased precipitation in both locations. Given that both of these locations are well above the equator, it can be inferred that the ITCZ had shifted to a more northerly average annual position in these regions as well. Thus, the results of the Burns et al. (2003) study support the findings of this study that the ITCZ shifted north rapidly at the onset of Interstadial 12. It is estimated that the ITCZ migrated its average annual position by approximately six degrees of latitude, or 600 to 700 km during the ~450 years spanning the abrupt onset of Interstadial 12.

5.3.2 The Abundance Records of Minor Contributing Species

The abundances of *G. ruber* (pink), *G. sacculifer*, *G. quinqueloba*, and *N. pachyderma* remain relatively low through the onset of Interstadial 12, making a definitive interpretation of their records difficult. These species do not provide much insight into what climate was like during the onset of Interstadial 12 because of either very low abundances or a lack of knowledge about their ecologies.

Although the pink and white morphotypes of *G. ruber* are the same species, they have slightly different ecological preferences. While their distribution and temperature tolerances are similar, plankton tow studies from the western Gulf of Mexico have shown

that pink *G. ruber* inhabits a region slightly deeper in the water column, between 25 and 65 m water depth (Bé, 1982). In addition, the white variety of *G. ruber* has been found to dominate sediments that underlie the central Sargasso Sea, while pink *G. ruber* are more typically found in the Caribbean Sea and Gulf of Mexico (Kipp, 1976). Plankton tow studies have also shown that pink *G. ruber* lives only during the warmer summer months, while the white variety lives year round (Bé and Tolderlund, 1971; Deuser and Ross, 1989). In the Cariaco Basin, abundance patterns of the two varieties also appear to be driven differently (Peterson et al., 1991). Pink *G. ruber* does not show the same dramatic change in average relative abundance that white *G. ruber* exhibits between anoxic and oxic sediment units (Peterson et al., 1991). The record of pink *G. ruber* for the onset of Interstadial 12 is distinctly different from that of white *G. ruber*. While abundances of white *G. ruber* drop off into the transition, abundances of the pink variety remain higher, and even peak to maximum absolute abundance just prior to the height of the interstadial.

It has been suggested by Peterson et al. (2000a) that the transition into Interstadial 12 marks a boundary between oxic and anoxic conditions in the Cariaco Basin, with oxic conditions during the stadial preceeding the interstadial. Increased surface productivity during Interstadial 12 facilitated anoxic conditions in the basin throughout the interstadial. Thus, the fact that pink *G. ruber* abundances remain high during the onset of Interstadial 12 while white *G. ruber* abundances drop off may be related to the basin's switch to anoxic conditions during the interstadial. It is also possible that pink *G. ruber*, as it lives slightly deeper in the water column than white *G. ruber*, was not as drastically impacted by the decline in surface water salinity at the onset of Interstadial 12. A third

possibility is that ecological preferences of pink *G. ruber* are not clearly understood yet, making a definitive interpretation of the record difficult.

Globigerinoides sacculifer is a tropical to subtopical species that, like other mixed layer dwelling species, flourishes in warm, oligotrophic waters (Bé and Tolderlund, 1971). *Globigerinoides sacculifer* is also an algal symbiont-bearing species that can do well in nutrient poor waters (Faul et al., 2000). The absolute abundance record for *G. sacculifer* resembles that of *O. universa*, with a drop at the abrupt onset into Interstadial 12. As both species do well under similar water column conditions, we would expect that their records would resemble on another. Thus, it is likely that the same driving factors are responsible for the patterns seen in both species during the onset of Interstadial 12.

Like *G. bulloides*, *G. quinqueloba* is also common in high productivity regions, such as coastal upwelling zones (Thiede, 1975). *Globigerina quinqueloba* is small and lives mostly in the photic zone (Tedesco and Thunell, 2003). A study of foraminifera in the Santa Barbara Basin suggested that *G. quinqueloba* may be a better indicator of upwelling than *G. bulloides* within that basin (Black et al., 2001). The absolute abundance record of *G. quinqueloba* in the Cariaco Basin exhibits an abrupt peak just into the transition into Interstadial 12 and then increases again just prior to and after the height of the interstadial. These peaks in the absolute abundance of *G. quinqueloba* at the onset of Interstadial 12 may be related to increased water column productivity, though given the low abundances, it is unclear if the two are related.

Neogloboquadrina pachyderma, albeit in very low abundances, is present in the Cariaco Basin during the transition into Interstadial 12. The species is most abundant in high latitude polar and subpolar regions (Thompson and Shackleton, 1980), so its

presence in the Cariaco Basin during Interstadial 12 is surprising. As such, the species does not provide much insight into what climate was like during Interstadial 12, due a lack of knowledge of the ecology of *N. pachyderma* and its presence in tropical waters.

5.3.3 The *Globorotalia menardii* record

The absolute abundances of *G. menardii* throughout Interstadial 12 remain low, making it difficult to determine if there is any significance in the values. However, the fact that *G. menardii* is present at all in the Cariaco Basin during Interstadial 12 is extremely surprising. According to Ericson and Wollin (1956), *G. menardii* appears and disappears from sediment cores from the tropical Atlantic throughout the Pleistocene, and likely corresponds to alternations between warm and cold climates, respectively. Indeed, the presence or absence of *G. menardii* in Atlantic cores is regularly used as a stratigraphic indicator for glacial and interglacial Quaternary sediments. As Interstadial 12 occurred during a Marine Isotope Stage 3, a glacial period, one would expect *G. menardii* to be completely absent from Cariaco Basin sediments, yet this species is present in this record, albeit in very small amounts. It may be that the Cariaco Basin acts as a refugia for this species during glacial periods, similar to what has been proposed for certain organisms (e.g., butterflies, woody angiosperms, etc.) in the Amazon Basin during dry climate phases (Prance, 1982). Alternatively, the Cariaco Basin may offer better preservation potential due to high sedimentation rates relative to the poor carbonate preservation in the North Atlantic during glacial periods.

5.4 Conclusions on Tropical Atlantic Climate Variability at the Onset of Interstadial 12

Much of the variability exhibited by the foraminifera in the Cariaco Basin at the onset of Interstadial 12 is the result of an abrupt transition from low productivity, nutrient depleted waters during the preceding stadial to highly productivity, nutrient rich waters during the interstadial. There is an overall shift from foraminifera that flourish in nutrient-poor environments to those that can outcompete other species during period of high productivity. Evidence from the Interstadial 12 data also supports enhanced regional rainfall as the mechanism by which these nutrients were delivered to the basin, as seen by a decline in species that have preferences for higher salinity waters. This evidence all supports a rapid northerly migration of the average annual position of the ITCZ during the abrupt transition into Interstadial 12. The results of the spectral analysis of the *G. bulloides* time series indicate significant tropical Atlantic variability on multiple time scales, ranging from interannual to multidecadal scale. These modes of variability are important as they represent a connection of the Cariaco Basin to wider-scale climate phenomenon from as far away as the North Atlantic. Another important finding of both the wavelet and spectral analysis results is that multidecadal variability, possibly linked to the AMO, only operated during the warm interval of the record. Thus, we see not only a response in the foraminiferal community to the abrupt changes occurring at the onset of Interstadial 12, but also a response in the dominant periodicities of climate variability.

VI. The Transition Out of Interstadial 12 – Results & Discussion

6.1 Introduction

While the onset of Interstadial 12 was characterized by a number of abrupt changes in global climate and ocean dynamics, the latter part of the interstadial and the transition back to stadial conditions occurred more gradually. This transition back to cooler climate conditions as inferred from the GISP2 $\delta^{18}O$ data began just after the height of the interstadial. Conditions in the tropics were changing as well during this period, as cooler North Atlantic temperatures likely resulted in increased surface pressure over the North Atlantic and a southward shift of the ITCZ as modern boundary conditions dynamics would suggest (Hastenrath and Greischar, 1993). The onset of Interstadial 12 provided the opportunity to examine how the tropical Atlantic responds to abrupt climate change, while the transition back to stadial conditions can show us how the tropics respond to more gradual change in a different direction (e.g. abrupt warming vs. gradual cooling).

6.2 Foraminiferal Census Results

Foraminiferal census data were collected on 540 samples representing the latter portion of Interstadial 12. The relative abundance of each species is expressed as a percentage value of the total counted foraminiferal population, while the absolute abundance represents the number of foraminifera normalized to per gram of dry

sediment. As stated earlier in Chapter 5, caution must be taken when looking just a relative abundance data, due to the "closed sum problem."

6.2.1 *Globigerina bulloides*

The absolute abundance record of *G. bulloides* for the latter part of Interstadial 12 (Figure 6.1, upper panel) begins by increasing from 800 *G. bulloides*/g to 1600 *G. bulloides*/g at 43,845 yBP. Values then decline to 144 *G. bulloides*/g at 43,790 yBP. After increasing again to almost 1,700 *G. bulloides*/g at 43,719 yBP, absolute abundances then decline to around 400 *G. bulloides*/g. *Globigerina bulloides* then peaks in absolute abundance to 1290 *G. bulloides*/g at 43,410 yBP before decreasing to 134 *G. bulloides*/g at 43,388 yBP. Between 43,388 and 43,322 yBP, the absolute abundance of *G. bulloides* is highly variable, coming to an abrupt maximum of 2,005 *G. bulloides*/g at 43,349 yBP, decreasing abruptly to 390 *G. bulloides*/g at 43,341 yBP, and then increasing again to 1836 *G. bulloides*/g at 43,333 yBP. After these large swings, the absolute abundance record of *G. bulloides* gradually declines to levels around 200 *G. bulloides*/g for the remainder of the record.

The relative abundance record of *G. bulloides* for the latter part of Interstadial 12 (Figure 6.1, lower panel) shows little variability and averages 55%. Values never reach over 69% or under below 37%.

6.2.2 *Neogloboquadrina dutertrei*

The *N. dutertrei* absolute abundance record is highly variable during the latter part of Interstadial 12 (Figure 6.2, upper panel), until 43,216 yBP, when levels decline from around 100 *N. dutertrei*/g to 25 *N. dutertrei*/g. Values for the record begin around 300 *N. dutertrei*/g before declining to 45 *N. dutertrei*/g at 43,790 yBP. After increasing

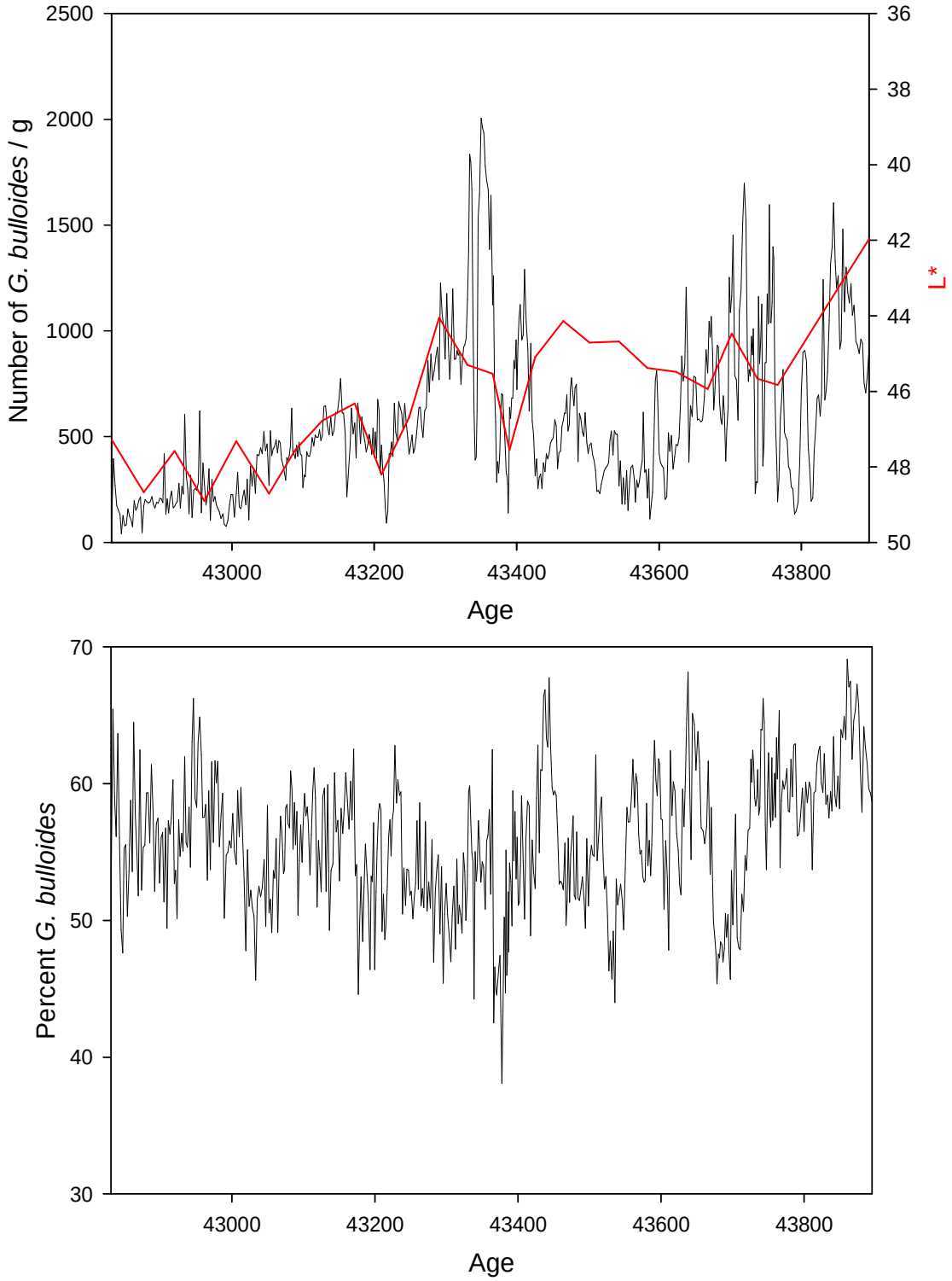

Figure 6.1: *Globigerina bulloides* absolute abundance (upper panel, reflectivity plotted in red) and relative abundance (lower panel) for the termination of Interstadial 12 (43,895 – 42,831 yBP). The relative abundance is expressed as a percentage value of the total counted foraminiferal population, while the absolute abundance represents the number of *G. bulloides* normalized to per gram of dry sediment.

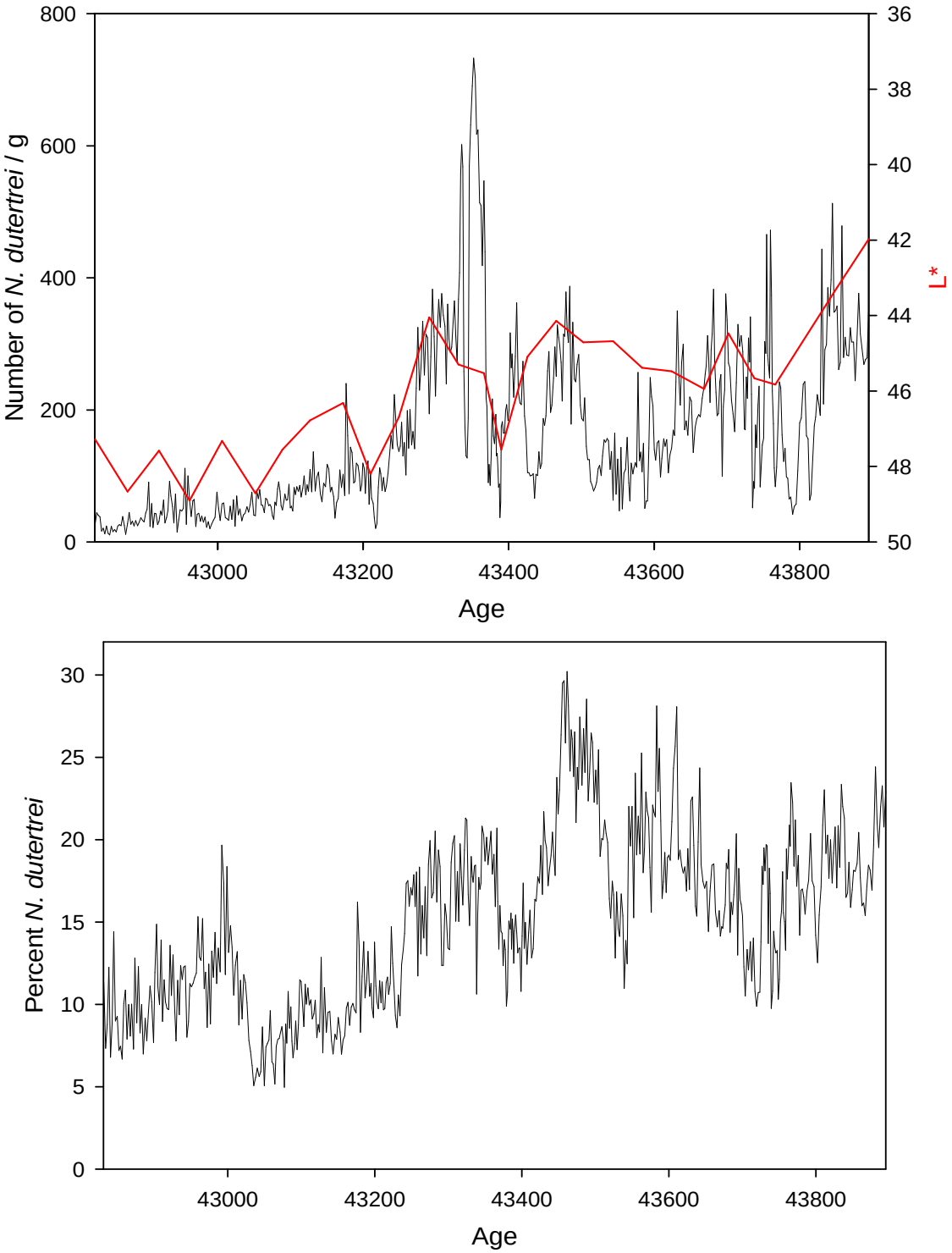

Figure 6.2: *Neogloboquadrina dutertrei* absolute abundance (upper panel, reflectivity plotted in red) and relative abundance (lower panel) for the termination of Interstadial 12 (45,810 – 44,668 yBP). The relative abundance is expressed as a percentage value of the total counted foraminiferal population, while the absolute abundance represents the number of *N. dutertrei* normalized to per gram of dry sediment.

abruptly to 470 *N. dutertrei*/g at 43,760 yBP, absolute abundances gradually decline to 48 *N. dutertrei*/g at 43,551. Values then peak twice to 390 *N. dutertrei*/g and 362 *N. dutertrei*/g at 43,483 yBP and 43,411 yBP, respectively. At 43,352 yBP, the absolute abundance of *N. dutertrei* comes to an abrupt maximum of 732 *N. dutertrei*/g, which is the highest value reached for the termination of Interstadial 12.

The contribution of *N. dutertrei* to the total foraminiferal population for the termination of Interstadial 12 (Figure 6.2, lower panel) varies between 5% and 30%. The maximum relative percentage of *N. dutertrei* of 30% occurs at 43,460 yBP. The higher relative percentages of *N. dutertrei* are seen in the first half of the record, while percentages do not reach over 21% in the latter half of the record.

6.2.3 *Orbulina universa*

The absolute abundance record of *O. universa* for the termination of Interstadial 12 (Figure 6.3, upper panel) displays a shift in variability at 43,357 yBP. Before this point, variability is low, ranging from 0 *O. universa*/g to 15 *O. universa*/g. After 43,357 yBP, the absolute abundance record is more variable, ranging from 0 *O. universa*/g to 26 *O. universa*/g.

Orbulina universa contributes <1% to the total foraminiferal population until 43,291 yBP, when relative abundances gradually begin to increase over the remainder of the record (Figure 6.3, lower panel). A peak of 6.5% is reached at 42,898 yBP.

6.2.4 *Globigerinella aequilateralis*

Globigerinella aequilateralis generally has absolute abundances of <20 *G. aequilateralis*/g for the time period exiting Interstadial 12 (Figure 6.4, upper panel);

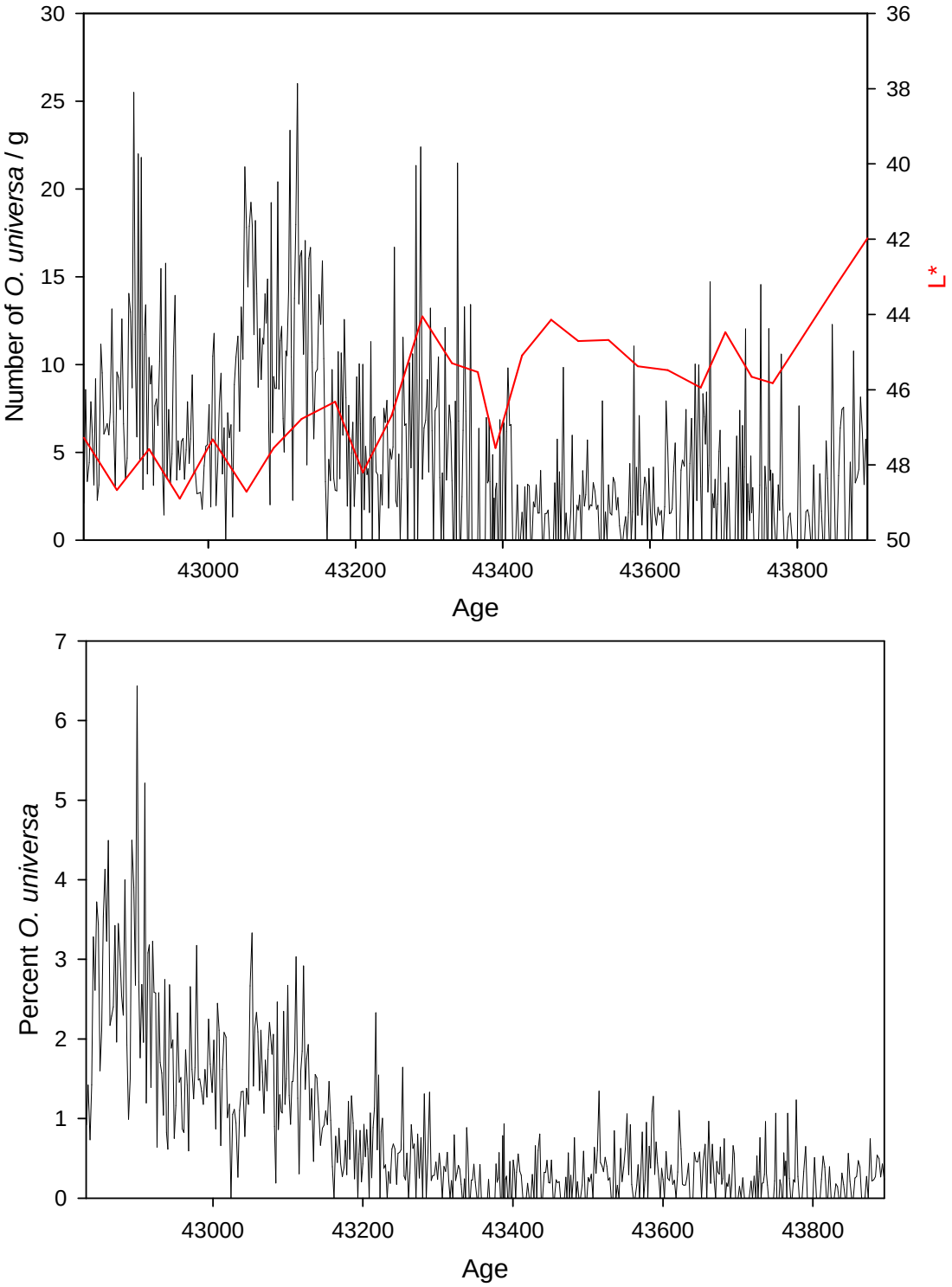

Figure 6.3: *Orbulina universa* absolute abundance (upper panel, reflectivity plotted in red) and relative abundance (lower panel) for the termination of Interstadial 12 (43,895 – 42,831 yBP). The relative abundance is expressed as a percentage value of the total counted foraminiferal population, while the absolute abundance represents the number of *O. universa* normalized to per gram of dry sediment.

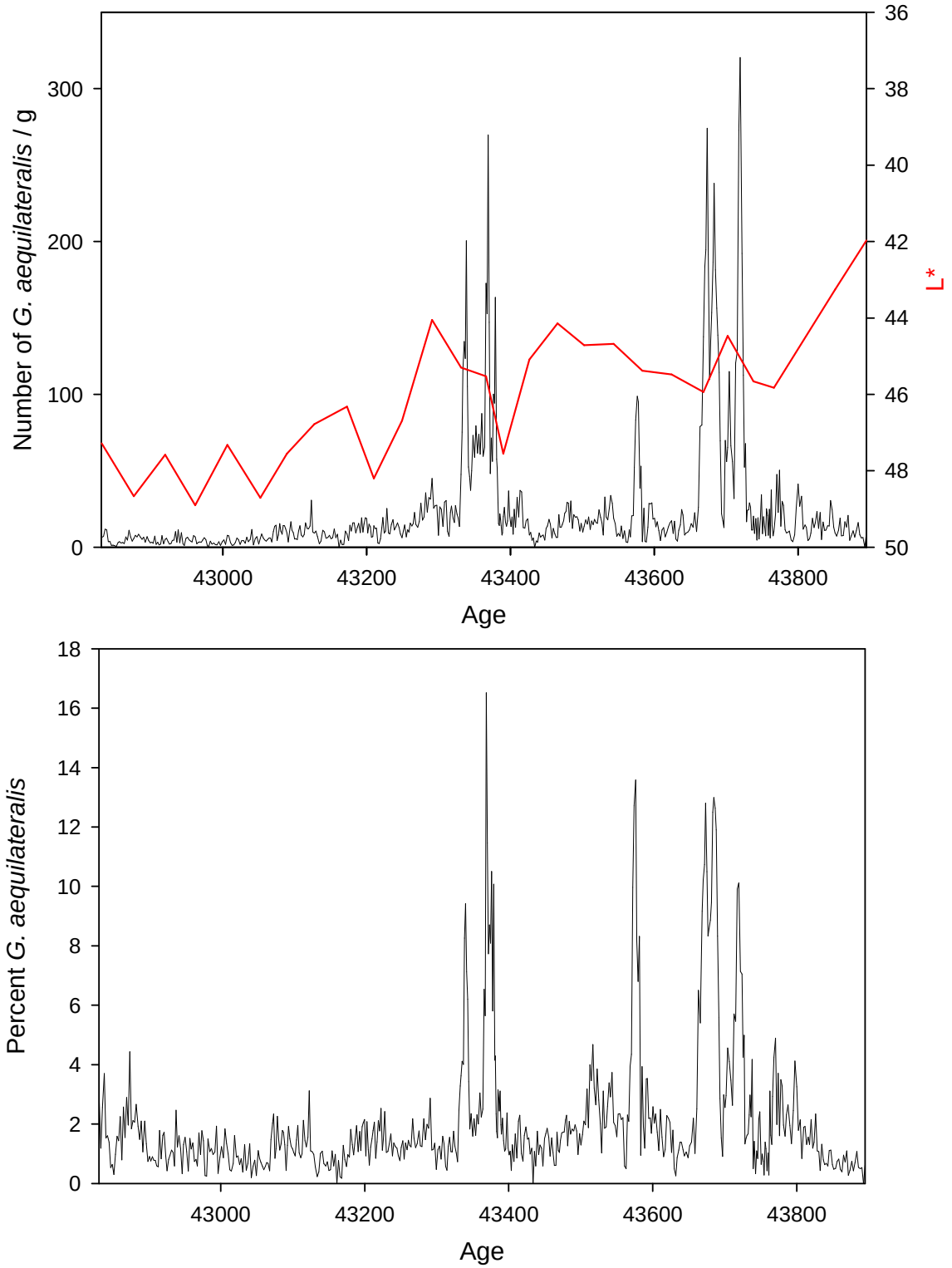

Figure 6.4: *Globigerinella aequilateralis* absolute abundance (upper panel, reflectivity plotted in red) and relative abundance (lower panel) for the termination of Interstadial 12 (43,895 – 42,831 yBP). The relative abundance is expressed as a percentage value of the total counted foraminiferal population, while the absolute abundance represents the number of *G. aequilateralis* normalized to per gram of dry sediment.

however, there are three periods of abrupt increase. From 43,727 to 43,662 yBP, values come to a maximum of 320 *G. aequilateralis*/g and from 43,381 to 43,330 yBP, absolute abundances of *G. aequilateralis* reach 270 *G. aequilateralis*/g. A smaller peak of 100 *G. aequilateralis*/g is reached between 43,583 to 43,567 yBP.

Throughout the termination of Interstadial 12, the relative abundance of *G. aequilateralis* averages 2% (Figure 6.4, lower panel). There are 6 prominent peaks that punctuate the record, with values of 10%, 13%, 16%, and 9% that occur at 43,719 yBP, 43,575 yBP, 43,368 yBP, and 43,339 yBP, respectively. A double peak of relative abundances of 13% occurs between 43,693 and 43,661 yBP.

6.2.5 *Globorotalia crassaformis*

Absolute abundances of *G. crassaformis* are low throughout the termination of Interstadial 12 (Figure 6.5, upper panel), ranging between 0 *G. crassaformis*/g and 17 *G. crassaformis/g*, with an average of 1.5 *G. crassaformis*/g. The maximum value of 17 *G. crassaformis*/g is reached at 43,257 yBP.

Throughout the latter part of Interstadial 12, relative abundances of *G. crassaformis* are generally <1% (Figure 6.5, lower panel), but reach just over 2% at 43,257 yBP, the same point as the maximum absolute abundance of *G. crassaformis.*

6.2.6 *Globorotalia menardii*

Globorotalia menardii does not appear often in the absolute abundance record (Figure 6.6, upper panel) until 43,212 yBP, after which the species is more prevalent. Values are low throughout the record, and when *G. menardii* is present, absolute abundances are generally <2 *G. menardii*/g and never reaches over 8 *G. menardii*/g.

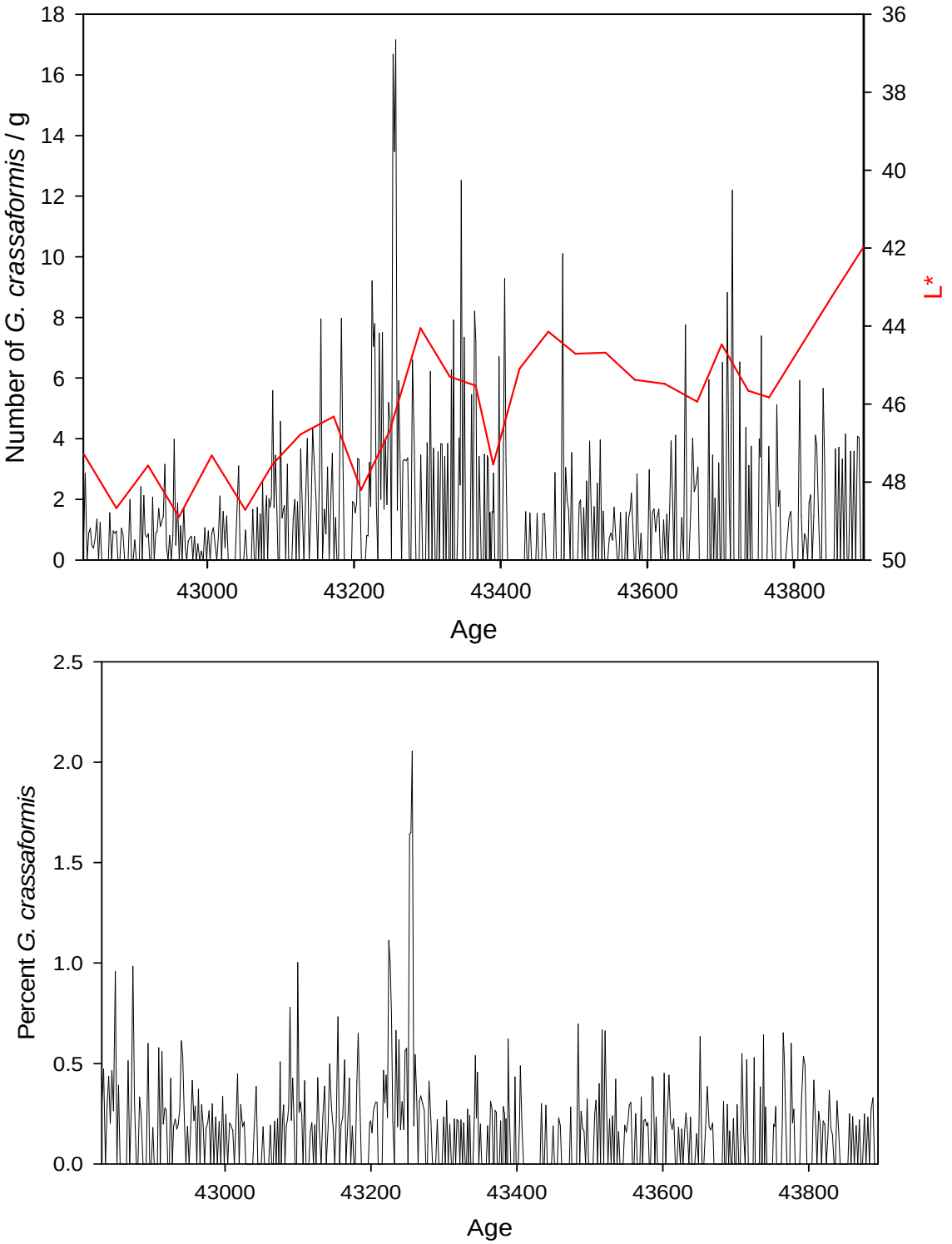

Figure 6.5: *Globorotalia crassaformis* absolute abundance (upper panel, reflectivity plotted in red) and relative abundance (lower panel) for the termination of Interstadial 12 (43,895 – 42,831 yBP). The relative abundance is expressed as a percentage value of the total counted foraminiferal population, while the absolute abundance represents the number of *G. crassaformis* normalized to per gram of dry sediment.

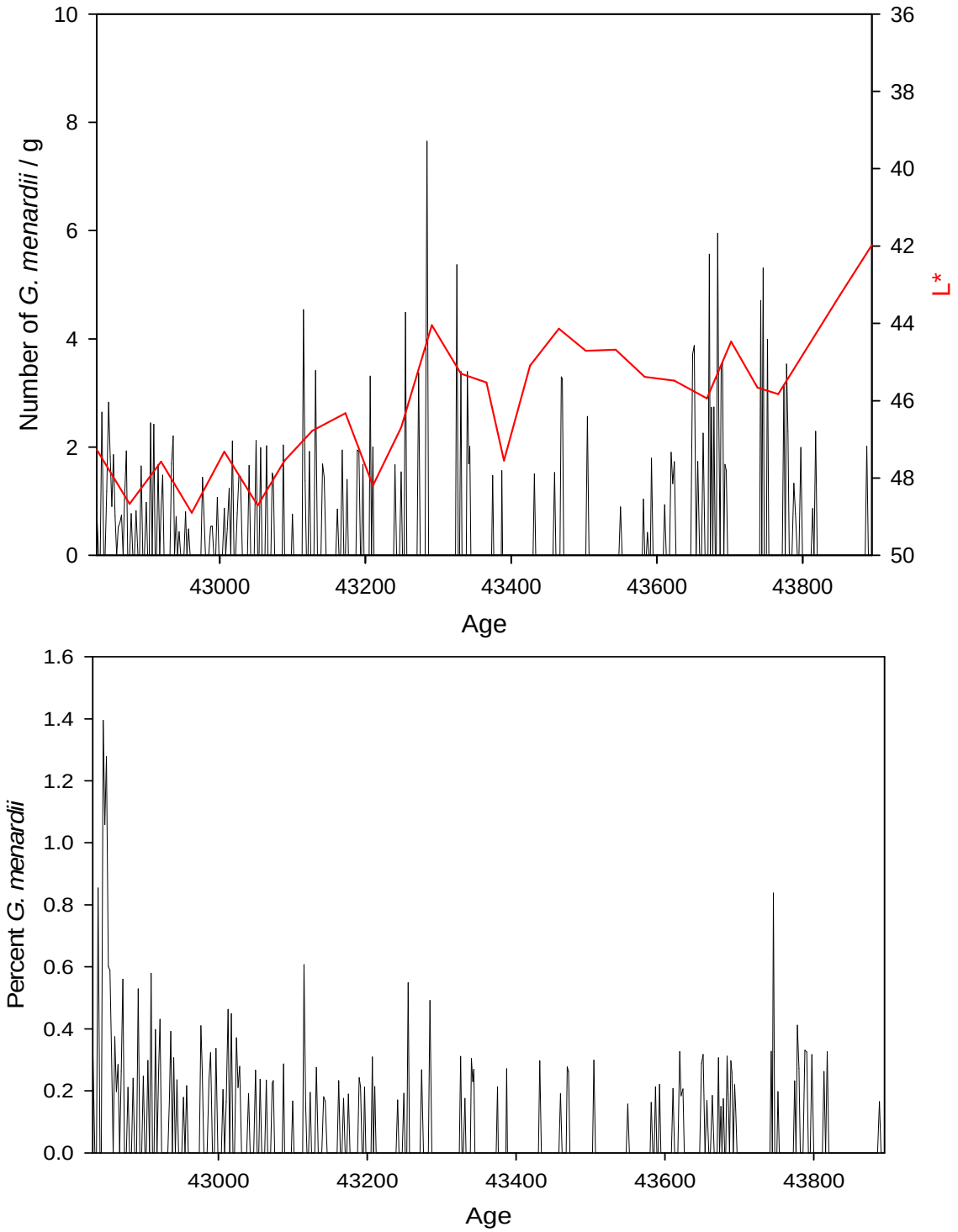

Figure 6.6: *Globorotalia menardii* absolute abundance (upper panel, reflectivity plotted in red) and relative abundance (lower panel) for the termination of Interstadial 12 (43,895 – 42,831 yBP). The relative abundance is expressed as a percentage value of the total counted foraminiferal population, while the absolute abundance represents the number of *G. menardii* normalized to per gram of dry sediment.

When *G. menardii* is present in the Interstadial 12 termination record, relative abundances are <1%, but comes to a peak of 1.4% at 42,845 yBP (Figure 6.6, lower panel)

6.2.7 *Globigerinoides ruber* (white morphotype)

The absolute abundance record of white *G. ruber* (Figure 6.7, upper panel) comes to two very abrupt peaks of 453 white *G. ruber*/g and 581 white *G. ruber*/g at 43,409 yBP and 43,354 yBP, respectively. Two smaller peaks occur at 43,845 yBP and 43,533 yBP, with absolute abundances of 158 white *G. ruber*/g and 210 white *G. ruber*/g, respectively. Aside from these peaks, levels remain generally <50 white *G. ruber*/g for the rest of the record.

White *G. ruber* generally contributes <5% to the total foraminiferal population for the termination of Interstadial 12 (Figure 6.7, lower panel). There are, however, two periods of abrupt increase in relative percentage between 43,566 and 43,518 yBP, when values reach over 20%, and between 43,435 and 43,330 yBP, when the relative percent of white *G. ruber* reaches a maximum of just over 23%. Beginning at 43,128 yBP, values gradually increase from around 1% to 10%, reached at 42,831 yBP.

6.2.8 *Globigerinoides ruber* (pink morphotype)

Pink *G. ruber* increases at the beginning of the Interstadial 12 termination (Figure 6.8, upper panel) between 43,895 and 43,697 yBP, when a sustained peak in absolute abundance of over 330 pink *G. ruber*/g is reached. This peak continues until 43,697 yBP, when values decline to levels <100 pink *G. ruber*/g. After this, there are three peaks in absolute abundance of 119, 141, and 105 pink *G. ruber*/g, at 43,530, 43,469, and 43,045

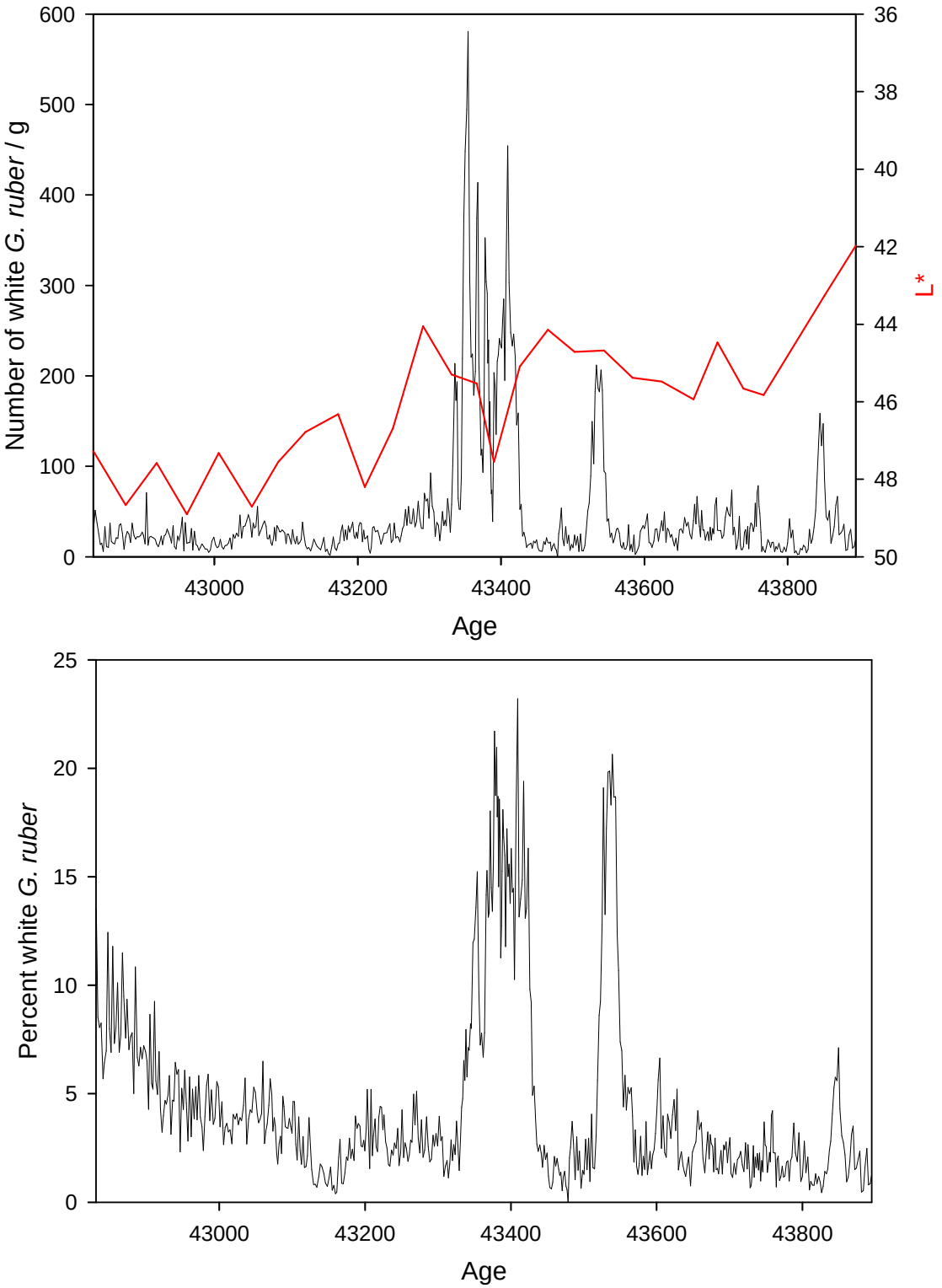

Figure 6.7: White *Globigerinoides ruber* absolute abundance (upper panel, reflectivity plotted in red) and relative abundance (lower panel) for the termination of Interstadial 12 (43,895 – 42,831 yBP). The relative abundance is expressed as a percentage value of the total counted foraminiferal population, while the absolute abundance represents the number of white *G. ruber* normalized to per gram of dry sediment.

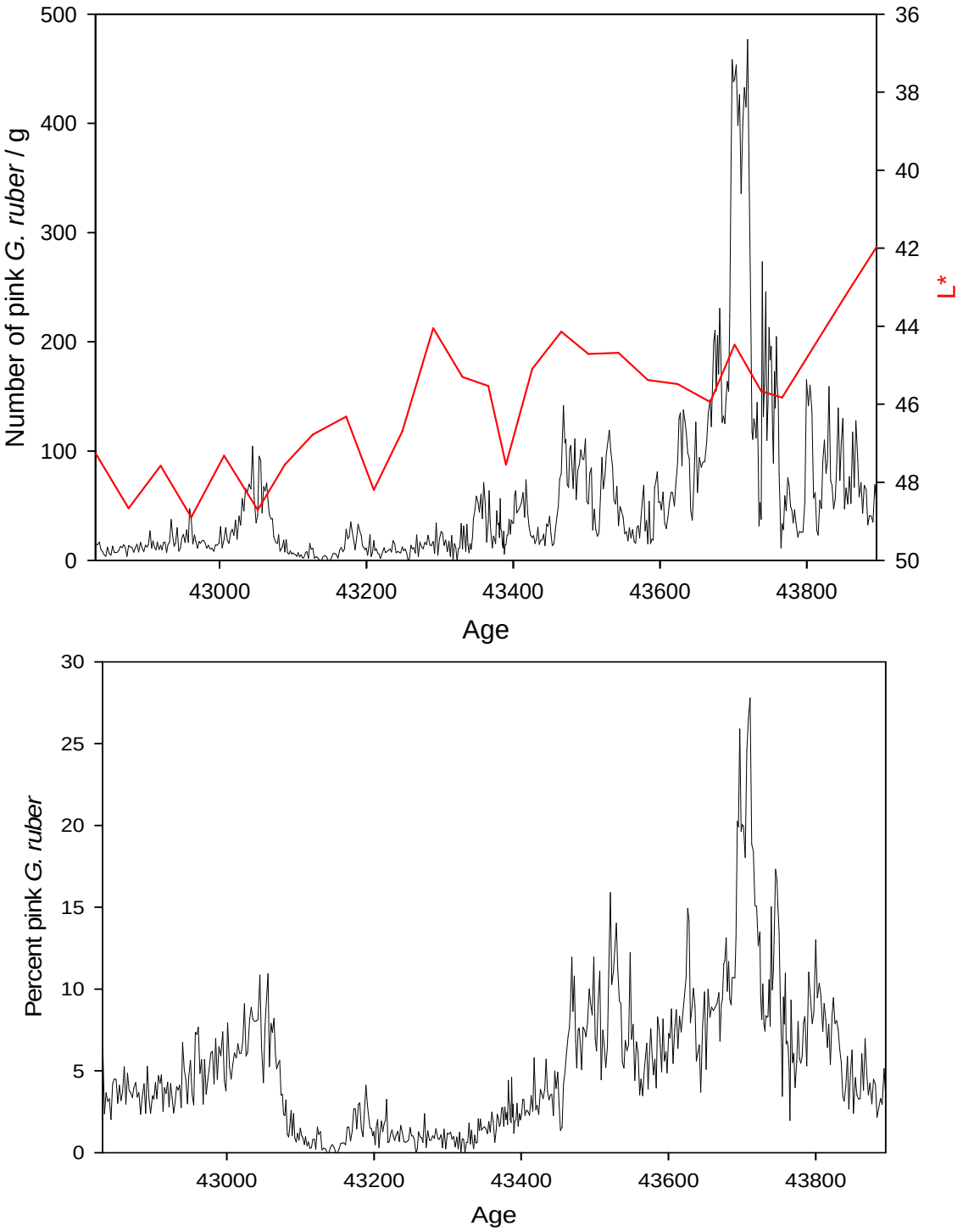

Figure 6.8: Pink *Globigerinoides ruber* absolute abundance (upper panel, reflectivity plotted in red) and relative abundance (lower panel) for the termination of Interstadial 12 (43,895 – 42,831 yBP). The relative abundance is expressed as a percentage value of the total counted foraminiferal population, while the absolute abundance represents the number of pink *G. ruber* normalized to per gram of dry sediment.

yBP, respectively. A maximum in absolute abundance of pink *G. ruber* for the Interstadial 12 termination record is reached at 43,710 yBP, with 477 pink *G. ruber*/g. The relative abundance of pink *G. ruber* (Figure 6.8, lower panel) peaks to almost 28% at 43,711 yBP. After a gradual decline to levels <1%, there is an abrupt increase to over 10% at 43,057 yBP. Values then decline gradually to around 3% for the remainder of the record.

6.2.9 *Globigerinoides sacculifer*

The absolute abundances of *G. sacculifer* (Figure 6.9, upper panel) are generally low throughout the termination of Interstadial 12 (<20 *G. sacculifer*/g), except for an abrupt peak in the middle of the record, when values come to a maximum of 422 *G. sacculifer*/g at 43,338 yBP.

At its peak in absolute abundance, *G. sacculifer* contributes over 17% to the total foraminiferal population (Figure 6.9, lower panel), while values are generally below 2% for the rest of the record. There is a gradual increase to around 5% at the very end of the Interstadial 12 termination, between 43,121 and 42,183 yBP.

6.2.10 *Globigerina rubescens*

Peaks in the absolute abundance of *G. rubescens* (Figure 6.10, upper panel), from 35 to 55 *G. rubescens*/g, occur in the beginning (before 43,710 yBP) and middle of the record, between 43,339 and 43,286 yBP. Absolute abundances remain <10 *G. rubescens*/g for all other times in the record of the termination of Interstadial 12.

The highest relative abundance of *G. rubescens* (Figure 6.10, lower panel) occurs at 43,866 yBP, when *G. rubescens* contributes just over 2.5% to the total foraminiferal population. Values remain low for the rest of the record, and are generally <1%.

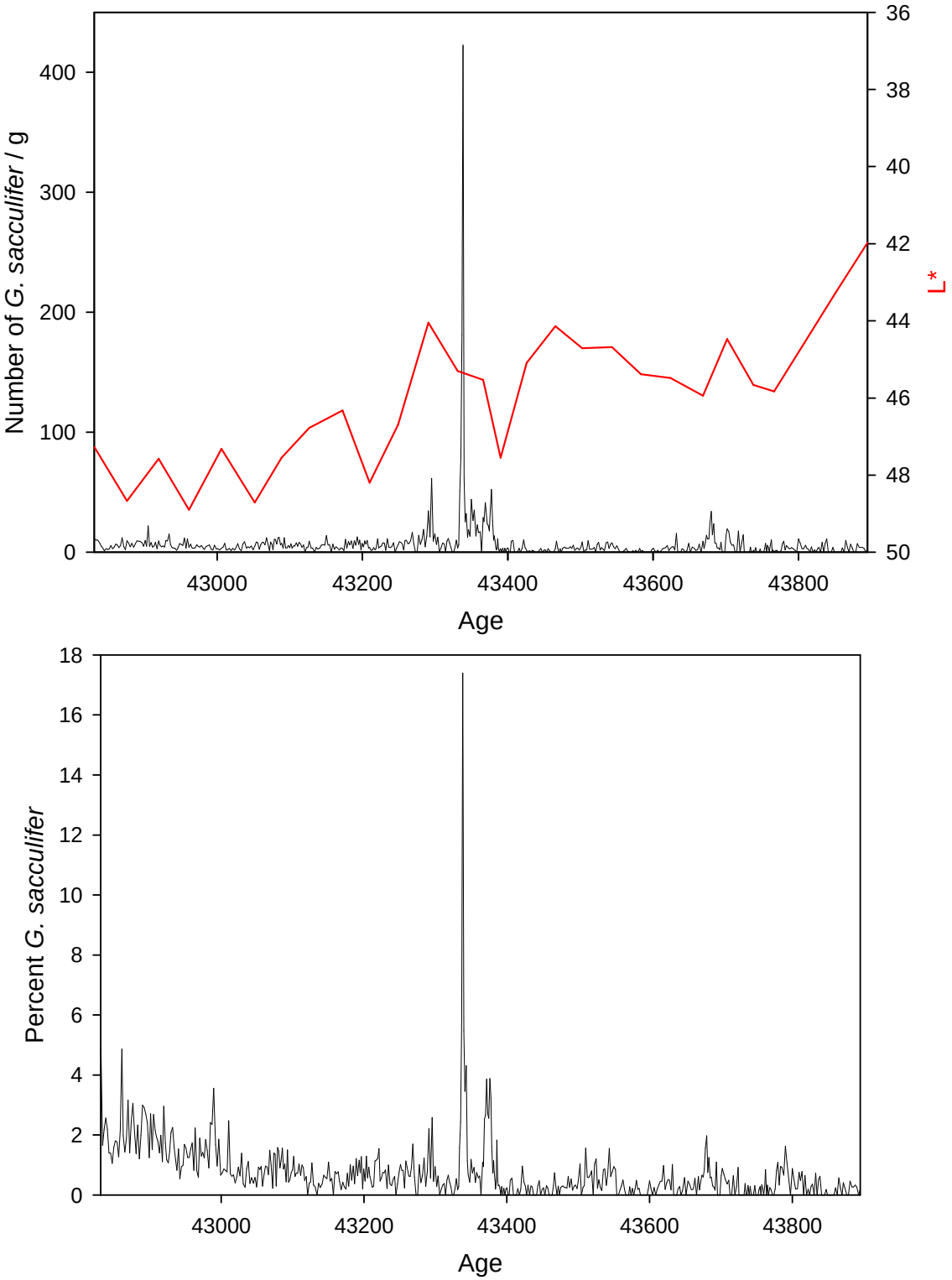

Figure 6.9: *Globigerinoides sacculifer* absolute abundance (upper panel, reflectivity plotted in red) and relative abundance (lower panel) for the termination of Interstadial 12 (43,895 – 42,831 yBP). The relative abundance is expressed as a percentage value of the total counted foraminiferal population, while the absolute abundance represents the number of *G. sacculifer* normalized to per gram of dry sediment.

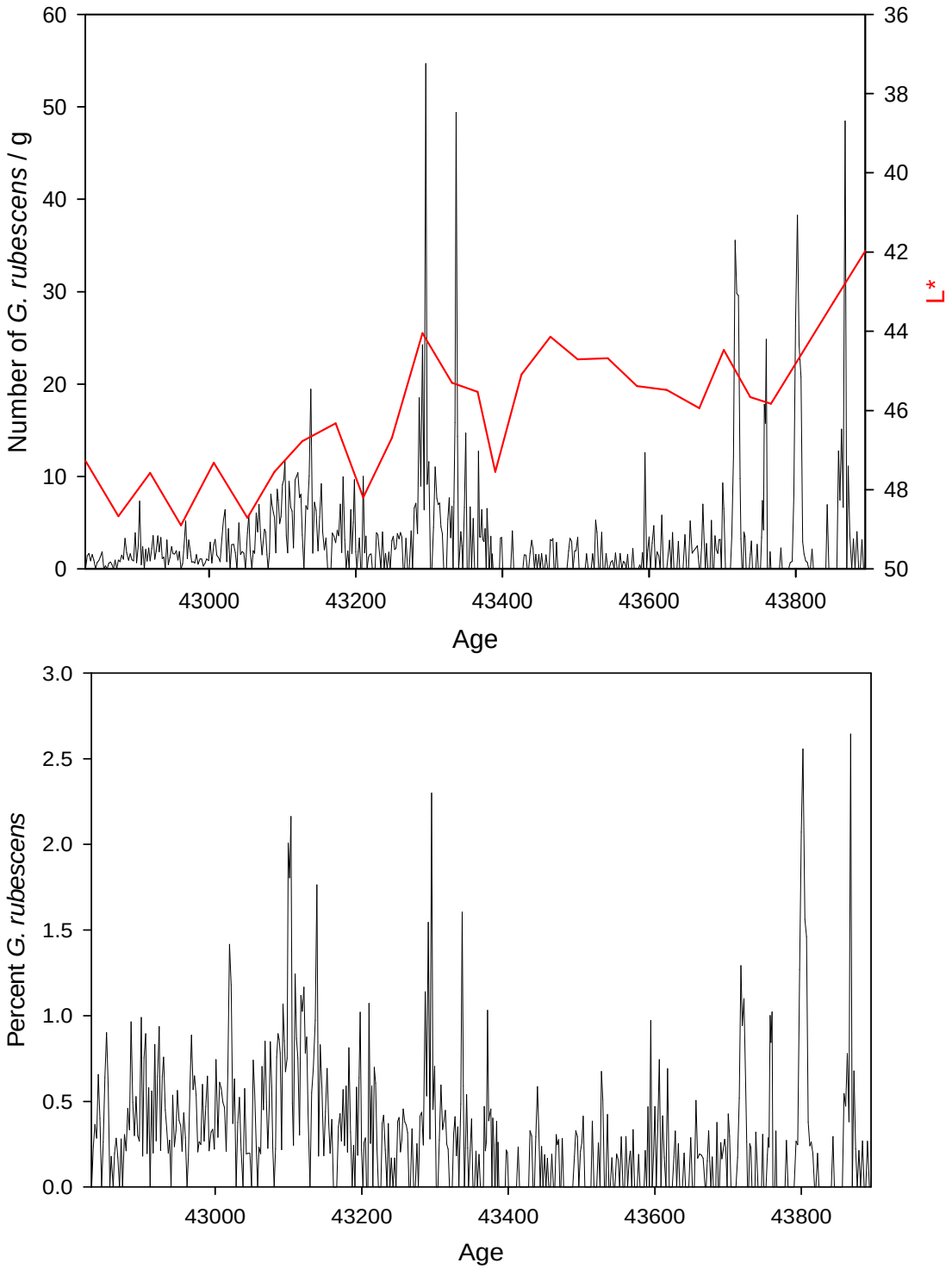

Figure 6.10: *Globigerina rubescens* absolute abundance (upper panel, reflectivity plotted in red) and relative abundance (lower panel) for the termination of Interstadial 12 (43,895 – 42,831 yBP). The relative abundance is expressed as a percentage value of the total counted foraminiferal population, while the absolute abundance represents the number of *G. rubescens* normalized to per gram of dry sediment.

6.2.11 *Globorotalia truncatulinoides*

Globorotalia truncatulinoides reaches its maximum absolute abundance (Figure 6.11, upper panel), 36 *G. truncatulinoides*/g, just into the record at 43,858 yBP. After this maximum, values are variable between 0 *G. truncatulinoides*/g and 41 *G. truncatulinoides*/g, but show a gradual decline throughout the remainder of the record.

In spite of *G. truncatulinoides* reaching its maximum absolute abundance in the beginning of the record, maximum relative abundances (Figure 6.11, lower panel) are reached at the very end of the termination of Interstadial 12. At this point, relative abundance values reach just over 1.5% at 42,850 yBP. Over the rest of the record, values are quite a low and generally do not reach over 1%.

6.2.12 *Globigerina quinqueloba*

The absolute abundance of *G. quinqueloba* (Figure 6.12, upper panel) remains low, ranging from 0 *G. quinqueloba*/g to almost 30 *G. quinqueloba*/g, for the first half of the period transitioning out of Interstadial 12. Values increase abruptly from the lower levels at 43,370 yBP to 87 *G. quinqueloba*/g at 43,335 yBP. After this point, absolute abundances of *G. quinqueloba* are more variable throughout the remainder of the record, ranging from 1 *G. quinqueloba*/g to just over 50 *G. quinqueloba*/g.

Despite its peak in absolute abundance at 43,355 yBP, *G. quinqueloba* contributes <2% to the total foraminiferal population until 43,293 yBP (Figure 6.12, lower panel). After this point, relative abundances increase gradually until a maximum of just over 12% is reached at 42,851 yBP, after which values drop abruptly.

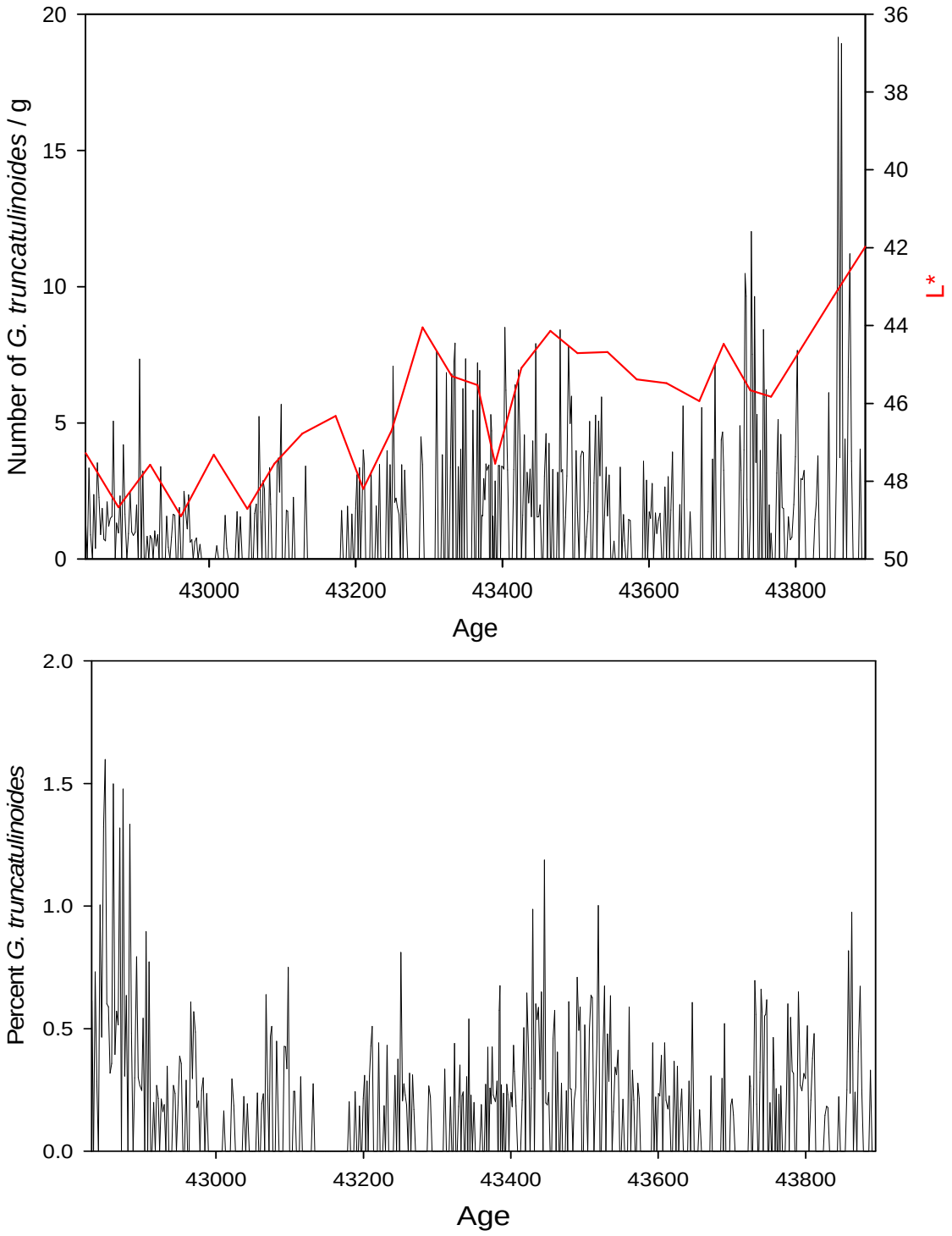

Figure 6.11: *Globorotalia truncatulinoides* absolute abundance (upper panel, reflectivity plotted in red) and relative abundance (lower panel) for the termination of Interstadial 12 (43,895 – 42,831 yBP). The relative abundance is expressed as a percentage value of the total counted foraminiferal population, while the absolute abundance represents the number of *G. truncatulinoides* normalized to per gram of dry sediment.

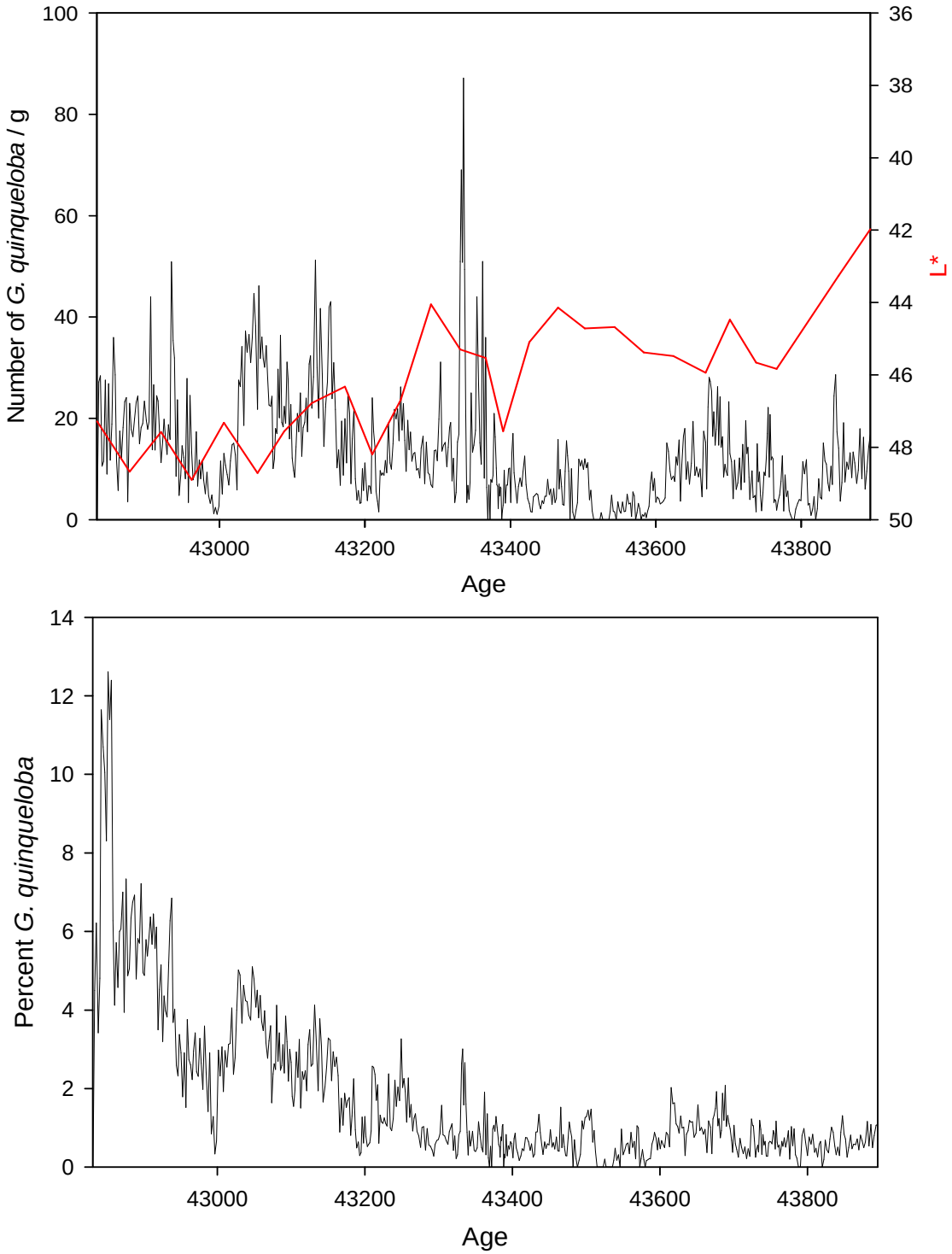

Figure 6.12: *Globigerina quinqueloba* absolute abundance (upper panel, reflectivity plotted in red) and relative abundance (lower panel) for the termination of Interstadial 12 (43,895 – 42,831 yBP). The relative abundance is expressed as a percentage value of the total counted foraminiferal population, while the absolute abundance represents the number of *G. quinqueloba* normalized to per gram of dry sediment.

6.2.13 *Pulleniatina obliquiloculata*

Pulleniatina obliquiloculata's presence is sporadic in the latter part of Interstadial 12 (Figure 6.13, upper panel), with absolute abundances of <4 *P. obliquiloculata*/g when it is present. When *P. obliquiloculata* is present in the assemblage, it contributes between <0.4% to the total foraminiferal population (Figure 6.13, lower panel).

6.3 Discussion

The latter portion of Interstadial 12 in MD03-2622 represents the gradual transition out of the interstadial and back to stadial conditions. As Interstadial 12 occurred after a Heinrich event, the sea level change at the onset of the interstadial was more abrupt and pronounced. Interstadial 12 is also the beginning for a longer-term Bond cycle, which is characteristic of a gradual, long-term cooling trend over the three or four interstadials following a Heinrich event (Bond et al., 1993). Sea level shows a similar trend, whereby a more abrupt and pronounced change occurred following a Heinrich event, and sea level gradually declined over the course of a few interstadial events (Siddall et al., 2003). Thus, while sea level rose between 20 and 30 m during the transition into Interstadial 12 (a level equivalent to 60 – 70 m below present levels), sea level regressed only ~10 m (a level equivalent to 70 – 80 m below present levels) throughout the gradual transition out of the interstadial (Siddall et al., 2003).

The discussion in this chapter will focus on the varying abundances of key foraminiferal species during the transition out of Interstadial 12 and the climatological forcing that may account for their patterns. Much of the background on species distributions and ecological preferences will be excluded from this discussion, as they

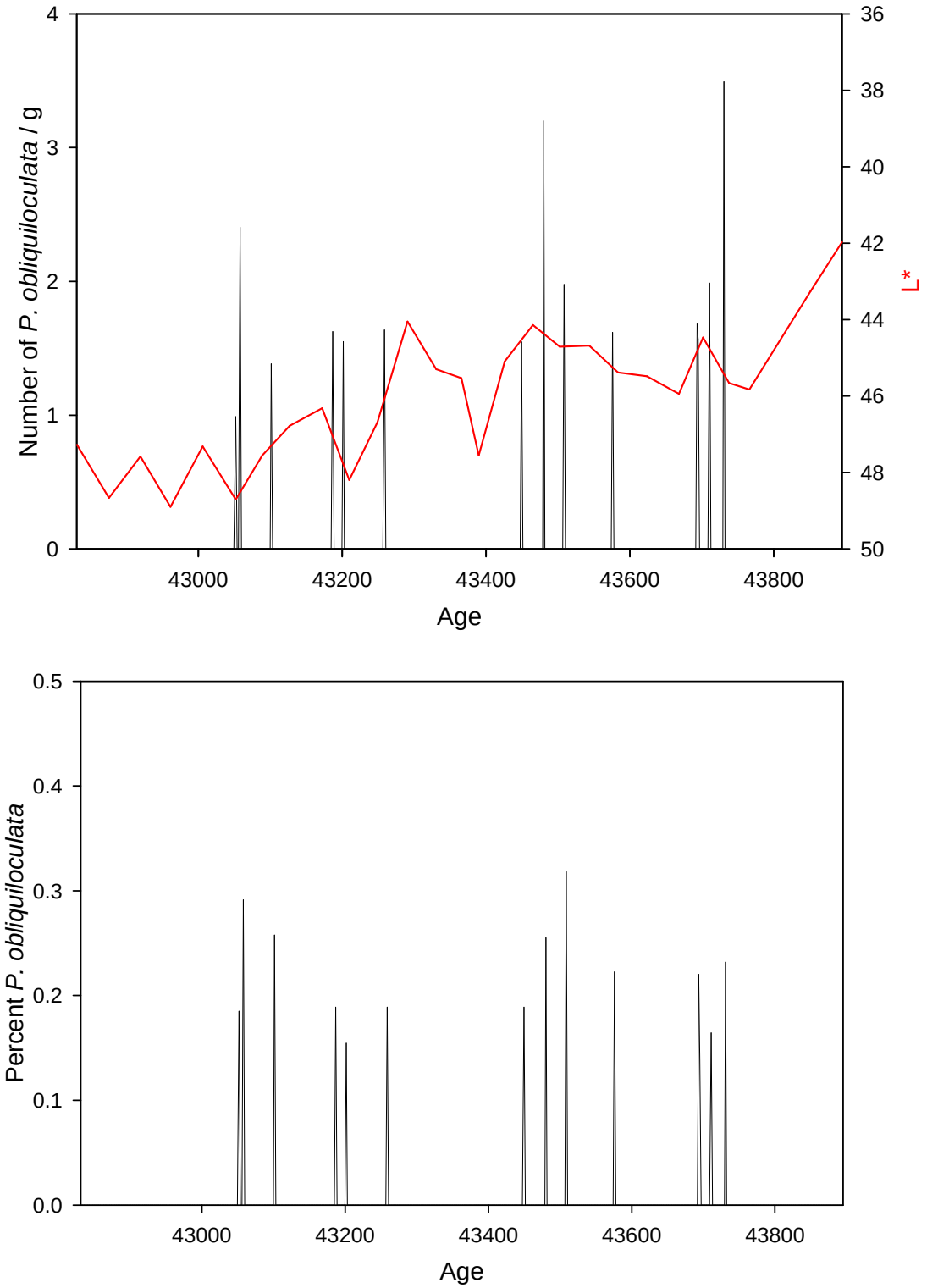

Figure 6.13: *Pulleniatinia obliquiloculata* absolute abundance (upper panel, reflectivity plotted in red) and relative abundance (lower panel) for the termination of Interstadial 12 (43,895 – 42,831 yBP). The relative abundance is expressed as percentage value of the total counted foraminiferal population, while the absolute abundance represents the number of P. *obliquiloculata* normalized to per gram of dry sediment.

were previously discussed in Chapter 5. In addition, most of this discussion will also only focus on those species that represent a significant proportion of the total foraminiferal population for the latter portion of Interstadial 12 and the transition back to stadial conditions.

6.3.1 The *Globigerina bulloides* Record and Supporting Species *Neogloboquadrina dutertrei* and *Orbulina universa*

The interpretation of the *G. bulloides* record for the onset of Interstadial 12 was not straightforward, as the transition into the interstadial was marked by rising sea level and a more northerly ITCZ average annual position. These competing influences contributed to a weakly correlated *G. bulloides* abundance record and sediment reflectivity record (Figure 5.1, upper panel). While still not entirely straightforward, the *G. bulloides* record for the latter part of Interstadial 12 and the transition back to stadial conditions more closely follows the sediment reflectance record (Figure 6.1, upper panel). Sediment reflectivity in the Cariaco Basin for the latter part of Interstadial 12 exhibits a gradual increase back to high sediment reflectance values characteristic of stadial periods (Figure 6.14). As sediment reflectivity is a proxy for surface productivity, this increase in reflectivity is interpreted as a gradual decline in productivity during the latter part of Interstadial 12 and the transition back to stadial conditions. The decline in productivity at the end of the interstadial is responsible for the transition back to oxic conditions in the basin, first noted by Peterson et al. (2000a). The improved similarity between the sediment reflectivity record and the *G. bulloides* abundance record indicates that the species' abundance fluctuations are likely related to upwelling-induced productivity fluctuations over the Cariaco Basin. A southern position for the ITCZ

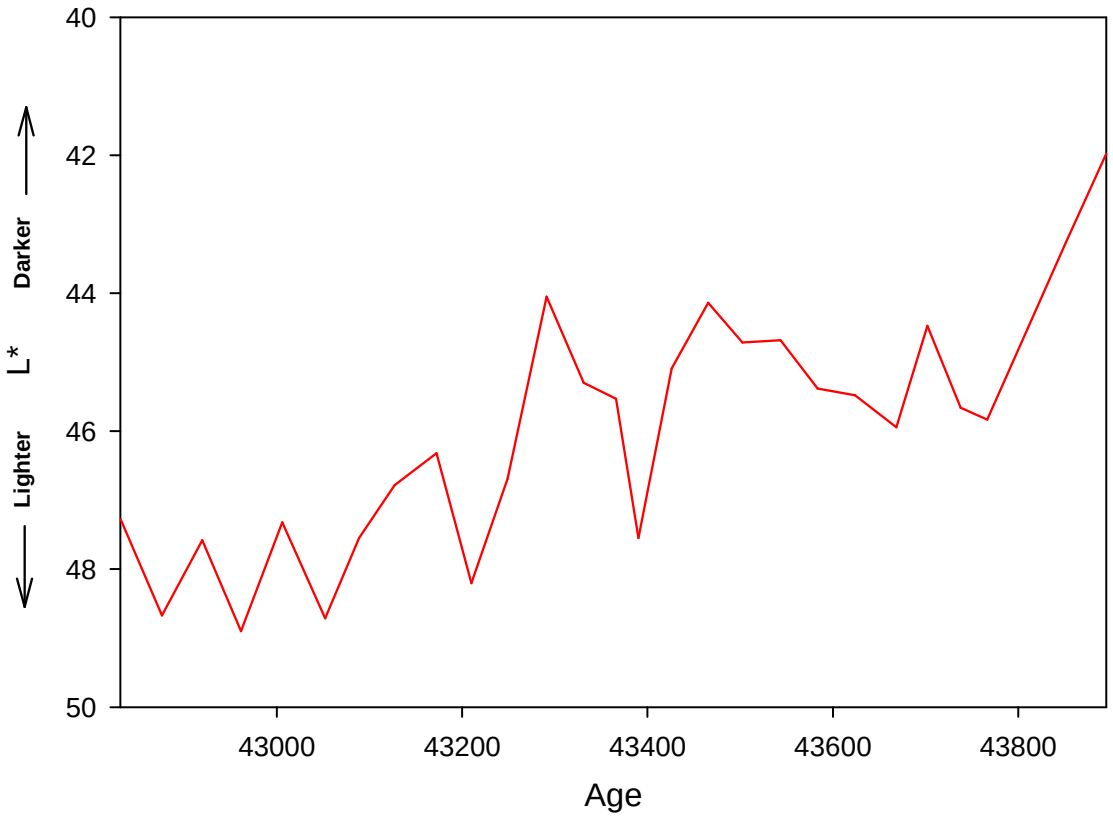

Figure 6.14: Sediment reflectivity measurements for the latter part of Interstadial 12 (43,895 – 42,831 yBP). Sediment color variations in the Cariaco Basin are driven by changing surface productivity, with increased organic rain leading to darker sediments (decreased reflectivity). Peterson et al. (2000) noted the deposition of dark sediments during warm interstadial times (e.g. Interstadial 12) and deposition of light-colored sediments during colder stadial intervals of the last glacial.

during stadials was suggested by Peterson et al. (2000a), thus the transition out of Interstadial 12 represents a time when the ITCZ was shifting from a more northerly ITCZ average annual position to a more southern one. As sea level did not decrease fully back to pre-Interstadial 12 levels at the transition out of the interstadial, a southern shift in the ITCZ would have initially enhanced upwelling over the basin. It has been shown that upwelling did occur in the basin when sea level was 60-70 m below present levels during the Younger Dryas event (Hughen et al, 1996; Fairbanks, 1989). It therefore seems probable that upwelling was a major contributing factor to *G. bulloides'* abundance for the latter part of Interstadial 12, as sea level declined from 60-70 m below present to 70-80 m below present at the termination of the interstadial.

Declining values for both *G. bulloides* abundance and sediment reflectivity after ~43,300 yBP may be due to sea level reaching a critical point for diminishing upwelling, as the basin was becoming progressively more isolated as sea level declined. Cooler North Atlantic SSTs (like those leading into and during stadials) result in increased surface pressure over the North Atlantic and a southward shift of the ITCZ (Hastenrath and Greischar, 1993), which under modern boundary conditions would drive stronger upwelling over the Cariaco Basin. Given the cooling over Greenland inferred from the GISP2 $\delta^{18}O$ data, we expect that North Atlantic SSTs would have cooled. One might predict more intense upwelling over the Cariaco Basin during stadial conditions as a result, however, nutrient limitations imposed by lower sea level and shallower sills appear to have kept stadial productivity low (Peterson et al., 2000a). This is not to say upwelling was necessarily reduced, but rather the water being upwelled was nutrient-depleted. In addition, the southward shift of the ITCZ during stadials acted to decrease

regional precipitation around the Cariaco Basin, resulting in a decrease in fluvially-derived nutrients.

Census data for *N. dutertrei* for the latter part of Interstadial 12 provides additional evidence that upwelling may have played a more important role in species' abundances following the height of the interstadial. As mentioned earlier in Chapter 5, the preferred habitat of *N. dutertrei* is a well stratified photic zone, however, the highest flux of *N. dutertrei* in the modern Cariaco Basin occurs during the spring upwelling season, when the highest chlorophyll values occur and the chlorophyll maximum shoals to around 0-25m (Tedesco and Thunell, 2003b; Muller-Karger et al., 2001). The record of *N. dutertrei* for the latter part of Interstadial 12 is nearly identical to the abundance record of *G. bulloides*, indicating that the same forcing mechanisms are likely driving the patterns seen in both records. As *G. bulloides* has been used in previous Cariaco Basin studies as an upwelling indicator (Overpeck et al., 1989; Peterson et al., 1991; Black et al., 1999), and the highest fluxes of *N. dutertrei* have been shown to occur during the upwelling season (Tedesco and Thunell, 2003b), it seems highly likely that enhanced upwelling during the latter part of Interstadial 12 is driving the variations in both species' abundance records. While *N. dutertrei* may prefer a highly stratified water column, it also inhabits a region close to the chlorophyll maximum, thus its response to upwelling during the latter part of Interstadial 12 may due to increased chlorophyll driven by enhanced upwelling.

As with *G. bulloides*, the abundance of *N. dutertrei* declines to much lower levels after ~43,300 yBP, indicating a weakening of the forcing mechanism responsible for both species' abundance records. As sea level was declining, the Cariaco Basin became

increasingly isolated from the Caribbean Sea, acting to restrict the exchange of surface waters. Thus, any upwelling that would have occurred once the basin became isolated would not have increased the abundances of *G. bulloides* and *N. dutertrei*, as nutrient-depleted waters were unable to leave the basin. Additional evidence for the basin becoming isolated at the termination of Interstadial 12 comes from a finding by Peterson et al. (2000a), who indicated that the transition out of Interstadial 12 was marked by a shift in the Cariaco basin from anoxic interstadial conditions to oxic stadial conditions. Despite being more restricted during stadials, the basin's deep waters were oxic due to decreased organic carbon export from the surface waters.

A third species that reinforces the notion of declining productivity in the Cariaco Basin at the transition back to stadial conditions is *Orbulina universa*. The abundance of *O. universa* for the latter portion of Interstadial 12 remains low until ~43,350 yBP, around which time the abundances of *G. bulloides* and *N. dutertrei* decline significantly. As *Orbulina universa* flourishes in nutrient depleted surface waters, the increase in *O. universa* serves as another example of a transition from high to low productivity in the Cariaco Basin during the transition out of Interstadial 12, which is likely related to the basin becoming increasingly isolated as sea level declined.

As was done for the *G. bulloides* abundance record for the onset of Interstadial 12, spectral analysis was performed on the *G. bulloides* abundance record for the latter part of Interstadial 12. The results revealed concentrations of variance in the interannual (4.3 years), decadal to interdecadal (14.5 – 15.5 years, 17 – 18 years, 20 – 21 years), and multicentennial (200 – 400 years) modes (Figure 6.15). Similar to the transition into

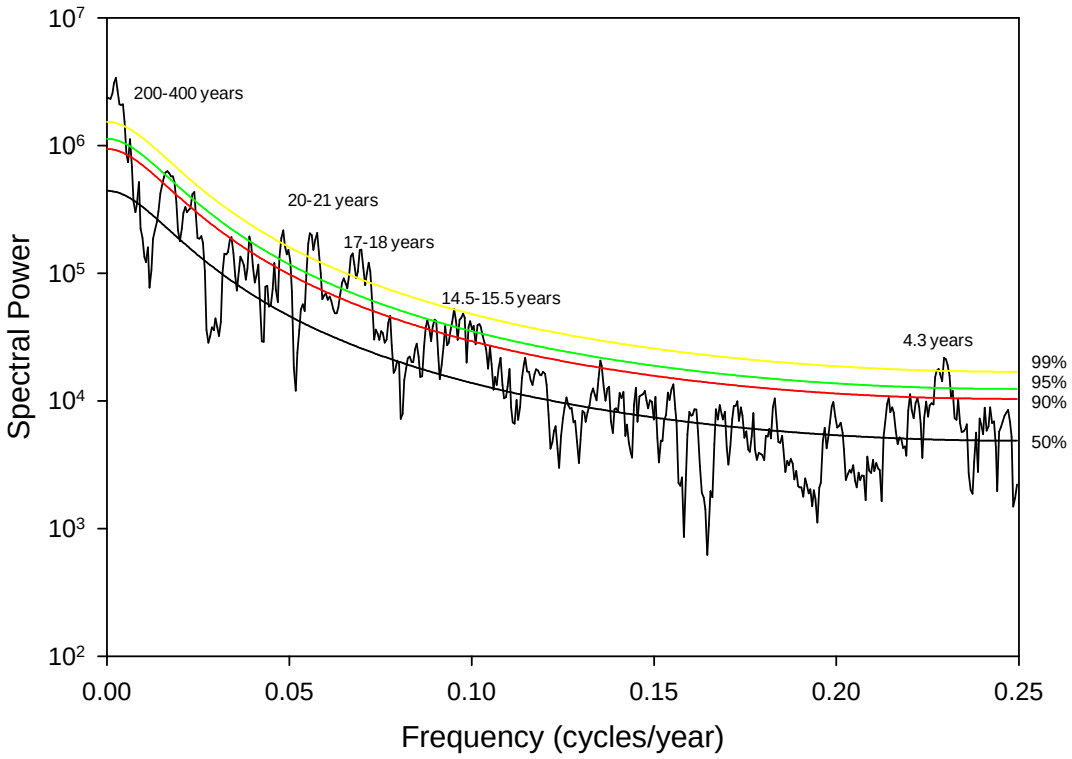

Figure 6.15: Spectral analysis results from the *Globigerina bulloides* absolute abundance time series for the termination of Interstadial 12 (43,895 to 42,831 yBP). Frequencies are converted to periodicities for peaks above the 99% confidence level.

Interstadial 12, the length of this record (1080 years) makes is difficult to infer anything significant from the multicentennial mode.

As stated in the discussion for Chapter 5, the interannual variance exhibited in the record is possibly related to the Atlantic Niño phenomenon. Given that the variability from 7.7 – 7.8 years in only present for the onset of Interstadial 12, it seems even more plausible that the interannual variance is really centered around 4.3 – 4.8 years, and the 7.7 – 7.8 year period of variability may be a harmonic of this. If the interannual variability is centered on 4.3 – 4.8 years, an Atlantic Niño type forcing is more likely than Pacific ENSO as the Atlantic Niño occurs more frequently than the Pacific ENSO (Wang, 2005). However, ENSO frequencies, if ENSO existed at this time, may have been different than they are today. Furthermore, the Atlantic Niño has an observed period range of 3-5 years (Chang et al., 2006), which is right at the edge of the Nyquist frequency for my samples, thus additional evidence would be needed to confirm the Atlantic Niño variability observed in the spectral analysis results.

It is significant to note the lack of a multidecadal period of variability in the spectral analysis results for the latter part of Interstadial 12 and the transition back into stadial conditions. Multidecadal-scale variability was also not evident in the earlier part of the record for the onset of Interstadial 12, a period when climate was still in cold stadial conditions. The latter part of Interstadial 12 represents a period of gradual cooling and the transition back into cold stadial conditions. The lack of multidecadal-scale variability provides additional evidence that AMO-type variability may only operate during warm climate periods, as the period matching the AMO was only present in the latter part of the record for the onset of Interstadial 12. It is important to note that

spectral analysis for the latter part of Interstadial 12 was performed on the whole time series, and not split into separate sections like was done for the onset of Interstadial 12. The exact point of transition out of the interstadial and back to stadial conditions is less well-defined, thus it is possible that AMO-type variability may have been significant in the latter part of Interstadial 12, but performing the analysis on the whole record weakened the significance of multidecadal-scale variability.

As was done for the onset of Interstadial 12, wavelet analysis was also performed on the *G. bulloides* absolute abundance record for the latter part of Interstadial 12 to see how significant periods of climate variability evolved during the transition back to stadial conditions. Wavelet analysis allowed for examining potential multidecadal scale variability in the earlier part of the record for the latter part of Interstadial 12, which spectral analysis did not allow for. The results revealed significant AMO-type variability in the earlier and middle sections of the record when climate was still substantially warmer than stadial conditions, but as climate transitioned back into cold stadial conditions, significant multidecadal-scale variability is not present (Figure 6.16). This provides yet more evidence that AMO-type variability may only operate during warmer climate periods.

Like the onset of Interstadial 12, the observed decadal and interdecadal modes of variability for the latter part of Interstadial 12 are periods which have no modern analogs, thus it is difficult to infer what climate phenomena they may be related to. Similarly, the periodicities also do not show up in other high resolution climate reconstructions. As stated earlier in Chapter 5, it may be that there was climate variability occurring on these scales during Interstadial 12 that we do not see in the modern climate system, or there are

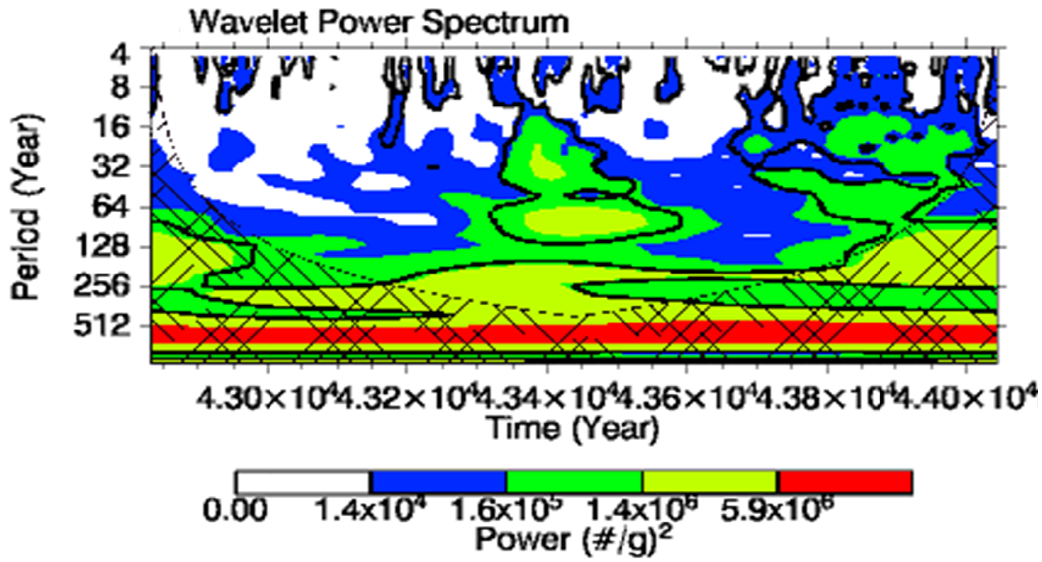

Figure 6.16: Wavelet analysis results for the *Globigerina bulloides* absolute abundance time series for the latter part of Interstadial 12 and the transition back to stadial conditions (42,831 to 43,895 yBP). Power outlined in black represents variability significant above the 99% confidence level. Variability under the black dotted line that is hatch marked is below the cone of influence, meaning no inferences can be made about the periods of variability in this region based on the length of the time series.

climate phenomena occurring on these periodicities in the modern climate system, but they have not yet been identified.

The results discussed above provide additional support for a gradual switch to a more southerly average annual position of the ITCZ during the latter part of Interstadial 12 and the transition back to stadial conditions. The foraminiferal census results imply a gradual decline in precipitation over the Cariaco Basin and surrounding regions as the ITCZ migrated to a more southerly position. Coincident with this, it would be expected that central South America experienced wetter conditions as the ITCZ would have been located further south over the South American landmass. Drier conditions would also be expected over northwest Africa as the ITCZ would have been pulled further south over the African landmass. The study by Burns et al. (2003) comparing $\delta^{18}O$ records of stalagmites collected from caves in China and Yemen showed that both records display a gradual shift to more positive $\delta^{18}O$ during the latter part of Interstadial 12, indicative of a gradual decline in precipitation in both locations. Given that both of these locations are well above the equator, it can be inferred that the ITCZ had shifted to a more southerly average annual position in these regions as well, resulting in reduced precipitation. Thus, the results of the Burns et al. (2003) study support the findings of this study that the ITCZ shifted south gradually during the latter part of the interstadial and the transition back to stadial conditions.

An important aspect of the north/south migration of the average annual position of the ITCZ throughout interstadial/stadial periods of the last glacial period is determining the forcing mechanism responsible for it. Solar insolation did not vary significantly during Interstadial 12, thus it is unlikely that this acted to influence the migration of the

ITCZ. Greenhouse gases may have played a role in modulation the extent of temperature changes across the interstadial, however, the resolution of existing records of greenhouse gases methane and carbon dioxide is too low to determine if gas levels were increasing prior to or following temperature changes in the high latitudes. A third possible forcing mechanism, and the one that seems most likely responsible, is related to variations in thermohaline circulation and Atlantic meridional overturning circulation. Reduced deepwater formation in the North Atlantic, which likely occurred during the last glacial period, would have acted to slow thermohaline circulation, reducing the export of warm, high salinity from the tropics and into the North Atlantic. A buildup of warm, high-salinity water in the equatorial Atlantic region would have weakened the Atlantic cross-equatorial sea surface temperature gradient and reduced the surface pressure gradient, leading to a southward displacement of the ITCZ. Eventually, the accumulating warm, high salinity water in the tropics would have kick-started the system to begin the rapid transport of the water to the high latitudes, leading to rapidly warming temperatures (interstadial conditions) (Broecker et al., 1990). Strengthened thermohaline circulation would have enhanced the Atlantic cross-equatorial sea surface temperature gradient, increasing the surface pressure gradient, leading to a northward displacement of the ITCZ.

6.3.2 The Abundance Records of Minor Contributing Species

The abundance records of white *G. ruber* and pink *G. ruber* remain relatively low through the latter part of Interstadial 12 and the transition back to stadial conditions, making a solid interpretation of their records difficult. While it is possible that their abundances may not be enough to provide insight on what climate was like during the

latter part of Interstadial 12, it could also be that we do not understand their ecologies well enough to make an interpretation.

The absolute abundances of white *G. ruber* remain low for the latter part of Interstadial 12, except for a few major peaks in the middle of the record. As white *G. ruber* has preferences for warm, saline water, these peaks may be due to sudden, abrupt declines in precipitation. The abundance records of both *G. bulloides* and *N. dutertrei* suggest that the ITCZ began a shift back to a more southerly stadial position, and as such, we would expect precipitation in and around the Cariaco Basin to decline. It seems unlikely that this shift occurred abruptly, and as such, an abrupt decline in precipitation is probably not a satisfactory explanation for white *G. ruber*'s abundance record.

As stated in the discussion for Chapter 5, the pink morphotype of *G. ruber* behaves quite differently than its white version. The records for both varieties for the transition out of Interstadial 12 are indeed both different, with the two species peaking to maximum absolute abundances ~400 years apart. The major peak in the pink *G. ruber* record for the latter part of Interstadial 12 occurs at the same time of high abundances of *G. bulloides* and *N. dutertrei*, indicating that the same forcing mechanism may be responsible for the patterns exhibited by all three species. However, the relationship drops off and pink *G. ruber* abundances remain low for the remainder of the transition out of Interstadial 12, while *G. bulloides* and *N. dutertrei* abundances remain high. It is interesting that the peak in pink *G. ruber* coincides with the first periods of maximum for *G. bulloides* and *N. dutertrei*, while white *G. ruber* is synchronous with the second peaks in abundance of *G. bulloides* and *N. dutertrei*. Conditions may have been more favorable

for pink *G. ruber* in the early part of the record, while white *G. ruber* flourished further into the transition back to stadial conditions.

6.4 Conclusions on Tropical Atlantic Climate Variability during the Latter Part of Interstadial 12

The foraminiferal abundance records for the latter part of Interstadial 12 and the transition back to stadial conditions suggest that the ITCZ began a gradual shift back to a southerly stadial position following the height of the interstadial. This acted to enhance upwelling in the Cariaco Basin, as seen by increases in both *G. bulloides* and *N. dutertrei*. The species' disconnect at the onset of the interstadial is likely due to the fact that changes were occurring abruptly as Interstadial 12 began, while the transition out of the interstadial occurred much more gradually. This makes it difficult to pinpoint exact forcing mechanisms as their responses to different modes of climate variability are not well known. In addition, as sea level gradually declined as the interstadial came to an end, the basin became progressively isolated, limiting exchange with Caribbean Sea water, which in turn facilitated an oligotrophic water column. Thus, as with the interpretation of the foraminiferal abundance records for the onset of Interstadial 12, the interpretation for this part of the interstadial is not entirely clear either, with competing forcing mechanisms of a southerly shift of the ITCZ and a gradually declining sea level. The results of the spectral analysis of the *G. bulloides* time series indicate significant tropical Atlantic variability on multiple time scales, ranging from interannual to interdecadal scale. The interannual period of variability provides additional evidence for an Altantic Niño-type oscillation during Interstadial 12, however, the resolution of the

record makes this a difficult determination. Multidecadal, AMO-type variability is not present in the full-record spectral analysis results, however, the results of wavelet analysis of the *G. bulloides* time series indicated a decline in multidecadal-scale variability as climate transitioned back into stadial conditions. The findings provide additional evidence that AMO-type variability may only operate during warm climate periods.

VII. Conclusions

This study is the first time a record capable of resolving subdecadal-scale variability has been created for an interstadial event in the tropical Atlantic, allowing for the examination of climate variability on these scales. The unusually high-resolution record allowed me to characterize the nature of interannual- to multicentennial-scale climate variability in the tropical Atlantic during a period of abrupt climate change and during a time when boundary conditions were very different from today. Climate variability on these scales, especially the role and response of the tropics, represents a major void in our understanding of the Earth's climate system. Interstadial 12 was used as a model for abrupt climate change as this time period is characterized by an estimated change in temperature over Greenland of over 10°C in a matter of a few hundred years (Landais et al., 2004). While the time period is not a perfect analogy for potential future anthropogenic climate change as the boundary conditions are not the same, examining climate variability during Interstadial 12 has provided us with the opportunity to understand how the climate system responds to a similar direction of change.

The chronology created for the Interstadial 12 portion of MD03-2622 was based on seasonal variations iron abundances in the Cariaco Basin, as seen from high-resolution sediment x-ray fluorescence data. The idea behind creating an age model in this way is the high iron input to the basin during the summer Venezuelan rainy season. Peaks in iron abundances were counted, with each peak representing a different year. A minimum and maximum number of peaks were counted and averaged as a way to take into account

that some years may have a stronger or weaker iron signal than others. The average number of peaks was then added to a starting date determined by a tie point between the MD03-2622 sediment reflectance record and the Greenland Ice Sheet Project 2 $\delta^{18}O$ record. This method of age model creation was successful, and is a quick, non-destructive way to create a high-resolution chronology. It is the first time that sediment chemical variations have been used to create an age model, and could prove to be critical for creating age models for other Cariaco Basin cores for intervals beyond the range of carbon-14 dating or for sediments whose laminae are too faint to count for a varve chronology. Still, it would be useful to try this method for studies of recent sediment and compare the carbon-14 dating method to that of an iron-based age model.

The results of the foraminiferal census study showed significantly different foraminiferal abundance patters for the onset and termination of Interstadial 12, and likely different forcing mechanisms responsible for their patterns. Interpreting the Interstadial 12 onset *Globogerina bulloides* abundance record was not straightforward due to the combined and competing effects of rising sea level on Ekman-induced upwelling within the Cariaco Basin and migrating ITCZ-associated variations in trade wind location and fluvial nutrient delivery to the basin. However, the *G. bulloides* data and the data from several supporting species support the notion of a rising sea level and a northward shift of the average annual position of the ITCZ at the onset of Interstadial 12. The abundance and reflectivity data suggests a northward shift in the ITCZ's annual average position of 600-700 miles in as little as a few centuries, with most of the shift occurring in less than 75 years. The *G. bulloides* record for the latter part of Interstadial 12, along with that of *Neogloboquadrina dutertrei,* provides evidence for a southward

shift of the ITCZ that drove enhanced upwelling over the Cariaco Basin. This upwelling was possible as sea level had not entirely retreated to pre-Interstadial 12 levels. However, as the interstadial came to an end and transitioned back to stadial conditions, the Cariaco basin became increasingly isolated from the open Caribbean Sea, and upwelling that was occurring in the basin was bringing nutrient depleted water to the surface, acting to decrease productivity within the basin.

Thus, the tropical Atlantic response to abrupt climate forcing was manifested by a shift in the average annual position of the ITCZ, and this likely had wide-reaching implications for the climatologies of other tropical regions. While the Cariaco Basin and surrounding regions, as well as Northwest Africa, experienced enhanced precipitation at the onset of Interstadial 12, regions in central South America were likely drier. The opposite likely occurred during the transition out of Interstadial 12, with northern South America and Northwest Africa experiencing drier conditions, while central South America received enhanced precipitation. The most probable potential forcing mechanism of a north/south migration of the ITCZ during the interstadial/stadial periods of the last glacial period is likely related to the surface expression of variation in Atlantic meridional overturning circulation.

Spectral analyses of the *G. bulloides* absolute abundance records for the onset and termination of Interstadial 12 were performed to identify possible forcing mechanisms and related linkages. The results confirmed the importance of interannual, interdecadal, and multidecadal scale variability in the tropical Atlantic, some of which are likely related to equatorial Atlantic Ocean dynamics, important air-sea interactions, and potential teleconnections. North Atlantic Oscillation-type climate variability may be

characteristic of the cold stadials of the last glacial period. In addition, Atlantic Niño-type variability may be related to the interannual variability observed throughout Interstaidial 12, however, the resolution of data collection impedes a conclusive finding here. In addition to the findings of the spectral analysis, wavelet analysis of the *G. bulloides* time series indicates significant Atlantic Multidecadal Oscillation (AMO)-type climate variability during the latter part of the onset of Interstadial 12, and in the early part of the transition out of the interstadial. This may indicate that AMO-type variability may only operate during warm climate periods, something that has significant implications for modern and near-future climate variability.

Future geochemical studies of the Interstadial 12 sediment from MD03-2622 may provide additional information on stadial and interstadial climate dynamics and water column characteristics. The Mg/Ca ratio of foraminiferal calcite will yield insight into Interstadial 12 sea surface temperatures, which may provide additional information on the tropical Atlantic expression of abrupt climate warming. Measuring the calcite $\delta^{18}O$ may provide additional support of north/south migrations of the ITCZ during the interstadials/stadials of the last glacial period, as the proxy can yield information on fresh water input to the basin during Interstadial 12 (via enhanced river drainage and precipitation). Additionally, it would be useful to complete the foraminiferal census study for the middle portion of Interstadial 12 that was not completed in this thesis. Doing so will create a longer, continuous record of the interstadial that will allow for the examination of centennial- and multicentennial-scale climate variability during Interstadial 12, as the shorter lengths of the two separate records created here prohibited this.

References

Alley, R. B., S. Anandakrishnan, and P. Jung (2001), Stochastic resonance in the North Atlantic, *Paleoceanography*, *16*(2), 190-198.

Alvera-Azcárate, A., A. Barth, and R. H. Weisberg (2009), A nested model of the Cariaco Basin (Venezuela): description of the basin's interior hydrography and interactions with the open ocean, *Ocean Dynamics*, *59*(1), 97-120.

Astor, Y., F. Muller-Karger, and M. I. Scranton (2003), Seasonal and interannual variation in the hydrography of the Cariaco Basin: implications for basin ventilation, *Continental Shelf Research*, *23*(1), 125-144.

Barker, S., P. Diz, M. J. Vautravers, J. Pike, G. Knorr, I. R. Hall, and W. S. Broecker (2009), Interhemispheric Atlantic seesaw response during the last deglaciation, *Nature*, *457*(7233), 1097-1102.

Bé, A. W. H. (1982), Biology of planktonic foraminifera, in *Foraminifera: Notes for a short course*, *Studies in Geology*, edited by T. Broadhead, University of Tennessee, 51-92.

Bé, A. W. H. and D. S. Tolderlund (1971), Distribution and ecology of living planktonic foraminifera in surface waters of the Atlantic and Indian Oceans, in B. M. Funnell and W. R. Riedel (eds.), *The Micropaleontology of the Oceans*, Cambridge University Press, Cambridge, United Kingdom, 105-149.

Beer, J., W. Mende, and R. Stellmacher (2000), The role of the sun in climate forcing, *Quaternary Science Reviews*, *19*(1-5), 403-415.

Bijma, J., W. W. Faber, and C. Hemleben (1990), Temperature and salinity limits for growth and survival of some planktonic foraminifera in laboratory cultures, *Journal of Foraminiferal Research*, *20*, 95-116.

Black, D. E., R. C. Thunell, and E. J. Tappa (2001), Planktonic foraminiferal response to the 1997-1998 El Nino: A sediment-trap record from the Santa Barbara Basin, *Geology*, *29*(12), 1075-1078.

Black, D. E., R. C. Thunell, A. Kaplan, L. C. Peterson, and E. J. Tappa (2004), A 2000-year record of Caribbean and tropical North Atlantic hydrographic variability, *Paleoceanography*, *19*(2).

Black, D. E., L. C. Peterson, J. T. Overpeck, A. Kaplan, M. N. Evans, and M. Kashgarian (1999), Eight centuries of North Atlantic Ocean atmosphere variability, *Science, 286*(5445), 1709-1713.

Black, D. E., M. A. Abahazi, R. C. Thunell, A. Kaplan, E. J. Tappa, and L. C. Peterson (2007), An 8-century tropical Atlantic SST record from the Cariaco Basin: Baseline variability, twentieth-century warming, and Atlantic hurricane frequency, *Paleoceanography, 22*.

Blunier, T., and E. J. Brook (2001), Timing of millennial-scale climate change in Antarctica and Greenland during the last glacial period, *Science, 291*(5501), 109-112.

Bond, G., W. Broecker, S. Johnsen, J. McManus, L. Labeyrie, J. Jouzel, and G. Bonani (1993), Correlations between climate records from North-Atlantic sediments and Greenland ice, *Nature, 365*(6442), 143-147.

Boyle, E. A. (2000), Is ocean thermohaline circulation linked to abrupt stadial/interstadial transitions?, *Quaternary Science Reviews, 19*(1-5), 255-272.

Broecker, W. S. (1994), Massive iceberg discharges as triggers for global climate-change, *Nature, 372*(6505), 421-424.

Broecker, W. S. (1997), Thermohaline circulation, the Achilles heel of our climate system: Will man-made CO2 upset the current balance?, *Science, 278*(5343), 1582-1588.

Broecker, W. S., G. Bond, M. Klas, G. Bonani, and W. Wolfli (1990), A salt oscillator in the glacial Atlantic? 1. The concept, Paleoceanography, 5, 469-477.

Cane, M. A. (1998), Climate change - A role for the tropical Pacific, *Science, 282*(5386), 59-61.

Cane, M. A. (2005), The evolution of El Nino, past and future, *Earth and Planetary Science Letters, 230*(3-4), 227-240.

Cane, M. A. and Clement, A. C. (1999), A role for the tropical Pacific coupled ocean-atmosphere system on Milankovitch and millennial timescales. Part II: Global impacts, in P.U. Clark, R.S. Webb, and L.D. Keigwin (eds.), *Mechanisms of Global Climate Change at Millennial Time Scales, Geophysical Monograph Series*, 112, American Geophysical Union, Washington, DC, 363 – 371.

Chang, P., L. Ji, and H. Li (1997), A decadal climate variation in the tropical Atlantic Ocean from thermodynamic air-sea interactions, *Nature, 385*(6616), 516-518.

Chang, P., T. Yamagata, P. Schopf, S. k. Behera, J. Carton, W. S. Kessler, G. Meyers, T. Qu, F. Schott, S. Shetye, and S. -P. Xie (2006), Climate fluctuations of tropical coupled systems - The role of ocean dynamics, *Journal of Climate, 19*, 5122-5174.

Chiang, J. C. H (2004), Present-day climate variability in the tropical Atlantic: a model for paleoclimate changes? In *The Hadley circulation: past, present, and future*, HF Diaz and R Bradley (eds), Springer, pp. 465-488

Chiang, J. C. H. (2009), The tropics in paleoclimate, *Annual Review of Earth and Planetary Sciences*, *37*, 263-297.

Chiang, J. C. H., Y. Kushnir, and A. Giannini (2002), Deconstructing Atlantic ITCZ variability: influence of the local cross-equatorial SST gradient, and remote forcing from the eastern equatorial Pacific, *Journal of Geophysical Research*, 107(D1).

Chiang, J. C. H., Y. Kushnir, and S. E. Zebiak (2000), Interdecadal changes in eastern Pacific ITCZ variability and its influence on the Atlantic ITCZ, *Geophysical Research Letters*, 27, 3687-3690.

Clement, A. C., and M. A. Cane (1999), A role for the tropical Pacific coupled ocean-atmosphere system on Milankovitch and millennial timescales. Part I: A modeling study of tropical Pacific variability, in P.U. Clark, R.S. Webb, and L.D. Keigwin (eds.), *Mechanisms of Global Climate Change at Millennial Time Scales, Geophysical Monograph Series*, 112, American Geophysical Union, Washington, DC, 363 – 371.

Clement, A. C., M. A. Cane, and R. Seager (2001), An orbitally driven tropical source for abrupt climate change, *Journal of Climate*, *14*(11), 2369-2375.

Curtis, J. H., D. A. Hodell, and M. Brenner (1996), Climate variability on the Yucatan Peninsula (Mexico) during the past 3500 years, and implications for Maya cultural evolution, *Quaternary Research*, *46*(1), 37-47.

Dansgaard, W., H. B. Clausen, N. Gundestrup, C. U. Hammer, S. F. Johnsen, P. M. Kristinsdottir, and N. Reeh (1982), A new Greenland deep ice core, *Science*, *218*(4579), 1273-1277.

Dansgaard, W., et al. (1993), Evidence for general instability of past climate from a 250-kyr ice-core record, *Nature*, *364*(6434), 218-220.

Delworth, T. L., and R. J. Greatbatch (2000), Multidecadal thermohaline circulation variability driven by atmospheric surface flux forcing, *Journal of Climate*, *13*(9), 1481-1495.

Deuser, W. G. (1987), Seasonal-variations in isotopic composition and deep-water fluxes of the tests of perennially abundant planktonic-foraminifera of the Sargasso Sea - Results from sediment-trap collections and their paleoceanographic significance, *Journal of Foraminiferal Research, 17*(1), 14-27.

Deuser, W. G. and E. H. Ross (1989), Seasonally abundant planktonic foraminifera of the Sargasso Sea: Succession, deep-water fluxes, isotopic composition, and paleoceanographic implications, *Journal of Foraminiferal Research, 19*, 268-293.

Dima, M., and G. Lohmann (2007), A hemispheric mechanism for the Atlantic multidecadal oscillation, *Journal of Climate, 20*(11), 2706-2719.

Eden, C., and J. Willebrand (2001), Mechanism of interannual to decadal variability of the North Atlantic circulation, *Journal of Climate, 14*(10), 2266-2280.

Elmore, A. C., R. C. Thunell, R. Styles, D. Black, R. W. Murray, N. Martinez, and Y. Astor (2009), Quantifying the seasonal variations in fluvial and eolian sources of terrigenous material to Cariaco Basin, Venezuela, *Journal of South American Earth Sciences, 27*(2-3), 197-210.

Enfield, D. B., and D. A. Mayer (1997), Tropical Atlantic sea surface temperature variability and its relation to El Nino Southern Oscillation, *Journal of Geophysical Research-Oceans, 102*(C1), 929-945.

Ericson, D. B., and G. Wollin (1956), Micropaleontological and isotopic determinations of Pleistocene climates, *Micropaleontology, 2*(3), 257-270.

Fairbanks, R. G., M. Sverdlove, R. Free, P. H. Wiebe, and A. W. H. Bé (1982), Vertical-distribution and isotopic fractionation of living planktonic-foraminifera from the Panama Basin, *Nature, 298*(5877), 841-844.

Faul, K. L., A. C. Ravelo, and M. L. Delaney (2000), Reconstructions of upwelling, productivity, and photic zone depth in the eastern equatorial Pacific Ocean using planktonic foraminiferal stable isotopes and abundances, *Journal of Foraminiferal Research, 30*(2), 110-125.

Ferraz-Reyes, E. (1983), Estudio del fitoplancton en la Cuenca Tuy-Cariaco, Venezuela, *Boletin del Instituto Oceanogragrafico de Venezuela Universidad de Oriente, 22,* 111-124.

Ghil, M., R. M. Allen, M. D. Dettinger, K. Ide, D. Kondrashov, M. E. Mann, A. Robertson, A. Saunders, Y. Tian, F. Varadi, and P. Yiou (2002), Advanced spectral methods for climatic time series, *Rev. Geophys., 40*(1), 3.1-3.41.

Gildor, H., and E. Tziperman (2000), Sea ice as the glacial cycles' climate switch: Role of seasonal and orbital forcing, *Paleoceanography, 15*(6), 605-615.

Goldenberg, S. B., C. W. Landsea, A. M. Mestas-Nunez, and W. M. Gray (2001), The recent increase in Atlantic hurricane activity: Causes and implications, *Science*, *293*(5529), 474-479.

González, C., and L. A. Dupont (2009), Tropical salt marsh succession as sea-level indicator during Heinrich events, *Quaternary Science Reviews*, *28*(9-10), 939-946.

González, C., L. M. Dupont, K. Mertens, and G. Wefer (2008), Reconstructing marine productivity of the Cariaco Basin during marine isotope stages 3 and 4 using organic-walled dinoflagellate cysts, *Paleoceanography*, *23*(3).

Hastenrath, S., and L. Greischar (1993), Further work on the prediction of Northeast Brazil rainfall anomalies, *Journal of Climate*, *6*(4), 743-758.

Haug, G. H., K. A. Hughen, D. M. Sigman, L. C. Peterson, and U. Röhl (2001), Southward migration of the intertropical convergence zone through the Holocene, *Science*, *293*(5533), 1304-1308.

Haug, G. H., T. F. Pedersen, D. M. Sigman, S. E. Calvert, B. Nielsen, and L. C. Peterson (1998), Glacial/interglacial variations in production and nitrogen fixation in the Cariaco Basin during the last 580 kyr, *Paleoceanography*, *13*(5), 427-432.

Haug, G. H., D. Gunther, L. C. Peterson, D. M. Sigman, K. A. Hughen, and B. Aeschlimann (2003), Climate and the collapse of Maya civilization, *Science*, *299*(5613), 1731-1735.

Hays, J. D., J. Imbrie, and N. J. Shackleton (1976), Variations in Earth's orbit - Pacemaker of ice ages, *Science*, *194*(4270), 1121-1132.

Heezen, B., R. Menzies, W. Broecker, and M. Ewing (1958), Date of stagnation of the Cariaco Trench, southeast Caribbean, *Bulletin of the Geological Society of America*, *67*, 1579.

Heezen, B., R. J. Menzies, W. S. Broecker, and M. Ewing (1959), Stagnation of the Cariaco Trench, in *International Oceanography Congress*, edited by M. Sears, Am. Assoc. for Adv. Sci., 99-102.

Heinrich, H. (1988), Origin and consequences of cyclic ice rafting in the Northeast Atlantic-Ocean during the past 130,000 years, *Quaternary Research*, *29*(2), 142-152.

Hemming, S. R. (2004), Heinrich events: Massive late pleistocene detritus layers of the North Atlantic and their global climate imprint, *Reviews of Geophysics*, *42*(1).

Hodell, D. A., M. Brenner, J. H. Curtis, and T. Guilderson (2001), Solar forcing of drought frequency in the Maya lowlands, *Science*, *292*(5520), 1367-1370.

Houghton, J.T., Ding, Y., Griggs, D.J., Noguer, M., van der Linden, P.J., Dai, X., Maskell, K., Johnson, C.A. (Eds.) (2001), *Climate Change 2001, The Scientific Basis*. Cambridge Univ. Press, Cambridge.

Huber, C., M. Leuenberger, R. Spahni, J. Fluckiger, J. Schwander, T. F. Stocker, S. Johnsen, A. Landals, and J. Jouzel (2006), Isotope calibrated Greenland temperature record over Marine Isotope Stage 3 and its relation to CH4, *Earth and Planetary Science Letters*, *243*(3-4), 504-519.

Hughen, K., J. Southon, S. Lehman, C. Bertrand, and J. Turnbull (2006), Marine-derived C-14 calibration and activity record for the past 50,000 years updated from the Cariaco Basin, *Quaternary Science Reviews*, *25*(23-24), 3216-3227.

Hughen, K., S. Lehman, J. Southon, J. Overpeck, O. Marchal, C. Herring, and J. Turnbull (2004), C-14 activity and global carbon cycle changes over the past 50,000 years, *Science*, *303*(5655), 202-207.

Hughen, K. A., D. P. Schrag, S. B. Jacobsen, and W. Hantoro (1999), El Niño during the last interglacial period recorded by a fossil coral from Indonesia, *Geophysical Research Letters*, *26*(20), 3129-3132.

Hughen, K. A., J. T. Overpeck, L. C. Peterson, and S. Trumbore (1996), Rapid climate changes in the tropical Atlantic region during the last deglaciation, *Nature*, *380*(6569), 51-54.

Hurrell, J.W., Y. Kushnir, M. Visbeck, and G. Ottersen, 2003, An overview of the North Atlantic Oscillation in *The North Atlantic Oscillation: Climate Significance and Environmental Impact*, J.W. Hurrell, Y. Kushnir, G. Ottersen, and M. Visbeck, Eds. *Geophysical Monograph Series*, 134, 1-35.

Imbrie, J., and N. G. Kipp (1971), A new micropaleontological method for quantitative paleoclimatology: Application to a late Pleistocene Caribbean core, in *The late Cenozoic glacial ages*, edited by K. Turekian, Yale University Press, New Haven, CT, 71-181.

Imbrie, J., et al. (1993), On the structure and origin of major glaciation cycles .2. The 100,000-year cycle, *Paleoceanography*, *8*(6), 699-735.

Jouzel, J., C. Lorius, J. R. Petit, C. Genthon, N. I. Barkov, V. M. Kotlyakov, and V. M. Petrov (1987), Vostok ice core - A continuous isotope temperature record over the last climatic cycle (160,000 years), *Nature*, *329*(6138), 403-408.

Kanfoush, S. L., D. A. Hodell, C. D. Charles, T. P. Guilderson, P. G. Mortyn, and U. S. Ninnemann (2000), Millennial-scale instability of the antarctic ice sheet during the last glaciation, *Science, 288*(5472), 1815-1818.

Kemle-von Mücke, S., and H. Oberhänsli (1999), The distribution of living planktonic foraminifera in relation to Southeast Atlantic oceanography, in *Use of Proxies in Paleoceanography: Examples from the South Atlantic*, edited by G. Fischer and G. Wefer, Springer-Verlag, Berlin, 91-115.

Kiefer, T. (1998), Produktivität und temperaturen im subtropischen Nordatlantik: zyklische und abrupte Veränderungen im späten Quartär, *Berichte-Reports 90*, Geologisch-Paläontologisches Institut, Christian-Albrechts Universität zu Kiel, Germany, pp. 127.

Kiefer, T., M. Sarnthein, H. Erlenkeuser, P. M. Grootes, and A. P. Roberts (2001), North Pacific response to millennial-scale changes in ocean circulation over the last 60 kyr, *Paleoceanography*, *16*(2), 179-189.

Kipp, N. G. (1971), New transfer function for estimating sea-surface conditions from sea-bed distribution of planktonic foraminiferal assemblages in the North Atlantic, in R. M. Cline and J. D. Hays (eds.), *Investigation of Late Quaternary Paleoceanography and Paleoclimatology, Mem. Geol. Soc. Amer., 145,* 3-42.

Kipp, N. G., and D. P. Towner (1975), The last millennium of climate: Foraminiferal records from coastal basin sediments, in *Proceedings of the WHO/IAMAP Symposium on Long-Term Climate Fluctuations*, World Meterological Organization, Geneva, 119-126.

Klein, S. A., B. J. Soden, and N. C. Lau (1999), Remote sea surface temperature variations during ENSO: Evidence for a tropical atmospheric bridge, *Journal of Climate*, *12*(4), 917-932.

Knight, J. R., C. K. Folland, and A. A. Scaife (2006), Climate impacts of the Atlantic Multidecadal Oscillation, *Geophysical Research Letters*, *33*(17).

Kudrass, H. R., A. Hofmann, H. Doose, K. Emeis, and H. Erlenkeuser (2001), Modulation and amplification of climatic changes in the Northern Hemisphere by the Indian summer monsoon during the past 80 k.y, *Geology*, *29*(1), 63-66.

Laj, C. (2004). Cruise report: MD 132 – P.I.C.A.S.S.O images XI, Fortaleza-Baltimore-Bresi, Mai Juin 2003, Institute Polaire Fr. Paul Emile Victor, Plouzané, France, pp. 53.

Landais, A., N. Caillon, C. Goujon, A. M. Grachev, J. M. Barnola, J. Chappellaz, J. Jouzel, V. Masson-Delmotte, M. Leuenberger (2004), Quantification of rapid temperature change during DO event 12 and phasing with methane inferred from air isotopic measurements, *Earth and Planetary Science Letters, 225*(1-2), 221-234.

Latif, M. and A. Grotzner (2000), The equatorial Atlantic oscillation and its response to ENSO, *Climate Dynamics, 16*(2-3), 213-218.

Lea, D. W., D. K. Pak, L. C. Peterson, and K. A. Hughen (2003), Synchroneity of tropical and high-latitude Atlantic temperatures over the last glacial termination, *Science, 301*(5638), 1361-1364.

Lidz, L., W. B. Charm, M. M. Ball, and S. Valdes (1969), Marine basins off coast of Venezuela, *Bulletin of Marine Science, 19*(1).

Lin, H. L., L. C. Peterson, J. T. Overpeck, S. E. Trumbore, and D. W. Murray (1997), Late Quaternary climate change from delta O-18 records of multiple species of planktonic foraminifera: High-resolution records from the anoxic Cariaco Basin, Venezuela, *Paleoceanography, 12*(3), 415-427.

Lorenzoni, L., R. C. Thunell, C. R. Benitez-Nelson, D. Hollander, N. Martinez, E. Tappa, R. Varela, Y. Astor, and F. E. Muller-Karger (2009), The importance of subsurface nepheloid layers in transport and delivery of sediments to the eastern Cariaco Basin, Venezuela, *Deep-Sea Research Part I-Oceanographic Research Papers*, *56*(12), 2249-2262.

Mann, M. E., and J. Park (1994), Global-scale modes of surface-temperature variability on interannual to century timescales, *Journal of Geophysical Research-Atmospheres, 99*(D12), 25819-25833.

Marshall, J., Y. Kushner, D. Battisti, P. Chang, A. Czaja, R. Dickson, J. Hurrell, M. McCartney, R. Saravanan, and M. Visbeck (2001), North Atlantic climate variability: Phenomena, impacts and mechanisms, *International Journal of Climatology, 21*(15), 1863-1898.

Martin, J. H. and S. E. Fitzwater (1988), Iron deficiency limits phytoplankton growth in the north-east Pacific subarctic, *Nature, 331*, 341-343.

Martinez, N. C., R. W. Murray, R. C. Thunell, L. C. Peterson, F. Muller-Karger, Y. Astor, and R. Varela (2007), Modern climate forcing of terrigenous deposition in the tropics (Cariaco Basin, Venezuela), *Earth and Planetary Science Letters, 264*(3-4), 438-451.

Martinez, N. C., R. W. Murray, R. C. Thunel, L. C. Peterson, F. Muller-Karger, L. Lorenzoni, Y. Astor, and R. Varela (2010), Local and regional geochemical signatures of surface sediments from the Cariaco Basin and Orinoco Delta, Venezuela, *Geology*, *38*(2), 159-162.

McConnell, M., Thunell, R., Peterson, L., and D. Black (2004), Tropical sea surface temperature variability during marine isotope stage 3: Mg/Ca results from the Cariaco Basin, Venezuela. *Eos Trans. AGU*, 85(47), Fall meeting supplement, Abstract OS33A-0579.

McConnell, M., Thunell, R., Peterson, L., and D. Black (2006), Timing and magnitude of tropical climate variability in the Cariaco Basin, Venezuela during marine isotope stage 3. *Eos Trans. AGU*, 87(52), Fall meeting supplement, Abstract PP13A-1586.

McConnell, M., Thunell, R., Peterson, L., Black, D., and D. Lea (2007), Tropical climate variability during Marine Isotope Stage 3: Results from the Cariaco Basin. *Eos Trans. AGU*, 88(52), Fall meeting supplement, Abstract OS43C-05.

McConnell, M., Thunell, R., Peterson, L., and Y. Astor (2008), Shell weight variability from the Cariaco Basin: Insights into carbon dioxide concentrations during the last glacial. *Eos Trans. AGU*, 89(53), Fall meeting supplement, Abstract PP41D-1478.

McConnell, M. C., R. C. Thunell, L. Lorenzoni, Y. Astor, J. D. Wright, and R. Fairbanks (2009), Seasonal variability in the salinity and oxygen isotopic composition of seawater from the Cariaco Basin, Venezuela: Implications for paleosalinity reconstructions, *Geochemistry Geophysics Geosystems*, 10.

Miró, M. (1971), Los foraminiferous planctonicos vivos y sedimentados del margen continental de Venezuela, *Acta Geologica Hispanica*, *VI*, 102-108.

Muller-Karger, F., et al. (2001), Annual cycle of primary production in the Cariaco Basin: Response to upwelling and implications for vertical export, *Journal of Geophysical Research-Oceans*, *106*(C3), 4527-4542.

Overpeck, J. T., L. C. Peterson, N. Kipp, J. Imbrie, and D. Rind (1989), Climate change in the circum-North Atlantic region during the last deglaciation, *Nature*, *338*(6216), 553-557.

Park, W., and M. Latif (2008), Multidecadal and multicentennial variability of the meridional overturning circulation, *Geophysical Research Letters*, *35*(22).

Peristykh, A. N., and P. E. Damon (2003), Persistence of the Gleissberg 88-year solar cycle over the last similar to 12,000 years: Evidence from cosmogenic isotopes, *Journal of Geophysical Research-Space Physics*, *108*(A1).

Peterson, L. C., and G. H. Haug (2006), Variability in the mean latitude of the Atlantic Intertropical Convergence Zone as recorded by riverine input of sediments to the Cariaco Basin (Venezuela), *Palaeogeography Palaeoclimatology Palaeoecology*, *234*(1), 97-113.

Peterson, L. C., J. T. Overpeck, N. G. Kipp, and J. Imbrie (1991), A high-resolution late Quaternary upwelling record from the anoxic Cariaco Basin, Venezuela, *Paleoceanography*, *6*(1), 99-119.

Peterson, L. C., G. H. Haug, K. A. Hughen, and U. Rohl (2000a), Rapid changes in the hydrologic cycle of the tropical Atlantic during the last glacial, *Science*, *290*(5498), 1947-1951.

Peterson, L. C., G. H. Haug, R. W. Murray, K. M. Yarincik, J. W. King, T. J. Bralower, K. Kameo, S. D. Rutherford, and R. B. Pearce (2000b), Late Quaternary stratigraphy and sedimentation at ODP Site 1002, Cariaco Basin (Venezuela), in *Proc. ODP. Scientific Results*, edited by R. M. Leckie, H. Sigurdsson, G. D. Acton and G. Draper, College Station TX (Ocean Drilling Program), 85-99.

Philander, S. G. (1999), El Nino and La Nina predictable climate fluctuations, *Reports on Progress in Physics*, *62*(2), 123-142.

Philander, S. G. (1990), *El Nino, La Nina and the Southern Oscillation*, International Geophysics Series, 46, Academic Press.

Philander, S. G. (1983), El-Nino Southern Oscillation phenomena, *Nature*, *302*(5906), 295-301.

Pierrehumbert, R.T. (2000), Climate change and the tropical Pacific: The sleeping dragon wakes. *Proceedings of the National Academy of Sciences*, 97, 1355 – 1358.

Prance, G. T. (ed.) (1982), Biological diversification in the tropics. New York: Columbia University Press.

Prell, W. L. and W. B. Curry (1981), Faunal and isotopic indices of monsoonal upwelling: Western Arabian Sea, *Oceanologica Acta*, *4*, 91-98.

Rahmstorf, S. (1994), Rapid climate transitions in a coupled ocean-atmosphere model, *Nature*, *372*(6501), 82-85.

Rahmstorf, S. (1995), Bifurcations of the Atlantic thermohaline circulation in response to changes in the hydrological cycle, *Nature*, *378*(6553), 145-149.

Reynolds, L., and R. C. Thunell (1985), Seasonal succession of planktonic-foraminifera in the subpolar North Pacific, *Journal of Foraminiferal Research*, *15*(4), 282-301.

Richards, F. A. (1975), The Cariaco Basin (trench), *Oceanography and Marine Biology: An Annual Review*, *13*, 11-67.

Roberts, A. P., B. Lehman, R. J. Weeks, K. L. Verosub, and C. Laj (1997), Relative paleointensity of the geomagnetic field over the last 200,000 years from ODP Sites 883 and 884, North Pacific Ocean, *Earth and Planetary Science Letters*, *152*(1-4), 11-23.

Rohling, E. J., K. Grant, C. Hemleben, M. Kucera, A. P. Roberts, I. Schmeltzer, H. Schulz, M. Siccha, M. Siddall, and G. Trommer (2008), New constraints on the timing of sea level fluctuations during early to middle marine isotope stage 3, *Paleoceanography*, *23*(3).

Sachs, J. P., and S. J. Lehman (1999), Subtropical North Atlantic temperatures 60,000 to 30,000 years ago, *Science*, *286*(5440), 756-759.

Schmidt, M. W., M. J. Vautravers, and H. J. Spero (2006), Rapid subtropical North Atlantic salinity oscillations across Dansgaard-Oeschger cycles, *Nature*, *443*(7111), 561-564.

Schubert, C. (1982), Origin of Cariaco Basin, Southern Caribbean Sea, *Marine Geology*, *47*(3-4), 345-360.

Scranton, M. I., M. McIntyre, G. T. Taylor, F. Muller-Karger, K. Fanning, and Y. Astor (2006), Temporal variability in the nutrient chemistry of the Cariaco Basin, in *Past and Present Marine Water Column Anoxia*, edited by L. N. Neretin, Springer Press, 139-160

Shackleton, N. J. (2000), The 100,000-year ice-age cycle identified and found to lag temperature, carbon dioxide, and orbital eccentricity, *Science*, *289*(5486), 1897-1902.

Siddall, M., E. J. Rohling, W. G. Thompson, and C. Waelbroeck (2008), Marine Isotope Stage 3 sea level fluctuations: Data synthesis and new outlook, *Reviews of Geophysics*, *46*(4).

Siddall, M., E. J. Rohling, A. Almogi-Labin, C. Hemleben, D. Meischner, I. Schmelzer, and D. A. Smeed (2003), Sea-level fluctuations during the last glacial cycle, *Nature*, *423*(6942), 853-858.

Stauffer, B., et al. (1998), Atmospheric CO_2 concentration and millennial-scale climate change during the last glacial period, *Nature*, *392*(6671), 59-62.

Stuiver, M., and T. F. Braziunas (1993), Modeling atmospheric C-14 influences and C-14 ages of marine samples to 10,000 BC, *Radiocarbon*, *35*(1), 137-189.

Stuiver, M., and P. M. Grootes (2000), GISP2 oxygen isotope ratios, *Quaternary Research*, *53*(3), 277-283.

Sutton, R. T., S. P. Jewson, and D. P. Rowell (2000), The elements of climate variability in the tropical Atlantic region, *Journal of Climate*, *13*(18), 3261-3284.

Tedesco, K. A., and R. C. Thunell (2003a), High resolution tropical climate record for the last 6,000 years, *Geophysical Research Letters*, *30*(17).

Tedesco, K. A., and R. C. Thunell (2003b), Seasonal and interannual variations in planktonic foraminiferal flux and assemblage composition in the Cariaco Basin, Venezuela, *Journal of Foraminiferal Research*, *33*(3), 192-210.

Thiede, J. (1975), Distribution of foraminifera in surface waters of a coastal upwelling area, *Nature*, *253*(5494), 712-714.

Thompson, P. R., and N. J. Shackleton (1980), North Pacific paleo-oceanography - Late Quaternary coiling variations of planktonic foraminifer *Neogloboquadrina pachyderma*, *Nature*, *287*(5785), 829-833.

Thunell, R. C., and L. A. Reynolds (1984), Sedimentation of planktonic-foraminifera - Seasonal-changes in species flux in the Panama Basin, *Micropaleontology*, *30*(3), 243-262.

Torrence, C. and G. P. Compo (1998), A Practical Guide to Wavelet Analysis, *Bull. Amer. Meteor. Soc.*, 79, 61-78.

Tudhope, A. W., C. P. Chilcott, M. T. McCulloch, E. R. Cook, J. Chappell, R. M. Ellam, D. W. Lea, J. M. Lough, and G. B. Shimmield (2001), Variability in the El Niño-Southern Oscillation through a glacial-interglacial cycle, *Science*, *291*(5508), 1151-1517.

Vellinga, M., and P. L. Wu (2004), Low-latitude freshwater influence on centennial variability of the Atlantic thermohaline circulation, *Journal of Climate*, *17*(23), 4498-4511.

Viles, H. A., and A. S. Goudie (2003), Interannual, decadal and multidecadal scale climatic variability and geomorphology, *Earth-Science Reviews*, *61*(1-2), 105-131.

Visbeck, M., Chassignet, E. P., Curry, R. G., Delworth, T. L., Dickson, R. R., & Krahmann, G., 2003, The ocean's response to North Atlantic Oscillation variability *in The North Atlantic Oscillation: Climatic Significance and Environmental Impact, Geophysical Monograph 134*, AGU, 113-145.

Visbeck, M. H., J. W. Hurrell, L. Polvani, and H. M. Cullen (2001), The North Atlantic Oscillation: Past, present, and future, *Proceedings of the National Academy of Sciences of the United States of America*, *98*(23), 12876-12877.

Voelker, A. H. L. (2002), Global distribution of centennial-scale records for Marine Isotope Stage (MIS) 3: a database, *Quaternary Science Reviews*, *21*(10), 1185-1212.

Wang, C. (2005), ENSO, Atlantic climate variability, and the Walker and Hadley circulations, in H. F. Diaz and R. S. Bradley, *The Hadley Circulation: Present, Past and Future*, Kluwer Academic Publishers, Netherlands, 173-202.

Wang, C. (2002), Atlantic climate variability and its associated atmospheric circulation cells, *Journal of Climate, 15*, 1516-1536.

Wang, H. J., R. H. Zhang, J. Cole, and F. Chavez (1999), El Nino and the related phenomenon Southern Oscillation (ENSO): The largest signal in interannual climate variation, *Proceedings of the National Academy of Sciences of the United States of America*, *96*(20), 11071-11072.

Wang, Y. J., H. Cheng, R. L. Edwards, Z. S. An, J. Y. Wu, C. C. Shen, and J. A. Dorale (2001), A high-resolution absolute-dated Late Pleistocene monsoon record from Hulu Cave, China, *Science*, *294*(5550), 2345-2348.

Yarincik, K. M., R. W. Murray, and L. C. Peterson (2000b), Climatically sensitive eolian and hemipelagic deposition in the Cariaco Basin, Venezuela, over the past 578,000 years: Results from Al/Ti and K/Al, *Paleoceanography*, *15*(2), 210-228.

Yarincik, K. M., R. W. Murray, T. W. Lyons, L. C. Peterson, and G. H. Haug (2000a), Oxygenation history of bottom waters in the Cariaco Basin, Venezuela, over the past 578,000 years: Results from redox-sensitive metals (Mo, V, Mn, and Fe), *Paleoceanography*, *15*(6), 593-604.

Zabel, M., T. Wagner, and P. deMenocal (2003), Terrigenous signals in sediments of the low-latitude Atlantic – indications to environmental variations during the late quaternary: Part II: Lithogenic matter, *Sonderforschungsbereich*, *261*, 323–345.

Appendix I: Split core photographs of MD03-2622 and the marked intervals containing evidence of microturbidite deposition. See table 4.1 for additional information.

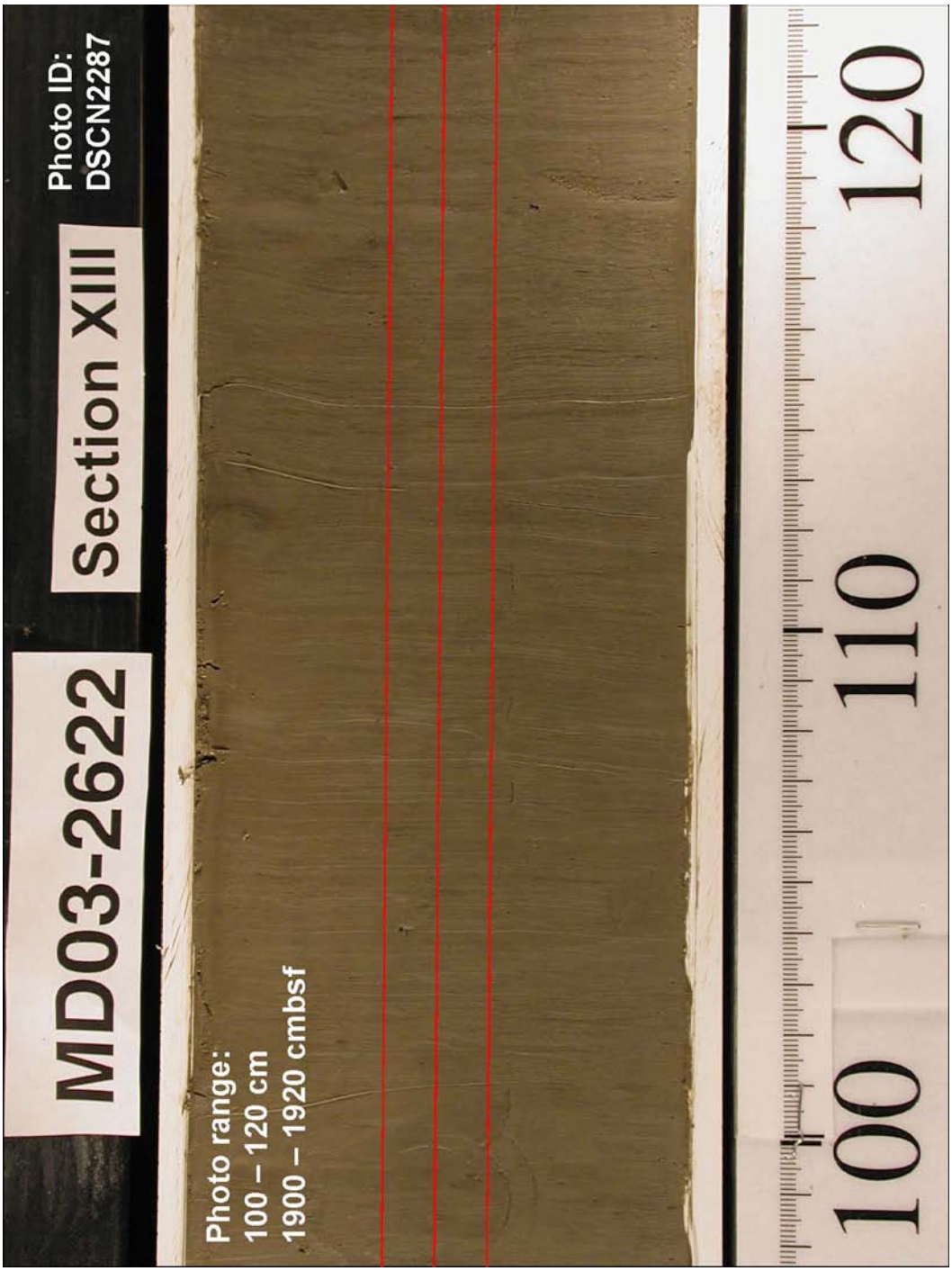

Split core photographs of MD03-2622 and the marked intervals containing evidence of microturbidite deposition. See table 4.1 for additional information. (continued)

Split core photographs of MD03-2622 and the marked intervals containing evidence of microturbidite deposition. See table 4.1 for additional information. (continued)

Split core photographs of MD03-2622 and the marked intervals containing evidence of microturbidite deposition. See table 4.1 for additional information. (continued)

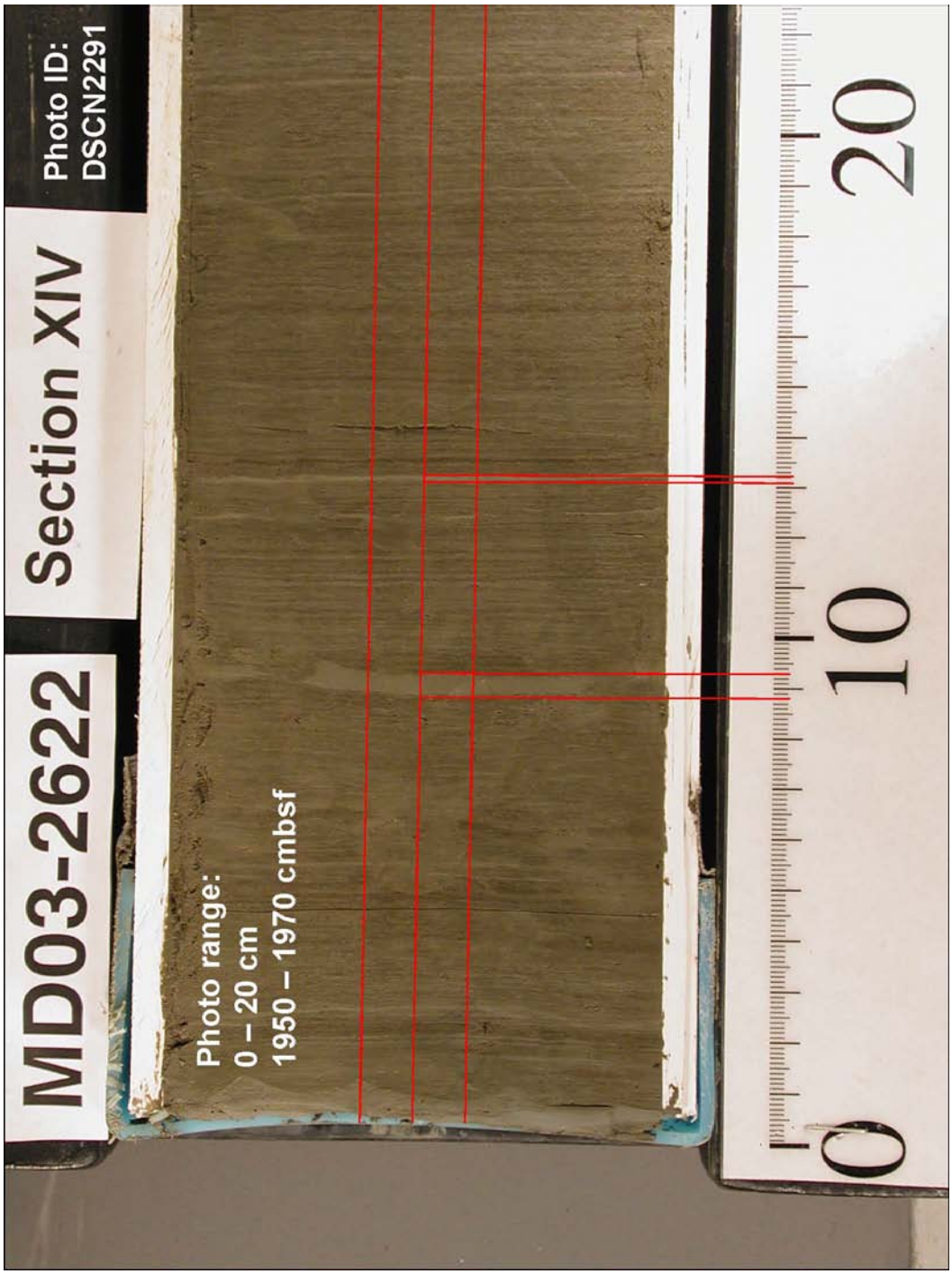

Split core photographs of MD03-2622 and the marked intervals containing evidence of microturbidite deposition. See table 4.1 for additional information. (continued)

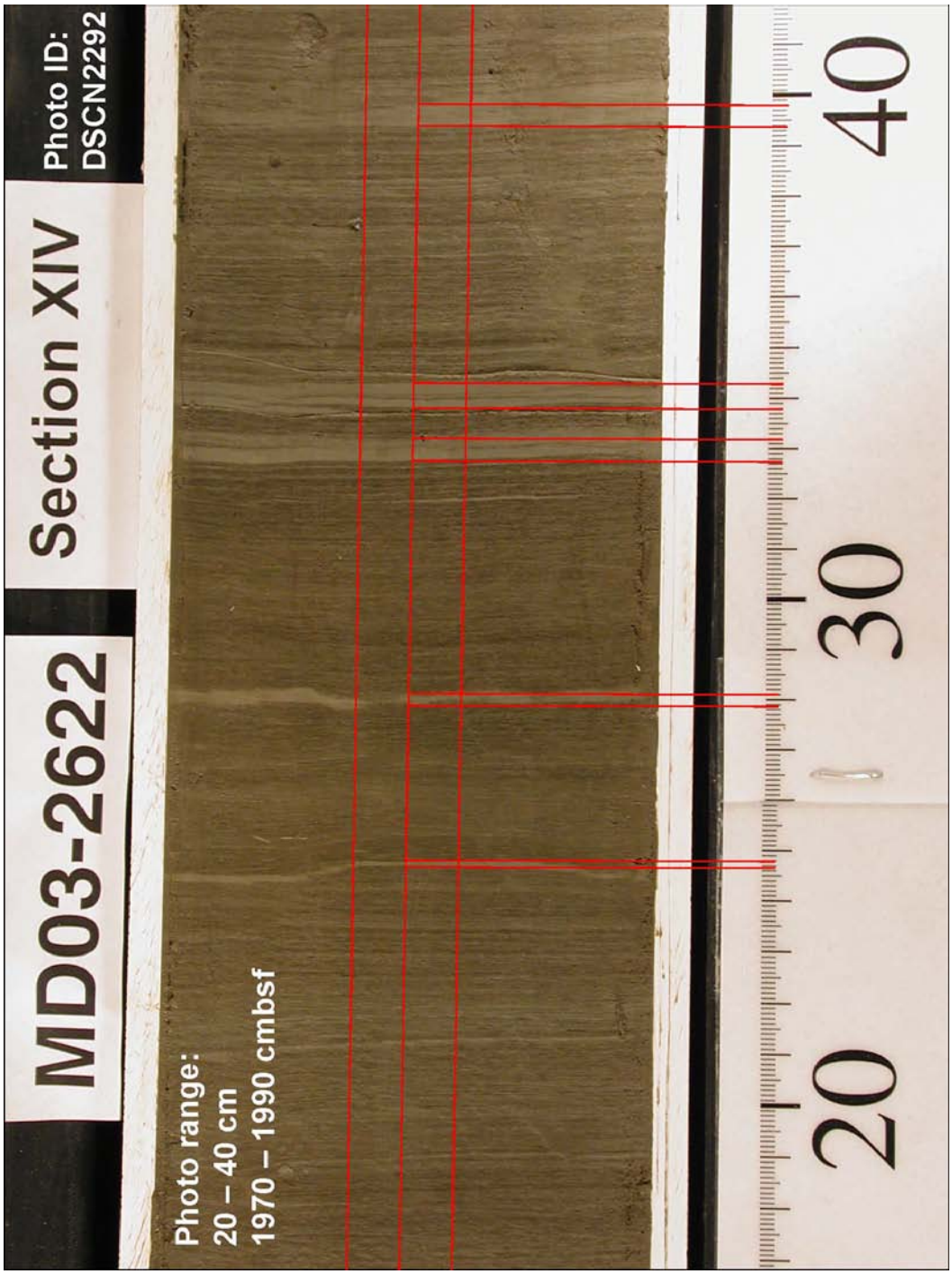

Split core photographs of MD03-2622 and the marked intervals containing evidence of microturbidite deposition. See table 4.1 for additional information. (continued)

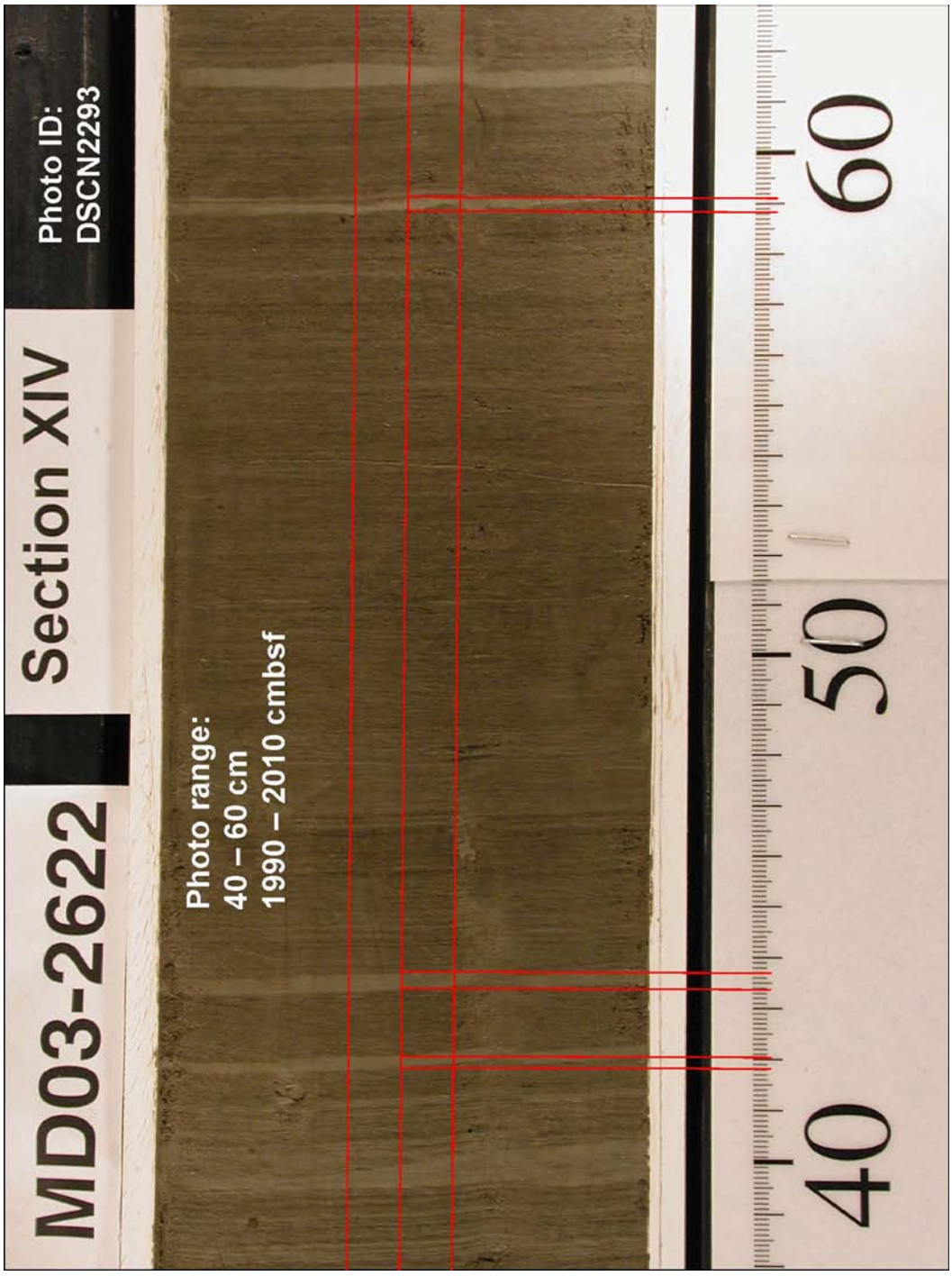

Split core photographs of MD03-2622 and the marked intervals containing evidence of microturbidite deposition. See table 4.1 for additional information. (continued)

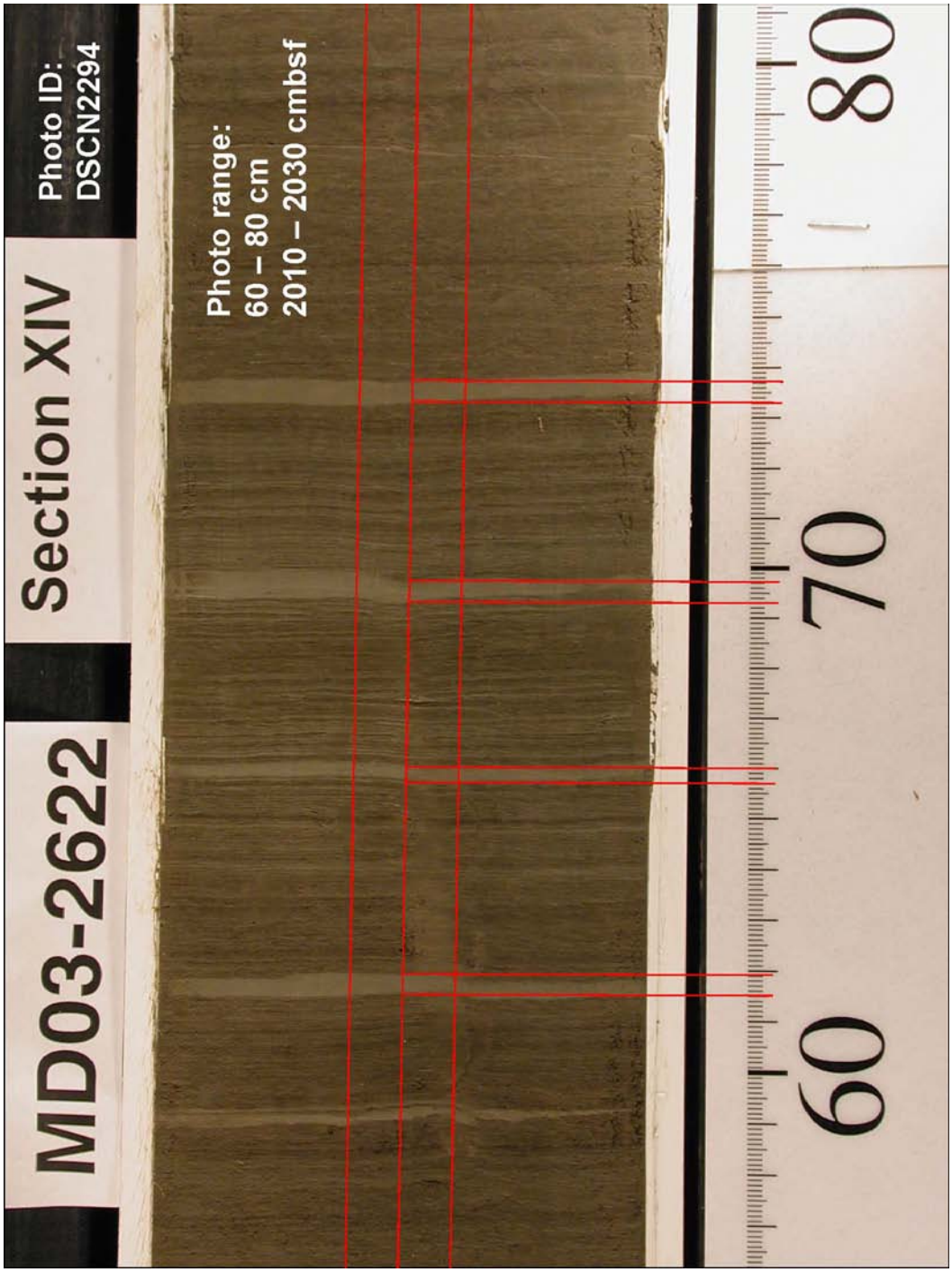

Split core photographs of MD03-2622 and the marked intervals containing evidence of microturbidite deposition. See table 4.1 for additional information. (continued)

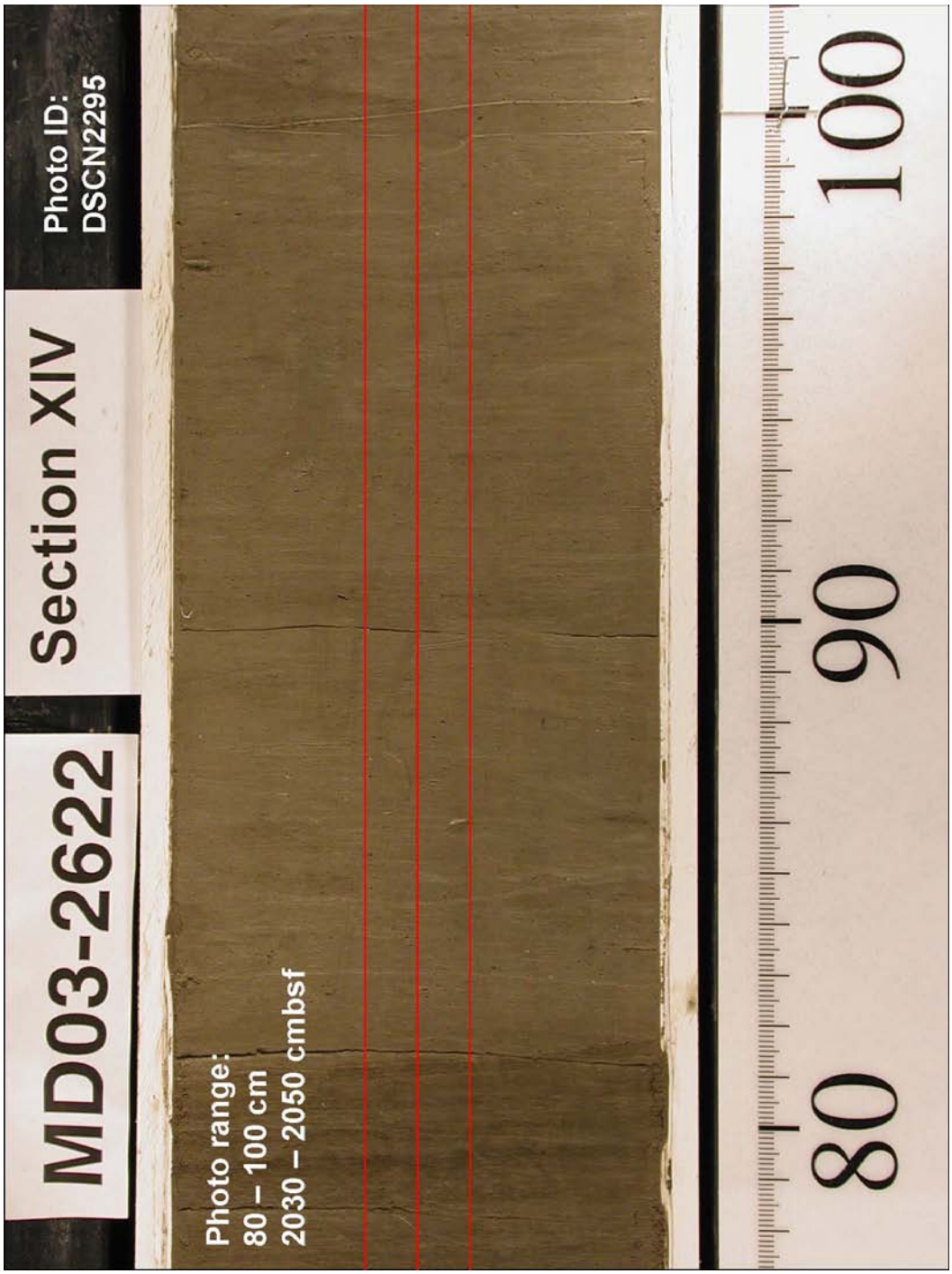

Appendix II: Core MD03-2622 Relative Abundance Data

G.b = Globigerina bulloides, *N.d = Neogloboquadrina dutertrei*, *O.u = Orbulina universa*, *G.a = Globigerinella aequilateralis*, *G.c = Globorotalia crassiformis*, *P.o = Pulleniatina obliquiloculata*, *G.m = Globorotalia menardii*, *G.r*(p) = *Globigerinoides ruber* (pink), *G.r*(w) = *Globigerinoides ruber* (white), *G.s = Globigerinoides sacculifer*, *G.g = Globigerinita glutinata*, *G.t = Globorotalia truncatulinoides*, *G.rs = Globigerina rubescens*, *N.p*(l) = *Neogloboquadrina pachyderma* (left-coiling), *N.p*(r) = *Neogloboquadrina pachyderma* (right coiling), *G.q = Globigerina quinqueloba*

Depth (cm)	Age (yBP)	*G.b* (%)	*N.d* (%)	*O.u* (%)	*G.a* (%)	*G.c* (%)	*P.o* (%)	*G.m* (%)	*G.r*(p) (%)	*G.r*(w) (%)	*G.s* (%)	*G.g* (%)	*G.t* (%)	*G.rs* (%)	*N.p*(l) (%)	*N.p*(r) (%)	*G.q* (%)	Other (%)
1900.0	42831.5	53.3	11.4	0.9	2.8	0.3	0.0	0.3	6.5	13.5	4.9	0.3	0.6	0.0	0.0	0.0	0.0	5.2
1900.1	42833.8	65.4	7.3	1.4	1.2	0.5	0.0	0.0	2.4	8.5	1.7	0.0	0.0	0.2	0.0	0.0	4.5	6.9
1900.2	42836.0	59.0	8.8	0.7	2.6	0.0	0.0	0.0	3.7	8.0	2.2	0.4	0.7	0.4	0.0	0.0	6.2	7.3
1900.3	42838.3	56.1	12.3	1.4	3.7	0.3	0.0	0.9	3.1	8.3	2.6	0.0	0.3	0.3	0.0	0.0	3.4	7.4
1900.4	42840.5	63.7	6.8	3.3	1.5	0.4	0.0	0.0	3.3	5.7	2.2	0.7	0.0	0.7	0.0	0.0	4.8	7.0
1900.5	42842.8	56.0	8.8	2.6	1.6	0.2	0.0	0.0	2.0	6.4	1.4	0.2	1.0	0.4	0.0	0.0	11.6	7.6
1900.6	42845.0	49.3	14.4	3.7	1.4	0.5	0.0	1.4	4.2	7.0	1.4	0.9	0.5	0.0	0.0	0.0	10.7	4.7
1900.7	42847.3	47.6	9.0	3.4	0.5	0.3	0.0	1.1	4.5	12.4	1.1	0.3	1.3	0.3	0.0	0.0	10.1	8.2
1900.8	42849.5	55.3	9.3	1.6	0.6	1.0	0.0	1.3	4.5	8.0	1.6	0.6	1.6	0.6	0.0	0.0	8.3	5.8
1900.9	42851.8	55.6	7.2	2.1	0.3	0.0	0.0	0.6	3.0	6.9	1.8	0.3	0.6	0.9	0.0	0.0	12.6	8.1
1901.0	42854.0	50.3	7.5	3.5	1.0	0.4	0.0	0.6	4.1	11.8	1.8	0.6	0.6	0.6	0.0	0.0	11.4	5.9
1901.1	42856.2	53.6	6.7	4.1	1.6	0.0	0.0	0.3	3.2	7.3	1.3	0.6	0.3	0.0	0.0	0.0	12.4	8.6
1901.2	42858.4	58.8	10.0	3.2	1.4	0.0	0.0	0.0	3.8	8.1	2.2	0.4	0.4	0.2	0.0	0.0	6.3	5.4
1901.3	42860.6	53.6	10.9	4.5	2.2	0.0	0.0	0.4	5.2	10.1	4.9	0.0	1.5	0.0	0.0	0.0	4.1	2.6
1901.4	42862.8	64.5	7.9	2.2	0.8	0.0	0.0	0.2	3.0	6.9	2.0	0.8	0.4	0.2	0.0	0.0	5.7	5.5
1901.5	42865.0	57.7	10.0	2.3	2.6	0.0	0.0	0.3	4.9	7.7	1.4	0.3	0.6	0.3	0.0	0.0	4.6	7.4
1901.6	42867.2	54.9	8.1	2.4	1.5	0.5	0.0	0.0	3.8	11.5	1.9	1.2	0.5	0.2	0.0	0.0	6.0	7.5
1901.7	42869.4	51.8	10.0	3.4	2.9	0.0	0.0	0.3	3.7	9.5	3.2	0.8	1.3	0.0	0.0	0.0	6.1	7.1
1901.8	42871.6	62.5	7.3	2.0	2.0	0.3	0.0	0.6	3.4	7.6	1.4	0.3	0.0	0.3	0.0	0.0	7.0	5.6
1901.9	42873.8	52.2	12.8	3.4	4.4	1.0	0.0	0.0	3.9	9.4	2.5	0.0	1.5	0.0	0.0	0.0	3.9	4.9
1902.0	42876.0	55.4	8.9	3.1	1.8	0.3	0.0	0.0	4.3	7.0	3.1	0.6	0.3	0.3	0.0	0.0	7.3	7.6
1902.1	42878.3	55.5	12.3	2.5	2.1	0.0	0.0	0.2	3.4	7.6	2.1	0.2	0.6	0.2	0.0	0.0	4.9	8.3

Core MD03-2622 Relative Abundance Data (continued)

Depth (cm)	Age (yBP)	*G.b* (%)	*N.d* (%)	*O.u* (%)	*G.a* (%)	*G.c* (%)	*P.o* (%)	*G.m* (%)	*G.r*(p) (%)	*G.r*(w) (%)	*G.s* (%)	*G.g* (%)	*G.t* (%)	*G.rs* (%)	*N.p*(l) (%)	*N.p*(r) (%)	*G.q* (%)	Other (%)
1902.2	42880.6	59.3	8.3	2.3	2.1	0.0	0.0	0.0	3.7	7.8	1.4	0.5	0.0	0.5	0.0	0.0	5.1	9.2
1902.3	42882.9	59.3	10.0	4.0	2.7	0.3	0.0	0.0	2.3	5.0	2.3	0.3	1.3	0.3	0.0	0.0	6.3	5.7
1902.4	42885.2	55.7	7.0	1.9	1.9	0.2	0.0	0.2	3.4	10.8	1.2	0.2	0.5	1.0	0.0	0.0	6.7	9.2
1902.5	42887.5	61.4	9.2	1.0	1.5	0.0	0.0	0.0	4.2	6.7	2.0	0.0	0.0	0.5	0.0	0.0	6.9	6.7
1902.6	42889.8	58.1	7.8	1.5	2.1	0.0	0.0	0.0	2.4	6.3	3.0	0.3	0.3	0.3	0.0	0.0	4.8	13.2
1902.7	42892.1	52.1	9.5	4.5	1.1	0.0	0.0	0.5	5.3	7.1	2.9	0.0	0.8	0.5	0.0	0.0	5.8	9.8
1902.8	42894.4	57.1	11.1	3.9	2.1	0.6	0.0	0.0	3.3	6.6	2.7	0.3	0.3	0.3	0.0	0.0	5.7	6.0
1902.9	42896.7	57.5	10.2	2.7	1.3	0.0	0.0	0.0	2.4	7.2	2.4	0.3	0.3	0.3	0.0	0.0	7.2	8.3
1903.0	42899.0	52.7	7.7	6.4	0.7	0.0	0.0	0.2	3.5	6.9	1.2	0.5	0.2	1.0	0.0	0.0	5.0	13.9
1903.1	42901.1	56.1	11.9	2.7	0.9	0.2	0.0	0.0	3.3	6.5	2.7	0.4	0.5	0.2	0.0	0.0	4.9	9.8
1903.2	42903.1	56.4	14.9	1.8	0.8	0.0	0.0	0.0	4.3	4.3	1.5	0.3	0.0	0.8	0.0	0.0	5.8	9.3
1903.3	42905.2	51.3	11.0	2.7	0.9	0.0	0.0	0.3	3.3	8.7	2.7	0.9	0.9	0.9	0.0	0.0	5.4	11.0
1903.4	42907.2	56.8	10.0	2.0	0.8	0.0	0.0	0.0	4.7	5.5	2.2	0.6	0.0	0.2	0.0	0.0	5.9	11.5
1903.5	42909.3	49.4	13.9	5.2	0.8	0.6	0.0	0.6	4.2	5.2	1.9	0.0	0.8	0.6	0.0	0.0	6.4	10.4
1903.6	42911.3	57.3	9.0	1.2	0.6	0.0	0.0	0.0	4.8	9.3	1.8	0.3	0.0	0.0	0.0	0.0	5.7	10.1
1903.7	42913.4	56.3	11.5	3.1	0.6	0.6	0.0	0.0	2.5	5.6	1.4	0.6	0.0	0.6	0.0	0.0	6.4	10.9
1903.8	42915.4	57.5	10.1	3.2	1.8	0.2	0.0	0.4	4.0	5.0	2.0	0.4	0.2	0.2	0.0	0.0	5.6	9.5
1903.9	42917.5	60.3	9.7	1.4	0.8	0.3	0.0	0.0	3.6	6.9	1.1	0.6	0.0	0.8	0.0	0.0	6.1	8.3
1904.0	42919.5	52.7	9.7	3.2	1.6	0.3	0.0	0.3	4.3	4.3	3.0	0.0	0.3	0.3	0.0	0.0	3.5	16.7
1904.1	42921.6	53.7	13.6	2.6	1.7	0.0	0.0	0.4	2.8	3.2	1.7	0.2	0.2	0.6	0.0	0.0	4.5	14.7
1904.2	42923.6	50.1	10.5	2.6	0.9	0.0	0.0	0.0	4.2	4.0	1.2	0.2	0.0	0.9	0.0	0.0	5.2	20.1
1904.3	42925.7	57.4	13.0	0.6	0.4	0.4	0.0	0.0	3.4	4.7	1.1	0.2	0.2	0.2	0.0	0.0	3.2	15.1
1904.4	42927.7	54.7	9.7	2.6	0.8	0.0	0.0	0.0	2.4	4.5	1.5	0.2	0.2	0.6	0.0	0.0	4.4	18.5
1904.5	42929.8	56.4	7.8	1.7	0.9	0.2	0.0	0.0	3.0	4.9	2.1	0.6	0.2	0.8	0.0	0.0	4.0	17.5
1904.6	42931.8	55.1	11.5	1.6	1.1	0.2	0.0	0.0	4.0	5.8	2.2	0.0	0.0	0.4	0.0	0.0	3.8	14.2
1904.7	42933.9	62.0	9.4	1.0	1.0	0.2	0.0	0.2	3.8	3.1	1.6	0.5	0.3	0.3	0.0	0.0	5.2	11.3
1904.8	42935.9	55.7	12.4	2.7	0.6	0.2	0.0	0.4	4.1	4.7	1.2	0.4	0.0	0.2	0.0	0.0	6.3	11.2
1904.9	42938.0	55.3	11.5	0.8	2.5	0.3	0.0	0.0	2.7	4.7	0.8	0.0	0.0	0.3	0.0	0.0	6.8	14.2

Core MD03-2622 Relative Abundance Data (continued)

Depth (cm)	Age (yBP)	*G.b* (%)	*N.d* (%)	*O.u* (%)	*G.a* (%)	*G.c* (%)	*P.o* (%)	*G.m* (%)	*G.r*(p) (%)	*G.r*(w) (%)	*G.s* (%)	*G.g* (%)	*G.t* (%)	*G.rs* (%)	*N.p*(l) (%)	*N.p*(r) (%)	*G.q* (%)	Other (%)
1905.0	42940.0	58.3	12.3	0.6	1.2	0.6	0.0	0.3	6.7	6.4	1.5	0.3	0.0	0.0	0.0	0.0	3.7	8.0
1905.1	42942.2	53.9	12.3	2.7	1.6	0.5	0.0	0.0	5.1	5.9	0.5	0.5	0.3	0.5	0.0	0.0	4.0	12.1
1905.2	42944.3	63.1	8.0	1.9	1.2	0.2	0.0	0.2	4.5	6.1	0.9	0.5	0.2	0.2	0.0	0.0	2.6	10.4
1905.3	42946.5	66.2	8.9	2.0	0.3	0.0	0.0	0.0	3.0	2.3	1.0	0.7	0.0	0.3	0.0	0.0	2.3	12.9
1905.4	42948.6	58.9	11.3	0.8	1.3	0.2	0.0	0.0	4.7	5.3	1.7	0.4	0.2	0.6	0.0	0.0	3.4	11.4
1905.5	42950.8	58.3	11.1	1.2	1.6	0.0	0.0	0.0	5.6	4.3	1.6	0.4	0.4	0.4	0.0	0.0	2.9	12.4
1905.6	42952.9	63.0	11.3	2.3	1.1	0.2	0.0	0.2	3.6	6.1	1.3	0.7	0.4	0.4	0.0	0.0	1.8	7.9
1905.7	42955.1	64.9	11.6	1.5	0.4	0.4	0.0	0.0	2.9	4.6	1.2	0.4	0.0	0.2	0.0	0.0	2.9	8.9
1905.8	42957.2	62.1	11.9	1.5	1.5	0.2	0.0	0.2	7.4	2.8	1.5	0.4	0.0	0.4	0.0	0.0	1.5	8.4
1905.9	42959.4	57.5	15.3	0.9	1.2	0.3	0.0	0.0	7.2	5.8	1.7	0.3	0.3	0.3	0.0	0.0	3.8	5.5
1906.0	42961.5	57.5	12.9	0.8	1.4	0.0	0.0	0.0	7.7	3.0	0.8	0.3	0.0	0.0	0.0	0.0	2.7	12.9
1906.1	42963.6	58.5	12.7	1.9	0.7	0.4	0.0	0.0	4.8	5.2	2.2	0.2	0.0	0.2	0.0	0.0	2.6	10.6
1906.2	42965.7	52.9	15.2	1.4	0.8	0.0	0.0	0.0	5.7	3.9	0.8	0.4	0.6	0.6	0.0	0.0	2.2	15.4
1906.3	42967.8	59.5	10.9	0.6	0.6	0.3	0.0	0.0	3.0	5.3	0.6	0.3	0.3	0.9	0.0	0.0	3.0	14.8
1906.4	42969.9	53.7	12.0	2.7	1.7	0.2	0.0	0.0	5.7	3.8	1.9	0.6	0.6	0.6	0.0	0.0	3.4	13.3
1906.5	42972.0	61.6	8.6	1.6	1.0	0.0	0.0	0.0	3.6	5.8	1.3	0.2	0.5	0.6	0.0	0.0	2.4	12.8
1906.6	42974.1	55.7	12.5	1.2	1.8	0.2	0.0	0.0	4.4	3.9	1.4	0.7	0.2	0.5	0.0	0.0	2.3	15.1
1906.7	42976.2	61.7	8.8	1.6	1.4	0.2	0.0	0.4	5.1	3.5	1.2	0.6	0.2	0.2	0.0	0.0	3.3	11.7
1906.8	42978.3	60.1	13.2	3.2	0.3	0.3	0.0	0.3	6.1	2.4	1.9	0.3	0.0	0.3	0.0	0.0	2.6	9.3
1906.9	42980.4	61.6	11.6	1.5	0.2	0.0	0.0	0.0	6.2	4.0	1.5	0.2	0.2	0.2	0.0	0.0	2.0	10.6
1907.0	42982.5	55.4	14.4	1.5	1.5	0.3	0.0	0.0	4.2	5.4	0.9	0.3	0.3	0.6	0.0	0.0	3.6	11.7
1907.1	42984.9	57.6	11.3	1.3	1.1	0.0	0.0	0.0	7.0	5.9	2.4	0.3	0.0	0.3	0.0	0.0	2.4	10.5
1907.2	42987.2	59.3	13.4	1.2	1.2	0.2	0.0	0.2	4.5	3.8	2.4	0.2	0.2	0.5	0.0	0.0	1.4	11.5
1907.3	42989.6	50.2	12.0	1.6	1.0	0.0	0.0	0.3	6.5	5.2	3.6	0.0	0.0	0.6	0.0	0.0	2.9	16.2
1907.4	42991.9	54.8	19.7	1.3	1.1	0.2	0.0	0.0	5.9	3.6	1.7	0.2	0.0	0.2	0.0	0.0	0.8	10.6
1907.5	42994.3	55.0	17.4	2.3	1.9	0.0	0.0	0.0	7.4	3.9	1.0	0.3	0.0	0.3	0.0	0.0	1.3	9.3
1907.6	42996.6	55.8	11.8	1.7	0.3	0.3	0.0	0.3	4.4	5.6	1.9	0.0	0.0	0.3	0.0	0.0	0.3	17.2
1907.7	42999.0	55.3	18.4	1.3	0.9	0.0	0.0	0.0	3.8	5.3	0.7	0.2	0.0	0.2	0.0	0.0	0.7	13.3

Core MD03-2622 Relative Abundance Data (continued)

Depth (cm)	Age (yBP)	*G.b* (%)	*N.d* (%)	*O.u* (%)	*G.a* (%)	*G.c* (%)	*P.o* (%)	*G.m* (%)	*G.r*(p) (%)	*G.r*(w) (%)	*G.s* (%)	*G.g* (%)	*G.t* (%)	*G.rs* (%)	*N.p*(l) (%)	*N.p*(r) (%)	*G.q* (%)	Other (%)
1907.8	43001.3	57.8	13.2	2.0	1.2	0.2	0.0	0.0	7.9	3.5	0.7	0.2	0.0	0.7	0.0	0.0	3.0	9.4
1907.9	43003.7	55.1	14.8	0.9	0.9	0.0	0.0	0.0	5.2	4.6	0.9	0.0	0.0	0.3	0.0	0.0	2.3	15.1
1908.0	43006.0	54.1	13.5	2.4	1.8	0.2	0.0	0.2	4.5	2.7	0.8	0.4	0.0	0.6	0.0	0.0	3.1	15.7
1908.1	43008.3	59.5	10.6	2.1	1.3	0.2	0.0	0.0	5.4	3.5	0.8	0.4	0.0	0.6	0.0	0.0	1.9	13.8
1908.2	43010.5	56.1	12.4	0.7	1.0	0.2	0.0	0.2	6.1	3.6	2.5	0.3	0.2	0.5	0.0	0.0	3.0	13.4
1908.3	43012.8	59.7	13.2	1.6	0.5	0.0	0.0	0.5	5.8	3.2	0.7	0.2	0.0	0.5	0.0	0.0	2.5	11.6
1908.4	43015.0	56.3	8.8	2.1	0.4	0.2	0.0	0.0	6.7	3.3	0.6	0.2	0.0	0.2	0.0	0.0	3.1	18.1
1908.5	43017.3	52.8	11.5	2.0	0.7	0.4	0.0	0.4	6.1	2.7	0.7	0.4	0.0	0.7	0.0	0.0	3.1	18.4
1908.6	43019.5	47.8	9.1	1.0	1.6	0.0	0.0	0.0	6.1	4.0	0.4	0.0	0.0	1.4	0.0	0.0	4.0	24.5
1908.7	43021.8	55.2	11.8	1.2	0.9	0.3	0.0	0.0	6.8	3.8	0.6	0.3	0.3	1.2	0.0	0.0	2.4	15.3
1908.8	43024.0	51.0	11.3	0.0	0.9	0.2	0.0	0.4	9.1	4.1	0.9	0.4	0.2	0.4	0.0	0.0	2.8	18.4
1908.9	43026.3	52.2	10.1	1.1	0.6	0.2	0.0	0.2	5.9	3.6	0.6	0.4	0.0	0.6	0.0	0.0	4.0	20.4
1909.0	43028.5	50.9	7.8	1.1	0.8	0.0	0.0	0.3	6.1	3.9	1.4	0.8	0.0	0.0	0.0	0.0	5.0	21.8
1909.1	43030.9	50.3	7.2	0.9	0.4	0.0	0.0	0.0	8.1	3.8	0.4	0.2	0.0	0.4	0.0	0.0	4.9	23.5
1909.2	43033.2	45.6	6.3	0.3	1.3	0.0	0.0	0.0	8.9	4.4	0.3	0.3	0.0	0.5	0.0	0.0	3.7	28.5
1909.3	43035.6	51.5	5.1	1.1	0.4	0.0	0.0	0.0	8.1	5.7	0.9	0.4	0.0	0.2	0.0	0.0	4.6	21.8
1909.4	43037.9	52.5	5.6	1.3	0.7	0.0	0.0	0.0	8.0	2.7	1.1	0.4	0.2	0.0	0.0	0.0	4.2	23.2
1909.5	43040.3	51.7	6.1	1.3	1.3	0.2	0.0	0.2	8.0	3.8	0.4	0.4	0.0	0.6	0.0	0.0	4.2	21.6
1909.6	43042.6	52.4	5.6	0.8	0.2	0.4	0.0	0.0	8.1	4.3	0.6	0.4	0.2	0.2	0.0	0.0	3.9	23.0
1909.7	43045.0	54.4	5.9	1.4	0.6	0.0	0.0	0.0	10.8	4.1	0.4	0.2	0.0	0.2	0.0	0.0	3.7	18.1
1909.8	43047.3	49.6	8.6	1.2	0.8	0.0	0.0	0.0	6.5	5.3	0.6	0.4	0.0	0.2	0.0	0.0	5.1	21.8
1909.9	43049.7	58.4	5.1	2.7	0.3	0.0	0.0	0.3	4.3	5.1	0.3	0.3	0.0	0.0	0.0	0.0	4.8	18.7
1910.0	43052.0	50.6	7.4	3.3	1.1	0.2	0.2	0.0	7.8	4.1	0.9	0.6	0.0	0.7	0.0	0.0	4.1	19.1
1910.1	43054.0	51.5	7.6	1.4	0.8	0.0	0.0	0.0	9.3	3.7	0.8	0.3	0.0	0.6	0.0	0.0	4.5	19.4
1910.2	43056.0	49.1	7.8	2.1	0.7	0.0	0.0	0.2	10.9	3.8	1.0	0.2	0.2	0.2	0.0	0.0	3.8	19.7
1910.3	43058.0	53.6	9.6	2.3	0.6	0.0	0.3	0.0	5.2	4.1	0.3	0.6	0.0	0.0	0.0	0.0	4.4	19.0
1910.4	43060.0	53.1	6.5	2.1	0.5	0.0	0.0	0.0	7.9	6.5	0.7	0.2	0.0	0.2	0.0	0.0	3.7	18.6
1910.5	43062.0	56.0	6.4	1.4	0.6	0.2	0.0	0.0	7.3	2.7	1.0	0.0	0.2	0.2	0.0	0.0	3.5	20.7

Core MD03-2622 Relative Abundance Data (continued)

Depth (cm)	Age (yBP)	*G.b* (%)	*N.d* (%)	*O.u* (%)	*G.a* (%)	*G.c* (%)	*P.o* (%)	*G.m* (%)	*G.r*(p) (%)	*G.r*(w) (%)	*G.s* (%)	*G.g* (%)	*G.t* (%)	*G.rs* (%)	*N.p*(l) (%)	*N.p*(r) (%)	*G.q* (%)	Other (%)
1910.6	43064.0	49.1	5.2	2.1	0.7	0.0	0.0	0.2	8.2	3.3	0.9	0.2	0.2	0.7	0.0	0.0	4.0	25.1
1910.7	43066.0	54.2	7.4	1.6	0.7	0.0	0.0	0.0	6.1	3.6	0.7	0.0	0.0	0.5	0.0	0.0	3.2	22.1
1910.8	43068.0	57.6	7.9	1.1	0.4	0.2	0.0	0.0	5.1	4.5	1.5	0.4	0.6	0.9	0.0	0.0	2.8	17.0
1910.9	43070.0	56.4	7.9	1.7	1.5	0.0	0.0	0.0	5.4	5.7	1.0	0.2	0.2	0.5	0.0	0.0	3.2	16.1
1911.0	43072.0	53.4	8.3	1.3	2.0	0.2	0.0	0.2	5.6	4.9	0.2	0.4	0.0	0.2	0.0	0.0	3.6	19.3
1911.1	43073.7	53.7	8.6	1.9	2.3	0.0	0.0	0.2	3.5	3.3	1.4	1.2	0.5	0.5	0.0	0.0	1.6	21.3
1911.2	43075.4	58.2	7.8	2.2	0.8	0.5	0.0	0.0	3.6	3.9	1.4	0.3	0.5	0.8	0.0	0.0	2.4	17.5
1911.3	43077.1	58.5	5.0	2.0	1.2	0.0	0.0	0.0	2.3	3.5	0.3	0.3	0.0	0.6	0.0	0.0	2.6	23.7
1911.4	43078.8	57.1	8.8	1.8	2.3	0.2	0.0	0.0	2.3	2.3	1.6	0.2	0.0	0.2	0.0	0.0	2.5	20.8
1911.5	43080.5	56.8	7.6	2.1	1.5	0.3	0.0	0.0	3.2	1.8	1.5	0.6	0.0	0.0	0.0	0.0	4.1	20.6
1911.6	43082.2	60.9	10.8	0.9	1.1	0.0	0.0	0.0	1.1	2.7	0.9	0.2	0.4	0.2	0.0	0.0	2.7	18.0
1911.7	43083.9	59.6	8.5	0.2	1.3	0.2	0.0	0.0	0.9	3.0	1.1	0.4	0.2	0.8	0.0	0.0	3.4	20.3
1911.8	43085.6	55.2	9.9	2.5	1.8	0.2	0.0	0.0	1.6	2.2	1.6	0.4	0.0	0.9	0.0	0.0	2.5	21.3
1911.9	43087.3	58.6	7.8	0.9	1.7	0.3	0.0	0.3	2.6	4.9	0.9	0.6	0.0	0.9	0.0	0.0	2.6	18.1
1912.0	43089.0	55.5	6.8	1.3	1.3	0.8	0.0	0.0	1.0	4.4	1.0	0.8	0.0	0.8	0.0	0.0	3.1	23.1
1912.1	43090.8	58.0	7.6	1.1	0.4	0.2	0.0	0.0	2.4	3.5	0.4	0.4	0.0	0.2	0.0	0.0	2.4	23.3
1912.2	43092.6	50.4	9.0	1.1	1.3	0.4	0.0	0.0	0.9	3.4	1.5	0.4	0.4	1.1	0.0	0.0	3.9	26.3
1912.3	43094.4	54.4	7.2	2.3	1.9	0.2	0.0	0.0	0.6	3.4	0.4	0.4	0.4	0.9	0.0	0.0	3.2	24.5
1912.4	43096.2	57.0	8.7	1.2	1.5	0.0	0.0	0.0	1.2	3.9	0.5	1.0	0.3	0.7	0.0	0.0	2.2	21.8
1912.5	43098.0	54.3	11.5	1.5	1.3	0.0	0.0	0.0	0.8	3.5	0.8	0.5	0.8	0.8	0.0	0.0	3.0	21.5
1912.6	43099.8	57.0	11.4	2.7	1.2	1.0	0.0	0.2	1.5	3.2	0.8	1.7	0.0	2.0	0.0	0.0	2.7	14.7
1912.7	43101.6	59.3	10.1	1.3	1.0	0.3	0.3	0.0	1.0	4.6	1.3	1.0	0.0	1.8	0.0	0.0	1.8	16.2
1912.8	43103.4	57.7	8.7	0.9	0.9	0.3	0.0	0.0	0.9	4.6	0.6	3.1	0.0	2.2	0.0	0.0	1.5	18.5
1912.9	43105.2	58.3	11.2	1.5	1.5	0.2	0.0	0.0	0.5	2.7	0.7	0.7	0.2	0.5	0.0	0.0	2.0	20.0
1913.0	43107.0	57.0	10.0	1.5	2.0	0.0	0.0	0.0	1.0	2.0	0.7	1.0	0.2	0.2	0.0	0.0	2.9	21.5
1913.1	43109.0	53.3	11.0	1.9	1.0	0.4	0.0	0.0	0.4	3.9	1.0	0.6	0.0	1.2	0.0	0.0	2.3	22.8
1913.2	43111.0	56.3	10.0	3.0	0.9	0.0	0.0	0.0	0.6	2.4	0.6	0.9	0.0	0.9	0.0	0.0	3.2	21.2
1913.3	43113.0	59.4	10.3	1.3	1.0	0.0	0.0	0.0	0.3	1.8	1.0	0.3	0.0	0.8	0.0	0.0	1.5	22.6

Core MD03-2622 Relative Abundance Data (continued)

Depth (cm)	Age (yBP)	*G.b* (%)	*N.d* (%)	*O.u* (%)	*G.a* (%)	*G.c* (%)	*P.o* (%)	*G.m* (%)	*G.r*(p) (%)	*G.r*(w) (%)	*G.s* (%)	*G.g* (%)	*G.t* (%)	*G.rs* (%)	*N.p*(l) (%)	*N.p*(r) (%)	*G.q* (%)	Other (%)
1913.4	43115.0	61.2	9.1	0.3	2.1	0.0	0.0	0.6	0.3	3.0	0.9	0.6	0.3	0.3	0.0	0.0	2.4	18.8
1913.5	43117.0	58.9	9.4	1.6	1.4	0.2	0.0	0.2	0.8	1.6	0.5	0.8	0.0	1.1	0.0	0.0	2.2	21.2
1913.6	43119.0	51.0	10.3	1.8	1.2	0.2	0.0	0.0	0.8	1.6	0.6	1.2	0.0	1.0	0.0	0.0	2.5	27.7
1913.7	43121.0	55.8	8.0	2.9	1.6	0.0	0.0	0.0	0.2	2.1	0.0	1.2	0.0	1.2	0.0	0.0	1.9	25.1
1913.8	43123.0	54.1	8.8	1.4	3.1	0.2	0.0	0.2	1.6	3.9	0.4	1.0	0.0	0.8	0.0	0.0	3.1	21.5
1913.9	43125.0	52.1	8.3	1.8	1.1	0.0	0.0	0.0	1.1	2.6	0.4	0.7	0.0	0.9	0.0	0.0	3.5	27.6
1914.0	43127.0	59.1	12.9	1.9	1.1	0.4	0.0	0.0	1.3	1.5	1.1	0.6	0.0	0.4	0.0	0.0	2.6	17.1
1914.1	43129.4	59.7	7.0	1.0	1.0	0.2	0.0	0.0	0.2	0.8	0.3	0.2	0.0	0.0	0.0	0.0	2.6	27.0
1914.2	43131.7	52.1	11.0	1.4	0.6	0.0	0.0	0.3	0.3	0.8	0.3	0.6	0.3	0.6	0.0	0.0	4.1	27.8
1914.3	43134.1	59.9	8.3	0.5	0.2	0.2	0.0	0.0	0.2	0.7	0.0	0.2	0.0	0.7	0.0	0.0	3.2	25.8
1914.4	43136.4	49.3	9.5	1.6	0.4	0.4	0.0	0.0	0.0	1.2	0.4	0.6	0.0	1.0	0.0	0.0	1.9	33.8
1914.5	43138.8	53.7	9.6	1.5	1.0	0.0	0.0	0.0	0.0	1.8	0.3	0.3	0.0	1.8	0.0	0.0	3.8	26.4
1914.6	43141.1	54.1	7.8	1.1	1.1	0.2	0.0	0.2	0.4	1.6	0.4	0.5	0.0	0.2	0.0	0.0	3.1	29.4
1914.7	43143.5	60.8	7.0	0.7	0.7	0.5	0.0	0.2	0.5	1.3	0.7	0.3	0.0	0.8	0.0	0.0	1.7	24.9
1914.8	43145.8	56.5	8.2	0.9	0.6	0.3	0.0	0.0	0.3	0.9	0.6	0.3	0.0	0.6	0.0	0.0	2.0	28.9
1914.9	43148.2	57.3	7.9	0.9	0.7	0.2	0.0	0.0	0.0	0.7	0.5	0.4	0.0	0.2	0.0	0.0	2.6	28.6
1915.0	43150.5	52.9	9.2	1.1	0.4	0.0	0.0	0.0	0.0	1.1	1.1	0.0	0.0	0.4	0.0	0.0	3.3	30.5
1915.1	43152.7	58.2	8.3	0.9	0.5	0.2	0.0	0.0	0.2	1.6	0.5	0.5	0.0	0.7	0.0	0.0	3.2	25.2
1915.2	43154.9	56.4	7.0	1.5	1.1	0.7	0.0	0.0	0.5	0.5	0.5	0.5	0.0	0.4	0.0	0.0	2.2	28.6
1915.3	43157.1	58.0	7.8	1.0	0.6	0.0	0.0	0.0	0.6	0.8	0.0	0.6	0.0	0.2	0.0	0.0	2.9	27.5
1915.4	43159.3	60.8	8.1	0.4	1.0	0.2	0.0	0.0	0.6	0.4	0.8	0.2	0.0	0.4	0.0	0.0	2.6	24.6
1915.5	43161.5	58.7	9.8	0.0	0.0	0.2	0.0	0.2	0.5	0.5	0.7	0.0	0.0	0.0	0.0	0.0	2.8	26.6
1915.6	43163.7	56.7	10.1	0.8	0.8	0.5	0.0	0.0	1.6	2.1	0.8	0.3	0.0	0.0	0.0	0.0	2.3	24.1
1915.7	43165.9	60.2	8.7	0.4	0.2	0.0	0.0	0.0	1.6	2.9	0.4	0.0	0.0	0.0	0.0	0.0	0.9	24.6
1915.8	43168.1	57.3	9.8	0.9	0.2	0.2	0.0	0.2	0.7	0.9	0.2	0.7	0.0	0.4	0.0	0.0	1.8	26.9
1915.9	43170.3	62.5	10.1	0.4	1.3	0.4	0.0	0.0	1.3	0.9	0.4	0.4	0.0	0.4	0.0	0.0	1.1	20.8
1916.0	43172.5	53.3	9.7	0.3	0.8	0.0	0.0	0.0	2.7	1.3	0.3	0.5	0.0	0.3	0.0	0.0	1.9	29.0
1916.1	43174.6	54.1	9.5	0.4	0.6	0.2	0.0	0.2	2.7	2.1	0.2	0.6	0.0	0.6	0.0	0.0	1.5	27.5

Core MD03-2622 Relative Abundance Data (continued)

Depth (cm)	Age (yBP)	*G.b* (%)	*N.d* (%)	*O.u* (%)	*G.a* (%)	*G.c* (%)	*P.o* (%)	*G.m* (%)	*G.r*(p) (%)	*G.r*(w) (%)	*G.s* (%)	*G.g* (%)	*G.t* (%)	*G.rs* (%)	*N.p*(l) (%)	*N.p*(r) (%)	*G.q* (%)	Other (%)
1916.2	43176.6	44.6	16.2	0.7	1.0	0.0	0.0	0.0	1.5	1.9	0.7	0.5	0.0	0.2	0.0	0.0	1.7	31.0
1916.3	43178.7	49.9	13.6	0.3	0.9	0.0	0.0	0.0	2.9	2.9	0.3	0.6	0.0	0.6	0.0	0.0	1.8	26.3
1916.4	43180.7	53.2	8.3	1.2	1.8	0.4	0.0	0.0	3.0	2.0	1.0	0.2	0.2	0.2	0.0	0.0	0.8	27.6
1916.5	43182.8	48.5	11.7	0.5	1.3	0.7	0.0	0.0	1.5	2.4	0.5	0.3	0.0	0.8	0.0	0.0	1.3	30.6
1916.6	43184.8	52.4	13.8	1.3	1.0	0.3	0.0	0.0	1.0	1.9	1.0	0.0	0.0	0.3	0.0	0.0	2.2	24.7
1916.7	43186.9	55.6	10.4	0.9	1.5	0.0	0.2	0.0	2.5	4.0	0.4	0.2	0.0	0.0	0.0	0.0	0.9	23.4
1916.8	43188.9	53.3	11.4	0.2	1.9	0.0	0.0	0.2	4.1	3.4	1.2	1.5	0.2	0.2	0.0	0.0	0.5	21.6
1916.9	43191.0	51.4	13.2	0.9	1.1	0.0	0.0	0.2	3.0	3.6	0.6	0.9	0.0	0.0	0.0	0.0	0.6	24.5
1917.0	43193.0	46.4	10.5	0.0	1.7	0.0	0.0	0.0	2.0	3.5	1.2	0.3	0.0	0.6	0.0	0.0	0.3	33.5
1917.1	43194.7	53.2	11.3	0.6	1.1	0.0	0.0	0.0	1.5	2.6	0.7	0.7	0.2	0.2	0.0	0.0	0.4	27.5
1917.2	43196.4	52.8	9.8	0.9	1.9	0.0	0.0	0.2	1.5	2.6	1.3	0.6	0.0	0.6	0.0	0.0	1.3	26.6
1917.3	43198.1	57.1	9.2	0.2	2.0	0.2	0.0	0.0	1.0	2.9	0.2	0.6	0.0	1.0	0.0	0.0	0.6	24.9
1917.4	43199.8	46.4	13.8	0.4	2.2	0.2	0.0	0.0	1.3	2.4	0.9	0.6	0.2	0.2	0.0	0.0	1.3	30.1
1917.5	43201.5	52.1	11.1	0.9	0.9	0.2	0.2	0.0	0.5	3.4	0.5	0.5	0.3	0.0	0.0	0.0	0.8	28.7
1917.6	43203.2	55.3	10.1	0.5	2.1	0.3	0.0	0.0	1.6	5.2	1.3	0.5	0.0	0.3	0.0	0.0	0.5	22.4
1917.7	43204.9	57.9	9.7	0.9	1.1	0.3	0.0	0.0	2.0	3.2	0.6	0.3	0.3	0.3	0.0	0.0	0.6	22.9
1917.8	43206.6	58.5	11.4	0.6	0.6	0.3	0.0	0.3	0.3	1.5	0.9	0.3	0.0	0.0	0.0	0.0	0.6	24.4
1917.9	43208.3	58.1	10.1	0.0	1.2	0.3	0.0	0.0	1.2	5.2	0.6	0.3	0.3	0.0	0.0	0.0	0.9	21.7
1918.0	43210.0	49.2	11.4	1.1	1.5	0.0	0.0	0.2	1.9	2.1	0.4	0.2	0.4	1.1	0.0	0.0	2.6	27.9
1918.1	43211.8	51.9	9.7	0.3	1.8	0.0	0.0	0.0	1.3	3.1	0.3	0.3	0.5	0.3	0.0	0.0	2.5	28.2
1918.2	43213.6	48.6	9.7	0.9	2.1	0.0	0.0	0.0	1.8	3.8	0.3	0.3	0.0	0.6	0.0	0.0	2.4	29.5
1918.3	43215.4	49.6	11.3	1.1	0.8	0.0	0.0	0.0	2.0	2.5	1.1	0.3	0.0	0.0	0.0	0.0	1.7	29.5
1918.4	43217.2	52.4	11.7	2.3	1.4	0.5	0.0	0.0	3.3	2.3	1.2	0.5	0.0	0.7	0.0	0.0	2.1	21.7
1918.5	43219.0	56.1	10.6	0.6	2.1	0.3	0.0	0.0	0.6	3.9	1.2	0.0	0.0	0.6	0.0	0.0	0.6	23.3
1918.6	43220.8	57.3	11.3	1.5	1.8	0.4	0.0	0.0	0.7	4.4	1.5	0.9	0.4	0.2	0.0	0.0	1.3	18.1
1918.7	43222.6	54.7	14.7	0.0	2.5	0.2	0.0	0.0	1.1	4.4	0.5	0.0	0.0	0.0	0.0	0.0	1.1	20.7
1918.8	43224.4	57.4	12.5	0.8	1.1	1.1	0.0	0.0	1.4	3.3	0.6	0.6	0.0	0.0	0.0	0.0	1.1	20.0
1918.9	43226.2	58.0	11.1	1.0	1.5	1.0	0.0	0.0	1.0	4.0	0.8	0.0	0.0	0.0	0.0	0.0	1.3	20.4

Core MD03-2622 Relative Abundance Data (continued)

Depth (cm)	Age (yBP)	*G.b* (%)	*N.d* (%)	*O.u* (%)	*G.a* (%)	*G.c* (%)	*P.o* (%)	*G.m* (%)	*G.r*(p) (%)	*G.r*(w) (%)	*G.s* (%)	*G.g* (%)	*G.t* (%)	*G.rs* (%)	*N.p*(l) (%)	*N.p*(r) (%)	*G.q* (%)	Other (%)
1919.0	43228.0	62.8	9.3	0.4	2.4	0.7	0.0	0.0	0.7	2.8	0.7	0.2	0.2	0.4	0.0	0.0	1.1	18.2
1919.1	43230.1	58.6	8.6	0.4	1.0	0.2	0.0	0.0	1.0	2.5	0.8	0.4	0.0	0.4	0.0	0.0	1.0	24.9
1919.2	43232.2	60.3	10.6	0.0	1.1	0.0	0.0	0.0	1.3	1.7	0.2	0.4	0.4	0.2	0.0	0.0	2.4	21.4
1919.3	43234.3	59.1	9.3	0.3	1.3	0.7	0.0	0.0	0.7	1.7	1.0	0.0	0.0	0.0	0.0	0.0	1.0	24.9
1919.4	43236.4	59.4	12.4	0.2	1.7	0.2	0.0	0.0	1.7	2.4	0.4	0.2	0.0	0.4	0.0	0.0	0.9	20.2
1919.5	43238.5	50.5	13.3	0.6	0.9	0.6	0.0	0.0	1.2	2.2	0.3	0.3	0.0	0.0	0.0	0.0	1.2	28.8
1919.6	43240.6	53.8	14.3	0.7	1.4	0.2	0.0	0.2	0.7	2.7	0.5	0.7	0.0	0.2	0.0	0.0	2.2	22.5
1919.7	43242.7	51.1	17.3	0.6	1.2	0.3	0.0	0.0	0.6	2.5	0.6	0.6	0.3	0.0	0.0	0.0	1.5	23.2
1919.8	43244.8	53.7	17.5	0.2	1.2	0.2	0.0	0.0	0.7	3.4	0.0	0.5	0.0	0.2	0.0	0.0	2.0	20.4
1919.9	43246.9	53.7	15.9	0.6	0.9	0.6	0.0	0.0	0.8	1.7	0.4	0.4	0.4	0.0	0.0	0.0	1.7	23.1
1920.0	43249.0	51.8	17.1	0.6	0.8	0.6	0.0	0.2	1.5	2.3	0.8	0.2	0.0	0.4	0.0	0.0	3.3	20.5
1920.1	43251.0	52.1	16.6	0.6	1.2	0.0	0.0	0.0	1.0	4.3	1.0	0.2	0.8	0.4	0.0	0.0	2.0	19.7
1920.2	43252.9	50.1	17.9	1.6	1.4	1.6	0.0	0.0	1.0	2.1	0.8	0.8	0.2	0.2	0.0	0.0	2.3	19.9
1920.3	43254.9	51.6	15.9	0.3	0.8	1.6	0.0	0.5	0.8	2.7	0.8	0.3	0.3	0.3	0.0	0.0	1.9	22.0
1920.4	43256.8	52.7	18.0	0.2	1.4	2.1	0.0	0.0	0.0	2.5	0.2	0.7	0.2	0.5	0.0	0.0	1.1	20.3
1920.5	43258.8	57.3	11.7	0.6	1.1	0.2	0.2	0.0	0.2	1.9	1.1	0.2	0.2	0.4	0.0	0.0	2.3	22.7
1920.6	43260.7	52.3	18.3	0.0	1.5	0.5	0.0	0.0	1.3	2.2	0.9	0.9	0.0	0.4	0.0	0.0	1.3	20.5
1920.7	43262.7	58.6	13.1	0.3	1.3	0.3	0.0	0.0	1.0	2.9	0.6	0.6	0.3	0.3	0.0	0.0	1.6	19.1
1920.8	43264.6	51.1	16.0	0.9	1.2	0.0	0.0	0.0	0.9	2.8	0.6	0.3	0.0	0.0	0.0	0.0	0.9	25.2
1920.9	43266.6	52.3	14.0	0.6	2.2	0.3	0.0	0.0	0.6	5.0	0.9	0.3	0.3	0.0	0.0	0.0	1.2	22.1
1921.0	43268.5	50.9	17.1	0.7	1.5	0.3	0.0	0.0	2.4	3.6	1.7	0.5	0.2	0.3	0.0	0.0	1.4	19.4
1921.1	43270.8	57.2	13.0	0.0	1.2	0.3	0.0	0.0	0.3	5.1	0.6	0.0	0.0	0.0	0.0	0.0	0.9	21.4
1921.2	43273.0	50.7	18.5	0.8	1.3	0.3	0.0	0.3	1.3	2.9	0.0	0.8	0.0	0.0	0.0	0.0	0.8	22.3
1921.3	43275.3	52.8	19.9	0.3	1.8	0.0	0.0	0.0	0.8	2.3	0.0	0.3	0.0	0.3	0.0	0.0	0.5	21.2
1921.4	43277.5	50.9	16.5	0.8	1.3	0.0	0.0	0.0	0.8	3.8	1.0	0.3	0.0	0.0	0.0	0.0	1.0	23.8
1921.5	43279.8	55.9	16.8	0.0	1.2	0.4	0.0	0.0	1.0	2.1	0.4	0.2	0.0	0.4	0.0	0.0	1.0	20.5
1921.6	43282.0	46.9	20.5	1.3	2.2	0.2	0.0	0.0	0.9	2.4	0.7	0.7	0.0	0.4	0.0	0.0	0.4	23.4
1921.7	43284.3	52.1	16.2	0.0	1.5	0.0	0.0	0.5	1.5	3.9	1.2	0.2	0.0	0.2	0.0	0.0	1.0	21.6

Core MD03-2622 Relative Abundance Data (continued)

Depth (cm)	Age (yBP)	*G.b* (%)	*N.d* (%)	*O.u* (%)	*G.a* (%)	*G.c* (%)	*P.o* (%)	*G.m* (%)	*G.r*(p) (%)	*G.r*(w) (%)	*G.s* (%)	*G.g* (%)	*G.t* (%)	*G.rs* (%)	*N.p*(l) (%)	*N.p*(r) (%)	*G.q* (%)	Other (%)
1921.8	43286.5	53.8	19.4	0.6	2.0	0.0	0.0	0.0	0.9	2.6	0.3	0.0	0.0	1.1	0.0	0.0	0.6	18.8
1921.9	43288.8	54.8	18.4	1.3	1.9	0.0	0.0	0.0	0.8	1.9	0.8	0.3	0.3	0.5	0.0	0.0	0.5	18.6
1922.0	43291.0	49.0	12.4	0.2	2.9	0.2	0.0	0.0	1.1	2.0	2.2	0.2	0.2	1.5	0.0	0.0	0.4	27.6
1922.1	43293.2	53.9	12.4	0.3	1.1	0.0	0.0	0.0	0.3	3.1	0.6	0.0	0.0	0.3	0.0	0.0	0.3	27.8
1922.2	43295.3	45.4	16.1	0.3	1.1	0.0	0.0	0.0	1.4	2.6	2.6	0.0	0.0	2.3	0.0	0.0	0.6	27.6
1922.3	43297.5	50.5	15.4	0.5	1.4	0.0	0.0	0.0	0.2	3.2	0.5	0.2	0.0	0.5	0.0	0.0	0.7	27.1
1922.4	43299.6	52.7	13.4	0.2	0.5	0.2	0.0	0.0	1.2	2.6	0.9	0.5	0.0	0.7	0.0	0.0	0.7	26.4
1922.5	43301.8	50.4	13.3	0.6	1.1	0.0	0.0	0.0	1.1	4.0	0.3	0.3	0.0	0.0	0.0	0.0	0.8	28.0
1922.6	43303.9	48.9	18.6	0.3	1.3	0.3	0.0	0.0	1.3	2.8	0.6	0.3	0.0	0.0	0.0	0.0	1.6	24.0
1922.7	43306.1	47.0	19.8	0.0	0.8	0.0	0.0	0.0	0.8	3.0	0.0	0.3	0.0	0.3	0.0	0.0	0.8	27.2
1922.8	43308.2	50.4	20.2	0.4	1.6	0.2	0.0	0.0	1.0	1.2	0.2	0.4	0.0	0.6	0.0	0.0	0.8	23.0
1922.9	43310.4	52.5	15.1	0.3	1.3	0.0	0.0	0.0	0.3	1.7	0.3	0.3	0.3	0.3	0.0	0.0	0.7	26.8
1923.0	43312.5	47.9	18.1	0.6	0.6	0.0	0.0	0.0	1.0	1.9	0.4	0.2	0.0	0.4	0.0	0.0	0.6	28.5
1923.1	43314.4	54.5	15.0	0.2	0.4	0.2	0.0	0.0	0.2	1.1	0.0	0.0	0.0	0.4	0.0	0.0	0.9	26.9
1923.2	43316.2	49.8	19.8	0.0	1.3	0.0	0.0	0.0	1.3	1.8	0.5	0.5	0.0	0.3	0.0	0.0	1.0	24.0
1923.3	43318.1	51.1	17.7	0.2	1.5	0.2	0.0	0.0	0.0	2.9	0.7	0.4	0.2	0.2	0.0	0.0	1.1	23.7
1923.4	43319.9	50.4	16.0	0.0	1.1	0.2	0.0	0.0	0.9	1.9	0.4	0.6	0.0	0.0	0.0	0.0	0.4	28.0
1923.5	43321.8	49.1	19.4	0.8	1.1	0.0	0.0	0.0	0.8	2.7	0.3	0.0	0.0	0.0	0.0	0.0	0.8	25.2
1923.6	43323.6	54.9	21.3	0.2	1.8	0.2	0.0	0.0	0.0	2.2	0.0	0.4	0.4	0.0	0.0	0.0	0.2	18.2
1923.7	43325.5	53.6	21.2	0.3	1.2	0.0	0.0	0.3	0.6	3.7	0.0	0.3	0.0	0.3	0.0	0.0	0.3	18.1
1923.8	43327.3	50.0	16.7	0.4	1.0	0.2	0.0	0.0	0.6	2.7	0.2	0.2	0.0	0.4	0.0	0.0	0.8	26.7
1923.9	43329.2	52.4	14.8	0.4	0.7	0.0	0.0	0.0	1.8	1.5	0.5	0.0	0.2	0.2	0.0	0.0	0.9	26.6
1924.0	43331.0	59.4	19.0	0.2	2.5	0.0	0.0	0.2	0.5	3.0	0.2	0.4	0.4	0.4	0.0	0.0	2.6	11.4
1924.1	43332.5	59.8	17.8	0.0	3.3	0.3	0.0	0.0	1.4	4.4	0.3	0.3	0.0	0.0	0.0	0.0	3.0	9.6
1924.2	43334.0	57.2	17.4	0.0	3.6	0.0	0.0	0.0	0.7	4.8	1.6	0.7	0.2	0.2	0.0	0.0	1.6	12.0
1924.3	43335.5	55.0	18.4	0.2	4.1	0.2	0.0	0.0	0.2	6.5	2.4	0.2	0.2	0.5	0.0	0.0	2.7	9.2
1924.4	43337.0	54.3	18.4	0.0	4.0	0.0	0.0	0.0	1.1	5.6	5.9	0.3	0.0	1.6	0.0	0.0	1.6	7.2
1924.5	43338.5	44.2	10.6	0.9	8.3	0.0	0.0	0.0	0.6	8.0	17.4	2.1	0.0	0.6	0.0	0.0	0.9	6.5

Core MD03-2622 Relative Abundance Data (continued)

Depth (cm)	Age (yBP)	*G.b* (%)	*N.d* (%)	*O.u* (%)	*G.a* (%)	*G.c* (%)	*P.o* (%)	*G.m* (%)	*G.r*(p) (%)	*G.r*(w) (%)	*G.s* (%)	*G.g* (%)	*G.t* (%)	*G.rs* (%)	*N.p*(l) (%)	*N.p*(r) (%)	*G.q* (%)	Other (%)
1924.6	43340.0	55.0	15.5	0.6	9.4	0.0	0.0	0.3	0.6	5.8	5.5	1.8	0.3	0.0	0.0	0.0	0.3	4.9
1924.7	43341.5	52.9	17.7	0.0	7.1	0.2	0.0	0.2	2.1	7.1	3.4	0.5	0.0	0.2	0.0	0.0	0.9	7.6
1924.8	43343.0	53.9	17.0	0.0	6.2	0.5	0.0	0.3	1.3	7.0	4.3	1.3	0.5	0.5	0.0	0.0	0.5	6.5
1924.9	43344.5	57.3	17.4	0.2	3.4	0.2	0.0	0.0	2.1	8.2	1.1	0.0	0.0	0.2	0.0	0.0	0.7	9.1
1925.0	43346.0	56.1	20.8	0.2	1.8	0.5	0.0	0.0	1.4	8.0	0.7	0.5	0.2	0.0	0.0	0.0	0.9	8.9
1925.1	43348.0	52.8	20.3	0.4	2.4	0.0	0.0	0.0	1.5	12.0	0.4	0.4	0.0	0.2	0.0	0.0	0.4	9.2
1925.2	43350.0	54.3	18.7	0.2	1.6	0.2	0.0	0.0	1.6	12.1	1.2	0.4	0.2	0.4	0.0	0.0	0.4	8.7
1925.3	43352.0	53.9	20.1	0.0	2.2	0.0	0.0	0.0	1.5	13.6	0.7	0.0	0.0	0.0	0.0	0.0	0.5	7.5
1925.4	43354.0	50.8	18.5	0.0	1.6	0.0	0.0	0.0	1.2	15.2	0.9	0.2	0.0	0.0	0.0	0.0	1.2	10.4
1925.5	43356.0	55.8	19.4	0.4	2.3	0.0	0.0	0.0	1.9	9.7	0.4	0.2	0.0	0.2	0.0	0.0	0.8	8.8
1925.6	43358.0	56.3	20.5	0.0	2.0	0.0	0.0	0.0	1.3	7.3	0.8	0.5	0.0	0.0	0.0	0.0	0.5	11.0
1925.7	43360.0	58.1	17.9	0.0	3.0	0.2	0.0	0.0	2.5	7.8	0.6	0.6	0.2	0.2	0.0	0.0	0.4	8.6
1925.8	43362.0	51.9	19.1	0.0	2.2	0.0	0.0	0.0	1.9	6.7	0.6	0.6	0.0	0.0	0.0	0.0	1.9	15.0
1925.9	43364.0	62.5	15.9	0.0	2.5	0.3	0.0	0.0	0.6	7.8	0.0	0.6	0.0	0.0	0.0	0.0	0.3	9.4
1926.0	43366.0	42.5	20.7	0.0	6.5	0.3	0.0	0.0	1.4	14.2	1.1	0.8	0.3	0.0	0.0	0.0	1.4	10.9
1926.1	43367.5	46.6	16.2	0.2	5.6	0.0	0.0	0.0	2.4	15.3	0.9	1.6	0.0	0.5	0.0	0.0	0.2	10.4
1926.2	43368.9	44.9	13.3	0.0	16.5	0.0	0.0	0.0	2.1	13.1	2.5	0.4	0.4	0.2	0.0	0.0	0.0	6.4
1926.3	43370.4	44.5	16.0	0.0	11.5	0.3	0.0	0.0	1.6	13.3	2.7	0.8	0.0	0.3	0.0	0.0	0.5	8.5
1926.4	43371.8	45.6	14.4	0.0	7.7	0.3	0.0	0.0	1.8	18.0	3.9	0.5	0.3	1.0	0.0	0.0	0.0	6.4
1926.5	43373.3	46.6	14.3	0.0	8.7	0.0	0.0	0.0	2.7	14.5	2.7	0.4	0.2	0.4	0.0	0.0	1.0	8.5
1926.6	43374.7	47.4	12.3	0.0	8.1	0.0	0.0	0.2	2.8	13.4	2.6	0.6	0.4	0.4	0.0	0.0	1.1	10.6
1926.7	43376.2	43.4	13.9	0.0	10.5	0.0	0.0	0.0	1.6	15.8	3.9	0.2	0.2	0.5	0.0	0.0	0.9	9.1
1926.8	43377.6	38.1	13.3	0.4	5.8	0.2	0.0	0.0	2.8	21.7	3.2	0.2	0.2	0.0	0.0	0.0	1.3	12.7
1926.9	43379.1	43.3	9.9	0.2	10.1	0.0	0.0	0.0	2.0	18.8	1.6	0.6	0.2	0.4	0.0	0.0	1.0	11.9
1927.0	43380.5	50.2	10.7	0.2	4.1	0.0	0.0	0.0	2.4	21.0	0.7	1.0	0.2	0.2	0.0	0.0	0.7	8.3
1927.1	43381.5	50.1	13.2	0.6	4.3	0.3	0.0	0.0	1.7	17.8	1.1	2.3	0.3	0.0	0.0	0.0	0.6	7.7
1927.2	43382.4	44.7	15.1	0.3	2.3	0.3	0.0	0.0	4.4	18.7	0.8	1.0	0.0	0.0	0.0	0.0	0.5	11.9
1927.3	43383.4	55.1	14.8	0.0	1.8	0.3	0.0	0.0	3.3	14.5	0.5	0.3	0.0	0.3	0.0	0.0	0.3	9.0

Core MD03-2622 Relative Abundance Data (continued)

Depth (cm)	Age (yBP)	*G.b* (%)	*N.d* (%)	*O.u* (%)	*G.a* (%)	*G.c* (%)	*P.o* (%)	*G.m* (%)	*G.r*(p) (%)	*G.r*(w) (%)	*G.s* (%)	*G.g* (%)	*G.t* (%)	*G.rs* (%)	*N.p*(l) (%)	*N.p*(r) (%)	*G.q* (%)	Other (%)
1927.4	43384.3	46.0	14.6	0.0	1.5	0.0	0.0	0.0	2.9	18.6	0.2	0.2	0.6	0.4	0.0	0.0	0.8	14.4
1927.5	43385.3	46.8	15.5	0.0	3.2	0.2	0.0	0.0	2.0	16.7	0.5	0.2	0.7	0.0	0.0	0.0	0.7	13.5
1927.6	43386.2	52.1	13.4	0.8	2.9	0.0	0.0	0.0	1.8	11.3	1.8	0.3	0.0	0.3	0.0	0.0	1.0	14.4
1927.7	43387.2	47.7	15.2	0.0	2.4	0.0	0.0	0.3	4.6	12.7	0.5	1.4	0.3	0.0	0.0	0.0	1.1	13.8
1927.8	43388.1	54.2	14.3	0.9	3.1	0.6	0.0	0.0	2.2	15.3	0.3	1.2	0.0	0.0	0.0	0.0	0.0	7.8
1927.9	43389.1	53.6	12.5	0.0	2.0	0.3	0.0	0.0	3.0	18.1	0.3	0.7	0.0	0.0	0.0	0.0	0.3	9.2
1928.0	43390.0	52.8	14.5	0.2	1.7	0.2	0.0	0.0	1.2	16.8	0.2	0.5	0.2	0.0	0.0	0.0	0.2	11.4
1928.1	43391.5	49.6	15.4	0.3	2.2	0.0	0.0	0.0	1.9	16.0	0.0	0.6	0.0	0.0	0.0	0.0	0.8	13.2
1928.2	43393.0	59.5	14.4	0.0	1.4	0.0	0.0	0.0	2.0	11.8	0.3	0.6	0.0	0.0	0.0	0.0	0.3	9.8
1928.3	43394.5	54.4	13.1	0.0	1.1	0.0	0.0	0.0	3.0	17.2	0.0	0.8	0.3	0.0	0.0	0.0	0.5	9.6
1928.4	43396.0	58.0	13.4	0.5	1.2	0.0	0.0	0.0	1.6	15.0	0.2	1.8	0.2	0.0	0.0	0.0	0.5	7.6
1928.5	43397.5	53.0	13.4	0.0	2.4	0.4	0.0	0.0	2.4	15.6	0.0	2.2	0.0	0.2	0.0	0.0	0.6	9.7
1928.6	43399.0	56.1	10.8	0.0	1.2	0.0	0.0	0.0	2.0	13.8	0.2	3.0	0.2	0.2	0.0	0.0	0.6	12.0
1928.7	43400.5	51.1	14.1	0.5	1.0	0.0	0.0	0.0	2.4	16.3	0.2	3.6	0.2	0.0	0.0	0.0	0.2	10.3
1928.8	43402.0	51.4	17.4	0.4	1.1	0.0	0.0	0.0	3.3	14.3	0.0	3.8	0.2	0.0	0.0	0.0	0.7	7.6
1928.9	43403.5	54.0	13.4	0.0	0.4	0.2	0.0	0.0	3.2	14.5	0.0	2.6	0.4	0.0	0.0	0.0	0.9	10.4
1929.0	43405.0	59.1	15.0	0.3	1.3	0.5	0.0	0.0	2.3	10.3	0.5	2.1	0.3	0.0	0.0	0.0	0.5	7.8
1929.1	43407.1	54.4	12.4	0.6	0.7	0.2	0.0	0.0	2.6	18.0	0.6	2.0	0.2	0.0	0.0	0.0	0.4	8.0
1929.2	43409.2	50.1	14.4	0.3	1.7	0.0	0.0	0.0	2.5	23.2	0.0	0.7	0.0	0.0	0.0	0.0	0.2	7.0
1929.3	43411.3	56.0	15.7	0.3	0.9	0.0	0.0	0.0	2.3	13.1	0.0	3.7	0.0	0.0	0.0	0.0	0.3	7.7
1929.4	43413.4	58.7	12.8	0.0	2.1	0.0	0.0	0.0	3.5	14.0	0.0	0.5	0.0	0.2	0.0	0.0	0.5	7.7
1929.5	43415.5	58.4	13.4	0.0	2.3	0.0	0.0	0.0	2.5	14.9	0.2	0.2	0.2	0.0	0.0	0.0	0.4	7.5
1929.6	43417.6	48.9	16.4	0.0	1.0	0.0	0.0	0.0	5.8	19.4	0.0	1.0	0.5	0.0	0.0	0.0	0.8	6.3
1929.7	43419.7	55.9	16.3	0.2	0.7	0.0	0.0	0.0	2.6	13.1	0.2	0.2	0.0	0.0	0.0	0.0	0.7	10.1
1929.8	43421.8	53.5	17.7	0.0	1.6	0.0	0.0	0.0	2.9	13.5	1.0	0.0	0.6	0.0	0.0	0.0	0.6	8.4
1929.9	43423.9	52.3	17.4	0.0	1.9	0.0	0.0	0.0	2.3	16.3	0.4	0.2	0.4	0.0	0.0	0.0	0.4	8.3
1930.0	43426.0	58.9	19.6	0.3	1.5	0.0	0.0	0.0	3.9	9.8	0.3	0.3	0.0	0.0	0.0	0.0	0.6	4.8
1930.1	43428.0	62.8	16.7	0.0	1.5	0.0	0.0	0.0	3.6	9.2	0.0	0.3	0.3	0.0	0.0	0.0	0.3	5.4

Core MD03-2622 Relative Abundance Data (continued)

Depth (cm)	Age (yBP)	*G.b* (%)	*N.d* (%)	*O.u* (%)	*G.a* (%)	*G.c* (%)	*P.o* (%)	*G.m* (%)	*G.r*(p) (%)	*G.r*(w) (%)	*G.s* (%)	*G.g* (%)	*G.t* (%)	*G.rs* (%)	*N.p*(l) (%)	*N.p*(r) (%)	*G.q* (%)	Other (%)
1930.2	43429.9	54.9	21.7	0.7	1.0	0.0	0.0	0.0	3.3	4.9	0.3	1.0	1.0	0.3	0.0	0.0	0.3	10.5
1930.3	43431.9	61.0	19.9	0.0	1.2	0.0	0.0	0.3	3.9	5.4	0.0	0.0	0.0	0.3	0.0	0.0	0.9	7.1
1930.4	43433.8	61.0	19.5	0.6	0.0	0.3	0.0	0.0	5.7	3.9	0.3	0.3	0.6	0.0	0.0	0.0	0.9	6.9
1930.5	43435.8	66.4	17.2	0.8	1.1	0.0	0.0	0.0	3.8	2.7	0.3	0.3	0.5	0.0	0.0	0.0	1.3	5.6
1930.6	43437.7	66.9	18.2	0.0	0.6	0.0	0.0	0.0	3.2	2.3	0.0	0.3	0.6	0.3	0.0	0.0	0.9	6.7
1930.7	43439.7	63.3	19.1	0.0	1.8	0.3	0.0	0.0	3.5	2.6	0.0	0.6	0.3	0.6	0.0	0.0	0.6	7.3
1930.8	43441.6	62.7	20.5	0.3	1.0	0.0	0.0	0.0	3.6	2.3	0.0	0.6	0.6	0.3	0.0	0.0	0.3	7.8
1930.9	43443.6	67.7	19.0	0.3	1.3	0.0	0.0	0.0	2.3	1.6	0.3	0.3	0.0	0.0	0.0	0.0	0.6	6.5
1931.0	43445.5	62.9	17.8	0.5	1.2	0.0	0.0	0.0	5.0	2.6	0.5	0.5	1.2	0.2	0.0	0.0	0.5	7.1
1931.1	43447.5	59.7	23.8	0.2	0.6	0.0	0.0	0.0	3.9	2.0	0.0	0.2	0.2	0.0	0.0	0.0	0.6	8.8
1931.2	43449.5	59.2	21.6	0.2	1.5	0.2	0.2	0.0	4.9	2.3	0.2	0.4	0.2	0.2	0.0	0.0	0.6	8.5
1931.3	43451.5	59.5	23.0	0.5	1.7	0.0	0.0	0.0	2.9	1.2	0.2	0.2	0.2	0.0	0.0	0.0	1.0	9.6
1931.4	43453.5	59.1	26.4	0.0	1.9	0.0	0.0	0.0	1.4	0.7	0.0	0.2	0.0	0.2	0.0	0.0	0.5	9.8
1931.5	43455.5	56.5	29.5	0.0	1.6	0.0	0.0	0.0	1.6	0.6	0.3	0.0	0.0	0.0	0.0	0.0	0.6	9.3
1931.6	43457.5	52.6	29.7	0.2	0.9	0.2	0.0	0.0	4.1	0.9	0.2	0.0	0.5	0.0	0.0	0.0	0.5	10.1
1931.7	43459.5	52.9	25.9	0.2	1.5	0.2	0.0	0.2	5.0	2.1	0.0	0.2	0.6	0.2	0.0	0.0	0.8	10.3
1931.8	43461.5	52.7	30.2	0.2	1.0	0.0	0.0	0.0	6.0	1.7	0.0	0.2	0.0	0.0	0.0	0.0	0.4	7.5
1931.9	43463.5	52.2	28.1	0.0	0.6	0.0	0.0	0.0	7.1	2.0	0.0	0.2	0.4	0.0	0.0	0.0	0.4	8.9
1932.0	43465.5	55.7	24.2	0.0	0.6	0.0	0.0	0.0	7.6	1.5	0.3	0.3	0.0	0.3	0.0	0.0	1.5	8.0
1932.1	43467.2	49.6	26.7	0.0	1.7	0.0	0.0	0.0	9.1	1.2	0.7	0.0	0.0	0.2	0.0	0.0	0.5	10.1
1932.2	43468.8	51.4	26.1	0.0	1.1	0.0	0.0	0.3	11.9	1.4	0.3	0.0	0.3	0.3	0.0	0.0	0.8	6.1
1932.3	43470.5	56.0	23.8	0.3	1.0	0.0	0.0	0.3	8.6	0.5	0.0	0.5	0.0	0.0	0.0	0.0	0.5	8.4
1932.4	43472.1	51.3	26.5	0.0	1.5	0.0	0.0	0.0	10.8	1.2	0.3	0.3	0.0	0.0	0.0	0.0	0.3	7.9
1932.5	43473.8	54.8	21.0	0.6	1.7	0.3	0.0	0.0	6.8	1.4	0.0	0.6	0.0	0.3	0.0	0.0	0.3	12.2
1932.6	43475.4	56.2	24.4	0.0	1.7	0.0	0.0	0.0	5.2	0.7	0.2	0.5	0.2	0.0	0.0	0.0	0.7	10.1
1932.7	43477.1	57.6	23.1	0.3	1.7	0.0	0.0	0.0	7.5	0.6	0.3	0.3	0.0	0.0	0.0	0.0	1.2	7.5
1932.8	43478.7	51.8	27.4	0.0	2.1	0.0	0.0	0.0	7.6	0.0	0.3	0.0	0.6	0.0	0.0	0.0	0.9	9.1
1932.9	43480.4	51.5	25.8	0.3	2.3	0.0	0.3	0.0	6.6	2.0	0.3	0.3	0.3	0.0	0.0	0.0	0.8	9.7

Core MD03-2622 Relative Abundance Data (continued)

Depth (cm)	Age (yBP)	*G.b* (%)	*N.d* (%)	*O.u* (%)	*G.a* (%)	*G.c* (%)	*P.o* (%)	*G.m* (%)	*G.r*(p) (%)	*G.r*(w) (%)	*G.s* (%)	*G.g* (%)	*G.t* (%)	*G.rs* (%)	*N.p*(l) (%)	*N.p*(r) (%)	*G.q* (%)	Other (%)
1933.0	43482.0	56.5	23.3	0.8	1.3	0.0	0.0	0.0	5.1	2.5	0.3	0.5	0.3	0.0	0.0	0.0	0.0	9.6
1933.1	43484.1	51.6	26.7	0.0	2.1	0.7	0.0	0.0	7.7	3.7	0.2	0.0	0.0	0.0	0.0	0.0	0.7	6.5
1933.2	43486.1	51.5	24.1	0.2	1.7	0.0	0.0	0.0	7.5	2.7	0.6	0.4	0.2	0.0	0.0	0.0	0.2	11.0
1933.3	43488.2	52.4	28.5	0.0	1.8	0.3	0.0	0.0	7.1	1.0	0.3	0.8	0.3	0.0	0.0	0.0	0.0	7.6
1933.4	43490.2	53.2	22.3	0.0	1.8	0.2	0.0	0.0	8.0	3.0	0.5	0.5	0.7	0.2	0.0	0.0	0.2	9.4
1933.5	43492.3	51.6	24.0	0.2	2.0	0.2	0.0	0.0	10.0	1.5	0.2	0.2	0.5	0.3	0.0	0.0	0.3	9.2
1933.6	43494.3	49.4	26.5	0.6	1.8	0.0	0.0	0.0	9.1	2.4	0.3	0.3	0.6	0.3	0.0	0.0	1.2	7.6
1933.7	43496.4	56.0	25.9	0.0	1.0	0.3	0.0	0.0	8.4	0.6	0.3	0.0	0.0	0.0	0.0	0.0	1.0	6.5
1933.8	43498.4	51.1	22.3	0.0	1.7	0.0	0.0	0.0	12.0	1.5	0.2	0.8	0.0	0.2	0.0	0.0	1.3	9.0
1933.9	43500.5	54.4	24.2	0.3	1.3	0.0	0.0	0.0	7.0	1.3	0.5	0.5	0.5	0.3	0.0	0.0	1.3	8.5
1934.0	43502.5	55.5	22.2	0.2	1.7	0.0	0.0	0.0	6.2	2.9	1.0	0.6	0.2	0.4	0.0	0.0	1.4	7.7
1934.1	43504.6	54.8	25.4	0.3	2.1	0.0	0.0	0.3	9.3	1.5	0.0	0.6	0.0	0.0	0.0	0.0	1.2	4.5
1934.2	43506.6	54.7	19.0	0.0	2.0	0.2	0.0	0.0	11.1	3.0	0.2	0.2	0.5	0.0	0.0	0.0	1.5	7.6
1934.3	43508.7	62.1	20.1	0.6	3.2	0.3	0.3	0.0	4.5	1.0	0.3	0.6	0.6	0.0	0.0	0.0	0.6	5.7
1934.4	43510.7	54.4	20.0	0.3	1.9	0.0	0.0	0.0	7.5	4.1	1.6	0.9	0.6	0.0	0.0	0.0	0.9	7.8
1934.5	43512.8	56.0	21.2	0.6	4.0	0.4	0.0	0.0	6.6	1.6	0.6	0.4	0.0	0.0	0.0	0.0	0.4	8.2
1934.6	43514.8	58.1	20.4	1.3	3.5	0.0	0.0	0.0	5.2	1.5	0.6	0.8	0.2	0.4	0.0	0.0	0.0	8.1
1934.7	43516.9	59.0	19.8	0.4	4.7	0.7	0.0	0.0	6.5	3.1	0.7	0.4	0.4	0.0	0.0	0.0	0.0	4.2
1934.8	43518.9	54.5	16.4	0.4	3.2	0.0	0.0	0.0	11.0	5.6	0.8	0.4	1.0	0.0	0.0	0.0	0.0	6.6
1934.9	43521.0	52.3	15.2	0.3	2.6	0.7	0.0	0.0	15.9	8.6	0.0	1.0	0.0	0.0	0.0	0.0	0.0	3.3
1935.0	43523.0	53.2	17.5	0.5	3.9	0.3	0.0	0.0	10.3	9.3	1.0	0.5	0.0	0.3	0.0	0.0	0.0	3.3
1935.1	43525.1	50.3	16.6	0.4	2.8	0.0	0.0	0.0	11.0	12.8	1.2	1.0	0.4	0.0	0.0	0.0	0.2	3.2
1935.2	43527.1	46.3	12.8	0.2	2.0	0.2	0.0	0.0	12.4	19.1	0.2	0.7	0.7	0.7	0.0	0.0	0.0	4.7
1935.3	43529.2	48.5	16.8	0.3	1.0	0.0	0.0	0.0	14.0	13.3	0.5	0.5	0.0	0.5	0.0	0.0	0.0	4.6
1935.4	43531.2	45.7	14.6	0.0	3.1	0.2	0.0	0.0	11.2	17.2	0.2	0.7	0.5	0.0	0.0	0.0	0.0	6.5
1935.5	43533.3	49.2	14.1	0.0	1.9	0.0	0.0	0.0	9.3	19.8	0.1	0.3	0.3	0.0	0.0	0.0	0.0	5.0
1935.6	43535.3	44.0	16.7	0.8	1.9	0.4	0.0	0.0	9.1	19.9	0.8	0.4	0.6	0.4	0.0	0.0	0.0	4.9
1935.7	43537.4	53.0	15.4	0.0	2.6	0.0	0.0	0.0	5.5	18.3	0.9	0.2	0.0	0.0	0.0	0.0	0.2	4.0

Core MD03-2622 Relative Abundance Data (continued)

Depth (cm)	Age (yBP)	*G.b* (%)	*N.d* (%)	*O.u* (%)	*G.a* (%)	*G.c* (%)	*P.o* (%)	*G.m* (%)	*G.r*(p) (%)	*G.r*(w) (%)	*G.s* (%)	*G.g* (%)	*G.t* (%)	*G.rs* (%)	*N.p*(l) (%)	*N.p*(r) (%)	*G.q* (%)	Other (%)
1935.8	43539.4	51.1	11.0	0.2	3.4	0.2	0.0	0.0	5.2	20.6	0.3	0.0	0.2	0.0	0.0	0.0	0.5	7.4
1935.9	43541.5	51.9	13.9	0.0	2.9	0.0	0.0	0.0	6.8	18.7	0.7	0.0	0.3	0.2	0.0	0.0	0.2	4.5
1936.0	43543.5	52.6	12.5	0.6	3.7	0.0	0.0	0.0	6.2	18.7	1.6	0.3	0.3	0.0	0.0	0.0	0.3	3.1
1936.1	43545.7	51.4	22.0	0.2	2.1	0.0	0.0	0.0	6.6	12.3	0.6	0.6	0.4	0.0	0.0	0.0	0.0	3.7
1936.2	43547.8	49.3	19.6	0.4	1.9	0.2	0.0	0.0	12.2	10.7	0.8	0.8	0.0	0.2	0.0	0.0	1.0	2.9
1936.3	43550.0	53.8	22.0	0.6	1.6	0.2	0.0	0.2	6.9	7.4	0.9	0.3	0.0	0.2	0.0	0.0	0.3	5.7
1936.4	43552.1	58.3	15.3	1.1	2.3	0.2	0.0	0.0	7.8	7.0	0.8	0.6	0.2	0.0	0.0	0.0	0.4	5.9
1936.5	43554.3	57.2	24.0	0.3	2.3	0.3	0.0	0.0	4.4	4.4	0.0	0.9	0.0	0.3	0.0	0.0	0.6	5.3
1936.6	43556.4	57.2	19.1	0.9	2.2	0.3	0.0	0.0	6.8	5.8	0.0	0.3	0.0	0.0	0.0	0.0	0.6	6.8
1936.7	43558.6	59.2	21.4	0.2	2.2	0.0	0.0	0.0	6.1	4.3	0.2	0.2	0.0	0.0	0.0	0.0	0.3	6.0
1936.8	43560.7	61.8	19.1	0.0	0.6	0.0	0.0	0.0	3.5	5.3	0.3	0.3	0.6	0.3	0.0	0.0	0.9	7.4
1936.9	43562.9	58.3	25.3	0.0	0.5	0.3	0.0	0.0	4.5	5.0	0.5	0.3	0.0	0.0	0.0	0.0	0.5	5.0
1937.0	43565.0	60.7	18.0	0.2	2.3	0.0	0.0	0.0	3.5	5.3	0.2	0.3	0.3	0.2	0.0	0.0	0.7	8.4
1937.1	43566.9	60.0	19.5	0.4	2.1	0.0	0.0	0.0	4.8	4.0	0.0	0.2	0.2	0.2	0.0	0.0	0.2	8.4
1937.2	43568.7	56.3	22.9	0.0	3.9	0.0	0.0	0.0	5.8	1.8	0.0	0.8	0.0	0.0	0.0	0.0	1.1	7.4
1937.3	43570.6	54.8	21.7	0.3	4.3	0.3	0.0	0.0	6.7	3.3	0.0	0.3	0.0	0.3	0.0	0.0	1.0	6.7
1937.4	43572.4	55.1	21.3	0.8	10.0	0.0	0.0	0.0	3.9	1.7	0.3	0.3	0.3	0.0	0.0	0.0	0.0	6.4
1937.5	43574.3	53.2	18.3	0.0	12.7	0.2	0.0	0.0	6.0	1.3	0.0	0.6	0.2	0.0	0.0	0.0	0.2	7.1
1937.6	43576.1	52.8	15.6	0.2	13.6	0.2	0.2	0.0	7.6	1.8	0.2	0.7	0.0	0.0	0.0	0.0	0.4	6.7
1937.7	43578.0	53.0	22.1	1.0	8.2	0.2	0.0	0.0	5.9	3.0	0.0	0.8	0.0	0.2	0.0	0.0	0.2	5.5
1937.8	43579.8	58.6	21.6	0.0	6.8	0.2	0.0	0.0	4.7	1.2	0.2	0.6	0.0	0.0	0.0	0.0	0.0	6.0
1937.9	43581.7	54.0	21.4	0.7	8.3	0.0	0.0	0.2	5.7	2.1	0.5	0.7	0.0	0.0	0.0	0.0	0.2	6.4
1938.0	43583.5	55.8	28.1	0.4	0.9	0.0	0.0	0.0	4.0	1.5	0.2	0.4	0.0	0.0	0.0	0.0	0.2	8.5
1938.1	43585.4	53.3	22.9	1.1	3.9	0.4	0.0	0.0	8.3	3.7	0.2	0.2	0.0	0.0	0.0	0.0	0.2	5.7
1938.2	43587.2	55.5	25.5	1.3	1.9	0.4	0.0	0.2	7.7	1.3	0.0	0.4	0.0	0.2	0.0	0.0	0.2	5.3
1938.3	43589.1	59.8	21.1	0.3	1.2	0.0	0.0	0.0	6.5	1.8	0.0	0.6	0.0	0.0	0.0	0.0	0.6	8.0
1938.4	43590.9	63.1	16.4	0.7	3.5	0.2	0.0	0.0	4.9	2.3	0.0	0.5	0.0	0.5	0.0	0.0	0.7	7.0
1938.5	43592.8	60.3	17.4	0.4	3.5	0.0	0.0	0.2	8.2	1.5	0.0	0.4	0.4	0.0	0.0	0.0	0.9	6.6

Core MD03-2622 Relative Abundance Data (continued)

Depth (cm)	Age (yBP)	*G.b* (%)	*N.d* (%)	*O.u* (%)	*G.a* (%)	*G.c* (%)	*P.o* (%)	*G.m* (%)	*G.r*(p) (%)	*G.r*(w) (%)	*G.s* (%)	*G.g* (%)	*G.t* (%)	*G.rs* (%)	*N.p*(l) (%)	*N.p*(r) (%)	*G.q* (%)	Other (%)
1938.6	43594.6	59.1	19.2	0.2	2.2	0.0	0.0	0.0	5.6	2.2	0.0	0.5	0.0	1.0	0.0	0.0	0.7	9.2
1938.7	43596.5	61.8	16.8	0.0	2.2	0.0	0.0	0.0	6.2	2.4	0.0	0.2	0.2	0.0	0.0	0.0	0.4	9.7
1938.8	43598.3	61.4	18.9	0.4	1.7	0.0	0.0	0.0	4.9	3.2	0.2	0.4	0.0	0.2	0.0	0.0	0.7	8.1
1938.9	43600.2	57.4	19.1	0.2	2.6	0.0	0.0	0.0	7.3	4.2	0.5	0.5	0.2	0.5	0.0	0.0	0.5	7.1
1939.0	43602.0	57.3	18.7	0.0	2.0	0.5	0.0	0.0	7.0	5.6	0.2	0.2	0.2	0.0	0.0	0.0	0.7	7.4
1939.1	43604.2	50.8	21.1	0.6	2.3	0.0	0.0	0.0	8.8	6.6	0.0	0.4	0.4	0.4	0.0	0.0	0.6	8.0
1939.2	43606.4	55.8	24.3	0.2	1.7	0.2	0.0	0.0	5.5	2.5	0.2	0.0	0.0	0.7	0.0	0.0	0.5	8.2
1939.3	43608.6	53.1	25.7	0.2	1.1	0.4	0.0	0.0	7.5	4.0	0.0	0.2	0.4	0.0	0.0	0.0	0.9	6.4
1939.4	43610.8	47.8	28.1	0.4	2.5	0.2	0.0	0.2	8.7	2.3	0.2	0.4	0.2	0.4	0.0	0.0	0.8	7.7
1939.5	43613.0	62.4	18.8	0.2	1.6	0.2	0.0	0.0	6.4	2.1	0.3	0.2	0.2	0.2	0.0	0.0	0.5	7.1
1939.6	43615.2	57.7	19.4	0.2	0.9	0.2	0.0	0.0	8.3	4.1	0.5	0.5	0.2	0.0	0.0	0.0	2.0	6.1
1939.7	43617.4	60.1	18.4	0.0	1.2	0.0	0.0	0.0	7.4	3.7	0.5	0.0	0.0	0.7	0.0	0.0	1.6	6.5
1939.8	43619.6	59.5	18.0	0.3	2.3	0.0	0.0	0.3	8.5	2.9	1.0	0.0	0.0	0.0	0.0	0.0	1.6	5.6
1939.9	43621.8	56.3	18.3	1.1	2.2	0.2	0.0	0.2	9.5	4.0	0.2	0.4	0.4	0.0	0.0	0.0	1.1	6.1
1940.0	43624.0	55.1	16.9	0.6	2.1	0.0	0.0	0.2	10.7	4.7	0.4	0.6	0.0	0.0	0.0	0.0	1.0	7.6
1940.1	43626.0	52.6	19.4	0.2	1.0	0.2	0.0	0.0	14.9	3.3	0.5	0.2	0.3	0.2	0.0	0.0	0.9	6.3
1940.2	43628.0	51.9	17.0	0.2	1.8	0.0	0.0	0.0	14.2	5.2	0.5	0.2	0.0	0.3	0.0	0.0	1.3	7.5
1940.3	43630.0	59.6	22.4	0.2	0.5	0.2	0.0	0.0	7.9	1.5	0.2	0.0	0.2	0.0	0.0	0.0	1.0	6.5
1940.4	43632.0	56.9	22.6	0.3	0.3	0.3	0.0	0.0	8.9	2.0	1.0	0.5	0.3	0.3	0.0	0.0	1.0	5.8
1940.5	43634.0	60.1	19.7	0.4	0.9	0.1	0.0	0.0	10.0	2.3	0.0	0.3	0.0	0.0	0.0	0.0	0.3	5.8
1940.6	43636.0	64.7	16.0	0.0	1.1	0.0	0.0	0.0	9.0	1.7	0.0	0.8	0.0	0.0	0.0	0.0	0.8	5.9
1940.7	43638.0	68.1	15.3	0.0	1.4	0.2	0.0	0.0	5.6	1.4	0.0	0.5	0.0	0.0	0.0	0.0	0.9	6.5
1940.8	43640.0	59.7	19.8	0.0	1.4	0.0	0.0	0.0	6.2	1.2	0.2	0.2	0.0	0.2	0.0	0.0	1.2	9.9
1940.9	43642.0	54.4	24.4	0.6	1.1	0.0	0.0	0.0	6.6	1.7	0.3	0.0	0.3	0.0	0.0	0.0	1.1	9.5
1941.0	43644.0	65.1	18.5	0.5	0.9	0.0	0.0	0.0	3.7	2.1	0.0	0.5	0.0	0.0	0.0	0.0	1.2	7.6
1941.1	43646.5	64.3	17.5	0.5	1.1	0.2	0.0	0.0	7.7	0.8	0.2	0.3	0.6	0.0	0.0	0.0	0.8	6.2
1941.2	43648.9	61.0	17.1	0.6	0.9	0.0	0.0	0.3	9.8	2.3	0.6	0.0	0.0	0.3	0.0	0.0	0.9	6.4
1941.3	43651.4	63.8	17.5	0.0	1.3	0.6	0.0	0.3	5.1	2.5	0.0	0.6	0.0	0.0	0.0	0.0	1.6	6.7

Core MD03-2622 Relative Abundance Data (continued)

Depth (cm)	Age (yBP)	*G.b* (%)	*N.d* (%)	*O.u* (%)	*G.a* (%)	*G.c* (%)	*P.o* (%)	*G.m* (%)	*G.r*(p) (%)	*G.r*(w) (%)	*G.s* (%)	*G.g* (%)	*G.t* (%)	*G.rs* (%)	*N.p*(l) (%)	*N.p*(r) (%)	*G.q* (%)	Other (%)
1941.4	43653.8	61.6	14.4	0.5	1.4	0.0	0.0	0.0	10.0	2.8	0.5	0.2	0.0	0.0	0.0	0.0	0.9	7.7
1941.5	43656.3	56.8	16.9	0.7	2.2	0.0	0.0	0.2	8.3	4.2	0.3	0.3	0.2	0.5	0.0	0.0	1.0	8.4
1941.6	43658.7	56.5	18.5	0.0	1.0	0.2	0.0	0.0	8.9	3.4	0.2	0.5	0.0	0.2	0.0	0.0	0.8	9.9
1941.7	43661.2	55.6	18.5	1.0	2.5	0.4	0.0	0.0	8.7	3.7	0.2	0.0	0.0	0.2	0.0	0.0	1.0	8.3
1941.8	43663.6	56.9	15.6	0.2	6.5	0.2	0.0	0.2	8.9	2.0	0.6	0.6	0.0	0.2	0.0	0.0	0.4	7.8
1941.9	43666.1	61.7	14.7	0.7	5.4	0.2	0.0	0.0	9.1	1.4	0.0	0.3	0.0	0.2	0.0	0.0	1.2	5.2
1942.0	43668.5	53.4	15.7	0.2	9.2	0.2	0.0	0.0	9.8	2.6	0.6	0.4	0.0	0.0	0.0	0.0	1.0	6.9
1942.1	43670.2	58.3	14.1	0.0	10.2	0.0	0.0	0.0	6.8	3.2	0.2	0.2	0.0	0.0	0.0	0.0	0.3	6.6
1942.2	43671.8	53.5	14.7	0.5	10.7	0.0	0.0	0.3	9.0	2.0	0.5	0.3	0.3	0.2	0.0	0.0	1.2	6.7
1942.3	43673.5	49.9	14.6	0.3	12.8	0.0	0.0	0.0	9.4	3.1	0.7	0.5	0.0	0.3	0.0	0.0	1.3	7.1
1942.4	43675.1	48.7	15.3	0.3	10.5	0.0	0.0	0.1	11.5	2.7	0.6	0.7	0.0	0.1	0.0	0.0	1.5	7.8
1942.5	43676.8	47.6	16.0	0.6	8.3	0.0	0.0	0.0	11.8	2.6	0.9	1.1	0.0	0.0	0.0	0.0	1.9	9.2
1942.6	43678.4	45.4	18.6	0.2	8.6	0.0	0.0	0.2	13.1	1.4	1.6	1.4	0.0	0.2	0.0	0.0	1.1	8.4
1942.7	43680.1	47.5	18.2	0.2	8.9	0.0	0.0	0.0	9.9	3.0	2.0	2.0	0.0	0.0	0.0	0.0	1.2	7.1
1942.8	43681.7	47.3	19.4	0.7	9.5	0.0	0.0	0.0	11.7	1.5	0.7	1.0	0.0	0.0	0.0	0.0	0.7	7.5
1942.9	43683.4	48.4	14.4	0.0	12.5	0.3	0.0	0.3	9.4	1.6	1.3	0.6	0.0	0.0	0.0	0.0	0.9	10.3
1943.0	43685.0	48.2	16.2	0.2	13.0	0.0	0.0	0.2	9.0	1.3	0.6	1.3	0.0	0.4	0.0	0.0	1.9	7.7
1943.1	43686.7	47.0	15.5	0.1	12.6	0.0	0.0	0.0	10.7	1.9	0.6	0.6	0.3	0.0	0.0	0.0	1.2	9.5
1943.2	43688.4	47.9	16.7	0.3	11.9	0.3	0.0	0.3	10.7	2.4	0.3	0.6	0.0	0.0	0.0	0.0	2.1	6.5
1943.3	43690.1	50.5	17.7	0.0	8.3	0.0	0.0	0.3	10.7	1.3	0.3	0.3	0.5	0.3	0.0	0.0	1.0	8.9
1943.4	43691.8	48.8	20.4	0.2	5.6	0.2	0.0	0.0	13.1	2.6	0.2	0.2	0.0	0.2	0.0	0.0	1.3	7.4
1943.5	43693.5	50.4	13.0	0.7	2.9	0.0	0.2	0.2	20.3	2.4	1.1	0.0	0.0	0.2	0.0	0.0	1.1	7.5
1943.6	43695.2	47.6	18.2	0.6	1.5	0.0	0.1	0.1	19.9	2.8	0.0	0.4	0.0	0.3	0.0	0.0	1.0	7.4
1943.7	43696.9	45.7	16.4	0.0	0.9	0.2	0.0	0.0	25.9	1.8	0.0	0.2	0.0	0.2	0.0	0.0	0.7	8.0
1943.8	43698.6	53.6	16.1	0.0	3.0	0.0	0.0	0.0	19.6	2.4	0.0	0.2	0.2	0.0	0.0	0.0	0.4	4.5
1943.9	43700.3	49.7	15.4	0.0	2.6	0.0	0.0	0.0	20.0	3.0	0.6	0.4	0.2	0.4	0.0	0.0	1.1	6.6
1944.0	43702.0	52.8	12.3	0.1	3.0	0.3	0.0	0.0	20.0	1.3	0.9	0.7	0.1	0.3	0.0	0.0	0.6	7.5
1944.1	43704.2	57.8	10.5	0.0	4.6	0.0	0.0	0.0	18.0	1.1	0.7	0.2	0.0	0.0	0.0	0.0	0.5	6.6

Core MD03-2622 Relative Abundance Data (continued)

Depth (cm)	Age (yBP)	*G.b* (%)	*N.d* (%)	*O.u* (%)	*G.a* (%)	*G.c* (%)	*P.o* (%)	*G.m* (%)	*G.r*(p) (%)	*G.r*(w) (%)	*G.s* (%)	*G.g* (%)	*G.t* (%)	*G.rs* (%)	*N.p*(l) (%)	*N.p*(r) (%)	*G.q* (%)	Other (%)
1944.2	43706.4	48.7	13.3	0.3	4.1	0.0	0.0	0.0	24.6	1.8	0.5	0.8	0.0	0.0	0.0	0.0	0.3	5.6
1944.3	43708.6	48.0	12.1	0.0	3.5	0.5	0.0	0.0	26.6	1.3	0.4	0.4	0.0	0.0	0.0	0.0	0.7	6.6
1944.4	43710.8	47.9	13.8	0.0	2.6	0.2	0.2	0.0	27.8	2.0	0.5	0.5	0.0	0.0	0.0	0.0	0.5	4.1
1944.5	43713.0	51.9	11.4	0.0	5.7	0.0	0.0	0.0	18.9	2.1	0.0	0.5	0.0	0.2	0.0	0.0	0.3	9.0
1944.6	43715.2	50.6	14.0	0.0	5.5	0.5	0.0	0.0	18.4	2.3	0.0	0.0	0.0	0.5	0.0	0.0	0.5	7.5
1944.7	43717.4	54.7	10.8	0.2	9.9	0.0	0.0	0.0	15.1	1.7	0.6	0.2	0.0	1.3	0.0	0.0	0.2	5.2
1944.8	43719.6	53.6	9.9	0.0	10.1	0.0	0.0	0.0	15.1	1.4	0.0	0.5	0.0	0.9	0.0	0.0	0.5	8.0
1944.9	43721.8	56.6	10.7	0.3	7.1	0.0	0.0	0.0	12.6	2.7	0.3	0.3	0.0	1.1	0.0	0.0	0.3	8.0
1945.0	43724.0	56.7	10.7	0.0	7.1	0.0	0.0	0.0	13.5	1.5	0.9	0.6	0.3	0.6	0.0	0.0	1.2	6.7
1945.1	43725.4	61.8	13.8	0.5	4.2	0.5	0.0	0.0	9.5	2.7	0.0	0.3	0.3	0.3	0.0	0.0	1.1	5.0
1945.2	43726.8	60.1	18.4	0.0	5.0	0.0	0.0	0.0	8.1	1.8	0.0	0.5	0.0	0.0	0.0	0.0	1.0	5.0
1945.3	43728.2	62.5	17.3	0.3	1.3	0.0	0.0	0.0	10.3	0.7	0.0	0.3	0.0	0.0	0.0	0.0	0.7	6.6
1945.4	43729.6	61.5	19.5	0.8	1.5	0.0	0.0	0.0	7.8	0.8	0.0	0.5	0.3	0.3	0.0	0.0	0.3	6.8
1945.5	43731.0	58.9	18.1	0.0	1.6	0.0	0.2	0.0	7.4	1.4	0.0	0.0	0.7	0.2	0.0	0.0	0.5	10.9
1945.6	43732.4	58.4	19.7	0.2	1.7	0.0	0.0	0.0	8.4	2.6	0.0	0.2	0.6	0.0	0.0	0.0	0.6	7.8
1945.7	43733.8	59.0	19.6	0.2	2.3	0.4	0.0	0.0	8.3	1.2	0.4	0.6	0.2	0.0	0.0	0.0	0.4	7.5
1945.8	43735.2	61.0	13.7	0.3	3.0	0.0	0.0	0.0	8.3	2.1	0.0	0.6	0.0	0.0	0.0	0.0	1.2	9.8
1945.9	43736.6	57.7	18.3	1.0	2.2	0.0	0.0	0.0	10.6	1.6	0.0	1.0	0.0	0.0	0.0	0.0	1.0	6.7
1946.0	43738.0	58.2	16.7	0.3	4.2	0.6	0.0	0.0	7.7	2.3	0.3	1.0	0.3	0.3	0.0	0.0	0.3	7.7
1946.1	43739.6	64.0	9.8	0.2	0.5	0.0	0.0	0.0	15.0	1.5	0.0	0.3	0.7	0.2	0.0	0.0	0.8	7.1
1946.2	43741.1	63.9	10.8	0.0	1.4	0.3	0.0	0.0	9.9	2.3	0.3	0.6	0.6	0.0	0.0	0.0	0.6	9.4
1946.3	43742.7	66.2	14.4	0.0	0.3	0.0	0.0	0.3	11.1	1.0	0.0	0.3	0.0	0.0	0.0	0.0	0.7	5.6
1946.4	43744.2	64.5	13.5	0.0	1.1	0.0	0.0	0.0	14.0	1.9	0.0	0.0	0.6	0.0	0.0	0.0	0.3	4.1
1946.5	43745.8	57.0	13.1	0.0	0.8	0.0	0.0	0.8	17.3	1.4	0.0	0.6	0.6	0.0	0.0	0.0	0.3	8.1
1946.6	43747.3	53.7	13.3	0.0	2.2	0.0	0.0	0.0	16.7	3.7	0.3	0.0	0.6	0.3	0.0	0.0	0.6	8.6
1946.7	43748.9	59.4	10.3	0.2	2.4	0.0	0.0	0.0	14.9	2.6	0.0	0.2	0.0	0.0	0.0	0.0	0.7	9.2
1946.8	43750.4	62.3	11.5	1.1	0.6	0.0	0.0	0.0	13.4	2.6	0.0	0.4	0.0	0.0	0.0	0.0	0.6	7.5
1946.9	43752.0	58.0	15.0	0.0	1.0	0.2	0.0	0.2	9.7	1.4	0.0	0.0	0.2	0.0	0.0	0.0	0.6	13.8

Core MD03-2622 Relative Abundance Data (continued)

Depth (cm)	Age (yBP)	*G.b* (%)	*N.d* (%)	*O.u* (%)	*G.a* (%)	*G.c* (%)	*P.o* (%)	*G.m* (%)	*G.r*(p) (%)	*G.r*(w) (%)	*G.s* (%)	*G.g* (%)	*G.t* (%)	*G.rs* (%)	*N.p*(l) (%)	*N.p*(r) (%)	*G.q* (%)	Other (%)
1947.0	43753.5	56.8	15.7	0.0	0.7	0.2	0.0	0.0	6.5	1.9	0.2	0.2	0.0	0.2	0.0	0.0	0.9	16.6
1947.1	43754.8	61.9	18.1	0.0	0.3	0.3	0.0	0.0	3.4	2.3	0.3	0.6	0.0	0.3	0.0	0.0	0.9	11.7
1947.2	43756.1	57.3	15.5	0.2	1.4	0.0	0.0	0.0	9.5	1.9	0.0	0.5	0.5	0.2	0.0	0.0	0.5	12.5
1947.3	43757.4	58.4	15.0	0.2	1.2	0.0	0.0	0.0	7.8	4.0	0.3	0.7	0.3	1.0	0.0	0.0	1.2	9.8
1947.4	43758.7	60.8	13.3	0.0	0.4	0.0	0.0	0.0	11.0	4.2	0.2	0.6	0.0	0.8	0.0	0.0	0.6	8.0
1947.5	43760.0	57.5	19.4	0.0	1.0	0.0	0.0	0.0	6.6	2.3	0.0	0.8	0.3	1.0	0.0	0.0	0.5	10.5
1947.6	43761.3	63.4	17.6	0.6	0.3	0.0	0.0	0.0	6.8	2.3	0.3	0.9	0.0	0.0	0.0	0.0	0.6	7.4
1947.7	43762.6	60.3	19.0	0.3	3.1	0.0	0.0	0.0	6.5	2.3	0.8	1.4	0.0	0.0	0.0	0.0	0.3	5.9
1947.8	43763.9	62.9	20.9	0.5	1.6	0.2	0.0	0.0	5.1	0.7	0.0	1.2	0.2	0.0	0.0	0.0	0.5	6.3
1947.9	43765.2	65.4	19.6	0.0	1.3	0.7	0.0	0.0	2.0	2.0	0.3	0.3	0.0	0.3	0.0	0.0	0.7	7.5
1948.0	43766.5	53.9	23.5	1.1	2.9	0.5	0.0	0.0	9.3	2.1	0.0	0.8	0.3	0.0	0.0	0.0	0.5	5.1
1948.1	43768.4	58.8	22.3	0.3	4.3	0.3	0.0	0.0	5.5	1.0	0.3	0.5	0.0	0.0	0.0	0.0	0.8	6.3
1948.2	43770.3	60.2	18.4	0.0	4.9	0.0	0.0	0.0	6.1	1.2	0.2	0.7	0.0	0.0	0.0	0.0	0.5	7.9
1948.3	43772.2	59.6	21.2	0.0	2.0	0.0	0.0	0.0	4.0	1.7	0.0	0.7	0.0	0.0	0.0	0.0	0.7	10.3
1948.4	43774.1	60.1	17.2	0.2	3.7	0.0	0.0	0.2	5.6	1.2	0.0	0.7	0.2	0.0	0.0	0.0	0.9	10.0
1948.5	43776.0	61.1	19.0	0.2	1.6	0.6	0.0	0.0	8.0	1.2	0.2	0.2	0.6	0.0	0.0	0.0	0.2	7.0
1948.6	43777.9	58.0	14.2	1.2	3.5	0.2	0.0	0.4	5.8	1.9	0.8	0.8	0.0	0.0	0.0	0.0	1.0	12.1
1948.7	43779.8	57.9	16.9	0.3	3.3	0.3	0.0	0.3	5.5	1.9	1.1	0.5	0.5	0.3	0.0	0.0	0.5	10.7
1948.8	43781.7	61.8	17.0	0.0	2.0	0.0	0.0	0.0	5.9	1.0	0.3	0.7	0.3	0.0	0.0	0.0	1.0	10.1
1948.9	43783.6	59.0	16.5	0.0	1.6	0.0	0.0	0.0	7.9	1.9	1.0	0.3	0.3	0.0	0.0	0.0	0.3	11.1
1949.0	43785.5	62.8	15.5	0.0	2.3	0.0	0.0	0.0	8.3	2.1	0.9	0.5	0.0	0.0	0.0	0.0	0.2	7.4
1949.1	43787.9	62.9	16.9	0.3	2.6	0.0	0.0	0.3	5.3	3.6	0.7	1.0	0.0	0.0	0.0	0.0	0.0	6.3
1949.2	43790.3	56.2	17.5	0.6	1.9	0.3	0.0	0.3	11.0	2.3	1.6	0.3	0.6	0.0	0.0	0.0	0.0	7.1
1949.3	43792.7	56.3	20.4	0.0	1.3	0.5	0.0	0.0	9.7	1.9	1.1	1.3	0.3	0.3	0.0	0.0	0.8	6.2
1949.4	43795.1	57.6	17.5	0.0	2.5	0.5	0.0	0.0	7.9	3.2	0.5	1.0	0.2	0.2	0.0	0.0	1.0	7.9
1949.5	43797.5	59.7	17.1	0.0	4.1	0.0	0.0	0.3	8.6	1.0	0.0	1.0	0.3	1.3	0.0	0.0	0.6	6.0
1949.6	43799.9	56.5	14.2	0.0	3.3	0.0	0.0	0.0	13.0	1.2	0.9	1.2	0.3	2.1	0.0	0.0	0.3	7.1
1949.7	43802.3	60.1	12.5	0.5	1.8	0.0	0.0	0.0	9.5	2.8	0.5	0.0	0.5	2.6	0.0	0.0	0.8	8.4

Core MD03-2622 Relative Abundance Data (continued)

Depth (cm)	Age (yBP)	*G.b* (%)	*N.d* (%)	*O.u* (%)	*G.a* (%)	*G.c* (%)	*P.o* (%)	*G.m* (%)	*G.r*(p) (%)	*G.r*(w) (%)	*G.s* (%)	*G.g* (%)	*G.t* (%)	*G.rs* (%)	*N.p*(l) (%)	*N.p*(r) (%)	*G.q* (%)	Other (%)
1949.8	43804.7	58.6	15.4	0.0	2.1	0.0	0.0	0.0	10.4	1.4	0.2	0.4	0.0	1.6	0.0	0.0	0.6	9.4
1949.9	43807.1	60.1	17.1	0.0	0.8	0.4	0.0	0.0	9.6	2.1	0.2	1.3	0.2	1.5	0.0	0.0	0.8	5.8
1950.0	43809.5	59.6	20.9	0.0	1.9	0.2	0.0	0.0	7.4	0.6	0.8	0.4	0.4	0.4	0.0	0.0	0.4	7.2
1950.1	43811.6	53.7	23.0	0.2	1.9	0.0	0.0	0.0	9.1	1.0	0.5	0.5	0.5	0.2	0.0	0.0	0.5	8.9
1950.2	43813.7	59.3	19.2	0.5	1.3	0.3	0.0	0.3	8.1	0.8	0.8	1.0	0.0	0.3	0.0	0.0	0.3	7.9
1950.3	43815.8	59.5	20.3	0.4	1.6	0.2	0.0	0.0	6.4	0.8	0.0	0.4	0.0	0.2	0.0	0.0	0.6	9.7
1950.4	43817.9	61.4	17.6	0.0	1.3	0.0	0.0	0.3	7.8	1.3	0.7	0.0	0.0	0.0	0.0	0.0	0.7	8.8
1950.5	43820.0	62.4	20.0	0.0	2.2	0.2	0.0	0.0	5.4	0.9	0.0	0.6	0.0	0.0	0.0	0.0	0.0	8.4
1950.6	43822.1	62.7	17.4	0.4	1.2	0.2	0.0	0.0	8.3	1.2	0.2	0.6	0.0	0.2	0.0	0.0	0.2	7.5
1950.7	43824.2	60.0	19.2	0.0	1.4	0.0	0.0	0.0	9.5	0.9	0.0	0.2	0.0	0.0	0.0	0.0	0.7	8.1
1950.8	43826.3	59.4	20.8	0.0	2.3	0.1	0.0	0.0	7.9	0.4	0.3	0.3	0.1	0.0	0.0	0.0	0.4	7.9
1950.9	43828.4	62.2	17.1	0.0	1.1	0.4	0.0	0.0	8.1	0.7	0.4	0.6	0.2	0.0	0.0	0.0	0.4	9.0
1951.0	43830.5	58.5	20.9	0.2	1.1	0.2	0.0	0.0	7.5	1.4	0.0	0.2	0.2	0.0	0.0	0.0	0.7	9.3
1951.1	43832.6	59.2	18.3	0.1	0.4	0.1	0.0	0.0	6.4	1.3	0.7	0.7	0.0	0.0	0.0	0.0	1.0	11.6
1951.2	43834.7	57.5	23.3	0.0	1.3	0.0	0.0	0.0	5.5	1.5	0.0	0.4	0.0	0.0	0.0	0.0	0.9	9.5
1951.3	43836.8	59.4	22.0	0.0	0.8	0.0	0.0	0.0	3.4	2.4	0.5	0.3	0.0	0.0	0.0	0.0	0.5	10.6
1951.4	43838.9	58.0	21.3	0.3	0.6	0.3	0.0	0.0	3.1	2.8	0.6	0.6	0.0	0.0	0.0	0.0	0.3	11.9
1951.5	43841.0	63.4	16.5	0.2	0.7	0.2	0.0	0.0	4.1	4.1	0.0	0.3	0.0	0.0	0.0	0.0	0.5	10.0
1951.6	43843.1	59.1	16.8	0.0	0.6	0.0	0.0	0.0	5.9	5.3	0.0	0.3	0.0	0.3	0.0	0.0	0.3	11.5
1951.7	43845.2	58.3	18.6	0.0	1.1	0.0	0.0	0.0	2.7	5.8	0.0	0.2	0.2	0.0	0.0	0.0	0.9	12.2
1951.8	43847.3	60.6	15.9	0.6	1.1	0.0	0.0	0.0	4.9	5.6	0.2	0.4	0.0	0.0	0.0	0.0	1.3	9.5
1951.9	43849.4	58.2	16.9	0.2	0.6	0.0	0.0	0.0	6.3	7.1	0.0	0.2	0.0	0.0	0.0	0.0	0.8	9.6
1952.0	43851.5	64.0	18.1	0.0	0.5	0.0	0.0	0.0	2.4	4.3	0.0	0.5	0.0	0.0	0.0	0.0	0.7	9.5
1952.1	43853.8	63.4	18.1	0.0	0.5	0.0	0.0	0.0	4.6	3.1	0.0	0.3	0.0	0.0	0.0	0.0	0.3	9.9
1952.2	43856.0	64.9	18.5	0.3	0.8	0.3	0.0	0.0	3.5	2.8	0.0	0.3	0.3	0.0	0.0	0.0	0.5	8.0
1952.3	43858.3	63.2	20.4	0.3	0.8	0.0	0.0	0.0	3.3	2.2	0.0	0.3	0.8	0.5	0.0	0.0	0.8	7.4
1952.4	43860.5	69.1	17.7	0.5	0.5	0.2	0.0	0.0	3.3	0.9	0.2	0.5	0.2	0.5	0.0	0.0	0.5	5.9
1952.5	43862.8	67.1	16.0	0.4	0.4	0.0	0.0	0.0	6.0	1.2	0.0	0.0	1.0	0.8	0.0	0.0	0.6	6.6

Core MD03-2622 Relative Abundance Data (continued)

Depth (cm)	Age (yBP)	*G.b* (%)	*N.d* (%)	*O.u* (%)	*G.a* (%)	*G.c* (%)	*P.o* (%)	*G.m* (%)	*G.r*(p) (%)	*G.r*(w) (%)	*G.s* (%)	*G.g* (%)	*G.t* (%)	*G.rs* (%)	*N.p*(l) (%)	*N.p*(r) (%)	*G.q* (%)	Other (%)
1952.6	43865.0	67.5	16.2	0.0	1.0	0.2	0.0	0.0	3.8	1.9	0.6	0.6	0.0	0.4	0.0	0.0	0.6	7.4
1952.7	43867.3	61.8	15.4	0.0	0.7	0.0	0.0	0.0	7.0	3.1	0.2	0.5	0.2	2.6	0.0	0.0	0.7	7.7
1952.8	43869.5	64.6	17.1	0.0	1.1	0.2	0.0	0.0	4.8	3.5	0.0	0.2	0.0	0.0	0.0	0.0	0.4	7.9
1952.9	43871.8	65.4	18.5	0.3	0.3	0.0	0.0	0.0	3.5	1.5	0.4	0.5	0.4	0.7	0.0	0.0	0.8	7.7
1953.0	43874.0	67.3	18.2	0.0	0.4	0.0	0.0	0.0	4.3	1.6	0.2	0.4	0.7	0.2	0.0	0.0	0.7	6.1
1953.1	43876.4	65.7	16.9	0.7	0.7	0.2	0.0	0.0	3.0	2.0	0.0	1.0	0.2	0.0	0.0	0.0	0.5	9.0
1953.2	43878.7	61.1	19.7	0.2	0.4	0.0	0.0	0.0	4.5	2.4	0.0	0.4	0.0	0.2	0.0	0.0	0.6	10.5
1953.3	43881.1	57.9	24.4	0.2	0.7	0.2	0.0	0.0	4.2	0.5	0.5	0.5	0.0	0.0	0.0	0.0	1.2	9.8
1953.4	43883.4	64.2	21.0	0.3	1.1	0.0	0.0	0.0	2.2	0.5	0.3	0.5	0.0	0.3	0.0	0.0	0.5	9.2
1953.5	43885.8	62.6	19.5	0.5	0.5	0.3	0.0	0.0	2.7	1.6	0.3	0.3	0.0	0.0	0.0	0.0	1.1	10.6
1953.6	43888.1	61.5	22.0	0.5	0.5	0.3	0.0	0.2	3.3	2.5	0.3	0.2	0.3	0.0	0.0	0.0	0.5	7.9
1953.7	43890.5	59.6	23.3	0.3	0.5	0.0	0.0	0.0	2.9	0.8	0.3	0.8	0.0	0.3	0.0	0.0	0.8	10.4
1953.8	43892.8	59.3	20.8	0.4	0.0	0.0	0.0	0.0	5.1	0.9	0.0	0.4	0.0	0.0	0.0	0.0	1.1	12.0
1953.9	43895.2	58.6	23.1	0.2	0.7	0.0	0.0	0.0	3.3	1.3	0.2	0.0	0.0	0.0	0.0	0.0	1.1	11.5
1996.0	44668.0	46.8	3.8	0.6	0.9	0.0	0.0	0.0	4.1	0.0	0.9	0.3	0.3	0.0	0.6	0.0	2.3	39.5
1996.1	44670.2	42.4	6.1	0.4	0.2	0.4	0.2	0.0	3.8	0.6	0.4	0.6	0.0	0.0	0.2	0.0	4.0	40.9
1996.2	44672.3	41.4	7.3	0.0	0.4	0.0	0.0	0.0	5.5	0.6	0.2	1.0	0.2	0.0	0.0	0.0	4.1	39.4
1996.3	44674.5	41.3	8.7	0.2	0.2	0.0	0.2	0.2	6.2	0.9	0.2	0.4	0.7	0.0	0.0	0.0	2.1	38.8
1996.4	44676.6	40.0	10.3	0.2	1.0	0.2	0.0	0.2	3.3	0.6	0.6	1.2	0.0	0.0	0.0	0.0	2.3	40.0
1996.5	44678.8	40.2	10.3	0.7	1.3	0.0	0.2	0.0	5.1	0.7	0.0	1.5	0.2	0.0	0.4	0.0	2.6	36.7
1996.6	44680.9	40.2	12.3	0.5	0.0	0.0	0.0	0.3	5.4	0.3	0.8	0.3	0.0	0.0	0.3	0.0	2.4	37.3
1996.7	44683.1	43.1	12.5	0.6	0.9	0.3	0.0	0.3	7.0	0.3	0.9	1.2	0.6	0.0	0.0	0.0	4.3	27.8
1996.8	44685.2	44.5	6.5	0.8	1.4	0.0	0.3	0.0	3.7	0.6	1.4	0.6	0.0	0.0	0.0	0.0	3.1	37.1
1996.9	44687.4	37.4	12.3	0.2	0.9	0.2	0.0	0.2	5.0	1.3	0.4	0.9	0.0	0.0	0.4	0.0	2.9	37.9
1997.0	44689.5	44.6	11.5	0.4	0.8	0.2	0.2	0.0	5.4	0.6	0.8	0.8	0.2	0.0	0.0	0.0	3.3	31.0
1997.1	44691.9	45.2	10.0	0.2	1.1	0.4	0.0	0.0	4.5	0.9	0.2	0.2	0.2	0.0	0.2	0.0	2.6	34.2

Core MD03-2622 Relative Abundance Data (continued)

Depth (cm)	Age (yBP)	*G.b* (%)	*N.d* (%)	*O.u* (%)	*G.a* (%)	*G.c* (%)	*P.o* (%)	*G.m* (%)	*G.r*(p) (%)	*G.r*(w) (%)	*G.s* (%)	*G.g* (%)	*G.t* (%)	*G.rs* (%)	*N.p*(l) (%)	*N.p*(r) (%)	*G.q* (%)	Other (%)
1997.2	44694.3	44.6	7.6	0.0	0.7	0.0	0.2	0.0	4.0	0.2	0.7	0.9	0.0	0.2	0.4	0.0	4.2	36.5
1997.3	44696.7	43.1	9.6	0.4	0.2	0.7	0.0	0.0	5.9	0.2	0.7	0.4	0.2	0.0	0.2	0.0	4.6	33.8
1997.4	44699.1	38.2	14.7	0.2	0.2	0.0	0.0	0.2	5.8	0.4	0.4	0.8	0.2	0.0	0.6	0.0	4.0	34.2
1997.5	44701.5	47.1	11.2	0.2	0.5	0.5	0.0	0.0	4.8	1.0	0.5	0.2	0.2	0.0	0.2	0.0	1.7	31.8
1997.6	44703.9	42.6	11.7	0.3	0.8	0.0	0.0	0.3	6.1	0.5	0.5	0.8	0.0	0.0	0.5	0.0	1.5	34.5
1997.7	44706.3	42.8	9.1	0.3	0.3	0.0	0.0	0.0	4.7	0.8	0.3	0.8	0.5	0.0	0.0	0.0	1.6	38.9
1997.8	44708.7	38.1	7.0	0.2	0.7	0.0	0.0	0.2	3.5	1.1	0.2	1.1	0.7	0.0	0.2	0.0	2.6	44.3
1997.9	44711.1	40.7	10.5	0.0	0.9	0.2	0.0	0.0	4.3	0.2	0.2	0.2	0.7	0.0	0.2	0.0	2.5	39.3
1998.0	44713.5	41.3	9.8	0.6	0.9	0.4	0.2	0.4	3.7	0.4	0.2	0.4	0.2	0.0	0.4	0.0	2.4	38.9
1998.1	44715.6	41.9	9.9	1.1	1.1	0.0	0.0	0.0	5.4	0.5	0.0	0.3	0.5	0.0	0.0	0.0	1.6	37.6
1998.2	44717.7	42.1	9.0	0.5	1.2	0.2	0.0	0.0	4.0	0.7	0.5	0.5	0.5	0.0	0.0	0.0	3.1	37.6
1998.3	44719.8	41.7	7.2	0.2	0.7	0.2	0.0	0.2	6.5	0.5	0.7	0.2	0.0	0.0	0.0	0.0	3.6	38.3
1998.4	44721.9	42.1	11.4	0.8	0.3	0.0	0.3	0.0	3.9	0.5	0.0	0.5	0.3	0.0	0.0	0.0	3.1	37.0
1998.5	44724.0	43.4	11.6	1.0	0.0	0.0	0.3	0.0	5.8	0.3	0.3	1.3	0.0	0.0	0.0	0.0	2.3	33.8
1998.6	44726.1	38.5	11.9	0.2	0.7	0.7	0.4	0.0	5.8	0.7	0.2	0.9	0.7	0.0	0.0	0.0	1.3	38.0
1998.7	44728.2	40.9	10.8	0.5	1.1	0.0	0.8	0.0	5.5	0.3	0.0	0.8	0.3	0.0	0.0	0.0	2.6	36.4
1998.8	44730.3	41.3	9.9	0.2	0.6	0.2	0.0	0.0	6.3	0.4	0.6	0.7	0.6	0.0	0.0	0.0	1.9	37.4
1998.9	44732.4	37.6	14.1	0.8	0.3	0.6	0.0	0.0	3.9	1.4	0.8	0.3	0.0	0.0	0.0	0.0	2.5	37.8
1999.0	44734.5	38.0	12.8	0.5	0.8	0.0	0.0	0.0	8.4	0.5	0.0	0.5	0.8	0.0	0.0	0.0	1.6	35.9
1999.1	44736.2	42.5	8.7	0.0	0.6	0.3	0.0	0.0	4.5	0.0	0.6	1.4	0.6	0.0	0.0	0.0	2.0	39.1
1999.2	44737.9	42.5	10.2	0.0	0.3	0.6	0.0	0.0	3.2	0.3	0.6	1.0	0.0	0.0	0.0	0.0	3.8	37.5
1999.3	44739.6	40.9	9.7	0.0	0.0	0.5	0.0	0.2	6.2	0.7	0.5	0.7	0.7	0.0	0.0	0.0	3.1	36.8
1999.4	44741.3	46.5	11.6	0.6	0.6	0.0	0.3	0.0	5.9	0.3	0.6	0.6	0.0	0.0	0.0	0.0	2.8	30.3
1999.5	44743.0	60.2	5.6	0.0	0.0	0.6	0.0	0.0	3.1	0.6	0.0	0.0	0.0	0.0	0.0	0.0	3.1	26.7
1999.6	44744.7	46.1	11.1	1.0	0.2	0.2	0.2	0.0	6.0	0.7	0.2	0.5	0.0	0.0	0.0	0.0	2.2	31.4
1999.7	44746.4	38.2	16.1	0.3	0.8	0.5	0.3	0.0	7.3	0.8	0.3	0.8	0.3	0.0	0.0	0.0	2.6	31.9
1999.8	44748.1	44.1	9.6	1.0	0.8	0.5	0.3	0.0	7.6	1.0	0.5	0.3	0.3	0.0	0.3	0.0	1.3	32.7
1999.9	44749.8	49.2	7.1	0.0	0.6	0.4	0.0	0.4	4.5	0.2	0.0	0.2	0.2	0.0	0.0	0.0	3.0	34.0

Core MD03-2622 Relative Abundance Data (continued)

Depth (cm)	Age (yBP)	*G.b* (%)	*N.d* (%)	*O.u* (%)	*G.a* (%)	*G.c* (%)	*P.o* (%)	*G.m* (%)	*G.r*(p) (%)	*G.r*(w) (%)	*G.s* (%)	*G.g* (%)	*G.t* (%)	*G.rs* (%)	*N.p*(l) (%)	*N.p*(r) (%)	*G.q* (%)	Other (%)
2000.0	44751.5	46.6	9.2	0.0	0.5	0.0	0.0	0.0	3.3	0.8	0.0	0.3	0.5	0.0	0.0	0.0	1.9	36.9
2000.1	44754.1	43.0	11.4	0.2	0.0	0.0	0.0	0.0	4.4	1.0	0.0	0.2	0.0	0.0	0.2	0.0	3.6	35.9
2000.2	44756.6	48.2	8.4	0.0	0.2	0.2	0.2	0.0	3.0	0.2	0.2	0.2	0.9	0.0	0.5	0.0	1.4	36.4
2000.3	44759.2	51.7	10.4	0.2	0.4	0.0	0.2	0.0	2.1	0.4	0.0	0.2	0.0	0.0	0.0	0.0	2.3	31.9
2000.4	44761.7	52.7	11.4	0.0	0.0	0.5	0.0	0.0	3.4	0.3	0.0	0.0	0.0	0.0	0.0	0.0	2.1	29.7
2000.5	44764.3	52.4	14.0	0.0	0.0	0.0	0.0	0.0	3.9	0.3	0.0	0.3	0.0	0.0	0.0	0.0	1.0	28.0
2000.6	44766.8	56.8	10.3	0.0	0.3	0.0	0.0	0.0	3.6	0.3	0.0	0.0	0.0	0.0	0.0	0.0	1.8	26.9
2000.7	44769.4	59.2	10.1	0.0	0.5	0.0	0.3	0.0	3.9	0.5	0.0	0.0	0.0	0.0	0.0	0.0	1.6	23.9
2000.8	44771.9	54.3	10.6	0.0	0.0	0.0	0.0	0.0	3.8	0.2	0.0	0.2	0.2	0.0	0.4	0.0	2.6	27.7
2000.9	44774.5	56.4	10.6	0.0	0.2	0.0	0.0	0.0	3.6	0.4	0.0	0.2	0.0	0.0	0.0	0.0	1.8	26.7
2001.0	44777.0	55.3	8.8	0.0	0.0	0.2	0.0	0.0	4.0	0.9	0.0	0.0	0.0	0.0	0.0	0.0	4.0	26.9
2001.1	44779.1	55.4	11.5	0.0	0.0	0.0	0.0	0.0	2.9	0.2	0.2	0.5	0.2	0.0	0.0	0.0	1.8	27.1
2001.2	44781.2	57.3	10.3	0.0	0.2	0.0	0.0	0.0	1.6	0.8	0.0	0.0	0.2	0.0	0.0	0.0	2.0	27.6
2001.3	44783.3	50.8	14.1	0.4	0.2	0.0	0.0	0.0	3.4	0.0	0.4	0.0	0.2	0.0	0.0	0.0	2.4	28.1
2001.4	44785.4	57.8	9.5	0.3	0.3	0.0	0.3	0.0	1.8	0.3	0.0	0.0	0.3	0.0	0.0	0.0	1.8	28.0
2001.5	44787.5	53.9	7.8	0.0	0.0	0.0	0.2	0.0	4.3	0.7	0.0	0.0	0.5	0.0	0.0	0.0	1.9	30.6
2001.6	44789.6	58.3	8.9	0.0	0.0	0.3	0.3	0.0	3.1	0.3	0.0	0.0	0.0	0.0	0.0	0.0	1.7	27.1
2001.7	44791.7	53.0	10.2	0.0	0.3	0.3	0.0	0.0	7.0	0.3	0.0	0.0	0.0	0.0	0.0	0.0	2.1	26.9
2001.8	44793.8	53.3	9.7	0.4	0.0	0.2	0.0	0.0	5.3	0.2	0.4	0.2	0.4	0.0	0.0	0.0	3.9	26.1
2001.9	44795.9	51.6	10.2	0.8	0.5	0.3	0.0	0.0	7.0	0.5	0.3	0.0	0.0	0.0	0.0	0.0	2.1	26.8
2002.0	44798.0	55.2	8.1	0.8	0.0	0.0	0.0	0.3	6.4	0.8	0.3	0.0	0.8	0.0	0.0	0.0	2.0	25.2
2002.1	44800.3	56.6	12.7	0.0	0.0	0.0	0.0	0.0	3.5	0.3	0.9	0.3	0.0	0.0	0.0	0.0	1.8	23.9
2002.2	44802.6	55.6	12.1	0.3	0.0	0.0	0.3	0.0	6.1	1.0	0.0	0.0	0.6	0.0	0.0	0.0	1.6	22.4
2002.3	44804.9	53.3	12.5	0.0	0.0	0.0	0.0	0.0	5.3	0.3	0.0	0.5	0.3	0.0	0.0	0.0	1.6	26.3
2002.4	44807.2	59.4	11.7	0.0	0.0	0.0	0.0	0.0	2.9	0.3	0.3	0.0	0.6	0.0	0.0	0.0	2.3	22.4
2002.5	44809.5	57.0	10.6	0.0	0.0	0.6	0.3	0.0	5.6	0.9	0.3	0.3	0.6	0.0	0.0	0.0	3.4	20.2
2002.6	44811.8	53.0	11.6	0.0	0.2	0.2	0.0	0.0	4.2	0.6	0.2	0.0	0.0	0.0	0.0	0.0	3.4	26.6
2002.7	44814.1	51.3	15.6	0.0	0.0	0.0	0.3	0.0	5.1	0.5	0.3	0.0	0.3	0.0	0.0	0.0	2.6	24.1

Core MD03-2622 Relative Abundance Data (continued)

Depth (cm)	Age (yBP)	*G.b* (%)	*N.d* (%)	*O.u* (%)	*G.a* (%)	*G.c* (%)	*P.o* (%)	*G.m* (%)	*G.r*(p) (%)	*G.r*(w) (%)	*G.s* (%)	*G.g* (%)	*G.t* (%)	*G.rs* (%)	*N.p*(l) (%)	*N.p*(r) (%)	*G.q* (%)	Other (%)
2002.8	44816.4	54.2	10.8	0.0	0.0	0.0	0.7	0.0	2.3	1.3	0.3	0.0	0.0	0.0	0.0	0.0	2.9	27.5
2002.9	44818.7	52.5	13.2	0.0	0.5	0.0	0.0	0.0	4.7	0.3	0.0	0.3	0.3	0.0	0.0	0.0	3.4	25.1
2003.0	44821.0	55.5	10.2	0.4	0.8	0.0	0.2	0.0	4.0	1.0	0.2	0.2	0.2	0.0	0.0	0.0	1.8	25.5
2003.1	44822.9	56.5	11.0	0.0	0.0	0.0	0.3	0.0	4.5	0.6	0.6	0.0	0.3	0.0	0.0	0.0	3.4	23.0
2003.2	44824.7	50.1	16.5	0.0	0.0	0.2	0.2	0.0	4.0	0.9	0.7	0.2	0.2	0.0	0.0	0.0	3.8	23.2
2003.3	44826.6	59.4	10.1	0.0	0.0	0.5	0.5	0.0	4.4	0.3	0.3	0.0	0.3	0.0	0.0	0.0	2.5	21.8
2003.4	44828.4	56.0	10.4	0.2	0.2	0.4	0.4	0.0	2.2	0.9	0.6	0.2	0.0	0.0	0.0	0.0	2.2	26.3
2003.5	44830.3	47.9	15.8	0.0	0.0	0.6	0.0	0.0	6.4	0.6	0.0	0.0	0.3	0.0	0.0	0.0	4.2	24.2
2003.6	44832.1	56.0	13.0	0.3	0.3	0.0	0.0	0.0	3.2	0.3	0.6	0.0	0.0	0.0	0.0	0.0	2.9	23.3
2003.7	44834.0	49.8	11.3	0.3	0.3	0.3	0.3	0.0	7.8	0.6	0.3	0.0	0.3	0.0	0.3	0.0	4.2	23.9
2003.8	44835.8	49.4	13.6	0.0	0.3	0.6	0.0	0.0	5.3	0.9	0.6	0.3	0.0	0.0	0.0	0.0	2.4	26.6
2003.9	44837.7	54.4	10.5	0.3	0.3	0.3	0.0	0.0	4.7	0.3	0.0	0.3	0.6	0.0	0.0	0.0	2.8	25.7
2004.0	44839.5	50.8	11.2	0.3	0.8	0.0	0.0	0.0	6.1	0.5	0.3	0.3	0.5	0.0	0.0	0.0	2.4	26.7
2004.1	44841.7	54.3	9.7	0.0	0.0	0.5	0.3	0.0	2.9	0.3	0.0	0.3	0.0	0.0	0.0	0.0	1.8	30.0
2004.2	44843.9	56.6	7.7	0.0	0.0	0.3	0.3	0.0	3.9	0.3	0.0	0.3	0.3	0.0	0.0	0.0	3.3	27.1
2004.3	44846.1	56.7	11.1	0.3	0.0	0.3	0.0	0.0	4.6	0.3	0.0	0.0	0.6	0.0	0.0	0.0	3.1	23.1
2004.4	44848.3	58.1	8.6	0.0	0.2	0.4	0.0	0.0	2.7	0.2	0.0	0.2	0.0	0.4	0.0	0.0	3.6	25.5
2004.5	44850.5	58.7	7.4	0.2	0.4	0.2	0.4	0.0	3.5	0.6	0.4	0.6	0.2	0.2	0.4	0.0	2.5	24.4
2004.6	44852.7	60.0	6.3	0.2	0.0	0.2	0.0	0.0	4.0	0.0	0.2	0.0	0.0	0.0	0.0	0.0	2.3	26.7
2004.7	44854.9	64.3	7.7	0.2	0.9	0.5	0.0	0.0	1.6	0.2	0.0	0.7	0.0	0.0	0.7	0.0	1.4	21.6
2004.8	44857.1	61.9	7.3	0.0	0.8	0.3	0.0	0.0	2.5	0.8	0.0	0.3	0.0	0.0	0.0	0.0	0.3	26.0
2004.9	44859.3	53.9	10.8	0.3	0.3	0.0	0.0	0.3	5.2	0.3	0.0	0.5	0.0	0.0	0.8	0.0	1.0	26.8
2005.0	44861.5	56.0	5.3	0.0	0.0	0.0	0.2	0.0	3.3	0.2	0.2	0.0	0.0	0.0	1.4	0.0	3.8	29.4
2005.1	44863.5	52.7	9.1	0.2	0.2	0.2	0.4	0.0	6.4	0.4	0.0	0.6	0.0	0.0	0.4	0.0	1.2	28.2
2005.2	44865.4	62.9	10.5	0.0	0.9	0.0	0.0	0.9	6.2	1.3	0.0	0.6	0.2	0.0	0.0	0.0	0.4	16.1
2005.3	44867.4	62.1	4.5	0.0	0.3	0.0	0.5	0.3	5.3	0.8	0.0	1.0	0.5	0.0	0.0	0.0	0.5	24.4
2005.4	44869.3	56.0	11.1	0.3	0.3	0.3	0.0	0.0	6.5	1.9	0.3	1.6	0.0	0.0	0.5	0.0	2.4	18.8
2005.5	44871.3	63.4	8.6	0.0	0.3	0.3	0.3	0.0	3.5	1.0	0.0	0.3	0.0	0.0	0.3	0.0	1.6	20.4

Core MD03-2622 Relative Abundance Data (continued)

Depth (cm)	Age (yBP)	*G.b* (%)	*N.d* (%)	*O.u* (%)	*G.a* (%)	*G.c* (%)	*P.o* (%)	*G.m* (%)	*G.r*(p) (%)	*G.r*(w) (%)	*G.s* (%)	*G.g* (%)	*G.t* (%)	*G.rs* (%)	*N.p*(l) (%)	*N.p*(r) (%)	*G.q* (%)	Other (%)
2005.6	44873.2	51.4	10.1	0.0	0.2	0.0	0.0	0.0	6.7	1.9	0.2	0.6	0.4	0.0	0.0	0.0	0.8	27.7
2005.7	44875.2	50.2	13.0	0.0	0.0	0.6	0.0	0.0	7.3	0.6	0.0	0.3	0.0	0.0	1.0	0.0	2.9	24.1
2005.8	44877.1	51.5	8.6	0.2	0.0	0.2	0.0	0.0	5.2	1.1	0.4	0.6	0.2	0.2	0.0	0.0	0.2	31.5
2005.9	44879.1	54.9	8.9	0.0	0.3	0.0	0.0	0.0	5.2	0.0	0.0	0.3	0.3	0.0	0.0	0.0	5.5	24.5
2006.0	44881.0	52.6	8.6	0.7	0.9	0.4	0.0	0.0	3.9	0.9	0.2	0.4	0.0	0.0	0.2	0.0	1.8	29.4
2006.1	44882.9	54.2	7.4	0.0	0.4	0.2	0.0	0.0	5.1	0.4	0.0	0.2	0.2	0.0	0.2	0.0	2.1	29.4
2006.2	44884.8	55.9	8.3	0.5	0.3	0.0	0.0	0.0	3.2	1.1	0.0	0.8	0.3	0.0	0.0	0.0	1.9	27.7
2006.3	44886.7	55.0	10.2	0.0	0.0	0.0	0.0	0.0	4.1	1.5	0.0	0.3	0.3	0.3	0.6	0.0	2.0	25.7
2006.4	44888.6	57.0	8.3	0.0	0.9	0.0	0.0	0.0	5.7	1.4	0.3	1.4	0.3	0.0	0.0	0.0	0.3	24.5
2006.5	44890.5	51.7	12.3	0.5	0.5	0.0	0.2	0.0	4.0	0.9	0.5	0.7	0.0	0.0	0.0	0.0	1.2	27.6
2006.6	44892.4	54.6	9.8	0.0	0.6	0.3	0.0	0.0	4.9	0.9	0.0	0.6	0.0	0.0	0.3	0.0	1.7	26.3
2006.7	44894.3	43.5	9.6	0.2	0.2	0.2	0.0	0.2	7.2	1.8	0.0	0.4	0.0	0.0	0.6	0.0	3.6	32.5
2006.8	44896.2	51.6	11.1	0.2	0.4	0.2	0.0	0.2	6.2	0.8	0.6	1.4	0.2	0.2	0.2	0.0	1.4	25.5
2006.9	44898.1	55.4	10.6	0.9	0.6	0.9	0.0	0.3	8.3	0.9	0.0	0.6	0.0	0.0	0.6	0.0	3.1	18.0
2007.0	44900.0	54.7	10.4	0.0	1.4	0.0	0.0	0.0	8.2	0.4	0.6	0.6	0.2	0.0	0.0	0.0	1.6	21.8
2007.1	44902.1	47.5	6.6	0.0	0.2	0.0	0.0	0.0	7.9	1.1	0.0	0.6	0.2	0.0	0.4	0.0	1.7	33.8
2007.2	44904.1	43.6	6.4	0.0	0.5	0.7	0.0	0.0	7.5	1.1	0.5	0.5	0.0	0.0	0.2	0.0	0.7	38.4
2007.3	44906.2	47.2	6.9	0.0	0.7	0.0	0.0	0.0	6.9	1.3	0.0	0.0	0.0	0.0	0.0	0.0	1.7	35.3
2007.4	44908.2	43.0	9.7	0.3	0.5	0.0	0.3	0.0	4.9	1.0	0.2	0.3	0.5	0.0	0.7	0.0	2.2	36.2
2007.5	44910.3	54.1	6.5	0.2	0.2	0.2	0.0	0.0	2.2	0.2	0.0	0.2	0.0	0.0	0.2	0.0	2.5	33.2
2007.6	44912.3	41.6	9.5	0.2	0.2	0.0	0.0	0.0	4.0	1.6	0.2	0.5	0.2	0.0	0.7	0.0	2.3	38.8
2007.7	44914.4	43.2	10.4	0.2	0.4	0.0	0.2	0.0	3.1	0.6	0.2	0.4	0.4	0.0	0.4	0.0	3.5	36.7
2007.8	44916.4	43.5	6.0	0.4	0.4	0.0	0.2	0.0	6.0	0.7	0.2	0.4	0.2	0.0	0.2	0.0	4.0	37.7
2007.9	44918.5	45.0	9.0	0.2	0.5	0.2	0.2	0.0	3.6	1.4	0.0	0.5	0.2	0.0	0.5	0.0	2.0	36.7
2008.0	44920.5	43.9	7.6	0.2	0.2	0.2	0.2	0.0	6.6	0.5	0.2	0.2	0.2	0.0	0.7	0.0	1.7	37.3
2008.1	44921.9	45.6	6.6	0.2	0.2	0.2	0.0	0.0	7.0	0.8	0.2	0.2	0.2	0.0	0.6	0.0	0.6	37.5
2008.2	44923.2	40.0	7.0	0.7	0.0	0.5	0.5	0.0	4.6	1.7	0.7	0.5	0.0	0.0	0.5	0.0	0.5	42.7
2008.3	44924.6	46.0	6.5	0.3	0.0	0.0	0.3	0.0	4.6	1.1	0.0	0.8	0.3	0.0	0.3	0.0	1.9	38.2

Core MD03-2622 Relative Abundance Data (continued)

Depth (cm)	Age (yBP)	*G.b* (%)	*N.d* (%)	*O.u* (%)	*G.a* (%)	*G.c* (%)	*P.o* (%)	*G.m* (%)	*G.r*(p) (%)	*G.r*(w) (%)	*G.s* (%)	*G.g* (%)	*G.t* (%)	*G.rs* (%)	*N.p*(l) (%)	*N.p*(r) (%)	*G.q* (%)	Other (%)
2008.4	44925.9	39.2	5.7	0.3	0.3	0.3	0.0	0.0	4.6	0.5	0.0	1.1	0.0	0.0	0.5	0.0	4.1	43.3
2008.5	44927.3	40.7	8.4	0.0	0.9	0.0	0.3	0.0	4.1	0.9	0.3	0.0	0.3	0.0	0.0	0.0	1.7	42.4
2008.6	44928.6	39.3	7.8	0.2	0.4	0.0	0.2	0.0	3.0	0.4	0.4	0.2	0.0	0.0	0.0	0.0	2.0	46.3
2008.7	44930.0	35.1	5.2	0.0	0.2	0.2	0.2	0.0	3.7	0.2	0.2	0.2	0.0	0.0	0.0	0.0	4.0	50.6
2008.8	44931.3	36.3	4.0	0.0	0.4	0.0	0.0	0.2	5.3	0.2	0.0	0.4	0.2	0.0	0.0	0.0	4.4	48.5
2008.9	44932.7	37.9	6.5	0.2	0.0	0.2	0.0	0.0	4.9	0.2	0.4	0.2	0.4	0.0	0.0	0.0	4.7	44.4
2009.0	44934.0	49.9	7.7	0.0	0.0	0.0	0.0	0.0	1.7	0.0	0.0	0.5	0.7	0.0	0.2	0.0	4.5	34.7
2009.1	44935.9	45.7	6.4	0.0	0.3	0.0	0.0	0.0	3.7	0.3	0.0	0.5	0.0	0.0	0.5	0.0	4.5	38.0
2009.2	44937.8	46.6	4.9	0.0	0.2	0.0	0.5	0.0	4.2	0.5	0.0	0.5	0.7	0.2	0.7	0.0	7.4	33.6
2009.3	44939.7	46.6	4.7	0.0	0.3	0.3	0.0	0.0	6.0	0.3	0.0	0.5	1.0	0.0	0.5	0.0	5.5	34.3
2009.4	44941.6	48.4	4.4	0.6	1.1	0.4	0.0	0.0	3.6	0.2	0.0	0.8	0.8	0.0	0.6	0.0	5.5	33.4
2009.5	44943.5	50.4	7.2	0.0	0.2	0.0	0.0	0.0	4.1	0.2	0.5	0.5	0.7	0.0	0.5	0.0	4.8	30.8
2009.6	44945.4	47.7	4.7	0.0	0.3	0.3	0.0	0.0	8.2	0.3	0.0	0.5	0.5	0.0	0.5	0.0	6.3	30.7
2009.7	44947.3	46.0	7.4	0.0	0.3	0.0	0.0	0.0	5.9	0.6	0.6	0.3	0.0	0.0	0.3	0.0	4.7	33.8
2009.8	44949.2	43.6	8.7	0.3	0.6	0.3	0.0	0.0	9.0	0.9	0.3	0.3	0.0	0.0	0.6	0.0	3.5	32.0
2009.9	44951.1	45.2	6.0	0.0	0.0	0.2	0.2	0.0	8.4	1.0	0.5	0.5	0.2	0.0	0.0	0.0	3.8	34.0
2010.0	44953.0	46.8	9.4	0.0	0.2	0.0	0.4	0.0	7.2	0.2	0.2	0.7	0.2	0.0	0.2	0.0	4.4	30.0
2010.1	44955.1	51.2	4.7	0.6	0.0	0.0	0.0	0.0	5.6	0.3	0.0	0.3	0.0	0.0	0.3	0.0	4.0	32.9
2010.2	44957.2	46.2	7.8	0.2	0.2	0.0	0.0	0.0	7.6	0.7	0.0	0.4	0.2	0.0	0.4	0.0	4.6	31.7
2010.3	44959.3	48.1	7.9	0.8	1.3	0.3	0.0	0.0	5.0	0.5	0.0	0.0	0.0	0.0	0.0	0.0	4.2	31.7
2010.4	44961.4	46.9	5.5	0.7	0.2	0.0	0.0	0.0	5.1	0.5	0.7	0.5	0.2	0.0	0.5	0.0	1.8	37.5
2010.5	44963.5	44.0	6.3	0.5	0.7	0.2	0.4	0.2	5.3	0.9	0.4	0.9	0.4	0.0	0.4	0.0	3.2	36.4
2010.6	44965.6	43.9	7.3	0.4	0.2	0.0	0.0	0.2	6.6	1.3	1.2	0.6	0.2	0.0	0.0	0.0	4.6	33.5
2010.7	44967.7	45.0	7.2	1.0	0.3	0.0	0.3	0.0	6.5	0.5	1.0	0.5	0.0	0.0	0.0	0.0	3.4	34.4
2010.8	44969.8	48.0	5.9	0.2	1.4	0.9	0.2	0.0	6.8	1.6	1.4	0.5	0.0	0.0	0.2	0.0	3.0	30.0
2010.9	44971.9	49.7	8.4	0.4	0.8	0.0	0.2	0.2	5.3	0.8	0.4	0.8	0.2	0.0	0.0	0.0	2.9	29.9
2011.0	44974.0	48.7	7.7	1.0	1.6	1.0	0.0	0.3	3.9	0.6	1.0	1.0	0.3	0.0	0.0	0.0	2.3	30.6
2011.1	44975.3	42.2	8.6	0.5	0.0	0.5	0.0	0.3	6.4	1.3	0.5	0.3	0.5	0.0	0.3	0.0	4.8	33.7

Core MD03-2622 Relative Abundance Data (continued)

Depth (cm)	Age (yBP)	*G.b* (%)	*N.d* (%)	*O.u* (%)	*G.a* (%)	*G.c* (%)	*P.o* (%)	*G.m* (%)	*G.r*(p) (%)	*G.r*(w) (%)	*G.s* (%)	*G.g* (%)	*G.t* (%)	*G.rs* (%)	*N.p*(l) (%)	*N.p*(r) (%)	*G.q* (%)	Other (%)
2011.2	44976.5	41.5	9.3	0.0	0.2	0.5	0.3	0.2	6.6	1.2	0.7	0.9	0.3	0.0	0.0	0.0	4.0	34.3
2011.3	44977.8	44.6	9.9	0.3	0.0	0.0	0.3	0.0	6.0	0.3	0.9	0.6	0.0	0.0	0.0	0.0	3.6	33.4
2011.4	44979.0	40.8	10.3	0.3	0.5	0.0	0.3	0.0	6.1	1.1	0.3	1.1	0.5	0.0	0.3	0.0	3.2	35.5
2011.5	44980.3	40.1	11.7	0.3	0.3	0.0	1.2	0.0	6.7	0.0	0.3	1.2	0.3	0.0	0.0	0.0	2.6	35.4
2011.6	44981.5	35.0	12.7	0.4	0.2	0.7	0.4	0.0	6.9	0.0	0.2	0.6	0.2	0.0	0.4	0.0	2.0	40.4
2011.7	44982.8	39.6	11.6	0.3	0.3	0.0	0.0	0.0	7.3	0.3	0.3	0.3	0.0	0.0	0.3	0.0	4.0	35.6
2011.8	44984.0	42.3	8.8	0.2	0.0	0.0	0.2	0.0	9.2	0.6	0.0	0.2	0.4	0.0	0.0	0.0	1.7	36.5
2011.9	44985.3	38.0	11.7	0.0	0.0	0.0	0.3	0.0	8.2	0.6	0.3	0.3	0.6	0.0	0.3	0.0	2.3	37.4
2012.0	44986.5	39.4	7.4	0.2	0.0	0.0	0.0	0.2	9.3	0.2	0.4	0.6	0.0	0.0	0.0	0.0	3.1	39.2
2012.1	44988.7	36.8	8.3	0.2	0.4	0.2	0.0	0.0	9.1	0.4	0.0	1.4	0.0	0.0	0.0	0.0	5.5	37.7
2012.2	44990.8	39.1	11.0	0.0	0.2	0.2	0.0	0.0	10.4	0.5	0.5	0.7	0.5	0.0	0.0	0.0	3.7	33.1
2012.3	44993.0	39.9	9.7	0.5	0.5	0.0	0.0	0.0	11.2	0.5	0.3	0.3	0.8	0.0	0.0	0.0	2.3	33.9
2012.4	44995.1	42.9	10.3	0.3	0.0	0.0	0.3	0.0	9.5	0.3	0.3	0.5	1.3	0.0	0.0	0.0	4.0	30.6
2012.5	44997.3	40.0	12.6	0.9	0.3	0.3	0.3	0.0	9.2	0.3	0.0	0.0	0.6	0.0	0.0	0.0	4.0	31.4
2012.6	44999.4	38.0	11.4	0.5	0.3	0.3	0.2	0.0	8.2	0.3	0.2	0.5	0.3	0.0	0.0	0.0	4.4	35.3
2012.7	45001.6	41.1	13.9	0.3	0.5	0.3	0.0	0.0	7.2	0.0	0.0	0.8	0.8	0.0	0.0	0.0	4.0	31.2
2012.8	45003.7	38.5	11.3	0.2	0.5	0.0	0.0	0.5	10.4	0.5	0.0	0.5	0.7	0.0	0.0	0.0	5.0	32.1
2012.9	45005.9	36.8	6.9	0.0	0.0	0.3	0.3	0.0	15.2	0.3	0.0	1.0	0.5	0.0	0.3	0.0	7.7	30.8
2013.0	45008.0	38.9	12.8	0.6	0.0	0.0	0.0	0.0	11.6	0.3	0.0	0.3	0.3	0.0	0.0	0.0	4.5	30.9
2013.1	45010.3	41.8	12.1	0.2	0.0	0.4	0.4	0.0	8.6	0.2	0.0	0.4	0.2	0.0	0.0	0.0	3.3	32.6
2013.2	45012.5	40.8	13.8	0.2	0.2	0.0	0.4	0.0	8.1	0.6	0.2	0.4	0.6	0.0	0.0	0.0	2.5	32.3
2013.3	45014.8	43.1	10.3	0.7	0.2	0.2	0.6	0.2	6.4	0.4	0.4	0.4	0.2	0.0	0.0	0.0	3.9	33.1
2013.4	45017.0	43.7	13.1	0.5	0.0	0.0	0.2	0.0	7.4	0.2	0.7	0.5	0.0	0.2	0.0	0.0	2.4	31.0
2013.5	45019.3	40.7	10.4	0.2	0.2	0.0	0.0	0.2	8.4	1.0	0.2	0.0	0.5	0.0	0.2	0.0	3.6	34.2
2013.6	45021.5	44.2	8.9	0.4	0.4	0.2	0.0	0.4	7.8	0.4	0.4	0.0	1.3	0.0	0.0	0.0	1.6	33.8
2013.7	45023.8	45.4	8.4	0.2	0.2	0.2	0.0	0.0	4.9	0.4	0.2	0.0	0.2	0.0	0.0	0.0	3.8	36.1
2013.8	45026.0	42.1	6.3	0.0	0.3	0.0	0.0	0.0	8.9	0.9	0.0	0.3	0.6	0.0	0.0	0.0	4.3	36.4
2013.9	45028.3	46.8	6.0	0.4	0.2	0.2	0.4	0.2	7.6	0.6	0.0	0.4	0.0	0.0	0.2	0.0	2.4	34.6

Core MD03-2622 Relative Abundance Data (continued)

Depth (cm)	Age (yBP)	*G.b* (%)	*N.d* (%)	*O.u* (%)	*G.a* (%)	*G.c* (%)	*P.o* (%)	*G.m* (%)	*G.r*(p) (%)	*G.r*(w) (%)	*G.s* (%)	*G.g* (%)	*G.t* (%)	*G.rs* (%)	*N.p*(l) (%)	*N.p*(r) (%)	*G.q* (%)	Other (%)
2014.0	45030.5	44.6	5.6	0.2	0.0	0.2	0.2	0.2	4.2	1.0	0.6	0.8	0.4	0.0	0.2	0.0	6.7	35.0
2014.1	45032.5	45.3	4.8	0.4	0.4	0.4	0.0	0.0	6.1	0.2	0.2	0.5	0.5	0.0	0.2	0.0	6.8	34.3
2014.2	45034.5	45.2	4.2	0.3	0.3	0.2	0.2	0.0	3.2	1.0	0.0	0.2	0.3	0.0	0.3	0.0	4.9	39.7
2014.3	45036.5	49.2	4.5	0.2	0.2	0.0	0.0	0.0	3.4	0.9	0.0	0.0	0.4	0.0	0.2	0.0	3.7	37.2
2014.4	45038.5	43.4	8.6	0.2	0.2	0.4	0.0	0.0	6.1	0.4	0.2	0.4	0.0	0.0	0.0	0.0	3.5	36.5
2014.5	45040.5	43.4	3.4	0.8	0.3	0.0	0.0	0.0	4.1	1.3	0.3	1.0	0.0	0.0	0.5	0.0	5.2	39.8
2014.6	45042.5	50.0	4.5	0.0	0.0	0.0	0.3	0.0	4.0	0.3	0.3	0.5	0.5	0.3	0.0	0.0	2.5	36.9
2014.7	45044.5	50.3	4.1	0.3	0.9	0.0	0.0	0.0	4.1	1.2	0.3	0.0	0.0	0.0	0.0	0.0	3.6	35.2
2014.8	45046.5	49.1	4.8	0.6	0.3	0.3	0.3	0.0	5.1	0.3	0.0	0.3	0.6	0.0	0.0	0.0	4.8	33.5
2014.9	45048.5	42.2	6.6	0.6	0.0	0.4	0.2	0.4	6.6	0.2	0.4	0.6	0.2	0.0	0.4	0.0	6.1	35.0
2015.0	45050.5	48.2	6.0	0.5	0.8	0.0	0.3	0.0	4.3	0.5	0.3	0.5	0.0	0.0	0.0	0.0	2.5	36.2
2015.1	45051.7	47.2	4.9	0.4	0.4	0.2	0.0	0.0	6.2	1.0	0.2	0.2	0.6	0.2	0.2	0.0	3.1	35.3
2015.2	45052.8	51.0	6.7	0.0	0.3	0.0	0.0	0.6	7.0	0.6	0.0	0.3	0.3	0.0	0.0	0.0	1.8	31.4
2015.3	45054.0	50.0	3.5	0.0	0.0	0.3	0.3	0.3	6.4	0.6	0.6	0.6	1.3	0.0	0.0	0.0	3.8	32.1
2015.4	45055.1	46.2	3.8	0.2	0.0	0.0	0.2	0.0	4.9	0.8	0.2	0.0	0.6	0.0	0.0	0.0	3.2	39.9
2015.5	45056.3	43.2	7.2	0.0	0.8	0.0	0.3	0.0	2.7	1.1	0.3	0.5	0.3	0.0	0.0	0.0	3.7	40.0
2015.6	45057.4	46.8	7.1	0.0	0.8	0.0	0.0	0.2	3.2	0.2	0.2	0.2	0.2	0.2	0.2	0.0	2.2	38.5
2015.7	45058.6	44.4	7.6	0.4	0.2	0.0	0.0	0.0	3.7	0.9	0.2	0.4	0.2	0.0	0.6	0.0	3.9	37.5
2015.8	45059.7	47.3	9.3	0.5	0.7	0.2	0.3	0.2	6.3	0.5	0.8	0.5	0.3	0.2	0.2	0.0	3.2	29.6
2015.9	45060.9	43.5	7.1	0.0	0.6	0.0	0.2	0.0	3.7	0.6	0.4	0.6	0.4	0.0	0.2	0.0	4.4	38.5
2016.0	45062.0	38.9	5.8	0.2	0.2	0.0	0.0	0.0	4.8	0.8	0.2	0.6	0.4	0.0	0.2	0.0	6.0	42.0
2016.1	45063.9	53.5	4.5	0.0	0.0	0.2	0.0	0.0	4.5	1.3	0.2	0.2	0.0	0.0	0.0	0.0	3.3	32.3
2016.2	45065.7	44.2	5.9	0.2	0.0	0.2	0.0	0.0	5.5	0.6	0.4	0.2	0.2	0.0	0.2	0.0	4.7	37.8
2016.3	45067.6	42.6	8.6	0.7	0.2	0.0	0.0	0.0	7.3	0.7	0.2	0.2	0.0	0.0	0.0	0.0	4.2	35.3
2016.4	45069.4	42.0	5.2	0.4	1.0	0.2	0.0	0.0	7.7	0.0	1.0	0.2	0.0	0.0	0.2	0.0	5.4	36.5
2016.5	45071.3	41.8	6.3	0.0	0.5	0.2	0.4	0.0	4.3	1.8	0.5	0.2	0.5	0.0	0.4	0.0	4.5	38.4
2016.6	45073.1	39.9	6.2	0.3	0.3	0.3	0.0	0.0	6.5	0.6	1.2	0.9	0.9	0.0	0.6	0.0	3.7	38.3
2016.7	45075.0	37.8	8.1	0.7	0.9	0.2	0.0	0.2	7.9	0.9	1.4	0.5	0.9	0.0	0.9	0.0	2.5	37.1

Core MD03-2622 Relative Abundance Data (continued)

Depth (cm)	Age (yBP)	*G.b* (%)	*N.d* (%)	*O.u* (%)	*G.a* (%)	*G.c* (%)	*P.o* (%)	*G.m* (%)	*G.r*(p) (%)	*G.r*(w) (%)	*G.s* (%)	*G.g* (%)	*G.t* (%)	*G.rs* (%)	*N.p*(l) (%)	*N.p*(r) (%)	*G.q* (%)	Other (%)
2016.8	45076.8	42.7	5.5	0.0	0.3	0.0	0.0	0.0	7.0	0.6	0.9	0.9	0.6	0.0	0.9	0.0	2.4	38.2
2016.9	45078.7	38.5	6.3	0.8	1.0	0.3	0.0	0.0	8.1	1.0	1.8	0.0	0.3	0.0	0.8	0.0	3.6	37.5
2017.0	45080.5	37.1	8.0	0.9	0.0	0.3	0.3	0.3	11.8	0.6	0.3	0.0	0.6	0.0	0.0	0.0	2.3	37.6
2017.1	45082.9	42.0	9.7	0.0	0.3	0.0	0.0	0.0	8.5	0.6	1.6	0.0	0.3	0.0	0.6	0.0	2.2	34.2
2017.2	45085.2	41.3	10.5	0.6	0.2	1.5	0.0	0.0	9.9	1.0	2.1	0.0	0.2	0.0	0.0	0.0	2.7	30.0
2017.3	45087.6	37.7	11.5	0.5	0.3	0.0	0.0	0.0	9.0	0.3	0.5	0.0	0.3	0.0	0.8	0.0	1.4	37.7
2017.4	45089.9	38.4	10.7	0.9	0.6	0.0	0.3	0.0	12.1	0.6	2.0	0.3	0.6	0.0	0.3	0.0	0.9	32.4
2017.5	45092.3	32.2	10.3	0.0	1.3	1.0	0.0	0.0	9.6	1.3	0.0	0.0	0.6	0.0	1.0	0.0	1.3	41.5
2017.6	45094.6	42.3	7.3	0.0	0.3	0.3	0.0	0.0	10.6	1.2	1.2	0.3	0.9	0.0	0.3	0.0	0.6	34.7
2017.7	45097.0	41.6	11.4	0.7	0.2	0.2	0.0	0.0	12.0	0.7	0.9	0.4	0.4	0.0	0.4	0.0	0.7	30.3
2017.8	45099.3	36.3	11.0	0.0	0.4	0.4	0.2	0.0	7.9	1.1	0.6	0.0	0.2	0.0	0.4	0.0	1.1	40.3
2017.9	45101.7	37.9	6.6	0.0	0.9	0.0	0.0	0.0	8.1	0.6	0.9	0.3	0.3	0.0	0.9	0.0	1.8	41.8
2018.0	45104.0	34.5	9.5	0.5	0.0	0.5	0.5	0.3	7.6	0.8	0.5	0.3	0.0	0.0	0.5	0.0	2.1	42.4
2018.1	45106.1	47.4	8.1	0.7	0.4		0.2	0.0	5.3	0.9	0.2	0.0	0.4	0.0	0.7	0.0	0.9	34.9
2018.2	45108.2	50.5	5.0	0.7	0.7		0.2	0.0	7.1	1.8	1.1	0.0	0.5	0.0	0.2	0.0	0.2	32.0
2018.3	45110.3	45.4	9.2	0.4	0.2		0.6	0.2	3.3	0.2	0.6	0.2	0.4	0.0	0.0	0.0	0.4	38.8
2018.4	45112.4	45.5	6.5	0.9	0.2		0.0	0.0	5.0	0.7	2.0	0.2	0.2	0.0	1.3	0.0	0.0	37.5
2018.5	45114.5	44.3	8.9	0.3	0.3		0.0	0.0	6.1	0.9	0.3	0.6	0.0	0.0	0.3	0.0	0.3	37.6
2018.6	45116.6	38.1	7.4	0.3	0.3		0.3	0.3	8.3	1.1	1.7	0.3	0.6	0.0	0.9	0.0	0.0	40.4
2018.7	45118.7	35.7	11.1	0.5	0.3		0.5	0.0	8.4	1.5	1.0	0.0	0.3	0.0	0.3	0.0	0.3	40.3
2018.8	45120.8	38.3	7.7	0.3	0.6		0.0	0.3	7.1	2.5	0.9	0.3	0.3	0.0	0.6	0.0	0.0	41.0
2018.9	45122.9	38.3	10.5	0.9	0.9	0.6	0.0	0.3	7.8	3.6	1.5	0.3	1.2	0.0	0.6	0.0	0.3	33.7
2019.0	45125.0	41.5	6.9	1.0	0.7		0.7	0.3	8.8	2.0	1.3	1.0	0.7	0.0	0.7	0.0	0.7	34.0
2019.1	45126.2	43.8	7.5	0.5	0.3		0.0	0.3	7.8	1.6	0.8	0.3	0.5	0.0	0.5	0.0	0.3	35.8
2019.2	45127.4	35.0	9.8	0.7	0.5		0.0	0.0	9.8	2.4	1.2	0.2	1.2	0.0	1.2	0.0	0.0	37.9
2019.3	45128.6	43.1	10.9	0.3	1.3		0.3	0.0	9.6	1.3	1.3	0.3	1.6	0.0	1.3	0.0	0.6	28.1
2019.4	45129.8	37.9	7.5	1.1	1.1		0.2	0.2	10.9	2.5	1.1	0.5	0.5	0.0	0.9	0.0	0.0	35.6
2019.5	45131.0	40.6	8.0	0.6	1.1		0.6	0.2	7.6	1.7	0.9	0.2	1.3	0.0	1.1	0.0	0.0	36.1

Core MD03-2622 Relative Abundance Data (continued)

Depth (cm)	Age (yBP)	*G.b* (%)	*N.d* (%)	*O.u* (%)	*G.a* (%)	*G.c* (%)	*P.o* (%)	*G.m* (%)	*G.r*(p) (%)	*G.r*(w) (%)	*G.s* (%)	*G.g* (%)	*G.t* (%)	*G.rs* (%)	*N.p*(l) (%)	*N.p*(r) (%)	*G.q* (%)	Other (%)
2019.6	45132.2	43.6	7.1	0.6	0.2		0.6	0.2	9.1	2.0	0.8	0.2	1.0	0.0	1.0	0.0	0.0	33.5
2019.7	45133.4	36.4	8.9	0.2	0.2		0.5	0.0	10.2	1.8	1.4	0.2	1.6	0.0	1.1	0.0	0.2	37.3
2019.8	45134.6	38.1	7.7	0.8	0.2		0.0	0.2	8.1	2.4	1.6	0.0	0.6	0.0	1.6	0.0	0.0	38.9
2019.9	45135.8	47.7	7.5	0.3	0.6	0.6	0.3	0.3	6.5	2.2	1.9	0.0	0.3	0.0	0.6	0.0	0.0	31.8
2020.0	45137.0	46.0	8.5	0.8	0.6		0.4	0.0	7.9	3.2	1.0	0.2	0.6	0.0	0.8	0.0	0.0	30.0
2020.1	45139.5	47.6	6.5	0.4	0.2		0.6	0.0	6.1	2.2	1.1	0.2	0.2	0.2	1.3	0.0	0.0	33.3
2020.2	45141.9	44.2	9.1	0.4	0.9		0.2	0.0	5.8	1.3	1.5	0.2	0.2	0.0	1.5	0.0	0.0	34.7
2020.3	45144.4	43.5	9.9	0.4	0.9		0.7	0.0	8.1	0.9	2.0	0.4	0.0	0.0	1.8	0.0	0.0	31.4
2020.4	45146.8	39.9	10.9	0.4	0.6		0.0	0.2	7.7	2.4	1.0	0.2	0.6	0.0	1.6	0.0	0.2	34.3
2020.5	45149.3	36.5	13.4	0.2	0.4		0.6	0.0	8.8	2.3	1.3	0.4	0.8	0.0	1.5	0.0	0.4	33.4
2020.6	45151.7	37.3	12.1	0.0	0.5		0.8	0.0	8.1	2.0	1.0	0.0	0.5	0.0	1.5	0.0	0.0	36.3
2020.7	45154.2	38.5	14.8	0.3	0.3		0.9	0.0	5.2	0.6	2.2	0.0	0.3	0.0	0.6	0.0	0.0	36.3
2020.8	45156.6	39.0	9.0	0.0	0.5		0.0	0.0	10.0	1.0	0.7	0.2	0.7	0.0	1.2	0.0	0.5	37.3
2020.9	45159.1	48.0	16.0	0.2	0.0	0.6	0.0	0.0	7.7	0.2	1.8	0.0	0.9	0.0	0.5	0.0	0.0	24.8
2021.0	45161.5	46.7	13.0	0.0	0.4		0.2	0.2	8.9	0.6	0.2	0.0	1.2	0.0	0.2	0.0	0.0	28.4
2021.1	45163.8	40.6	12.6	1.4	0.0		0.5	0.2	5.5	0.9	0.5	0.2	0.5	0.2	0.9	0.0	0.0	36.1
2021.2	45166.0	38.1	11.4	0.0	0.3		0.0	0.0	8.7	1.3	1.3	0.3	0.8	0.0	0.8	0.0	0.0	37.0
2021.3	45168.3	40.8	10.4	0.7	0.7		0.0	0.0	8.9	1.0	0.7	0.0	0.7	0.0	1.2	0.0	0.2	34.5
2021.4	45170.5	37.4	9.4	0.8	0.5		0.0	0.5	7.1	1.0	0.5	0.5	0.8	0.0	1.3	0.0	0.0	40.2
2021.5	45172.8	37.6	12.7	0.2	0.9		0.0	0.0	8.8	0.7	0.2	0.4	0.9	0.0	0.7	0.0	0.0	36.9
2021.6	45175.0	43.3	14.4	0.2	0.2		0.0	0.2	5.4	0.9	1.6	0.2	1.2	0.0	2.8	0.0	0.0	29.4
2021.7	45177.3	43.3	12.6	0.9	0.6		0.0	0.4	10.9	0.6	0.2	0.0	1.5	0.0	2.1	0.0	0.2	26.7
2021.8	45179.5	41.9	13.4	0.3	0.0		0.0	0.0	8.3	1.0	0.0	0.3	0.6	0.0	2.2	0.0	0.0	31.9
2021.9	45181.8	49.0	10.6	2.0	0.3	0.0	0.0	0.0	6.0	0.7	1.3	0.0	0.7	0.0	1.0	0.0	0.0	28.5
2022.0	45184.0	38.2	16.2	0.2	1.0		0.2	0.2	8.4	1.0	0.6	0.0	0.6	0.0	0.0	0.0	0.0	33.3
2022.1	45186.4	42.3	20.6	1.0	0.8		0.2	0.2	9.0	1.3	0.8	0.0	1.3	0.0	0.2	0.0	0.0	22.3
2022.2	45188.7	44.2	19.4	1.2	2.1		0.0	0.3	6.7	1.2	1.2	0.3	0.6	0.0	0.6	0.0	0.0	22.1
2022.3	45191.1	48.6	16.9	0.3	0.5		0.3	0.0	5.5	1.6	1.9	0.5	0.8	0.0	0.3	0.0	0.3	22.4

Core MD03-2622 Relative Abundance Data (continued)

Depth (cm)	Age (yBP)	*G.b* (%)	*N.d* (%)	*O.u* (%)	*G.a* (%)	*G.c* (%)	*P.o* (%)	*G.m* (%)	*G.r*(p) (%)	*G.r*(w) (%)	*G.s* (%)	*G.g* (%)	*G.t* (%)	*G.rs* (%)	*N.p*(l) (%)	*N.p*(r) (%)	*G.q* (%)	Other (%)
2022.4	45193.4	47.1	19.4	0.7	0.4		0.2	0.0	7.8	1.3	1.5	0.2	2.4	0.0	1.1	0.0	1.1	16.8
2022.5	45195.8	46.0	19.9	0.0	2.4		0.0	0.3	6.5	0.9	0.6	0.9	1.5	0.0	0.3	0.0	1.2	19.6
2022.6	45198.1	45.1	23.4	0.6	0.6		0.8	0.6	6.2	0.6	2.0	0.6	1.4	0.0	0.8	0.0	1.4	15.8
2022.7	45200.5	43.5	22.1	1.5	1.5		0.6	0.0	6.5	2.6	1.2	0.6	1.5	0.0	1.2	0.0	1.5	15.9
2022.8	45202.8	51.3	18.7	1.2	0.9		0.0	0.6	5.5	2.0	0.9	0.0	1.2	0.0	0.6	0.0	0.6	16.6
2022.9	45205.2	52.0	18.9	1.1	0.5	0.5	0.3	0.0	5.4	1.6	0.8	0.3	1.9	0.0	1.3	0.0	1.1	14.8
2023.0	45207.5	50.4	23.5	1.1	1.6		0.3	0.0	5.1	1.1	1.3	0.3	2.1	0.0	0.5	0.0	0.8	12.0
2023.1	45208.6	52.3	21.2	0.0	0.3		0.7	0.0	7.3	1.7	1.7	0.0	1.0	0.0	0.7	0.0	1.0	12.3
2023.2	45209.7	46.1	20.1	0.2	1.1		0.6	0.4	8.0	1.9	0.6	0.2	2.6	0.0	0.4	0.0	1.1	16.5
2023.3	45210.8	45.7	20.4	0.0	1.6		0.3	0.3	7.6	0.7	0.7	0.7	2.0	0.0	0.7	0.0	1.0	18.4
2023.4	45211.9	41.7	23.2	0.2	1.1		0.0	0.0	9.5	1.3	2.7	0.2	1.1	0.0	1.3	0.0	1.1	16.8
2023.5	45213.0	42.8	21.5	1.0	0.8		0.3	0.3	9.7	0.8	3.6	0.0	0.5	0.0	0.5	0.0	1.5	16.7
2023.6	45214.1	46.7	23.2	1.2	1.2		0.3	0.3	8.7	0.9	1.5	0.0	0.9	0.0	0.6	0.0	0.9	13.6
2023.7	45215.2	45.7	20.5	0.8	1.9		0.0	0.0	7.6	2.7	1.1	0.3	0.8	0.0	0.5	0.0	1.6	16.5
2023.8	45216.3	48.3	19.6	0.2	1.4		0.0	0.0	12.0	0.5	0.2	0.2	0.5	0.0	0.0	0.0	2.4	14.6
2023.9	45217.4	46.9	22.5	0.8	1.7	0.0	0.3	0.0	9.0	2.5	1.1	0.0	1.1	0.0	0.6	0.0	2.0	11.5
2024.0	45218.5	50.8	20.8	0.0	1.7		0.3	0.0	6.4	2.2	1.1	0.0	1.1	0.0	0.3	0.0	2.5	12.8
2024.1	45220.9	50.0	19.3	0.0	2.1		0.6	0.0	8.6	3.0	1.2	0.0	4.2	0.0	0.9	0.0	1.2	8.9
2024.2	45223.2	50.5	19.3	0.3	0.3		0.0	0.0	11.3	3.3	1.7	0.0	1.7	0.0	0.0	0.0	2.0	9.6
2024.3	45225.6	48.1	25.1	0.3	1.9		0.3	0.0	8.3	1.9	1.6	0.0	0.8	0.0	0.3	0.0	2.7	8.8
2024.4	45227.9	53.5	22.2	1.3	0.5		0.3	0.3	6.8	2.9	0.8	0.0	2.3	0.0	0.3	0.0	1.6	7.3
2024.5	45230.3	49.4	20.2	1.4	1.9		0.6	0.3	7.5	3.0	0.6	0.3	1.9	0.3	0.3	0.0	1.9	10.5
2024.6	45232.6	54.4	19.9	0.2	0.2		0.2	0.2	5.6	2.7	2.5	0.2	1.7	0.0	0.7	0.0	0.7	10.5
2024.7	45235.0	53.7	25.7	0.5	0.8		0.0	0.0	5.6	1.0	0.0	0.0	1.0	0.0	1.0	0.0	2.3	8.4
2024.8	45237.3	52.8	19.9	0.4	0.6		0.6	0.0	5.4	3.5	0.4	0.2	0.0	0.0	0.4	0.0	1.3	14.3
2024.9	45239.7	60.2	15.4	0.6	0.3	0.3	0.9	0.0	4.2	1.2	0.6	0.0	0.6	0.0	0.0	0.0	2.1	13.9
2025.0	45242.0	62.2	14.4	0.8	1.1		0.0	0.0	5.3	1.6	0.3	0.8	1.3	0.0	1.1	0.0	3.2	8.0
2025.1	45244.5	56.9	14.7	0.6	0.6		0.0	0.3	4.9	1.8	1.8	0.0	0.0	0.0	0.6	0.0	6.1	11.6

Core MD03-2622 Relative Abundance Data (continued)

Depth (cm)	Age (yBP)	*G.b* (%)	*N.d* (%)	*O.u* (%)	*G.a* (%)	*G.c* (%)	*P.o* (%)	*G.m* (%)	*G.r*(p) (%)	*G.r*(w) (%)	*G.s* (%)	*G.g* (%)	*G.t* (%)	*G.rs* (%)	*N.p*(l) (%)	*N.p*(r) (%)	*G.q* (%)	Other (%)
2025.2	45247.0	53.1	22.4	1.1	1.1		0.2	0.0	4.3	2.2	1.3	0.2	0.2	0.0	1.1	0.0	2.8	10.1
2025.3	45249.5	58.1	20.2	0.3	0.9		0.0	0.0	3.7	2.8	0.0	0.3	0.3	0.0	0.6	0.0	3.4	9.3
2025.4	45252.0	47.9	24.0	0.2	0.4		0.0	0.0	5.0	2.9	0.6	0.0	0.4	0.0	0.8	0.0	5.6	12.1
2025.5	45254.5	52.0	16.5	0.9	1.4		0.0	0.0	3.8	1.4	3.1	0.5	0.4	0.0	0.7	0.0	5.6	13.7
2025.6	45257.0	58.8	14.8	0.3	0.5		0.3	0.0	3.8	1.1	1.1	0.0	0.3	0.0	0.8	0.0	6.5	11.9
2025.7	45259.5	53.9	14.9	0.2	0.7		0.4	0.0	5.5	1.1	1.8	0.2	0.7	0.0	0.9	0.0	7.9	11.8
2025.8	45262.0	56.1	14.7	0.4	0.2		0.2	0.0	3.9	1.4	1.2	0.0	1.2	0.0	1.0	0.0	7.3	12.5
2025.9	45264.5	53.8	16.7	0.7	0.5	0.2	0.2	0.0	4.7	1.6	0.5	0.0	0.9	0.0	0.9	0.0	6.5	13.1
2026.0	45267.0	55.3	15.9	0.3	0.3		0.0	0.0	5.0	1.1	1.7	0.0	0.3	0.0	0.6	0.0	7.5	12.0
2026.1	45269.4	60.1	13.5	0.2	0.2		0.2	0.0	4.6	1.2	1.9	0.2	0.2	0.0	1.0	0.0	5.6	10.9
2026.2	45271.7	55.6	16.2	0.3	1.8		0.3	0.0	2.4	2.1	1.2	0.0	0.9	0.0	0.6	0.0	9.3	9.3
2026.3	45274.1	55.1	16.2	0.0	0.7		1.0	0.0	4.0	2.0	0.3	0.0	0.3	0.0	0.0	0.0	11.6	8.9
2026.4	45276.4	50.3	16.6	0.3	0.6		0.3	0.0	2.7	2.4	0.0	0.6	0.3	0.0	0.6	0.0	13.0	12.4
2026.5	45278.8	44.5	21.3	0.0	1.3		0.4	0.0	2.2	0.9	0.6	0.2	0.9	0.0	0.2	0.0	14.2	13.3
2026.6	45281.1	53.6	19.2	0.0	0.2		0.2	0.0	2.6	1.1	0.4	0.2	0.7	0.0	0.7	0.0	9.3	11.9
2026.7	45283.5	53.0	18.9	0.0	0.3		0.3	0.0	2.5	1.4	0.8	0.3	0.0	0.0	0.3	0.0	8.5	13.9
2026.8	45285.8	48.1	23.4	0.3	0.5		0.3	0.5	3.0	1.3	0.5	0.3	1.0	0.0	0.5	0.0	5.5	14.9
2026.9	45288.2	46.0	26.5	0.5	0.5	0.7	0.2	0.2	3.0	0.5	0.2	0.2	0.5	0.0	0.2	0.0	5.2	16.1
2027.0	45290.5	53.1	18.4	0.5	0.7		0.0	0.2	3.4	0.9	0.5	0.0	0.7	0.0	0.5	0.0	7.6	13.6
2027.1	45292.7	51.2	17.9	0.5	1.2		0.0	0.2	2.6	1.4	1.2	0.0	0.7	0.0	0.0	0.0	5.0	18.1
2027.2	45294.9	46.6	24.1	1.1	1.1		0.2	0.0	3.8	1.5	0.9	0.2	0.7	0.0	0.0	0.0	5.8	14.0
2027.3	45297.1	48.3	28.7	1.2	1.0		0.0	0.2	3.1	1.0	0.2	0.0	0.5	0.0	0.5	0.0	4.8	10.4
2027.4	45299.3	51.3	26.5	1.2	1.2		0.0	0.2	2.8	1.9	0.9	0.2	0.2	0.0	0.2	0.0	3.5	9.7
2027.5	45301.5	53.9	24.2	0.6	0.8		0.4	0.0	4.5	1.9	0.8	0.2	0.4	0.0	0.2	0.0	2.3	9.6
2027.6	45303.7	31.1	34.0	0.6	3.2		0.3	0.0	5.1	1.9	1.9	0.0	0.6	0.0	1.6	0.0	0.0	19.6
2027.7	45305.9	47.4	29.5	0.6	0.6		0.6	0.2	8.5	2.5	2.9	0.2	0.8	0.0	0.0	0.0	0.0	6.0
2027.8	45308.1	50.7	24.4	1.6	0.8		0.8	0.3	7.3	1.8	2.4	0.0	0.5	0.0	0.0	0.0	0.5	8.9
2027.9	45310.3	49.7	23.7	0.9	1.1	0.5	1.3	0.0	7.3	2.6	2.2	0.4	1.8	0.0	0.2	0.0	0.0	8.8

Core MD03-2622 Relative Abundance Data (continued)

Depth (cm)	Age (yBP)	*G.b* (%)	*N.d* (%)	*O.u* (%)	*G.a* (%)	*G.c* (%)	*P.o* (%)	*G.m* (%)	*G.r*(p) (%)	*G.r*(w) (%)	*G.s* (%)	*G.g* (%)	*G.t* (%)	*G.rs* (%)	*N.p*(l) (%)	*N.p*(r) (%)	*G.q* (%)	Other (%)
2028.0	45312.5	44.8	32.8	1.4	0.9		0.3	0.0	8.6	1.1	0.6	0.3	0.6	0.0	0.0	0.0	0.0	8.6
2028.1	45314.9	41.6	32.1	0.3	0.8		0.3	0.0	7.1	1.8	1.6	0.3	0.8	0.0	0.5	0.0	0.0	12.9
2028.2	45317.3	44.4	34.5	0.3	1.3		0.0	0.0	2.9	2.6	1.3	0.0	0.0	0.0	0.6	0.0	0.3	11.8
2028.3	45319.7	44.3	33.0	0.8	1.0		0.0	0.0	3.8	1.3	0.5	0.3	0.0	0.0	1.0	0.0	0.3	13.9
2028.4	45322.1	40.4	36.7	0.2	1.6		0.2	0.0	2.6	1.4	1.2	0.0	0.0	0.0	0.9	0.0	0.0	14.7
2028.5	45324.5	39.6	36.0	0.0	2.1		0.0	0.0	3.9	0.9	0.6	0.0	0.6	0.0	0.6	0.0	0.0	15.8
2028.6	45326.9	33.3	40.6	0.2	2.5		0.6	0.0	3.9	3.3	0.8	0.0	0.6	0.2	0.4	0.0	0.2	13.3
2028.7	45329.3	39.2	36.3	0.7	2.3		0.5	0.0	5.0	0.7	0.5	0.2	0.2	0.0	0.2	0.0	0.0	14.4
2028.8	45331.7	33.7	42.4	0.0	1.2		0.4	0.4	7.3	1.0	0.4	0.0	0.6	0.0	0.4	0.0	0.0	12.1
2028.9	45334.1	32.3	45.5	0.0	1.6	0.0	0.3	0.3	8.1	1.9	0.3	0.0	0.3	0.0	0.6	0.0	0.6	8.1
2029.0	45336.5	34.2	44.5	0.7	2.2		0.2	0.0	6.0	0.9	0.2	0.2	0.0	0.0	0.9	0.0	0.0	9.8
2029.1	45338.9	36.2	34.8	0.8	2.8		0.6	0.0	8.3	2.5	1.4	0.3	0.0	0.0	0.6	0.0	0.0	11.9
2029.2	45341.3	31.3	52.2	0.0	1.9		0.5	0.0	4.6	1.4	0.5	0.0	0.3	0.0	1.4	0.0	0.0	6.0
2029.3	45343.7	35.9	42.7	0.0	1.8		0.6	0.0	5.9	1.5	0.6	0.0	0.0	0.0	0.0	0.0	1.2	9.8
2029.4	45346.1	36.3	41.3	1.2	0.3		0.0	0.0	4.4	1.8	0.9	0.3	0.3	0.0	1.2	0.0	0.9	11.2
2029.5	45348.5	37.6	43.0	0.5	1.5		0.8	0.0	3.9	1.5	0.0	0.3	0.0	0.0	0.5	0.0	0.0	10.3
2029.6	45350.9	43.0	36.1	0.6	1.0		0.0	0.0	4.8	1.6	0.2	0.2	0.2	0.0	0.6	0.0	0.0	11.6
2029.7	45353.3	42.8	40.6	0.4	0.2		0.4	0.0	5.3	1.0	0.2	0.0	0.4	0.0	0.6	0.0	0.4	7.7
2029.8	45355.7	40.1	39.3	0.3	0.3		0.3	0.0	4.1	2.3	0.3	0.0	0.3	0.0	0.5	0.0	0.8	11.6
2029.9	45358.1	41.2	40.3	0.9	0.0	0.0	0.6	0.0	4.1	2.2	0.3	0.0	0.0	0.0	0.6	0.0	0.3	9.4
2030.0	45360.5	59.6	20.2	0.2	0.4		0.4	0.4	4.2	2.2	0.9	0.0	0.7	0.2	1.1	0.0	0.0	9.5
2030.1	45363.0	52.9	20.9	0.3	0.5		1.1	0.0	7.0	0.8	1.3	0.5	0.3	0.0	0.3	0.0	0.0	14.2
2030.2	45365.4	56.4	21.3	0.8	1.7		0.0	0.2	5.6	2.1	1.7	0.2	0.6	0.0	0.6	0.0	0.0	8.9
2030.3	45367.9	55.7	17.0	0.3	0.3		0.3	0.0	9.2	1.6	1.3	0.0	0.0	0.3	0.3	0.0	0.0	13.4
2030.4	45370.3	58.5	10.5	0.7	0.7		0.2	0.0	8.6	1.4	1.2	0.0	0.5	0.0	0.9	0.0	0.0	16.8
2030.5	45372.8	55.1	9.5	1.3	1.0		0.3	0.0	10.0	1.8	3.1	0.3	0.0	0.0	1.0	0.0	0.3	16.4
2030.6	45375.2	59.5	9.8	1.4	0.6		0.0	0.0	7.5	2.3	1.7	0.3	0.0	0.0	0.6	0.0	0.0	16.2
2030.7	45377.7	56.4	7.0	2.5	0.6		1.0	0.0	10.8	3.5	4.1	0.0	0.0	0.0	1.0	0.0	0.0	13.1

Core MD03-2622 Relative Abundance Data (continued)

Depth (cm)	Age (yBP)	*G.b* (%)	*N.d* (%)	*O.u* (%)	*G.a* (%)	*G.c* (%)	*P.o* (%)	*G.m* (%)	*G.r*(p) (%)	*G.r*(w) (%)	*G.s* (%)	*G.g* (%)	*G.t* (%)	*G.rs* (%)	*N.p*(l) (%)	*N.p*(r) (%)	*G.q* (%)	Other (%)
2030.8	45380.1	59.6	4.3	1.6	1.9		0.3	0.3	8.9	2.4	3.0	0.0	0.0	0.0	0.8	0.0	0.0	17.0
2030.9	45382.6	63.1	3.8	2.2	1.0	0.0	0.0	0.0	10.3	2.2	4.8	0.0	0.3	0.0	0.3	0.0	0.0	11.9
2031.0	45385.0	59.1	4.9	2.0	1.4		0.0	0.0	14.3	2.6	2.3	0.0	0.0	0.0	0.3	0.0	0.0	13.1
2031.1	45387.3	59.8	5.0	2.6	2.0		0.0	0.0	10.2	2.9	2.0	0.3	0.0	0.0	0.6	0.0	0.0	14.6
2031.2	45389.6	57.1	7.0	1.2	1.2		0.0	0.0	13.0	1.4	1.7	0.0	0.0	0.0	0.3	0.0	0.0	17.1
2031.3	45391.9	64.4	2.4	1.6	1.3		0.0	0.0	10.4	3.5	4.3	0.0	0.0	0.0	0.5	0.0	0.0	11.7
2031.4	45394.2	55.3	5.8	1.9	1.1		0.0	0.0	11.4	1.9	3.9	0.0	0.8	0.0	0.3	0.0	0.0	17.5
2031.5	45396.5	52.5	4.7	2.5	1.3		0.0	0.0	13.6	2.8	3.5	0.3	0.3	0.0	0.0	0.0	0.0	18.4
2031.6	45398.8	57.2	4.5	1.3	2.6		0.3	0.0	11.5	2.2	3.8	0.0	0.0	0.0	0.6	0.0	0.0	16.0
2031.7	45401.1	55.1	4.2	2.3	3.9		0.0	0.0	15.8	1.6	3.1	0.0	0.0	0.0	0.3	0.0	0.0	13.8
2031.8	45403.4	58.2	5.2	2.4	2.7		0.0	0.0	10.3	3.0	3.9	0.0	0.0	0.0	0.9	0.0	0.0	13.3
2031.9	45405.7	51.2	4.7	2.4	0.6	0.0	0.9	0.0	13.2	3.5	2.4	0.0	0.0	0.3	0.6	0.0	0.3	20.0
2032.0	45408.0	48.7	6.3	1.6	1.8		0.4	0.4	14.6	3.4	4.3	0.0	0.7	0.7	0.4	0.0	0.4	16.4
2032.1	45410.4	53.6	5.4	0.9	1.7		0.3	0.0	11.7	2.0	4.0	0.3	0.0	0.0	0.6	0.0	0.3	19.2
2032.2	45412.7	53.1	5.3	3.5	1.2		0.0	0.0	10.6	4.1	3.8	0.6	0.0	0.3	1.2	0.0	0.0	16.4
2032.3	45415.1	50.9	5.6	0.8	1.3		0.5	0.0	17.2	3.2	3.5	0.0	0.0	0.0	1.1	0.0	0.3	15.5
2032.4	45417.4	55.8	6.6	1.5	1.5		0.2	0.2	10.0	4.1	3.6	0.0	0.0	0.5	1.0	0.0	0.0	15.0
2032.5	45419.8	53.4	6.5	3.3	1.1		0.3	0.8	13.6	3.3	2.4	0.0	0.0	0.0	0.8	0.0	0.3	14.4
2032.6	45422.1	53.5	3.3	1.7	1.0		0.0	0.0	15.3	3.0	3.7	0.0	0.0	0.0	0.7	0.0	0.0	17.9
2032.7	45424.5	55.6	4.6	2.9	1.1		0.0	0.0	12.6	4.0	3.2	0.3	0.3	0.0	2.0	0.0	0.0	13.5
2032.8	45426.8	55.7	5.1	2.6	2.1		0.0	0.0	12.6	4.0	4.0	0.4	0.0	0.2	0.6	0.0	0.0	12.6
2032.9	45429.2	54.2	4.6	3.0	2.4	0.5	0.2	0.2	11.3	4.8	3.8	0.4	0.0	0.4	0.6	0.0	0.4	13.5
2033.0	45431.5	52.4	4.5	1.8	2.1		0.3	0.5	10.2	7.9	3.7	0.3	0.0	0.0	1.0	0.0	0.5	14.9
2033.1	45433.9	52.2	5.8	2.0	2.6		0.3	0.3	14.2	2.6	5.5	0.3	0.0	0.0	0.9	0.0	0.3	13.0
2033.2	45436.3	50.7	6.1	4.2	1.1		0.0	0.3	14.7	2.5	4.4	1.1	0.3	0.0	0.8	0.0	0.0	13.9
2033.3	45438.7	51.6	5.9	3.3	2.1		0.3	0.0	11.6	4.2	3.3	0.9	0.0	0.0	1.2	0.0	0.0	15.7
2033.4	45441.1	53.9	6.1	2.3	1.9		0.0	0.2	10.4	4.4	3.8	0.6	0.2	0.0	1.9	0.0	0.2	14.2
2033.5	45443.5	53.3	4.9	3.3	2.3		0.0	0.0	13.2	5.9	3.6	0.0	0.0	0.0	1.6	0.0	0.0	11.8

Core MD03-2622 Relative Abundance Data (continued)

Depth (cm)	Age (yBP)	*G.b* (%)	*N.d* (%)	*O.u* (%)	*G.a* (%)	*G.c* (%)	*P.o* (%)	*G.m* (%)	*G.r*(p) (%)	*G.r*(w) (%)	*G.s* (%)	*G.g* (%)	*G.t* (%)	*G.rs* (%)	*N.p*(l) (%)	*N.p*(r) (%)	*G.q* (%)	Other (%)
2033.6	45445.9	58.4	6.1	2.3	1.3		0.0	0.0	13.2	3.2	3.9	0.3	0.3	0.0	1.0	0.0	0.0	10.0
2033.7	45448.3	60.1	2.0	5.2	1.4		0.0	0.3	11.5	3.4	3.4	0.0	0.0	0.0	0.9	0.0	0.0	11.8
2033.8	45450.7	61.2	4.6	2.3	1.6		0.0	0.0	12.5	3.9	3.6	0.0	0.0	0.0	0.7	0.0	0.0	9.5
2033.9	45453.1	60.6	4.6	2.0	1.3	0.3	0.0	0.0	12.7	3.6	1.6	0.7	0.0	0.0	1.3	0.0	0.0	11.7
2034.0	45455.5	58.7	3.0	1.5	0.9		0.0	0.0	14.0	5.2	1.2	0.0	0.0	0.3	1.5	0.0	0.0	13.7
2034.1	45457.7	57.1	3.4	2.0	1.3		0.0	0.0	13.3	3.8	2.7	0.0	0.0	0.0	1.1	0.0	0.0	15.3
2034.2	45459.8	59.1	4.1	1.0	1.5		0.0	0.2	11.9	3.9	3.9	0.0	0.0	0.0	1.0	0.0	0.0	13.6
2034.3	45462.0	61.8	4.4	1.8	1.5		0.2	0.0	12.5	4.2	3.5	0.2	0.2	0.0	0.2	0.0	0.0	9.4
2034.4	45464.1	59.2	6.9	1.9	1.6		0.0	0.3	10.1	5.3	3.5	0.0	0.3	0.0	0.8	0.0	0.0	10.1
2034.5	45466.3	58.6	4.5	1.4	2.0		0.0	0.0	12.7	3.9	3.5	0.4	0.0	0.0	1.2	0.0	0.0	11.7
2034.6	45468.4	60.6	5.1	2.6	2.1		0.2	0.0	8.8	3.5	3.5	0.0	0.2	0.0	1.4	0.0	0.0	12.1
2034.7	45470.6	59.2	4.4	2.7	2.0		0.0	0.0	12.0	4.4	2.4	0.0	0.0	0.2	0.7	0.0	0.0	12.0
2034.8	45472.7	59.9	3.6	2.2	2.0		0.0	0.0	11.8	4.2	2.0	0.0	0.0	0.0	0.6	0.0	0.0	13.7
2034.9	45474.9	62.3	2.5	1.2	1.6	0.0	0.0	0.0	12.1	4.7	1.9	0.3	0.0	0.0	0.0	0.0	0.0	13.4
2035.0	45477.0	57.0	3.1	2.6	2.0		0.0	0.0	15.3	3.3	3.1	0.0	0.5	0.0	0.5	0.0	0.0	12.5
2035.1	45479.2	59.4	5.4	2.2	1.1		0.6	0.0	12.9	2.6	3.2	0.2	0.0	0.0	0.4	0.0	0.0	12.0
2035.2	45481.4	58.3	4.6	1.8	1.8		0.2	0.4	11.1	4.6	2.4	0.0	0.0	0.0	0.8	0.0	0.0	14.1
2035.3	45483.6	64.2	3.6	1.0	2.1		0.0	0.2	11.9	3.6	2.3	0.0	0.0	0.0	0.2	0.0	0.0	10.9
2035.4	45485.8	63.1	2.9	1.8	2.6		0.0	0.0	12.1	2.9	2.9	0.2	0.0	0.0	0.4	0.0	0.0	11.0
2035.5	45488.0	56.3	1.3	2.2	1.6		0.0	0.0	14.6	2.9	2.9	0.2	0.0	0.0	2.2	0.0	0.0	15.7
2035.6	45490.2	53.5	2.8	0.6	0.9		0.0	0.0	17.2	4.3	4.6	0.0	0.0	0.0	1.2	0.0	0.0	14.8
2035.7	45492.4	55.8	3.6	1.0	1.0		0.0	0.0	17.8	3.9	3.9	0.3	0.0	0.0	0.8	0.0	0.0	11.9
2035.8	45494.6	56.8	5.3	1.4	1.1		0.0	0.0	14.4	4.1	4.1	0.5	0.0	0.0	0.9	0.0	0.0	11.4
2035.9	45496.8	53.0	1.9	2.8	1.2	0.5	0.0	0.2	20.1	5.0	3.3	0.0	0.2	0.0	0.5	0.0	0.0	11.8
2036.0	45499.0	60.3	2.1	1.2	2.7		0.0	0.0	14.5	4.5	3.9	0.0	0.0	0.0	0.9	0.0	0.0	9.7
2036.1	45500.9	60.6	4.8	0.4	1.5		0.0	0.2	14.4	1.5	4.2	0.0	0.2	0.0	1.1	0.0	0.0	10.9
2036.2	45502.7	55.1	3.0	1.5	1.2		0.3	0.0	17.2	5.4	2.4	0.0	0.3	0.0	0.9	0.0	0.0	12.7
2036.3	45504.6	56.2	4.3	1.7	1.5		0.0	0.4	15.0	3.4	5.1	0.0	0.0	0.0	0.6	0.0	0.0	11.8

Core MD03-2622 Relative Abundance Data (continued)

Depth (cm)	Age (yBP)	*G.b* (%)	*N.d* (%)	*O.u* (%)	*G.a* (%)	*G.c* (%)	*P.o* (%)	*G.m* (%)	*G.r*(p) (%)	*G.r*(w) (%)	*G.s* (%)	*G.g* (%)	*G.t* (%)	*G.rs* (%)	*N.p*(l) (%)	*N.p*(r) (%)	*G.q* (%)	Other (%)
2036.4	45506.4	61.8	2.4	1.3	1.7		0.0	0.9	13.4	2.4	5.0	0.0	0.2	0.0	0.0	0.0	0.0	10.8
2036.5	45508.3	61.4	3.1	0.9	0.9		0.0	0.0	12.9	4.4	4.2	0.0	0.4	0.0	0.4	0.0	0.0	11.3
2036.6	45510.1	62.3	2.2	1.5	1.3		0.0	0.0	12.9	2.6	2.2	0.4	0.4	0.2	0.4	0.0	0.0	13.8
2036.7	45512.0	64.3	2.7	1.5	1.5		0.0	0.0	11.2	3.6	2.9	0.0	0.0	0.0	0.7	0.0	0.0	11.7
2036.8	45513.8	64.2	4.5	1.8	2.7		0.0	0.0	8.7	2.1	3.6	0.0	0.0	0.0	0.9	0.0	0.0	11.6
2036.9	45515.7	66.6	3.2	2.0	1.0	0.0	0.0	0.0	12.8	2.6	2.4	0.0	0.4	0.2	0.0	0.0	0.0	8.7
2037.0	45517.5	63.7	3.5	0.9	1.3		0.0	0.6	14.0	4.1	2.4	0.0	0.2	0.0	0.0	0.0	0.0	9.4
2037.1	45519.9	66.6	3.3	1.9	0.9		0.2	0.0	9.5	4.8	2.9	0.2	0.0	0.0	0.9	0.0	0.0	8.8
2037.2	45522.3	71.7	1.6	3.4	0.6		0.0	0.3	10.0	5.0	0.6	0.0	0.0	0.0	0.6	0.0	0.0	6.2
2037.3	45524.7	73.9	3.2	1.6	1.3		0.0	0.3	7.1	4.7	1.1	0.0	0.0	0.0	0.0	0.0	0.0	6.9
2037.4	45527.1	68.4	0.9	1.8	1.2		0.0	0.0	14.0	2.3	1.8	0.3	0.0	0.3	0.6	0.0	0.0	8.5
2037.5	45529.5	69.3	1.5	1.5	0.9		0.0	0.0	15.2	3.8	0.6	0.0	0.0	0.0	0.6	0.0	0.0	6.7
2037.6	45531.9	70.7	1.4	3.4	1.1		0.0	0.0	9.8	4.5	1.4	0.0	0.0	0.0	0.6	0.0	0.0	7.3
2037.7	45534.3	73.9	1.5	1.3	2.2		0.0	0.0	7.6	2.7	1.3	0.2	0.4	0.0	0.4	0.0	0.0	8.7
2037.8	45536.7	82.0	2.3	0.5	0.5		0.0	0.0	4.9	1.8	1.6	0.0	0.0	0.0	0.5	0.0	0.0	5.7
2037.9	45539.1	72.0	3.1	1.2	2.3	0.0	0.0	0.0	7.0	3.5	0.8	0.0	0.2	0.0	0.8	0.0	0.0	8.9
2038.0	45541.5	76.7	1.7	1.5	0.8		0.0	0.0	8.4	2.1	1.9	0.0	0.4	0.0	1.1	0.0	0.0	5.5
2038.1	45543.8	75.7	1.7	1.5	0.9		0.0	0.4	8.3	2.8	1.3	0.4	0.0	0.0	0.4	0.0	0.0	6.6
2038.2	45546.1	72.6	2.5	1.3	0.5		0.2	0.2	9.8	3.3	1.3	0.2	0.2	0.0	0.7	0.0	0.0	7.2
2038.3	45548.4	71.2	3.3	1.4	0.5		0.0	0.0	10.3	3.3	2.4	0.0	0.3	0.0	0.8	0.0	0.0	6.5
2038.4	45550.7	73.8	3.3	1.3	0.4		0.0	0.2	9.3	4.3	1.5	0.0	0.0	0.0	0.4	0.0	0.0	5.4
2038.5	45553.0	71.1	2.7	0.6	0.4		0.2	0.0	11.3	3.7	1.2	0.0	0.2	0.0	0.2	0.0	0.0	8.2
2038.6	45555.3	72.5	3.6	0.3	0.7		0.0	0.0	7.9	3.6	1.3	0.0	0.0	0.0	1.0	0.0	0.0	8.9
2038.7	45557.6	69.2	3.0	0.8	1.9		0.0	0.0	11.8	3.2	1.3	0.2	0.4	0.0	0.4	0.0	0.0	7.8
2038.8	45559.9	74.9	2.2	1.6	0.6		0.0	0.0	10.2	3.2	1.3	0.0	0.3	0.3	0.0	0.0	0.0	5.4
2038.9	45562.2	68.3	1.0	2.3	1.6	0.0	0.0	0.7	11.8	3.9	2.3	0.0	0.0	0.0	0.3	0.0	0.0	7.8
2039.0	45564.5	70.2	2.0	0.3	2.3		0.0	0.0	8.9	4.9	1.3	0.0	0.0	0.0	1.0	0.0	0.0	9.2
2039.1	45566.6	69.5	2.9	1.4	1.2		0.5	0.0	11.2	3.1	1.4	0.0	0.0	0.0	0.5	0.0	0.0	8.4

Core MD03-2622 Relative Abundance Data (continued)

Depth (cm)	Age (yBP)	*G.b* (%)	*N.d* (%)	*O.u* (%)	*G.a* (%)	*G.c* (%)	*P.o* (%)	*G.m* (%)	*G.r*(p) (%)	*G.r*(w) (%)	*G.s* (%)	*G.g* (%)	*G.t* (%)	*G.rs* (%)	*N.p*(l) (%)	*N.p*(r) (%)	*G.q* (%)	Other (%)
2039.2	45568.7	70.4	1.4	1.7	1.7		0.0	0.3	10.0	4.0	1.4	0.3	0.0	0.0	0.9	0.0	0.0	8.0
2039.3	45570.8	74.1	2.0	1.7	0.3		0.0	0.0	13.0	1.7	1.7	0.0	0.0	0.0	0.7	0.0	0.0	5.0
2039.4	45572.9	71.3	3.6	1.9	0.6		0.0	0.0	9.2	5.6	1.1	0.0	0.0	0.0	1.1	0.0	0.0	5.6
2039.5	45575.0	70.5	2.0	1.5	0.7		0.0	0.2	12.6	3.7	1.1	0.2	0.2	0.0	0.2	0.0	0.0	7.0
2039.6	45577.1	66.8	2.2	1.3	0.6		0.0	0.2	14.0	4.7	1.5	0.0	0.2	0.0	0.6	0.0	0.0	7.8
2039.7	45579.2	65.4	4.2	1.0	0.7		0.0	0.0	11.8	6.2	2.0	0.0	0.0	0.0	1.0	0.0	0.0	7.8
2039.8	45581.3	78.5	2.1	2.4	0.5		0.0	0.0	4.5	2.1	2.9	0.0	0.0	0.0	0.3	0.0	0.0	6.8
2039.9	45583.4	82.1	2.0	1.5	1.0	0.0	0.0	0.0	3.8	2.6	1.0	0.0	0.0	0.3	0.5	0.0	0.0	5.1
2040.0	45585.5	73.5	2.5	3.7	1.8		0.0	0.4	7.0	3.3	1.1	0.4	0.0	0.0	0.4	0.0	0.0	6.1
2040.1	45587.8	78.5	1.5	2.2	1.1		0.0	0.2	8.5	2.0	0.5	0.0	0.2	0.2	0.5	0.0	0.0	4.5
2040.2	45590.0	74.0	2.7	1.2	0.9		0.0	0.0	11.6	2.7	0.6	0.0	0.3	0.0	1.5	0.0	0.0	4.5
2040.3	45592.3	76.6	2.1	1.0	1.2		0.0	0.0	10.3	2.7	1.0	0.2	0.0	0.4	0.4	0.0	0.0	4.1
2040.4	45594.5	75.8	2.5	1.9	0.6		0.0	0.0	8.5	3.5	0.6	0.0	0.0	0.0	0.3	0.0	0.0	6.3
2040.5	45596.8	79.9	1.7	1.5	1.0		0.0	0.0	6.7	2.0	1.0	0.2	0.2	0.3	0.3	0.0	0.0	5.1
2040.6	45599.0	80.2	2.9	1.4	0.7		0.0	0.0	5.7	2.2	0.9	0.0	0.0	0.0	0.7	0.0	0.0	5.3
2040.7	45601.3	81.0	2.6	1.3	1.1		0.0	0.0	5.3	2.1	1.3	0.0	0.0	0.0	0.0	0.0	0.0	5.3
2040.8	45603.5	78.0	2.0	1.7	1.0		0.0	0.0	5.7	4.7	1.7	0.0	0.0	0.0	0.2	0.0	0.0	5.0
2040.9	45605.8	82.9	1.7	1.2	0.7	0.2	0.0	0.0	3.7	2.0	1.0	0.0	0.2	0.0	0.5	0.0	0.0	6.1
2041.0	45608.0	82.4	2.4	0.7	0.9		0.0	0.0	3.3	3.5	1.6	0.0	0.0	0.3	0.3	0.0	0.0	4.7
2041.1	45610.4	83.9	1.6	1.9	1.4		0.0	0.0	2.1	1.6	1.4	0.0	0.2	0.2	0.7	0.0	0.0	4.9
2041.2	45612.7	81.2	1.4	1.1	1.8		0.0	0.0	2.3	2.3	1.1	0.0	0.2	0.0	0.9	0.0	0.0	7.7
2041.3	45615.1	82.4	2.7	0.8	1.2		0.0	0.2	2.5	1.2	1.4	0.0	0.0	0.0	1.0	0.0	0.0	6.5
2041.4	45617.4	78.9	3.3	0.5	1.3		0.0	0.0	2.3	2.0	1.0	0.5	0.3	0.0	0.8	0.0	0.0	9.1
2041.5	45619.8	76.6	3.0	2.4	1.5		0.0	0.3	4.4	2.4	1.5	0.0	0.0	0.0	0.9	0.0	0.0	7.1
2041.6	45622.1	76.5	3.2	1.6	1.9		0.0	0.2	2.1	6.0	1.8	0.0	0.2	0.0	0.2	0.0	0.0	6.5
2041.7	45624.5	77.5	2.8	2.5	1.5		0.3	0.0	4.0	3.0	1.5	0.5	0.0	0.0	0.3	0.0	0.0	6.3
2041.8	45626.8	75.8	3.8	2.2	1.0		0.0	0.3	4.1	3.5	2.2	0.0	0.0	0.3	0.6	0.0	0.0	6.1
2041.9	45629.2	72.6	4.4	0.6	1.5	0.0	0.0	0.0	3.2	3.5	3.5	0.9	0.0	0.0	1.2	0.0	0.0	8.5

Core MD03-2622 Relative Abundance Data (continued)

Depth (cm)	Age (yBP)	*G.b* (%)	*N.d* (%)	*O.u* (%)	*G.a* (%)	*G.c* (%)	*P.o* (%)	*G.m* (%)	*G.r*(p) (%)	*G.r*(w) (%)	*G.s* (%)	*G.g* (%)	*G.t* (%)	*G.rs* (%)	*N.p*(l) (%)	*N.p*(r) (%)	*G.q* (%)	Other (%)
2042.0	45631.5	76.4	3.4	2.2	1.9		0.0	0.3	4.0	2.8	0.9	0.0	0.0	0.3	1.2	0.0	0.0	6.5
2042.1	45633.7	80.7	3.3	2.2	1.8		0.0	0.0	2.0	3.1	0.6	0.0	0.0	0.0	1.0	0.0	0.0	5.3
2042.2	45635.8	78.3	2.2	1.7	2.2		0.0	0.0	3.6	3.6	2.2	0.0	0.0	0.0	1.0	0.0	0.0	5.3
2042.3	45638.0	76.8	2.3	1.0	1.5		0.0	0.2	4.9	3.4	2.0	0.0	0.2	0.2	0.5	0.0	0.0	7.0
2042.4	45640.1	74.9	3.5	1.3	1.5		0.0	0.0	5.5	3.0	1.8	0.2	0.0	0.0	0.8	0.0	0.0	7.4
2042.5	45642.3	78.4	3.5	2.4	0.8		0.0	0.0	2.2	2.7	1.9	0.0	0.0	0.3	1.9	0.0	0.0	5.9
2042.6	45644.4	78.2	3.0	1.4	0.7		0.0	0.2	3.2	2.3	3.6	0.0	0.0	0.0	1.1	0.0	0.0	6.4
2042.7	45646.6	77.5	3.1	2.0	0.3		0.2	0.0	1.9	3.4	2.0	0.3	0.2	0.0	0.5	0.0	0.0	8.6
2042.8	45648.7	76.5	3.6	2.2	1.5		0.0	0.0	1.7	3.8	2.6	0.0	0.2	0.3	0.5	0.0	0.0	7.0
2042.9	45650.9	72.5	4.3	2.0	1.2	0.0	0.0	0.0	3.5	3.5	2.8	0.0	0.0	0.0	0.6	0.0	0.0	9.6
2043.0	45653.0	71.1	5.0	1.6	1.2		0.0	0.0	4.1	3.3	4.7	0.0	0.0	0.0	1.0	0.0	0.0	8.1
2043.1	45655.4	68.3	6.5	1.9	1.5		0.0	0.2	5.0	3.0	3.9	0.2	0.0	0.2	0.6	0.0	0.0	8.6
2043.2	45657.7	69.9	6.1	0.9	0.9		0.0	0.0	3.7	4.4	4.4	0.0	0.2	0.0	0.7	0.0	0.0	9.0
2043.3	45660.1	67.6	4.1	3.2	0.9		0.0	0.3	3.8	4.4	5.0	0.0	0.0	0.0	0.9	0.0	0.0	9.9
2043.4	45662.4	68.3	6.2	2.7	0.5		0.0	0.0	2.7	3.3	3.8	0.0	0.0	0.3	0.5	0.0	0.0	11.7
2043.5	45664.8	68.1	5.2	3.3	1.0		0.0	0.0	2.6	3.6	3.9	0.0	0.0	0.0	0.3	0.0	0.0	12.1
2043.6	45667.1	65.2	5.1	2.8	2.0		0.0	0.0	4.5	5.6	3.9	0.3	1.1	0.0	0.3	0.0	0.0	9.3
2043.7	45669.5	68.2	4.2	3.3	1.2		0.0	0.3	3.9	4.2	2.4	0.0	0.0	0.3	1.5	0.0	0.0	10.5
2043.8	45671.8	64.7	3.7	3.0	2.3		0.0	0.0	4.6	4.4	3.4	0.0	0.0	0.0	0.9	0.0	0.0	13.1
2043.9	45674.2	68.5	2.9	2.6	1.5	0.0	0.0	0.0	2.6	4.7	4.4	0.0	0.0	0.3	1.7	0.0	0.0	10.8
2044.0	45676.5	65.6	5.6	2.9	2.9		0.0	0.3	2.9	5.1	4.8	0.0	0.0	0.3	0.5	0.0	0.0	9.1
2044.1	45679.0	70.8	2.7	2.4	1.9		0.0	0.0	3.8	2.7	3.5	0.0	0.3	0.3	0.3	0.0	0.0	11.4
2044.2	45681.4	66.1	4.5	2.5	1.8		0.0	0.0	2.9	5.4	3.6	0.0	0.2	0.2	1.6	0.0	0.0	11.1
2044.3	45683.9	68.1	4.9	1.7	1.2		0.0	0.0	3.0	7.2	2.6	0.0	0.0	0.2	0.7	0.0	0.0	10.5
2044.4	45686.3	66.6	3.4	4.3	1.9		0.0	0.2	3.1	6.0	3.1	0.2	0.0	0.0	1.4	0.0	0.0	9.6
2044.5	45688.8	69.3	4.1	1.8	1.2		0.0	0.2	3.9	4.5	3.3	0.2	0.2	0.0	0.6	0.0	0.0	10.8
2044.6	45691.2	71.7	4.4	3.0	1.3		0.2	0.0	3.8	5.9	1.3	0.0	0.0	0.0	1.3	0.0	0.0	7.2
2044.7	45693.7	71.7	6.4	1.3	0.7		0.0	0.0	3.8	6.6	2.0	0.0	0.0	0.2	0.9	0.0	0.0	6.4

Core MD03-2622 Relative Abundance Data (continued)

Depth (cm)	Age (yBP)	*G.b* (%)	*N.d* (%)	*O.u* (%)	*G.a* (%)	*G.c* (%)	*P.o* (%)	*G.m* (%)	*G.r*(p) (%)	*G.r*(w) (%)	*G.s* (%)	*G.g* (%)	*G.t* (%)	*G.rs* (%)	*N.p*(l) (%)	*N.p*(r) (%)	*G.q* (%)	Other (%)
2044.8	45696.1	72.8	3.3	1.0	0.7		0.0	0.0	4.6	7.9	3.3	0.0	0.0	0.0	1.0	0.0	0.0	5.6
2044.9	45698.6	71.8	4.3	1.6	1.6	0.8	0.0	0.0	4.5	5.3	1.6	0.2	0.0	0.0	1.4	0.0	0.0	7.7
2045.0	45701.0	68.0	5.0	2.3	1.1		0.0	0.0	3.8	8.4	3.0	0.0	0.4	0.0	1.5	0.0	0.0	6.5
2045.1	45703.3	73.8	3.6	1.9	1.3		0.0	0.2	2.8	4.9	1.7	0.0	0.0	0.2	1.9	0.0	0.0	7.7
2045.2	45705.5	71.6	2.5	2.5	1.5		0.0	0.0	1.9	7.6	3.2	0.0	0.0	0.0	1.0	0.0	0.0	8.2
2045.3	45707.8	77.5	4.6	1.1	1.4		0.0	0.0	3.1	4.3	2.0	0.0	0.0	0.0	0.9	0.0	0.0	5.1
2045.4	45710.0	76.3	2.0	2.2	1.3		0.0	0.2	2.2	5.4	2.0	0.2	0.0	0.0	0.7	0.0	0.0	7.6
2045.5	45712.3	73.7	2.0	3.7	1.6		0.2	0.0	2.0	6.7	2.0	0.0	0.0	0.0	1.0	0.0	0.0	7.3
2045.6	45714.5	69.7	3.1	2.7	2.0		0.0	0.0	2.9	7.1	2.7	0.2	0.2	0.4	1.3	0.0	0.0	7.7
2045.7	45716.8	72.2	4.1	2.8	1.7		0.0	0.0	1.7	6.7	2.8	0.0	0.0	0.0	1.3	0.0	0.0	6.7
2045.8	45719.0	69.9	5.0	2.6	2.4		0.0	0.0	1.5	6.5	1.5	0.2	0.0	0.0	1.5	0.0	0.0	9.0
2045.9	45721.3	73.6	2.7	1.9	1.6	0.0	0.0	0.3	0.5	6.5	2.4	0.0	0.0	0.0	1.4	0.0	0.0	9.0
2046.0	45723.5	71.1	7.5	3.0	0.7		0.0	0.0	2.3	3.9	1.6	0.0	0.0	0.0	0.7	0.0	0.0	9.2
2046.1	45725.6	73.2	2.3	3.5	1.9		0.0	0.2	2.1	7.7	1.7	0.0	0.0	0.0	1.0	0.0	0.0	6.4
2046.2	45727.7	75.2	3.3	2.1	1.7		0.0	0.2	3.1	6.1	0.7	0.0	0.0	0.0	0.9	0.0	0.0	6.6
2046.3	45729.8	81.1	2.9	2.2	0.6		0.0	0.0	1.6	5.1	0.3	0.0	0.0	0.0	0.3	0.0	0.0	5.8
2046.4	45731.9	77.2	2.9	2.4	1.0		0.2	0.0	1.6	6.0	1.9	0.0	0.0	0.0	0.9	0.0	0.0	5.9
2046.5	45734.0	76.4	3.5	2.0	1.0		0.0	0.0	1.4	4.5	2.4	0.0	0.0	0.0	0.4	0.0	0.0	8.4
2046.6	45736.1	74.3	3.2	0.9	2.3		0.0	0.0	2.6	5.2	2.6	0.0	0.0	0.0	1.2	0.0	0.0	7.8
2046.7	45738.2	77.3	1.8	1.0	0.6		0.2	0.0	2.4	6.1	2.8	0.0	0.0	0.0	1.0	0.0	0.0	6.9
2046.8	45740.3	77.7	1.0	2.7	0.7		0.0	0.0	2.3	5.0	2.3	0.0	0.0	0.0	0.7	0.0	0.0	7.6
2046.9	45742.4	78.1	2.7	1.8	0.3	0.0	0.0	0.0	2.1	3.6	2.4	0.0	0.0	0.0	0.6	0.0	0.0	8.2
2047.0	45744.5	80.5	1.6	2.8	0.7		0.2	0.0	1.1	4.9	1.9	0.0	0.0	0.0	0.9	0.0	0.0	5.5
2047.1	45746.8	80.5	2.3	1.2	2.0		0.0	0.0	1.2	4.1	1.5	0.0	0.0	0.0	0.9	0.0	0.0	6.4
2047.2	45749.1	81.4	2.1	0.7	1.2		0.0	0.0	0.7	4.0	1.9	0.0	0.0	0.0	1.7	0.0	0.0	6.4
2047.3	45751.4	81.6	1.9	1.2	1.2		0.0	0.0	1.5	4.8	1.9	0.0	0.0	0.0	0.7	0.0	0.0	5.1
2047.4	45753.7	85.2	1.1	0.6	2.0		0.0	0.0	0.8	4.5	0.8	0.0	0.0	0.0	1.1	0.0	0.0	3.9
2047.5	45756.0	76.7	2.1	2.7	0.8		0.0	0.0	0.8	4.5	2.7	0.0	0.0	0.0	2.1	0.0	0.0	7.5

Core MD03-2622 Relative Abundance Data (continued)

Depth (cm)	Age (yBP)	*G.b* (%)	*N.d* (%)	*O.u* (%)	*G.a* (%)	*G.c* (%)	*P.o* (%)	*G.m* (%)	*G.r*(p) (%)	*G.r*(w) (%)	*G.s* (%)	*G.g* (%)	*G.t* (%)	*G.rs* (%)	*N.p*(l) (%)	*N.p*(r) (%)	*G.q* (%)	Other (%)
2047.6	45758.3	80.0	2.5	1.5	1.7		0.0	0.0	2.7	4.0	1.7	0.0	0.0	0.0	0.2	0.0	0.0	5.7
2047.7	45760.6	77.9	2.3	2.1	0.2		0.0	0.0	2.1	5.0	1.8	0.0	0.0	0.0	0.5	0.0	0.0	8.2
2047.8	45762.9	78.4	1.5	1.5	1.5		0.0	0.0	2.3	6.7	1.5	0.0	0.0	0.0	0.8	0.0	0.0	5.7
2047.9	45765.2	80.9	1.9	0.9	1.4	0.0	0.0	0.0	1.4	4.0	1.4	0.0	0.0	0.0	0.7	0.0	0.0	7.4
2048.0	45767.5	80.6	1.6	2.7	0.7		0.0	0.0	1.3	4.9	1.3	0.0	0.0	0.0	1.1	0.0	0.0	5.8
2048.1	45769.5	76.7	3.4	1.0	1.2		0.0	0.0	1.5	5.7	2.0	0.0	0.0	0.0	1.7	0.0	0.0	6.9
2048.2	45771.4	82.0	3.2	1.5	0.7		0.0	0.0	0.7	4.0	1.2	0.0	0.0	0.0	0.2	0.0	0.0	6.4
2048.3	45773.4	81.3	2.7	2.5	0.9		0.0	0.0	0.7	4.3	1.6	0.0	0.0	0.0	0.0	0.0	0.0	5.9
2048.4	45775.3	78.6	1.4	1.4	1.4		0.0	0.0	1.4	5.0	2.3	0.0	0.0	0.0	1.8	0.0	0.0	6.8
2048.5	45777.3	76.5	3.5	2.1	0.8		0.0	0.0	2.1	5.3	1.6	0.0	0.0	0.0	1.9	0.0	0.0	6.1
2048.6	45779.2	84.2	1.5	1.0	0.6		0.0	0.0	1.3	4.4	2.1	0.0	0.0	0.0	1.7	0.0	0.0	3.1
2048.7	45781.2	74.2	3.8	1.8	2.0		0.0	0.0	1.3	5.4	2.0	0.0	0.0	0.0	2.5	0.0	0.0	7.0
2048.8	45783.1	74.9	5.0	1.8	2.9		0.0	0.0	0.7	4.5	1.6	0.0	0.0	0.0	0.7	0.0	0.0	7.9
2048.9	45785.1	78.8	3.7	1.1	1.1	0.0	0.0	0.0	1.7	3.2	1.1	0.0	0.0	0.0	1.3	0.0	0.0	8.0
2049.0	45787.0	78.2	1.7	0.3	0.6		0.0	0.0	1.2	4.7	1.7	0.0	0.0	0.0	2.6	0.0	0.0	9.0
2049.1	45789.3	80.8	1.7	0.6	0.3		0.0	0.0	1.7	7.6	2.6	0.0	0.0	0.0	0.0	0.0	0.0	4.7
2049.2	45791.6	76.8	2.3	1.8	0.7		0.0	0.0	2.3	6.4	2.3	0.0	0.0	0.0	0.9	0.0	0.0	6.4
2049.3	45793.9	80.1	2.5	1.9	1.4		0.0	0.0	1.4	5.3	2.2	0.0	0.0	0.0	0.8	0.0	0.0	4.4
2049.4	45796.2	78.6	2.8	0.6	1.2		0.0	0.3	1.2	4.7	1.6	0.0	0.0	0.0	0.9	0.0	0.0	8.1
2049.5	45798.5	77.3	3.8	1.6	0.6		0.0	0.0	0.6	4.7	1.6	0.0	0.0	0.0	5.0	0.0	0.0	4.7
2049.6	45800.8	69.2	6.1	0.9	0.6		0.0	0.0	3.7	7.9	1.8	0.0	0.3	0.0	2.4	0.0	0.0	7.0
2049.7	45803.1	70.0	3.9	1.8	0.4		0.0	0.0	1.8	8.1	1.8	0.0	0.0	0.0	5.3	0.0	0.0	7.0
2049.8	45805.4	56.4	5.0	2.0	1.7		0.0	0.0	3.6	9.8	2.5	0.0	0.3	0.0	10.1	0.0	0.0	8.7
2049.9	45807.7	61.8	7.9	2.3	2.0	0.0	0.0	0.0	2.7	5.9	1.1	0.0	0.0	0.0	11.3	0.0	0.0	5.0

Appendix III: Core MD03-2622 Absolute Abundance Data

G.b = Globigerina bulloides, *N.d = Neogloboquadrina dutertrei*, *O.u = Orbulina universa*, *G.a = Globigerinella aequilateralis*, *G.c = Globorotalia crassiformis*, *P.o = Pulleniatina obliquiloculata*, *G.m = Globorotalia menardii*, *G.r*(p) = *Globigerinoides ruber* (pink), *G.r*(w) = *Globigerinoides ruber* (white), *G.s = Globigerinoides sacculifer*, *G.g = Globigerinita glutinata*, *G.t = Globorotalia truncatulinoides*, *G.rs = Globigerina rubescens*, *N.p*(l) = *Neogloboquadrina pachyderma* (left-coiling), *N.p*(r) = *Neogloboquadrina pachyderma* (right coiling), *G.q = Globigerina quinqueloba*

Depth (cm)	Age (yBP)	*G.b* #/g	*N.d* #/g	*O.u* #/g	*G.a* #/g	*G.c* #/g	*P.o* #/g	*G.m* #/g	*G.r*(p) #/g	*G.r*(w) #/g	*G.s* #/g	*G.g* #/g	*G.t* #/g	*G.rs* #/g	*N.p*(l) #/g	*N.p*(r) #/g	*G.q* #/g	Other #/g
1900.0	42831.5	122.5	26.1	2.1	6.4	0.7	0.0	0.7	14.8	31.1	11.3	0.7	1.4	0.0	0.0	0.0	0.0	12.0
1900.1	42833.8	395.7	44.4	8.6	7.2	2.9	0.0	0.0	14.3	51.5	10.0	0.0	0.0	1.4	0.0	0.0	27.2	41.5
1900.2	42836.0	270.1	40.1	3.3	11.7	0.0	0.0	0.0	16.7	36.8	10.0	1.7	3.3	1.7	0.0	0.0	28.4	33.4
1900.3	42838.3	174.0	38.0	4.4	11.5	0.9	0.0	2.6	9.7	25.6	7.9	0.0	0.9	0.9	0.0	0.0	10.6	23.0
1900.4	42840.5	153.0	16.3	7.9	3.7	1.1	0.0	0.0	7.9	13.7	5.3	1.6	0.0	1.6	0.0	0.0	11.6	16.8
1900.5	42842.8	132.5	20.9	6.2	3.8	0.5	0.0	0.0	4.7	15.2	3.3	0.5	2.4	0.9	0.0	0.0	27.5	18.0
1900.6	42845.0	41.6	12.2	3.1	1.2	0.4	0.0	1.2	3.5	5.9	1.2	0.8	0.4	0.0	0.0	0.0	9.0	3.9
1900.7	42847.3	127.3	24.0	9.2	1.4	0.7	0.0	2.8	12.0	33.2	2.8	0.7	3.5	0.7	0.0	0.0	26.9	21.9
1900.8	42849.5	78.4	13.1	2.3	0.9	1.4	0.0	1.8	6.3	11.3	2.3	0.9	2.3	0.9	0.0	0.0	11.8	8.2
1900.9	42851.8	83.3	10.8	3.2	0.5	0.0	0.0	0.9	4.5	10.4	2.7	0.5	0.9	1.4	0.0	0.0	18.9	12.2
1901.0	42854.0	158.7	23.6	11.2	3.1	1.2	0.0	1.9	13.0	37.2	5.6	1.9	1.9	1.9	0.0	0.0	36.0	18.6
1901.1	42856.2	123.4	15.4	9.5	3.7	0.0	0.0	0.7	7.3	16.8	2.9	1.5	0.7	0.0	0.0	0.0	28.6	19.8
1901.2	42858.4	110.0	18.8	6.0	2.7	0.0	0.0	0.0	7.0	15.1	4.0	0.7	0.7	0.3	0.0	0.0	11.7	10.1
1901.3	42860.6	75.1	15.2	6.3	3.2	0.0	0.0	0.5	7.4	14.2	6.8	0.0	2.1	0.0	0.0	0.0	5.8	3.7
1901.4	42862.8	197.5	24.2	6.6	2.4	0.0	0.0	0.6	9.1	21.1	6.0	2.4	1.2	0.6	0.0	0.0	17.5	16.9
1901.5	42865.0	151.4	26.2	6.0	6.7	0.0	0.0	0.7	12.7	20.2	3.7	0.7	1.5	0.7	0.0	0.0	12.0	19.5
1901.6	42867.2	166.5	24.5	7.3	4.7	1.6	0.0	0.0	11.4	34.9	5.7	3.6	1.6	0.5	0.0	0.0	18.2	22.9
1901.7	42869.4	199.0	38.5	13.2	11.1	0.0	0.0	1.0	14.2	36.5	12.2	3.0	5.1	0.0	0.0	0.0	23.3	27.3
1901.8	42871.6	215.1	25.1	6.8	6.8	1.0	0.0	1.9	11.6	26.0	4.8	1.0	0.0	1.0	0.0	0.0	24.1	19.3
1901.9	42873.8	46.8	11.5	3.1	4.0	0.9	0.0	0.0	3.5	8.4	2.2	0.0	1.3	0.0	0.0	0.0	3.5	4.4
1902.0	42876.0	173.4	27.8	9.6	5.7	1.0	0.0	0.0	13.4	22.0	9.6	1.9	1.0	1.0	0.0	0.0	23.0	23.9
1902.1	42878.3	202.6	44.8	9.3	7.7	0.0	0.0	0.8	12.4	27.8	7.7	0.8	2.3	0.8	0.0	0.0	17.8	30.2

Core MD03-2622 Absolute Abundance Data (continued)

Depth (cm)	Age (yBP)	*G.b* #/g	*N.d* #/g	*O.u* #/g	*G.a* #/g	*G.c* #/g	*P.o* #/g	*G.m* #/g	*G.r*(p) #/g	*G.r*(w) #/g	*G.s* #/g	*G.g* #/g	*G.t* #/g	*G.rs* #/g	*N.p*(l) #/g	*N.p*(r) #/g	*G.q* #/g	Other #/g
1902.2	42880.6	192.0	26.8	7.4	6.7	0.0	0.0	0.0	11.9	25.3	4.5	1.5	0.0	1.5	0.0	0.0	16.4	29.8
1902.3	42882.9	186.9	31.5	12.6	8.4	1.0	0.0	0.0	7.3	15.7	7.3	1.0	4.2	1.0	0.0	0.0	19.9	17.8
1902.4	42885.2	191.3	24.0	6.6	6.6	0.8	0.0	0.8	11.6	37.3	4.1	0.8	1.7	3.3	0.0	0.0	23.2	31.5
1902.5	42887.5	216.3	32.3	3.5	5.2	0.0	0.0	0.0	14.8	23.5	7.0	0.0	0.0	1.7	0.0	0.0	24.4	23.5
1902.6	42889.8	182.0	24.4	4.7	6.6	0.0	0.0	0.0	7.5	19.7	9.4	0.9	0.9	0.9	0.0	0.0	15.0	41.3
1902.7	42892.1	162.9	29.8	14.1	3.3	0.0	0.0	1.7	16.5	22.3	9.1	0.0	2.5	1.7	0.0	0.0	18.2	30.6
1902.8	42894.4	189.9	37.0	13.0	7.0	2.0	0.0	0.0	11.0	22.0	9.0	1.0	1.0	1.0	0.0	0.0	19.0	20.0
1902.9	42896.7	186.5	33.0	8.7	4.3	0.0	0.0	0.0	7.8	23.4	7.8	0.9	0.9	0.9	0.0	0.0	23.4	26.9
1903.0	42899.0	208.9	30.4	25.5	2.9	0.0	0.0	1.0	13.7	27.5	4.9	2.0	1.0	3.9	0.0	0.0	19.6	54.9
1903.1	42901.1	205.2	43.7	9.9	3.3	0.7	0.0	0.0	11.9	23.8	9.9	1.3	2.0	0.7	0.0	0.0	17.9	35.7
1903.2	42903.1	188.4	49.6	5.9	2.5	0.0	0.0	0.0	14.3	14.3	5.0	0.8	0.0	2.5	0.0	0.0	19.3	31.1
1903.3	42905.2	420.5	90.5	22.0	7.3	0.0	0.0	2.4	26.9	70.9	22.0	7.3	7.3	7.3	0.0	0.0	44.0	90.5
1903.4	42907.2	133.5	23.5	4.6	1.8	0.0	0.0	0.0	11.0	12.9	5.1	1.4	0.0	0.5	0.0	0.0	13.8	27.2
1903.5	42909.3	206.7	58.1	21.8	3.2	2.4	0.0	2.4	17.8	21.8	8.1	0.0	3.2	2.4	0.0	0.0	26.6	43.6
1903.6	42911.3	138.9	21.7	2.9	1.4	0.0	0.0	0.0	11.6	22.4	4.3	0.7	0.0	0.0	0.0	0.0	13.7	24.6
1903.7	42913.4	214.1	43.7	11.7	2.1	2.1	0.0	0.0	9.6	21.3	5.3	2.1	0.0	2.1	0.0	0.0	24.5	41.5
1903.8	42915.4	242.1	42.7	13.4	7.5	0.8	0.0	1.7	16.8	20.9	8.4	1.7	0.8	0.8	0.0	0.0	23.5	40.2
1903.9	42917.5	163.5	26.4	3.8	2.3	0.8	0.0	0.0	9.8	18.8	3.0	1.5	0.0	2.3	0.0	0.0	16.6	22.6
1904.0	42919.5	170.0	31.2	10.4	5.2	0.9	0.0	0.9	13.9	13.9	9.5	0.0	0.9	0.9	0.0	0.0	11.3	53.8
1904.1	42921.6	184.6	46.7	8.9	5.9	0.0	0.0	1.5	9.6	11.1	5.9	0.7	0.7	2.2	0.0	0.0	15.6	50.4
1904.2	42923.6	193.1	40.6	9.9	3.6	0.0	0.0	0.0	16.2	15.3	4.5	0.9	0.0	3.6	0.0	0.0	19.9	77.6
1904.3	42925.7	279.6	63.4	3.1	2.1	2.1	0.0	0.0	16.6	22.9	5.2	1.0	1.0	1.0	0.0	0.0	15.6	73.8
1904.4	42927.7	162.0	28.7	7.6	2.4	0.0	0.0	0.0	7.2	13.4	4.3	0.5	0.5	1.9	0.0	0.0	12.9	55.0
1904.5	42929.8	265.7	36.7	8.1	4.5	0.9	0.0	0.0	14.3	23.3	9.8	2.7	0.9	3.6	0.0	0.0	18.8	82.3
1904.6	42931.8	228.7	47.6	6.5	4.7	0.9	0.0	0.0	16.8	24.3	9.3	0.0	0.0	1.9	0.0	0.0	15.9	58.8
1904.7	42933.9	605.9	91.6	10.2	10.2	1.7	0.0	1.7	37.3	30.5	15.3	5.1	3.4	3.4	0.0	0.0	50.9	110.3
1904.8	42935.9	314.0	69.7	15.5	3.3	1.1	0.0	2.2	23.2	26.5	6.6	2.2	0.0	1.1	0.0	0.0	35.4	63.0
1904.9	42938.0	257.8	53.6	3.8	11.5	1.3	0.0	0.0	12.8	21.7	3.8	0.0	0.0	1.3	0.0	0.0	31.9	66.4

Core MD03-2622 Absolute Abundance Data (continued)

Depth (cm)	Age (yBP)	*G.b* #/g	*N.d* #/g	*O.u* #/g	*G.a* #/g	*G.c* #/g	*P.o* #/g	*G.m* #/g	*G.r*(p) #/g	*G.r*(w) #/g	*G.s* #/g	*G.g* #/g	*G.t* #/g	*G.rs* #/g	*N.p*(l) #/g	*N.p*(r) #/g	*G.q* #/g	Other #/g
1905.0	42940.0	135.9	28.6	1.4	2.9	1.4	0.0	0.7	15.7	15.0	3.6	0.7	0.0	0.0	0.0	0.0	8.6	18.6
1905.1	42942.2	317.0	72.6	15.8	9.5	3.2	0.0	0.0	30.0	34.7	3.2	3.2	1.6	3.2	0.0	0.0	23.7	71.0
1905.2	42944.3	117.3	14.9	3.5	2.2	0.4	0.0	0.4	8.3	11.4	1.8	0.9	0.4	0.4	0.0	0.0	4.8	19.3
1905.3	42946.5	248.3	33.5	7.4	1.2	0.0	0.0	0.0	11.2	8.7	3.7	2.5	0.0	1.2	0.0	0.0	8.7	48.4
1905.4	42948.6	255.3	48.8	3.3	5.7	0.8	0.0	0.0	20.3	22.8	7.3	1.6	0.8	2.4	0.0	0.0	14.6	49.6
1905.5	42950.8	246.4	46.8	4.9	6.6	0.0	0.0	0.0	23.8	18.1	6.6	1.6	1.6	1.6	0.0	0.0	12.3	52.6
1905.6	42952.9	283.6	50.8	10.5	4.8	0.8	0.0	0.8	16.1	27.4	5.6	3.2	1.6	1.6	0.0	0.0	8.1	35.5
1905.7	42955.1	621.8	111.6	14.0	4.0	4.0	0.0	0.0	27.9	43.8	12.0	4.0	0.0	2.0	0.0	0.0	27.9	85.7
1905.8	42957.2	140.0	26.8	3.4	3.4	0.5	0.0	0.5	16.6	6.3	3.4	1.0	0.0	1.0	0.0	0.0	3.4	19.0
1905.9	42959.4	375.8	100.1	5.7	7.6	1.9	0.0	0.0	47.2	37.8	11.3	1.9	1.9	1.9	0.0	0.0	24.6	35.9
1906.0	42961.5	280.9	62.9	4.0	6.7	0.0	0.0	0.0	37.5	14.7	4.0	1.3	0.0	0.0	0.0	0.0	13.4	62.9
1906.1	42963.6	176.8	38.3	5.6	2.3	1.1	0.0	0.0	14.6	15.8	6.8	0.6	0.0	0.6	0.0	0.0	7.9	32.1
1906.2	42965.7	216.5	62.2	5.8	3.3	0.0	0.0	0.0	23.2	15.8	3.3	1.7	2.5	2.5	0.0	0.0	9.1	63.0
1906.3	42967.8	348.7	64.2	3.5	3.5	1.7	0.0	0.0	17.3	31.2	3.5	1.7	1.7	5.2	0.0	0.0	17.3	86.7
1906.4	42969.9	104.0	23.2	5.1	3.3	0.4	0.0	0.0	11.0	7.4	3.7	1.1	1.1	1.1	0.0	0.0	6.6	25.7
1906.5	42972.0	299.3	41.7	7.9	4.7	0.0	0.0	0.0	17.3	28.4	6.3	0.8	2.4	3.2	0.0	0.0	11.8	62.2
1906.6	42974.1	195.1	43.6	4.4	6.2	0.6	0.0	0.0	15.6	13.7	5.0	2.5	0.6	1.9	0.0	0.0	8.1	53.0
1906.7	42976.2	217.3	31.0	5.8	5.1	0.7	0.0	1.4	18.1	12.3	4.3	2.2	0.7	0.7	0.0	0.0	11.6	41.2
1906.8	42978.3	178.2	39.3	9.4	0.8	0.8	0.0	0.8	18.1	7.1	5.5	0.8	0.0	0.8	0.0	0.0	7.9	27.5
1906.9	42980.4	159.6	30.1	3.8	0.6	0.0	0.0	0.0	16.0	10.3	3.8	0.6	0.6	0.6	0.0	0.0	5.1	27.6
1907.0	42982.5	144.8	37.6	3.9	3.9	0.8	0.0	0.0	11.0	14.1	2.3	0.8	0.8	1.6	0.0	0.0	9.4	30.5
1907.1	42984.9	113.7	22.2	2.6	2.1	0.0	0.0	0.0	13.7	11.6	4.8	0.5	0.0	0.5	0.0	0.0	4.8	20.6
1907.2	42987.2	135.0	30.5	2.7	2.7	0.5	0.0	0.5	10.2	8.6	5.4	0.5	0.5	1.1	0.0	0.0	3.2	26.3
1907.3	42989.6	84.5	20.2	2.7	1.6	0.0	0.0	0.5	10.9	8.7	6.0	0.0	0.0	1.1	0.0	0.0	4.9	27.3
1907.4	42991.9	76.6	27.5	1.8	1.5	0.3	0.0	0.0	8.3	5.0	2.4	0.3	0.0	0.3	0.0	0.0	1.2	14.8
1907.5	42994.3	103.6	32.7	4.2	3.6	0.0	0.0	0.0	13.9	7.3	1.8	0.6	0.0	0.6	0.0	0.0	2.4	17.6
1907.6	42996.6	177.0	37.4	5.3	1.1	1.1	0.0	1.1	13.9	17.6	5.9	0.0	0.0	1.1	0.0	0.0	1.1	54.5
1907.7	42999.0	226.5	75.2	5.4	3.6	0.0	0.0	0.0	15.4	21.7	2.7	0.9	0.0	0.9	0.0	0.0	2.7	54.4

Core MD03-2622 Absolute Abundance Data (continued)

Depth (cm)	Age (yBP)	*G.b* #/g	*N.d* #/g	*O.u* #/g	*G.a* #/g	*G.c* #/g	*P.o* #/g	*G.m* #/g	*G.r*(p) #/g	*G.r*(w) #/g	*G.s* #/g	*G.g* #/g	*G.t* #/g	*G.rs* #/g	*N.p*(l) #/g	*N.p*(r) #/g	*G.q* #/g	Other #/g
1907.8	43001.3	225.3	51.3	7.7	4.8	1.0	0.0	0.0	30.9	13.5	2.9	1.0	0.0	2.9	0.0	0.0	11.6	36.8
1907.9	43003.7	119.9	32.2	1.9	1.9	0.0	0.0	0.0	11.4	10.1	1.9	0.0	0.0	0.6	0.0	0.0	5.1	32.8
1908.0	43006.0	231.4	57.6	10.5	7.9	0.9	0.0	0.9	19.2	11.4	3.5	1.7	0.0	2.6	0.0	0.0	13.1	67.2
1908.1	43008.3	332.0	58.9	11.8	7.5	1.1	0.0	0.0	30.0	19.3	4.3	2.1	0.0	3.2	0.0	0.0	10.7	77.1
1908.2	43010.5	167.6	37.0	2.0	3.0	0.5	0.0	0.5	18.2	10.8	7.4	1.0	0.5	1.5	0.0	0.0	8.9	39.9
1908.3	43012.8	160.1	35.4	4.3	1.2	0.0	0.0	1.2	15.5	8.7	1.9	0.6	0.0	1.2	0.0	0.0	6.8	31.0
1908.4	43015.0	209.9	32.6	7.8	1.6	0.8	0.0	0.0	24.9	12.4	2.3	0.8	0.0	0.8	0.0	0.0	11.7	67.6
1908.5	43017.3	248.3	53.9	9.5	3.2	2.1	0.0	2.1	28.5	12.7	3.2	2.1	0.0	3.2	0.0	0.0	14.8	86.6
1908.6	43019.5	178.0	33.9	3.8	6.0	0.0	0.0	0.0	22.6	15.1	1.5	0.0	0.0	5.3	0.0	0.0	15.1	91.3
1908.7	43021.8	299.3	64.0	6.4	4.8	1.6	0.0	0.0	36.8	20.8	3.2	1.6	1.6	6.4	0.0	0.0	12.8	83.2
1908.8	43024.0	107.5	23.9	0.0	2.0	0.4	0.0	0.8	19.2	8.6	2.0	0.8	0.4	0.8	0.0	0.0	5.9	38.7
1908.9	43026.3	359.8	69.6	7.3	4.4	1.5	0.0	1.5	40.6	24.7	4.4	2.9	0.0	4.4	0.0	0.0	27.6	140.7
1909.0	43028.5	266.4	40.9	5.8	4.4	0.0	0.0	1.5	32.1	20.4	7.3	4.4	0.0	0.0	0.0	0.0	26.3	113.9
1909.1	43030.9	351.4	50.0	6.6	2.6	0.0	0.0	0.0	56.6	26.3	2.6	1.3	0.0	2.6	0.0	0.0	34.2	164.5
1909.2	43033.2	231.7	31.9	1.3	6.6	0.0	0.0	0.0	45.2	22.6	1.3	1.3	0.0	2.7	0.0	0.0	18.6	144.8
1909.3	43035.6	415.1	40.8	8.9	3.5	0.0	0.0	0.0	65.6	46.1	7.1	3.5	0.0	1.8	0.0	0.0	37.3	175.6
1909.4	43037.9	409.9	43.5	10.4	5.2	0.0	0.0	0.0	62.7	20.9	8.7	3.5	1.7	0.0	0.0	0.0	33.1	181.0
1909.5	43040.3	448.5	53.2	11.6	11.6	1.7	0.0	1.7	69.8	33.2	3.3	3.3	0.0	5.0	0.0	0.0	36.5	187.7
1909.6	43042.6	419.7	45.0	6.2	1.6	3.1	0.0	0.0	65.2	34.1	4.7	3.1	1.6	1.6	0.0	0.0	31.0	184.6
1909.7	43045.0	523.7	56.9	13.3	5.7	0.0	0.0	0.0	104.4	39.8	3.8	1.9	0.0	1.9	0.0	0.0	36.1	174.6
1909.8	43047.3	433.5	75.5	10.3	6.9	0.0	0.0	0.0	56.7	46.4	5.2	3.4	0.0	1.7	0.0	0.0	44.6	190.6
1909.9	43049.7	465.5	40.4	21.3	2.1	0.0	0.0	2.1	34.0	40.4	2.1	2.1	0.0	0.0	0.0	0.0	38.3	148.8
1910.0	43052.0	270.0	39.6	17.8	5.9	1.0	1.0	0.0	41.5	21.8	4.9	3.0	0.0	4.0	0.0	0.0	21.8	101.9
1910.1	43054.0	527.9	77.9	14.4	8.7	0.0	0.0	0.0	95.2	37.5	8.7	2.9	0.0	5.8	0.0	0.0	46.2	199.1
1910.2	43056.0	410.5	65.6	17.9	6.0	0.0	0.0	2.0	91.5	31.8	8.0	2.0	2.0	2.0	0.0	0.0	31.8	165.0
1910.3	43058.0	442.6	79.4	19.2	4.8	0.0	2.4	0.0	43.3	33.7	2.4	4.8	0.0	0.0	0.0	0.0	36.1	156.3
1910.4	43060.0	453.6	55.6	17.9	4.0	0.0	0.0	0.0	67.5	55.6	6.0	2.0	0.0	2.0	0.0	0.0	31.8	158.8
1910.5	43062.0	484.7	55.2	11.7	5.0	1.7	0.0	0.0	63.5	23.4	8.4	0.0	1.7	1.7	0.0	0.0	30.1	178.9

Core MD03-2622 Absolute Abundance Data (continued)

Depth (cm)	Age (yBP)	*G.b* #/g	*N.d* #/g	*O.u* #/g	*G.a* #/g	*G.c* #/g	*P.o* #/g	*G.m* #/g	*G.r*(p) #/g	*G.r*(w) #/g	*G.s* #/g	*G.g* #/g	*G.t* #/g	*G.rs* #/g	*N.p*(l) #/g	*N.p*(r) #/g	*G.q* #/g	Other #/g
1910.6	43064.0	423.7	44.5	18.2	6.1	0.0	0.0	2.0	70.8	28.3	8.1	2.0	2.0	6.1	0.0	0.0	34.4	216.4
1910.7	43066.0	481.4	66.2	14.0	6.0	0.0	0.0	0.0	54.2	32.1	6.0	0.0	0.0	4.0	0.0	0.0	28.1	196.6
1910.8	43068.0	471.5	64.5	8.7	3.5	1.7	0.0	0.0	41.8	36.6	12.2	3.5	5.2	7.0	0.0	0.0	22.7	139.4
1910.9	43070.0	392.4	55.1	12.0	10.3	0.0	0.0	0.0	37.9	39.6	6.9	1.7	1.7	3.4	0.0	0.0	22.4	111.9
1911.0	43072.0	361.9	56.4	9.1	13.7	1.5	0.0	1.5	38.1	33.5	1.5	3.0	0.0	1.5	0.0	0.0	24.4	131.0
1911.1	43073.7	330.7	53.2	11.5	14.4	0.0	0.0	1.4	21.6	20.1	8.6	7.2	2.9	2.9	0.0	0.0	10.1	130.8
1911.2	43075.4	294.4	39.5	11.2	4.3	2.6	0.0	0.0	18.0	19.7	6.9	1.7	2.6	4.3	0.0	0.0	12.0	88.4
1911.3	43077.1	401.0	34.1	14.0	8.0	0.0	0.0	0.0	16.0	24.1	2.0	2.0	0.0	4.0	0.0	0.0	18.0	162.4
1911.4	43078.8	390.1	60.3	12.4	15.4	1.5	0.0	0.0	15.4	15.4	10.8	1.5	0.0	1.5	0.0	0.0	17.0	142.1
1911.5	43080.5	410.0	55.2	14.9	10.6	2.1	0.0	0.0	23.4	12.7	10.6	4.2	0.0	0.0	0.0	0.0	29.7	148.7
1911.6	43082.2	454.6	80.4	6.7	8.4	0.0	0.0	0.0	8.4	20.1	6.7	1.7	3.3	1.7	0.0	0.0	20.1	133.9
1911.7	43083.9	635.3	91.0	2.0	14.2	2.0	0.0	0.0	10.1	32.4	12.1	4.0	2.0	8.1	0.0	0.0	36.4	216.5
1911.8	43085.6	430.8	76.9	19.2	14.0	1.7	0.0	0.0	12.2	17.5	12.2	3.5	0.0	7.0	0.0	0.0	19.2	166.0
1911.9	43087.3	415.7	55.0	6.1	12.2	2.0	0.0	2.0	18.3	34.6	6.1	4.1	0.0	6.1	0.0	0.0	18.3	128.4
1912.0	43089.0	398.0	48.5	9.3	9.3	5.6	0.0	0.0	7.5	31.7	7.5	5.6	0.0	5.6	0.0	0.0	22.4	165.9
1912.1	43090.8	460.0	60.5	8.6	3.5	1.7	0.0	0.0	19.0	27.7	3.5	3.5	0.0	1.7	0.0	0.0	19.0	185.0
1912.2	43092.6	406.8	72.5	8.6	10.4	3.5	0.0	0.0	6.9	27.6	12.1	3.5	3.5	8.6	0.0	0.0	31.1	212.5
1912.3	43094.4	473.3	63.1	20.4	16.7	1.9	0.0	0.0	5.6	29.7	3.7	3.7	3.7	7.4	0.0	0.0	27.8	213.5
1912.4	43096.2	416.1	63.8	8.6	11.0	0.0	0.0	0.0	8.6	28.2	3.7	7.4	2.5	4.9	0.0	0.0	16.0	159.6
1912.5	43098.0	411.1	87.1	11.4	9.5	0.0	0.0	0.0	5.7	26.5	5.7	3.8	5.7	5.7	0.0	0.0	22.7	162.9
1912.6	43099.8	259.7	51.8	12.2	5.3	4.6	0.0	0.8	6.9	14.5	3.8	7.6	0.0	9.1	0.0	0.0	12.2	67.0
1912.7	43101.6	318.3	54.0	6.9	5.5	1.4	1.4	0.0	5.5	24.9	6.9	5.5	0.0	9.7	0.0	0.0	9.7	87.2
1912.8	43103.4	311.4	46.7	5.0	5.0	1.7	0.0	0.0	5.0	25.0	3.3	16.7	0.0	11.7	0.0	0.0	8.3	100.2
1912.9	43105.2	429.2	82.6	10.8	10.8	1.8	0.0	0.0	3.6	19.8	5.4	5.4	1.8	3.6	0.0	0.0	14.4	147.3
1913.0	43107.0	408.7	71.8	10.5	14.0	0.0	0.0	0.0	7.0	14.0	5.3	7.0	1.8	1.8	0.0	0.0	21.0	154.0
1913.1	43109.0	405.9	83.7	14.2	7.9	3.2	0.0	0.0	3.2	30.0	7.9	4.7	0.0	9.5	0.0	0.0	17.4	173.7
1913.2	43111.0	433.1	76.7	23.3	6.7	0.0	0.0	0.0	5.0	18.3	5.0	6.7	0.0	6.7	0.0	0.0	25.0	163.4
1913.3	43113.0	494.9	85.6	10.4	8.4	0.0	0.0	0.0	2.1	14.6	8.4	2.1	0.0	6.3	0.0	0.0	12.5	187.9

Core MD03-2622 Absolute Abundance Data (continued)

Depth (cm)	Age (yBP)	*G.b* #/g	*N.d* #/g	*O.u* #/g	*G.a* #/g	*G.c* #/g	*P.o* #/g	*G.m* #/g	*G.r*(p) #/g	*G.r*(w) #/g	*G.s* #/g	*G.g* #/g	*G.t* #/g	*G.rs* #/g	*N.p*(l) #/g	*N.p*(r) #/g	*G.q* #/g	Other #/g
1913.4	43115.0	457.2	68.1	2.3	15.9	0.0	0.0	4.5	2.3	22.7	6.8	4.5	2.3	2.3	0.0	0.0	18.2	140.7
1913.5	43117.0	508.1	81.2	13.8	12.4	1.4	0.0	1.4	6.9	13.8	4.1	6.9	0.0	9.6	0.0	0.0	19.3	183.1
1913.6	43119.0	496.6	99.9	18.0	12.0	2.0	0.0	0.0	8.0	16.0	6.0	12.0	0.0	10.0	0.0	0.0	24.0	269.8
1913.7	43121.0	497.8	71.1	26.0	13.9	0.0	0.0	0.0	1.7	19.1	0.0	10.4	0.0	10.4	0.0	0.0	17.3	223.7
1913.8	43123.0	533.4	86.5	13.5	30.8	1.9	0.0	1.9	15.4	38.4	3.8	9.6	0.0	7.7	0.0	0.0	30.8	211.4
1913.9	43125.0	481.4	76.9	16.2	10.1	0.0	0.0	0.0	10.1	24.3	4.0	6.1	0.0	8.1	0.0	0.0	32.4	254.9
1914.0	43127.0	505.2	110.0	16.5	9.2	3.7	0.0	0.0	11.0	12.8	9.2	5.5	0.0	3.7	0.0	0.0	22.0	146.7
1914.1	43129.4	642.2	75.9	10.6	10.6	1.8	0.0	0.0	1.8	8.8	3.5	1.8	0.0	0.0	0.0	0.0	28.2	291.1
1914.2	43131.7	646.3	136.6	17.1	6.8	0.0	0.0	3.4	3.4	10.2	3.4	6.8	3.4	6.8	0.0	0.0	51.2	344.9
1914.3	43134.1	558.4	77.3	4.3	2.1	2.1	0.0	0.0	2.1	6.4	0.0	2.1	0.0	6.4	0.0	0.0	30.1	240.5
1914.4	43136.4	508.2	98.2	16.0	4.0	4.0	0.0	0.0	0.0	12.0	4.0	6.0	0.0	10.0	0.0	0.0	20.0	348.9
1914.5	43138.8	591.9	105.6	16.7	11.1	0.0	0.0	0.0	0.0	19.5	2.8	2.8	0.0	19.5	0.0	0.0	41.7	291.8
1914.6	43141.1	504.9	72.7	10.1	10.1	1.7	0.0	1.7	3.4	15.2	3.4	5.1	0.0	1.7	0.0	0.0	28.8	274.0
1914.7	43143.5	528.8	60.7	5.8	5.8	4.3	0.0	1.4	4.3	11.6	5.8	2.9	0.0	7.2	0.0	0.0	14.4	216.7
1914.8	43145.8	614.9	89.1	9.5	6.4	3.2	0.0	0.0	3.2	9.5	6.4	3.2	0.0	6.4	0.0	0.0	22.3	315.0
1914.9	43148.2	609.1	83.7	9.7	7.8	1.9	0.0	0.0	0.0	7.8	5.8	3.9	0.0	1.9	0.0	0.0	27.2	303.6
1915.0	43150.5	675.3	117.6	14.0	5.6	0.0	0.0	0.0	0.0	14.0	14.0	0.0	0.0	5.6	0.0	0.0	42.0	389.1
1915.1	43152.7	774.3	110.6	12.3	6.1	3.1	0.0	0.0	3.1	21.5	6.1	6.1	0.0	9.2	0.0	0.0	43.0	334.9
1915.2	43154.9	611.7	75.6	15.9	11.9	8.0	0.0	0.0	6.0	6.0	6.0	6.0	0.0	4.0	0.0	0.0	23.9	310.3
1915.3	43157.1	612.2	82.7	10.3	6.2	0.0	0.0	0.0	6.2	8.3	0.0	6.2	0.0	2.1	0.0	0.0	31.0	289.5
1915.4	43159.3	516.5	68.6	3.3	8.4	1.7	0.0	0.0	5.0	3.3	6.7	1.7	0.0	3.3	0.0	0.0	21.8	209.3
1915.5	43161.5	215.6	35.9	0.0	0.0	0.9	0.0	0.9	1.7	1.7	2.6	0.0	0.0	0.0	0.0	0.0	10.3	97.5
1915.6	43163.7	335.6	59.9	4.6	4.6	3.1	0.0	0.0	9.2	12.3	4.6	1.5	0.0	0.0	0.0	0.0	13.8	142.8
1915.7	43165.9	456.2	66.1	3.4	1.7	0.0	0.0	0.0	11.9	22.0	3.4	0.0	0.0	0.0	0.0	0.0	6.8	186.6
1915.8	43168.1	634.9	108.9	9.7	1.9	1.9	0.0	1.9	7.8	9.7	1.9	7.8	0.0	3.9	0.0	0.0	19.4	297.5
1915.9	43170.3	513.3	82.6	3.5	10.5	3.5	0.0	0.0	10.5	7.0	3.5	3.5	0.0	3.5	0.0	0.0	8.8	170.5
1916.0	43172.5	565.0	102.6	2.9	8.6	0.0	0.0	0.0	28.5	14.3	2.9	5.7	0.0	2.9	0.0	0.0	20.0	307.8
1916.1	43174.6	400.5	70.3	2.8	4.2	1.4	0.0	1.4	19.7	15.5	1.4	4.2	0.0	4.2	0.0	0.0	11.2	203.8

Core MD03-2622 Absolute Abundance Data (continued)

Depth (cm)	Age (yBP)	*G.b* #/g	*N.d* #/g	*O.u* #/g	*G.a* #/g	*G.c* #/g	*P.o* #/g	*G.m* #/g	*G.r*(p) #/g	*G.r*(w) #/g	*G.s* #/g	*G.g* #/g	*G.t* #/g	*G.rs* #/g	*N.p*(l) #/g	*N.p*(r) #/g	*G.q* #/g	Other #/g
1916.2	43176.6	659.6	239.9	10.7	14.3	0.0	0.0	0.0	21.5	28.6	10.7	7.2	0.0	3.6	0.0	0.0	25.1	458.2
1916.3	43178.7	592.1	161.2	3.5	10.5	0.0	0.0	0.0	35.0	35.0	3.5	7.0	0.0	7.0	0.0	0.0	21.0	311.8
1916.4	43180.7	466.6	72.9	10.7	16.0	3.6	0.0	0.0	26.7	17.8	8.9	1.8	1.8	1.8	0.0	0.0	7.1	241.7
1916.5	43182.8	594.1	143.5	6.0	15.9	8.0	0.0	0.0	17.9	29.9	6.0	4.0	0.0	10.0	0.0	0.0	15.9	374.8
1916.6	43184.8	513.2	135.2	12.6	9.4	3.1	0.0	0.0	9.4	18.9	9.4	0.0	0.0	3.1	0.0	0.0	22.0	242.1
1916.7	43186.9	477.7	89.4	8.1	13.0	0.0	1.6	0.0	21.1	34.1	3.2	1.6	0.0	0.0	0.0	0.0	8.1	201.5
1916.8	43188.9	427.0	91.4	1.9	15.6	0.0	0.0	1.9	33.1	27.2	9.7	11.7	1.9	1.9	0.0	0.0	3.9	173.1
1916.9	43191.0	463.1	119.1	7.7	9.6	0.0	0.0	1.9	26.9	32.7	5.8	7.7	0.0	0.0	0.0	0.0	5.8	221.0
1917.0	43193.0	510.9	115.5	0.0	19.2	0.0	0.0	0.0	22.5	38.5	12.8	3.2	0.0	6.4	0.0	0.0	3.2	368.9
1917.1	43194.7	477.4	101.1	5.0	9.9	0.0	0.0	0.0	13.3	23.2	6.6	6.6	1.7	1.7	0.0	0.0	3.3	247.0
1917.2	43196.4	417.5	77.3	6.7	15.1	0.0	0.0	1.7	11.8	20.2	10.1	5.0	0.0	5.0	0.0	0.0	10.1	210.0
1917.3	43198.1	541.0	87.0	1.9	19.3	1.9	0.0	0.0	9.7	27.1	1.9	5.8	0.0	9.7	0.0	0.0	5.8	235.7
1917.4	43199.8	402.1	119.4	3.7	18.7	1.9	0.0	0.0	11.2	20.5	7.5	5.6	1.9	1.9	0.0	0.0	11.2	261.2
1917.5	43201.5	522.4	111.6	9.3	9.3	1.6	1.6	0.0	4.7	34.1	4.7	4.7	3.1	0.0	0.0	0.0	7.8	288.3
1917.6	43203.2	400.4	73.5	3.8	15.1	1.9	0.0	0.0	11.3	37.7	9.4	3.8	0.0	1.9	0.0	0.0	3.8	162.0
1917.7	43204.9	676.5	113.9	10.0	13.4	3.3	0.0	0.0	23.4	36.8	6.7	3.3	3.3	3.3	0.0	0.0	6.7	267.9
1917.8	43206.6	626.7	122.5	6.6	6.6	3.3	0.0	3.3	3.3	16.6	9.9	3.3	0.0	0.0	0.0	0.0	6.6	261.6
1917.9	43208.3	328.7	57.1	0.0	6.9	1.7	0.0	0.0	6.9	29.4	3.5	1.7	1.7	0.0	0.0	0.0	5.2	122.8
1918.0	43210.0	460.1	106.2	10.0	14.0	0.0	0.0	2.0	18.0	20.0	4.0	2.0	4.0	10.0	0.0	0.0	24.1	260.6
1918.1	43211.8	353.7	65.9	1.7	12.1	0.0	0.0	0.0	8.7	20.8	1.7	1.7	3.5	1.7	0.0	0.0	17.3	192.5
1918.2	43213.6	292.8	58.7	5.3	12.5	0.0	0.0	0.0	10.7	23.1	1.8	1.8	0.0	3.6	0.0	0.0	14.2	178.0
1918.3	43215.4	163.8	37.4	3.7	2.8	0.0	0.0	0.0	6.6	8.4	3.7	0.9	0.0	0.0	0.0	0.0	5.6	97.3
1918.4	43217.2	91.4	20.3	4.1	2.4	0.8	0.0	0.0	5.7	4.1	2.0	0.8	0.0	1.2	0.0	0.0	3.7	37.8
1918.5	43219.0	146.4	27.7	1.6	5.5	0.8	0.0	0.0	1.6	10.3	3.2	0.0	0.0	1.6	0.0	0.0	1.6	60.9
1918.6	43220.8	419.1	82.4	11.3	12.9	3.2	0.0	0.0	4.8	32.3	11.3	6.5	3.2	1.6	0.0	0.0	9.7	132.4
1918.7	43222.6	418.8	112.6	0.0	19.4	1.8	0.0	0.0	8.8	33.4	3.5	0.0	0.0	0.0	0.0	0.0	8.8	158.4
1918.8	43224.4	475.5	103.6	6.9	9.2	9.2	0.0	0.0	11.5	27.6	4.6	4.6	0.0	0.0	0.0	0.0	9.2	165.8
1918.9	43226.2	406.6	77.4	7.0	10.6	7.0	0.0	0.0	7.0	28.2	5.3	0.0	0.0	0.0	0.0	0.0	8.8	142.6

Core MD03-2622 Absolute Abundance Data (continued)

Depth (cm)	Age (yBP)	*G.b* #/g	*N.d* #/g	*O.u* #/g	*G.a* #/g	*G.c* #/g	*P.o* #/g	*G.m* #/g	*G.r*(p) #/g	*G.r*(w) #/g	*G.s* #/g	*G.g* #/g	*G.t* #/g	*G.rs* #/g	*N.p*(l) #/g	*N.p*(r) #/g	*G.q* #/g	Other #/g
1919.0	43228.0	657.9	97.5	3.9	25.3	7.8	0.0	0.0	7.8	29.2	7.8	1.9	1.9	3.9	0.0	0.0	11.7	191.0
1919.1	43230.1	520.3	76.2	3.7	9.3	1.9	0.0	0.0	9.3	22.3	7.4	3.7	0.0	3.7	0.0	0.0	9.3	221.1
1919.2	43232.2	484.5	84.9	0.0	8.7	0.0	0.0	0.0	10.4	13.9	1.7	3.5	3.5	1.7	0.0	0.0	19.1	171.6
1919.3	43234.3	666.5	104.8	3.7	15.0	7.5	0.0	0.0	7.5	18.7	11.2	0.0	0.0	0.0	0.0	0.0	11.2	280.8
1919.4	43236.4	640.6	133.9	2.0	18.0	2.0	0.0	0.0	18.0	26.0	4.0	2.0	0.0	4.0	0.0	0.0	10.0	217.9
1919.5	43238.5	611.6	161.3	7.5	11.3	7.5	0.0	0.0	15.0	26.3	3.8	3.8	0.0	0.0	0.0	0.0	15.0	349.0
1919.6	43240.6	529.9	140.9	6.7	13.4	1.7	0.0	1.7	6.7	26.8	5.0	6.7	0.0	1.7	0.0	0.0	21.8	221.3
1919.7	43242.7	657.4	223.1	8.0	15.9	4.0	0.0	0.0	8.0	31.9	8.0	8.0	4.0	0.0	0.0	0.0	19.9	298.8
1919.8	43244.8	576.2	187.8	1.8	12.8	1.8	0.0	0.0	7.3	36.5	0.0	5.5	0.0	1.8	0.0	0.0	21.9	218.8
1919.9	43246.9	495.0	147.1	5.2	8.7	5.2	0.0	0.0	6.9	15.6	3.5	3.5	3.5	0.0	0.0	0.0	15.6	212.9
1920.0	43249.0	416.1	137.2	4.6	6.2	4.6	0.0	1.5	12.3	18.5	6.2	1.5	0.0	3.1	0.0	0.0	26.2	164.9
1920.1	43251.0	454.7	145.1	5.3	10.6	0.0	0.0	0.0	8.8	37.2	8.8	1.8	7.1	3.5	0.0	0.0	17.7	171.6
1920.2	43252.9	508.9	181.4	16.7	14.6	16.7	0.0	0.0	10.4	20.9	8.3	8.3	2.1	2.1	0.0	0.0	22.9	202.3
1920.3	43254.9	421.9	130.1	2.2	6.7	13.5	0.0	4.5	6.7	22.4	6.7	2.2	2.2	2.2	0.0	0.0	15.7	179.5
1920.4	43256.8	440.4	150.6	1.9	11.4	17.2	0.0	0.0	0.0	21.0	1.9	5.7	1.9	3.8	0.0	0.0	9.5	169.7
1920.5	43258.8	495.6	101.4	4.9	9.8	1.6	1.6	0.0	1.6	16.4	9.8	1.6	1.6	3.3	0.0	0.0	19.6	196.3
1920.6	43260.7	567.7	199.1	0.0	15.8	5.9	0.0	0.0	13.8	23.7	9.9	9.9	0.0	3.9	0.0	0.0	13.8	222.7
1920.7	43262.7	636.8	141.9	3.5	13.8	3.5	0.0	0.0	10.4	31.1	6.9	6.9	3.5	3.5	0.0	0.0	17.3	207.6
1920.8	43264.6	640.0	200.5	11.6	15.4	0.0	0.0	0.0	11.6	34.7	7.7	3.9	0.0	0.0	0.0	0.0	11.6	316.1
1920.9	43266.6	548.5	146.9	6.5	22.9	3.3	0.0	0.0	6.5	52.2	9.8	3.3	3.3	0.0	0.0	0.0	13.1	231.8
1921.0	43268.5	497.3	167.4	6.6	14.9	3.3	0.0	0.0	23.2	34.8	16.6	5.0	1.7	3.3	0.0	0.0	13.3	189.0
1921.1	43270.8	622.4	140.9	0.0	13.1	3.3	0.0	0.0	3.3	55.7	6.6	0.0	0.0	0.0	0.0	0.0	9.8	232.6
1921.2	43273.0	637.0	232.6	10.1	16.9	3.4	0.0	3.4	16.9	37.1	0.0	10.1	0.0	0.0	0.0	0.0	10.1	279.7
1921.3	43275.3	860.0	325.1	4.1	28.8	0.0	0.0	0.0	12.3	37.0	0.0	4.1	0.0	4.1	0.0	0.0	8.2	345.7
1921.4	43277.5	710.9	229.9	10.6	17.7	0.0	0.0	0.0	10.6	53.1	14.1	3.5	0.0	0.0	0.0	0.0	14.1	332.5
1921.5	43279.8	891.2	267.3	0.0	19.8	6.6	0.0	0.0	16.5	33.0	6.6	3.3	0.0	6.6	0.0	0.0	16.5	326.8
1921.6	43282.0	764.6	334.3	21.3	35.6	3.6	0.0	0.0	14.2	39.1	10.7	10.7	0.0	7.1	0.0	0.0	7.1	380.5
1921.7	43284.3	811.2	252.5	0.0	23.0	0.0	0.0	7.7	23.0	61.2	19.1	3.8	0.0	3.8	0.0	0.0	15.3	336.7

Core MD03-2622 Absolute Abundance Data (continued)

Depth (cm)	Age (yBP)	*G.b* #/g	*N.d* #/g	*O.u* #/g	*G.a* #/g	*G.c* #/g	*P.o* #/g	*G.m* #/g	*G.r*(p) #/g	*G.r*(w) #/g	*G.s* #/g	*G.g* #/g	*G.t* #/g	*G.rs* #/g	*N.p*(l) #/g	*N.p*(r) #/g	*G.q* #/g	Other #/g
1921.8	43286.5	875.3	314.9	9.3	32.4	0.0	0.0	0.0	13.9	41.7	4.6	0.0	0.0	18.5	0.0	0.0	9.3	305.7
1921.9	43288.8	923.1	309.2	22.4	31.4	0.0	0.0	0.0	13.4	31.4	13.4	4.5	4.5	9.0	0.0	0.0	9.0	313.7
1922.0	43291.0	769.2	194.0	3.5	45.0	3.5	0.0	0.0	17.3	31.2	34.6	3.5	3.5	24.3	0.0	0.0	6.9	433.1
1922.1	43293.2	1225.5	280.8	6.4	25.5	0.0	0.0	0.0	6.4	70.2	12.8	0.0	0.0	6.4	0.0	0.0	6.4	631.9
1922.2	43295.3	1079.9	382.7	6.8	27.3	0.0	0.0	0.0	34.2	61.5	61.5	0.0	0.0	54.7	0.0	0.0	13.7	656.1
1922.3	43297.5	1020.5	311.2	9.2	27.5	0.0	0.0	0.0	4.6	64.1	9.2	4.6	0.0	9.2	0.0	0.0	13.7	549.1
1922.4	43299.6	867.5	220.7	3.9	7.7	3.9	0.0	0.0	19.4	42.6	15.5	7.7	0.0	11.6	0.0	0.0	11.6	433.8
1922.5	43301.8	1176.8	310.7	13.2	26.4	0.0	0.0	0.0	26.4	92.6	6.6	6.6	0.0	0.0	0.0	0.0	19.8	654.5
1922.6	43303.9	965.0	367.3	6.2	24.9	6.2	0.0	0.0	24.9	56.0	12.5	6.2	0.0	0.0	0.0	0.0	31.1	473.2
1922.7	43306.1	771.7	324.9	0.0	13.5	0.0	0.0	0.0	13.5	49.6	0.0	4.5	0.0	4.5	0.0	0.0	13.5	446.8
1922.8	43308.2	936.5	376.1	7.4	29.5	3.7	0.0	0.0	18.4	22.1	3.7	7.4	0.0	11.1	0.0	0.0	14.7	427.7
1922.9	43310.4	1198.4	343.5	7.6	30.5	0.0	0.0	0.0	7.6	38.2	7.6	7.6	7.6	7.6	0.0	0.0	15.3	610.7
1923.0	43312.5	866.4	327.1	10.4	10.4	0.0	0.0	0.0	17.4	34.8	7.0	3.5	0.0	7.0	0.0	0.0	10.4	514.9
1923.1	43314.4	867.9	239.3	3.6	7.1	3.6	0.0	0.0	3.6	17.9	0.0	0.0	0.0	7.1	0.0	0.0	14.3	428.6
1923.2	43316.2	907.1	360.1	0.0	22.8	0.0	0.0	0.0	22.8	31.9	9.1	9.1	0.0	4.6	0.0	0.0	18.2	437.6
1923.3	43318.1	886.1	306.9	3.8	26.9	3.8	0.0	0.0	0.0	49.9	11.5	7.7	3.8	3.8	0.0	0.0	19.2	410.4
1923.4	43319.9	904.1	287.3	0.0	19.2	3.8	0.0	0.0	15.3	34.5	7.7	11.5	0.0	0.0	0.0	0.0	7.7	501.8
1923.5	43321.8	746.9	294.7	12.1	16.1	0.0	0.0	0.0	12.1	40.4	4.0	0.0	0.0	0.0	0.0	0.0	12.1	383.5
1923.6	43323.6	855.0	331.7	3.4	27.4	3.4	0.0	0.0	0.0	34.2	0.0	6.8	6.8	0.0	0.0	0.0	3.4	283.9
1923.7	43325.5	924.1	365.3	5.4	21.5	0.0	0.0	5.4	10.7	64.5	0.0	5.4	0.0	5.4	0.0	0.0	5.4	311.6
1923.8	43327.3	934.5	311.5	7.7	19.2	3.8	0.0	0.0	11.5	50.0	3.8	3.8	0.0	7.7	0.0	0.0	15.4	500.0
1923.9	43329.2	964.0	272.1	6.7	13.4	0.0	0.0	0.0	33.6	26.9	10.1	0.0	3.4	3.4	0.0	0.0	16.8	490.4
1924.0	43331.0	1148.7	367.0	3.4	47.6	0.0	0.0	3.4	10.2	57.8	3.4	6.8	6.8	6.8	0.0	0.0	51.0	220.9
1924.1	43332.5	1374.4	407.9	0.0	75.3	6.3	0.0	0.0	31.4	100.4	6.3	6.3	0.0	0.0	0.0	0.0	69.0	219.7
1924.2	43334.0	1835.6	558.7	0.0	116.1	0.0	0.0	0.0	21.8	152.4	50.8	21.8	7.3	7.3	0.0	0.0	50.8	384.5
1924.3	43335.5	1798.1	602.0	7.9	134.7	7.9	0.0	0.0	7.9	213.9	79.2	7.9	7.9	15.8	0.0	0.0	87.1	301.0
1924.4	43337.0	1671.6	568.2	0.0	123.5	0.0	0.0	0.0	32.9	172.9	181.2	8.2	0.0	49.4	0.0	0.0	49.4	222.3
1924.5	43338.5	1074.5	257.9	21.5	200.6	0.0	0.0	0.0	14.3	193.4	422.6	50.1	0.0	14.3	0.0	0.0	21.5	157.6

Core MD03-2622 Absolute Abundance Data (continued)

Depth (cm)	Age (yBP)	*G.b* #/g	*N.d* #/g	*O.u* #/g	*G.a* #/g	*G.c* #/g	*P.o* #/g	*G.m* #/g	*G.r*(p) #/g	*G.r*(w) #/g	*G.s* #/g	*G.g* #/g	*G.t* #/g	*G.rs* #/g	*N.p*(l) #/g	*N.p*(r) #/g	*G.q* #/g	Other #/g
1924.6	43340.0	614.7	173.2	6.8	105.3	0.0	0.0	3.4	6.8	64.5	61.1	20.4	3.4	0.0	0.0	0.0	3.4	54.3
1924.7	43341.5	389.7	130.5	0.0	52.5	1.7	0.0	1.7	15.2	52.5	25.4	3.4	0.0	1.7	0.0	0.0	6.8	55.9
1924.8	43343.0	402.8	126.9	0.0	46.3	4.0	0.0	2.0	10.1	52.4	32.2	10.1	4.0	4.0	0.0	0.0	4.0	48.3
1924.9	43344.5	621.2	188.1	2.5	37.1	2.5	0.0	0.0	22.3	89.1	12.4	0.0	0.0	2.5	0.0	0.0	7.4	99.0
1925.0	43346.0	1533.5	569.6	6.3	50.1	12.5	0.0	0.0	37.6	219.1	18.8	12.5	6.3	0.0	0.0	0.0	25.0	244.1
1925.1	43348.0	1643.0	631.9	13.3	73.2	0.0	0.0	0.0	46.6	372.5	13.3	13.3	0.0	6.7	0.0	0.0	13.3	286.0
1925.2	43350.0	2006.2	690.8	7.3	58.8	7.3	0.0	0.0	58.8	448.3	44.1	14.7	7.3	14.7	0.0	0.0	14.7	323.3
1925.3	43352.0	1959.7	732.7	0.0	79.4	0.0	0.0	0.0	53.0	494.3	26.5	0.0	0.0	0.0	0.0	0.0	17.7	273.7
1925.4	43354.0	1936.2	704.1	0.0	61.6	0.0	0.0	0.0	44.0	580.9	35.2	8.8	0.0	0.0	0.0	0.0	44.0	396.0
1925.5	43356.0	1778.5	617.4	13.4	73.8	0.0	0.0	0.0	60.4	308.7	13.4	6.7	0.0	6.7	0.0	0.0	26.8	281.9
1925.6	43358.0	1712.2	624.0	0.0	60.9	0.0	0.0	0.0	38.0	220.7	22.8	15.2	0.0	0.0	0.0	0.0	15.2	334.8
1925.7	43360.0	1666.3	513.6	0.0	87.4	5.5	0.0	0.0	71.0	224.0	16.4	16.4	5.5	5.5	0.0	0.0	10.9	245.9
1925.8	43362.0	1385.5	510.0	0.0	59.5	0.0	0.0	0.0	51.0	178.5	17.0	17.0	0.0	0.0	0.0	0.0	51.0	399.5
1925.9	43364.0	1640.9	418.4	0.0	65.6	8.2	0.0	0.0	16.4	205.1	0.0	16.4	0.0	0.0	0.0	0.0	8.2	246.1
1926.0	43366.0	1122.6	546.9	0.0	172.7	7.2	0.0	0.0	36.0	374.2	28.8	21.6	7.2	0.0	0.0	0.0	36.0	287.8
1926.1	43367.5	1260.5	439.3	6.4	152.8	0.0	0.0	0.0	63.7	413.8	25.5	44.6	0.0	12.7	0.0	0.0	6.4	280.1
1926.2	43368.9	733.3	217.9	0.0	269.8	0.0	0.0	0.0	34.6	214.5	41.5	6.9	6.9	3.5	0.0	0.0	0.0	103.8
1926.3	43370.4	571.5	205.3	0.0	147.1	3.4	0.0	0.0	20.5	171.1	34.2	10.3	0.0	3.4	0.0	0.0	6.8	109.5
1926.4	43371.8	284.1	89.9	0.0	48.2	1.6	0.0	0.0	11.2	112.4	24.1	3.2	1.6	6.4	0.0	0.0	0.0	40.1
1926.5	43373.3	382.4	117.4	0.0	71.4	0.0	0.0	0.0	22.2	119.0	22.2	3.2	1.6	3.2	0.0	0.0	7.9	69.8
1926.6	43374.7	329.8	85.8	0.0	56.2	0.0	0.0	1.5	19.2	93.2	17.7	4.4	3.0	3.0	0.0	0.0	7.4	74.0
1926.7	43376.2	413.6	132.8	0.0	100.1	0.0	0.0	0.0	15.2	150.2	37.0	2.2	2.2	4.4	0.0	0.0	8.7	87.1
1926.8	43377.6	618.1	216.5	7.0	94.3	3.5	0.0	0.0	45.4	352.7	52.4	3.5	3.5	0.0	0.0	0.0	21.0	206.0
1926.9	43379.1	703.0	160.2	3.3	163.5	0.0	0.0	0.0	32.7	304.1	26.2	9.8	3.3	6.5	0.0	0.0	16.3	192.9
1927.0	43380.5	697.6	149.0	3.4	57.6	0.0	0.0	0.0	33.9	291.2	10.2	13.5	3.4	3.4	0.0	0.0	10.2	115.1
1927.1	43381.5	604.2	158.8	6.9	51.8	3.5	0.0	0.0	20.7	214.0	13.8	27.6	3.5	0.0	0.0	0.0	6.9	93.2
1927.2	43382.4	572.5	193.0	3.3	30.0	3.3	0.0	0.0	56.6	239.6	10.0	13.3	0.0	0.0	0.0	0.0	6.7	153.1
1927.3	43383.4	486.8	130.5	0.0	15.5	2.2	0.0	0.0	28.8	128.3	4.4	2.2	0.0	2.2	0.0	0.0	2.2	79.7

Core MD03-2622 Absolute Abundance Data (continued)

Depth (cm)	Age (yBP)	*G.b* #/g	*N.d* #/g	*O.u* #/g	*G.a* #/g	*G.c* #/g	*P.o* #/g	*G.m* #/g	*G.r*(p) #/g	*G.r*(w) #/g	*G.s* #/g	*G.g* #/g	*G.t* #/g	*G.rs* #/g	*N.p*(l) #/g	*N.p*(r) #/g	*G.q* #/g	Other #/g
1927.4	43384.3	423.9	134.2	0.0	14.1	0.0	0.0	0.0	26.5	171.3	1.8	1.8	5.3	3.5	0.0	0.0	7.1	132.5
1927.5	43385.3	326.2	108.2	0.0	22.0	1.6	0.0	0.0	14.1	116.1	3.1	1.6	4.7	0.0	0.0	0.0	4.7	94.1
1927.6	43386.2	323.0	82.8	4.9	17.9	0.0	0.0	0.0	11.4	69.8	11.4	1.6	0.0	1.6	0.0	0.0	6.5	89.3
1927.7	43387.2	275.9	87.8	0.0	14.1	0.0	0.0	1.6	26.7	73.7	3.1	7.8	1.6	0.0	0.0	0.0	6.3	80.0
1927.8	43388.1	138.8	36.7	2.4	8.0	1.6	0.0	0.0	5.6	39.1	0.8	3.2	0.0	0.0	0.0	0.0	0.0	19.9
1927.9	43389.1	255.8	59.6	0.0	9.4	1.6	0.0	0.0	14.1	86.3	1.6	3.1	0.0	0.0	0.0	0.0	1.6	43.9
1928.0	43390.0	639.0	174.8	2.9	20.1	2.9	0.0	0.0	14.3	203.5	2.9	5.7	2.9	0.0	0.0	0.0	2.9	137.6
1928.1	43391.5	586.1	182.3	3.3	26.0	0.0	0.0	0.0	22.8	188.9	0.0	6.5	0.0	0.0	0.0	0.0	9.8	156.3
1928.2	43393.0	683.3	165.1	0.0	16.5	0.0	0.0	0.0	23.1	135.3	3.3	6.6	0.0	0.0	0.0	0.0	3.3	112.2
1928.3	43394.5	682.6	164.6	0.0	13.7	0.0	0.0	0.0	37.7	216.1	0.0	10.3	3.4	0.0	0.0	0.0	6.9	120.1
1928.4	43396.0	861.0	199.0	6.9	17.2	0.0	0.0	0.0	24.0	223.0	3.4	27.4	3.4	0.0	0.0	0.0	6.9	113.2
1928.5	43397.5	821.4	207.9	0.0	36.9	6.7	0.0	0.0	36.9	241.4	0.0	33.5	0.0	3.4	0.0	0.0	10.1	150.9
1928.6	43399.0	957.2	183.9	0.0	20.4	0.0	0.0	0.0	34.1	235.0	3.4	51.1	3.4	3.4	0.0	0.0	10.2	204.4
1928.7	43400.5	722.6	200.2	6.8	13.6	0.0	0.0	0.0	33.9	230.7	3.4	50.9	3.4	0.0	0.0	0.0	3.4	145.9
1928.8	43402.0	937.6	316.9	6.6	19.8	0.0	0.0	0.0	59.4	260.8	0.0	69.3	3.3	0.0	0.0	0.0	13.2	138.7
1928.9	43403.5	1063.3	263.7	0.0	8.5	4.3	0.0	0.0	63.8	285.0	0.0	51.0	8.5	0.0	0.0	0.0	17.0	204.1
1929.0	43405.0	1123.7	284.8	6.2	24.8	9.3	0.0	0.0	43.3	195.0	9.3	40.2	6.2	0.0	0.0	0.0	9.3	148.6
1929.1	43407.1	958.2	219.1	9.8	13.1	3.3	0.0	0.0	45.8	317.2	9.8	36.0	3.3	0.0	0.0	0.0	6.5	140.6
1929.2	43409.2	980.6	281.1	6.5	32.7	0.0	0.0	0.0	49.0	454.4	0.0	13.1	0.0	0.0	0.0	0.0	3.3	137.3
1929.3	43411.3	1290.6	362.2	6.6	19.8	0.0	0.0	0.0	52.7	302.9	0.0	85.6	0.0	0.0	0.0	0.0	6.6	177.8
1929.4	43413.4	1040.0	227.0	0.0	37.1	0.0	0.0	0.0	61.9	247.6	0.0	8.3	0.0	4.1	0.0	0.0	8.3	136.2
1929.5	43415.5	916.5	210.2	0.0	36.1	0.0	0.0	0.0	39.4	233.2	3.3	3.3	3.3	0.0	0.0	0.0	6.6	118.3
1929.6	43417.6	620.6	207.9	0.0	12.8	0.0	0.0	0.0	73.6	246.3	0.0	12.8	6.4	0.0	0.0	0.0	9.6	80.0
1929.7	43419.7	940.5	273.7	3.1	12.6	0.0	0.0	0.0	44.0	220.2	3.1	3.1	0.0	0.0	0.0	0.0	12.6	169.9
1929.8	43421.8	575.8	190.8	0.0	17.3	0.0	0.0	0.0	31.2	145.7	10.4	0.0	6.9	0.0	0.0	0.0	6.9	90.2
1929.9	43423.9	510.0	169.3	0.0	18.6	0.0	0.0	0.0	22.7	159.0	4.1	2.1	4.1	0.0	0.0	0.0	4.1	80.5
1930.0	43426.0	314.4	104.8	1.6	7.9	0.0	0.0	0.0	20.6	52.4	1.6	1.6	0.0	0.0	0.0	0.0	3.2	25.4
1930.1	43428.0	395.1	104.8	0.0	9.7	0.0	0.0	0.0	22.6	58.1	0.0	1.6	1.6	0.0	0.0	0.0	1.6	33.9

Core MD03-2622 Absolute Abundance Data (continued)

Depth (cm)	Age (yBP)	*G.b* #/g	*N.d* #/g	*O.u* #/g	*G.a* #/g	*G.c* #/g	*P.o* #/g	*G.m* #/g	*G.r*(p) #/g	*G.r*(w) #/g	*G.s* #/g	*G.g* #/g	*G.t* #/g	*G.rs* #/g	*N.p*(l) #/g	*N.p*(r) #/g	*G.q* #/g	Other #/g
1930.2	43429.9	253.7	100.3	3.0	4.6	0.0	0.0	0.0	15.2	22.8	1.5	4.6	4.6	1.5	0.0	0.0	1.5	48.6
1930.3	43431.9	308.4	100.8	0.0	6.0	0.0	0.0	1.5	19.6	27.1	0.0	0.0	0.0	1.5	0.0	0.0	4.5	36.1
1930.4	43433.8	323.1	103.5	3.2	0.0	1.6	0.0	0.0	30.2	20.7	1.6	1.6	3.2	0.0	0.0	0.0	4.8	36.6
1930.5	43435.8	254.7	66.0	3.1	4.1	0.0	0.0	0.0	14.4	10.3	1.0	1.0	2.1	0.0	0.0	0.0	5.2	21.7
1930.6	43437.7	376.3	102.3	0.0	3.3	0.0	0.0	0.0	18.2	13.2	0.0	1.7	3.3	1.7	0.0	0.0	5.0	38.0
1930.7	43439.7	334.4	100.6	0.0	9.3	1.5	0.0	0.0	18.6	13.9	0.0	3.1	1.5	3.1	0.0	0.0	3.1	38.7
1930.8	43441.6	419.0	136.8	2.2	6.5	0.0	0.0	0.0	23.9	15.2	0.0	4.3	4.3	2.2	0.0	0.0	2.2	52.1
1930.9	43443.6	395.4	111.1	1.9	7.5	0.0	0.0	0.0	13.2	9.4	1.9	1.9	0.0	0.0	0.0	0.0	3.8	37.7
1931.0	43445.5	418.9	118.6	3.2	7.9	0.0	0.0	0.0	33.2	17.4	3.2	3.2	7.9	1.6	0.0	0.0	3.2	47.4
1931.1	43447.5	469.8	187.0	1.5	4.6	0.0	0.0	0.0	30.9	15.5	0.0	1.5	1.5	0.0	0.0	0.0	4.6	69.5
1931.2	43449.5	484.3	176.4	1.5	12.4	1.5	1.5	0.0	40.2	18.6	1.5	3.1	1.5	1.5	0.0	0.0	4.6	69.6
1931.3	43451.5	493.6	191.1	4.0	13.9	0.0	0.0	0.0	23.9	10.0	2.0	2.0	2.0	0.0	0.0	0.0	8.0	79.6
1931.4	43453.5	580.8	258.9	0.0	18.3	0.0	0.0	0.0	13.3	6.6	0.0	1.7	0.0	1.7	0.0	0.0	5.0	96.2
1931.5	43455.5	552.4	288.3	0.0	15.2	0.0	0.0	0.0	15.2	6.1	3.0	0.0	0.0	0.0	0.0	0.0	6.1	91.1
1931.6	43457.5	348.0	196.1	1.5	6.1	1.5	0.0	0.0	27.4	6.1	1.5	0.0	3.0	0.0	0.0	0.0	3.0	66.9
1931.7	43459.5	423.5	207.1	1.5	12.3	1.5	0.0	1.5	39.9	16.9	0.0	1.5	4.6	1.5	0.0	0.0	6.1	82.9
1931.8	43461.5	432.8	248.0	1.7	8.6	0.0	0.0	0.0	49.6	13.7	0.0	1.7	0.0	0.0	0.0	0.0	3.4	61.6
1931.9	43463.5	548.3	295.4	0.0	6.4	0.0	0.0	0.0	74.4	21.3	0.0	2.1	4.3	0.0	0.0	0.0	4.3	93.5
1932.0	43465.5	577.2	250.5	0.0	6.3	0.0	0.0	0.0	79.3	15.9	3.2	3.2	0.0	3.2	0.0	0.0	15.9	82.5
1932.1	43467.2	611.3	328.5	0.0	21.3	0.0	0.0	0.0	112.5	15.2	9.1	0.0	0.0	3.0	0.0	0.0	6.1	124.7
1932.2	43468.8	609.8	309.8	0.0	13.2	0.0	0.0	3.3	141.7	16.5	3.3	0.0	3.3	3.3	0.0	0.0	9.9	72.5
1932.3	43470.5	698.4	297.0	3.3	13.1	0.0	0.0	3.3	107.7	6.5	0.0	6.5	0.0	0.0	0.0	0.0	6.5	104.4
1932.4	43472.1	526.2	272.1	0.0	14.9	0.0	0.0	0.0	110.6	12.0	3.0	3.0	0.0	0.0	0.0	0.0	3.0	80.7
1932.5	43473.8	556.2	213.3	5.8	17.3	2.9	0.0	0.0	69.2	14.4	0.0	5.8	0.0	2.9	0.0	0.0	2.9	123.9
1932.6	43475.4	725.2	314.9	0.0	22.3	0.0	0.0	0.0	66.8	9.5	3.2	6.4	3.2	0.0	0.0	0.0	9.5	130.4
1932.7	43477.1	778.4	311.4	3.9	23.4	0.0	0.0	0.0	101.2	7.8	3.9	3.9	0.0	0.0	0.0	0.0	15.6	101.2
1932.8	43478.7	715.0	378.5	0.0	29.4	0.0	0.0	0.0	105.1	0.0	4.2	0.0	8.4	0.0	0.0	0.0	12.6	126.2
1932.9	43480.4	646.8	323.4	3.2	28.8	0.0	3.2	0.0	83.2	25.6	3.2	3.2	3.2	0.0	0.0	0.0	9.6	121.7

Core MD03-2622 Absolute Abundance Data (continued)

Depth (cm)	Age (yBP)	*G.b* #/g	*N.d* #/g	*O.u* #/g	*G.a* #/g	*G.c* #/g	*P.o* #/g	*G.m* #/g	*G.r*(p) #/g	*G.r*(w) #/g	*G.s* #/g	*G.g* #/g	*G.t* #/g	*G.rs* #/g	*N.p*(l) #/g	*N.p*(r) #/g	*G.q* #/g	Other #/g
1933.0	43482.0	731.9	301.9	9.8	16.4	0.0	0.0	0.0	65.6	32.8	3.3	6.6	3.3	0.0	0.0	0.0	0.0	124.7
1933.1	43484.1	747.9	387.4	0.0	30.3	10.1	0.0	0.0	111.2	53.9	3.4	0.0	0.0	0.0	0.0	0.0	10.1	94.3
1933.2	43486.1	381.7	178.5	1.5	12.3	0.0	0.0	0.0	55.4	20.0	4.6	3.1	1.5	0.0	0.0	0.0	1.5	81.6
1933.3	43488.2	610.7	332.8	0.0	21.4	3.1	0.0	0.0	82.4	12.2	3.1	9.2	3.1	0.0	0.0	0.0	0.0	88.5
1933.4	43490.2	586.8	246.5	0.0	19.6	2.0	0.0	0.0	88.0	33.3	5.9	5.9	7.8	2.0	0.0	0.0	2.0	103.7
1933.5	43492.3	520.9	242.2	1.7	19.9	1.7	0.0	0.0	101.2	14.9	1.7	1.7	5.0	3.3	0.0	0.0	3.3	92.9
1933.6	43494.3	501.9	268.9	6.0	17.9	0.0	0.0	0.0	92.6	23.9	3.0	3.0	6.0	3.0	0.0	0.0	11.9	77.7
1933.7	43496.4	613.6	283.8	0.0	10.6	3.5	0.0	0.0	92.2	7.1	3.5	0.0	0.0	0.0	0.0	0.0	10.6	70.9
1933.8	43498.4	474.9	207.2	0.0	15.6	0.0	0.0	0.0	111.4	13.7	2.0	7.8	0.0	2.0	0.0	0.0	11.7	84.0
1933.9	43500.5	419.8	187.0	2.0	9.9	0.0	0.0	0.0	53.7	9.9	4.0	4.0	4.0	2.0	0.0	0.0	9.9	65.7
1934.0	43502.5	459.5	183.4	1.7	13.7	0.0	0.0	0.0	51.4	24.0	8.6	5.1	1.7	3.4	0.0	0.0	12.0	63.4
1934.1	43504.6	469.8	218.2	2.6	18.0	0.0	0.0	2.6	79.6	12.8	0.0	5.1	0.0	0.0	0.0	0.0	10.3	38.5
1934.2	43506.6	417.1	144.7	0.0	15.0	1.9	0.0	0.0	84.5	22.5	1.9	1.9	3.8	0.0	0.0	0.0	11.3	58.2
1934.3	43508.7	385.7	124.6	4.0	19.8	2.0	2.0	0.0	27.7	5.9	2.0	4.0	4.0	0.0	0.0	0.0	4.0	35.6
1934.4	43510.7	338.9	124.6	1.9	11.7	0.0	0.0	0.0	46.7	25.3	9.7	5.8	3.9	0.0	0.0	0.0	5.8	48.7
1934.5	43512.8	241.1	91.3	2.6	17.2	1.7	0.0	0.0	28.4	6.9	2.6	1.7	0.0	0.0	0.0	0.0	1.7	35.3
1934.6	43514.8	246.6	86.6	5.7	14.7	0.0	0.0	0.0	22.0	6.5	2.4	3.3	0.8	1.6	0.0	0.0	0.0	34.3
1934.7	43516.9	230.3	77.3	1.7	18.2	2.6	0.0	0.0	25.2	12.2	2.6	1.7	1.7	0.0	0.0	0.0	0.0	16.5
1934.8	43518.9	274.7	82.8	2.0	16.2	0.0	0.0	0.0	55.6	28.3	4.0	2.0	5.1	0.0	0.0	0.0	0.0	33.3
1934.9	43521.0	310.1	90.3	2.0	15.7	3.9	0.0	0.0	94.2	51.0	0.0	5.9	0.0	0.0	0.0	0.0	0.0	19.6
1935.0	43523.0	339.1	111.4	3.3	24.6	1.6	0.0	0.0	65.5	59.0	6.6	3.3	0.0	1.6	0.0	0.0	0.0	21.3
1935.1	43525.1	351.5	116.2	2.8	19.6	0.0	0.0	0.0	77.0	89.6	8.4	7.0	2.8	0.0	0.0	0.0	1.4	22.4
1935.2	43527.1	363.0	100.4	1.8	15.9	1.8	0.0	0.0	96.9	149.8	1.8	5.3	5.3	5.3	0.0	0.0	0.0	37.0
1935.3	43529.2	376.1	130.7	2.0	7.9	0.0	0.0	0.0	108.9	102.9	4.0	4.0	0.0	4.0	0.0	0.0	0.0	35.6
1935.4	43531.2	484.0	154.6	0.0	32.9	2.5	0.0	0.0	119.1	182.4	2.5	7.6	5.1	0.0	0.0	0.0	0.0	68.4
1935.5	43533.3	526.1	151.0	0.0	19.8	0.0	0.0	0.0	99.1	212.0	1.5	3.0	3.0	0.0	0.0	0.0	0.0	53.4
1935.6	43535.3	412.4	156.6	7.9	17.8	4.0	0.0	0.0	85.2	186.4	7.9	4.0	5.9	4.0	0.0	0.0	0.0	45.6
1935.7	43537.4	528.1	153.1	0.0	25.8	0.0	0.0	0.0	55.0	182.3	8.6	1.7	0.0	0.0	0.0	0.0	1.7	39.6

Core MD03-2622 Absolute Abundance Data (continued)

Depth (cm)	Age (yBP)	*G.b* #/g	*N.d* #/g	*O.u* #/g	*G.a* #/g	*G.c* #/g	*P.o* #/g	*G.m* #/g	*G.r*(p) #/g	*G.r*(w) #/g	*G.s* #/g	*G.g* #/g	*G.t* #/g	*G.rs* #/g	*N.p*(l) #/g	*N.p*(r) #/g	*G.q* #/g	Other #/g
1935.8	43539.4	511.4	109.7	1.6	33.9	1.6	0.0	0.0	51.6	206.5	3.2	0.0	1.6	0.0	0.0	0.0	4.8	74.2
1935.9	43541.5	511.8	136.8	0.0	28.7	0.0	0.0	0.0	67.6	184.1	6.8	0.0	3.4	1.7	0.0	0.0	1.7	43.9
1936.0	43543.5	266.7	63.1	3.2	18.9	0.0	0.0	0.0	31.6	94.7	7.9	1.6	1.6	0.0	0.0	0.0	1.6	15.8
1936.1	43545.7	385.2	164.9	1.5	15.4	0.0	0.0	0.0	49.3	92.4	4.6	4.6	3.1	0.0	0.0	0.0	0.0	27.7
1936.2	43547.8	181.8	72.3	1.4	7.2	0.7	0.0	0.0	45.1	39.4	2.9	2.9	0.0	0.7	0.0	0.0	3.6	10.7
1936.3	43550.0	306.1	125.3	3.6	8.9	0.9	0.0	0.9	39.4	42.1	5.4	1.8	0.0	0.9	0.0	0.0	1.8	32.2
1936.4	43552.1	180.7	47.3	3.3	7.2	0.7	0.0	0.0	24.3	21.7	2.6	2.0	0.7	0.0	0.0	0.0	1.3	18.4
1936.5	43554.3	339.8	142.9	1.7	13.9	1.7	0.0	0.0	26.1	26.1	0.0	5.2	0.0	1.7	0.0	0.0	3.5	31.4
1936.6	43556.4	150.4	50.1	2.4	5.7	0.8	0.0	0.0	17.8	15.4	0.0	0.8	0.0	0.0	0.0	0.0	1.6	17.8
1936.7	43558.6	288.1	104.3	0.8	10.8	0.0	0.0	0.0	29.8	20.7	0.8	0.8	0.0	0.0	0.0	0.0	1.7	29.0
1936.8	43560.7	354.4	109.7	0.0	3.4	0.0	0.0	0.0	20.2	30.4	1.7	1.7	3.4	1.7	0.0	0.0	5.1	42.2
1936.9	43562.9	365.2	158.3	0.0	3.1	1.6	0.0	0.0	28.2	31.3	3.1	1.6	0.0	0.0	0.0	0.0	3.1	31.3
1937.0	43565.0	299.8	88.8	0.8	11.4	0.0	0.0	0.0	17.1	26.1	0.8	1.6	1.6	0.8	0.0	0.0	3.3	41.6
1937.1	43566.9	191.6	62.1	1.3	6.7	0.0	0.0	0.0	15.4	12.7	0.0	0.7	0.7	0.7	0.0	0.0	0.7	26.7
1937.2	43568.7	293.5	119.3	0.0	20.6	0.0	0.0	0.0	30.2	9.6	0.0	4.1	0.0	0.0	0.0	0.0	5.5	38.4
1937.3	43570.6	260.1	103.1	1.6	20.6	1.6	0.0	0.0	31.7	15.9	0.0	1.6	0.0	1.6	0.0	0.0	4.8	31.7
1937.4	43572.4	289.7	112.1	4.4	52.4	0.0	0.0	0.0	20.4	8.7	1.5	1.5	1.5	0.0	0.0	0.0	0.0	33.5
1937.5	43574.3	348.8	120.0	0.0	83.3	1.4	0.0	0.0	39.5	8.5	0.0	4.2	1.4	0.0	0.0	0.0	1.4	46.6
1937.6	43576.1	383.8	113.4	1.6	98.8	1.6	1.6	0.0	55.1	13.0	1.6	4.9	0.0	0.0	0.0	0.0	3.2	48.6
1937.7	43578.0	615.2	256.7	11.1	95.2	2.2	0.0	0.0	68.6	35.4	0.0	8.9	0.0	2.2	0.0	0.0	2.2	64.2
1937.8	43579.8	332.2	122.8	0.0	38.6	1.2	0.0	0.0	26.9	7.0	1.2	3.5	0.0	0.0	0.0	0.0	0.0	33.9
1937.9	43581.7	343.9	136.1	4.2	53.0	0.0	0.0	1.0	36.4	13.5	3.1	4.2	0.0	0.0	0.0	0.0	1.0	40.5
1938.0	43583.5	210.6	106.0	1.4	3.6	0.0	0.0	0.0	14.9	5.7	0.7	1.4	0.0	0.0	0.0	0.0	0.7	32.0
1938.1	43585.4	346.7	149.2	7.1	25.6	2.8	0.0	0.0	54.0	24.2	1.4	1.4	0.0	0.0	0.0	0.0	1.4	36.9
1938.2	43587.2	110.3	50.7	2.5	3.8	0.8	0.0	0.4	15.2	2.5	0.0	0.8	0.0	0.4	0.0	0.0	0.4	10.6
1938.3	43589.1	174.9	61.8	0.9	3.5	0.0	0.0	0.0	19.1	5.2	0.0	1.7	0.0	0.0	0.0	0.0	1.7	23.5
1938.4	43590.9	237.4	61.8	2.6	13.2	0.9	0.0	0.0	18.5	8.8	0.0	1.8	0.0	1.8	0.0	0.0	2.6	26.5
1938.5	43592.8	490.2	141.8	3.6	28.7	0.0	0.0	1.8	66.4	12.6	0.0	3.6	3.6	0.0	0.0	0.0	7.2	53.9

Core MD03-2622 Absolute Abundance Data (continued)

Depth (cm)	Age (yBP)	*G.b* #/g	*N.d* #/g	*O.u* #/g	*G.a* #/g	*G.c* #/g	*P.o* #/g	*G.m* #/g	*G.r*(p) #/g	*G.r*(w) #/g	*G.s* #/g	*G.g* #/g	*G.t* #/g	*G.rs* #/g	*N.p*(l) #/g	*N.p*(r) #/g	*G.q* #/g	Other #/g
1938.6	43594.6	765.6	248.9	3.2	28.4	0.0	0.0	0.0	72.5	28.4	0.0	6.3	0.0	12.6	0.0	0.0	9.5	119.7
1938.7	43596.5	811.7	220.3	0.0	29.0	0.0	0.0	0.0	81.2	31.9	0.0	2.9	2.9	0.0	0.0	0.0	5.8	127.6
1938.8	43598.3	669.5	206.1	4.1	18.4	0.0	0.0	0.0	53.1	34.7	2.0	4.1	0.0	2.0	0.0	0.0	8.2	87.8
1938.9	43600.2	421.3	139.9	1.7	19.0	0.0	0.0	0.0	53.5	31.1	3.5	3.5	1.7	3.5	0.0	0.0	3.5	51.8
1939.0	43602.0	378.5	123.7	0.0	13.4	3.0	0.0	0.0	46.2	37.3	1.5	1.5	1.5	0.0	0.0	0.0	4.5	49.2
1939.1	43604.2	361.3	150.1	4.2	16.7	0.0	0.0	0.0	62.5	47.3	0.0	2.8	2.8	2.8	0.0	0.0	4.2	57.0
1939.2	43606.4	351.9	153.3	1.6	10.9	1.6	0.0	0.0	34.4	15.6	1.6	0.0	0.0	4.7	0.0	0.0	3.1	51.6
1939.3	43608.6	203.2	98.2	0.8	4.2	1.7	0.0	0.0	28.8	15.2	0.0	0.8	1.7	0.0	0.0	0.0	3.4	24.6
1939.4	43610.8	215.1	126.3	1.9	11.2	0.9	0.0	0.9	39.3	10.3	0.9	1.9	0.9	1.9	0.0	0.0	3.7	34.6
1939.5	43613.0	518.7	156.2	1.4	12.9	1.4	0.0	0.0	53.0	17.2	2.9	1.4	1.4	1.4	0.0	0.0	4.3	58.8
1939.6	43615.2	430.8	144.7	1.7	6.7	1.7	0.0	0.0	62.3	30.3	3.4	3.4	1.7	0.0	0.0	0.0	15.1	45.4
1939.7	43617.4	505.6	155.0	0.0	9.7	0.0	0.0	0.0	62.0	31.0	3.9	0.0	0.0	5.8	0.0	0.0	13.6	54.2
1939.8	43619.6	346.5	104.7	1.9	13.3	0.0	0.0	1.9	49.5	17.1	5.7	0.0	0.0	0.0	0.0	0.0	9.5	32.4
1939.9	43621.8	405.7	132.1	7.9	15.9	1.3	0.0	1.3	68.7	29.1	1.3	2.6	2.6	0.0	0.0	0.0	7.9	43.6
1940.0	43624.0	463.3	141.8	5.2	17.3	0.0	0.0	1.7	89.9	39.8	3.5	5.2	0.0	0.0	0.0	0.0	8.6	64.0
1940.1	43626.0	458.4	169.4	1.5	9.1	1.5	0.0	0.0	130.1	28.7	4.5	1.5	3.0	1.5	0.0	0.0	7.6	54.5
1940.2	43628.0	492.9	161.2	1.6	17.1	0.0	0.0	0.0	134.9	49.6	4.7	1.6	0.0	3.1	0.0	0.0	12.4	71.3
1940.3	43630.0	646.6	242.5	1.8	5.4	1.8	0.0	0.0	86.2	16.2	1.8	0.0	1.8	0.0	0.0	0.0	10.8	70.0
1940.4	43632.0	881.2	350.1	3.9	3.9	3.9	0.0	0.0	137.7	31.5	15.7	7.9	3.9	3.9	0.0	0.0	15.7	90.5
1940.5	43634.0	762.6	249.3	5.5	11.1	1.8	0.0	0.0	127.4	29.5	0.0	3.7	0.0	0.0	0.0	0.0	3.7	73.9
1940.6	43636.0	838.8	207.0	0.0	14.5	0.0	0.0	0.0	116.2	21.8	0.0	10.9	0.0	0.0	0.0	0.0	10.9	76.3
1940.7	43638.0	1206.4	271.7	0.0	24.7	4.1	0.0	0.0	98.8	24.7	0.0	8.2	0.0	0.0	0.0	0.0	16.5	115.3
1940.8	43640.0	902.0	299.7	0.0	21.0	0.0	0.0	0.0	92.9	18.0	3.0	3.0	0.0	3.0	0.0	0.0	18.0	149.8
1940.9	43642.0	379.6	169.8	4.0	8.0	0.0	0.0	0.0	45.9	12.0	2.0	0.0	2.0	0.0	0.0	0.0	8.0	65.9
1941.0	43644.0	646.4	183.4	4.6	9.2	0.0	0.0	0.0	36.7	20.6	0.0	4.6	0.0	0.0	0.0	0.0	11.5	75.6
1941.1	43646.5	595.6	161.5	4.2	9.8	1.4	0.0	0.0	71.6	7.0	1.4	2.8	5.6	0.0	0.0	0.0	7.0	57.6
1941.2	43648.9	785.5	219.6	7.4	11.2	0.0	0.0	3.7	126.6	29.8	7.4	0.0	0.0	3.7	0.0	0.0	11.2	81.9
1941.3	43651.4	779.4	213.3	0.0	15.5	7.8	0.0	3.9	62.0	31.0	0.0	7.8	0.0	0.0	0.0	0.0	19.4	81.4

Core MD03-2622 Absolute Abundance Data (continued)

Depth (cm)	Age (yBP)	*G.b* #/g	*N.d* #/g	*O.u* #/g	*G.a* #/g	*G.c* #/g	*P.o* #/g	*G.m* #/g	*G.r*(p) #/g	*G.r*(w) #/g	*G.s* #/g	*G.g* #/g	*G.t* #/g	*G.rs* #/g	*N.p*(l) #/g	*N.p*(r) #/g	*G.q* #/g	Other #/g
1941.4	43653.8	579.0	135.5	4.4	13.1	0.0	0.0	0.0	93.9	26.2	4.4	2.2	0.0	0.0	0.0	0.0	8.7	72.1
1941.5	43656.3	583.3	173.6	6.9	22.6	0.0	0.0	1.7	85.1	43.4	3.5	3.5	1.7	5.2	0.0	0.0	10.4	86.8
1941.6	43658.7	570.5	186.2	0.0	10.2	1.7	0.0	0.0	89.7	33.9	1.7	5.1	0.0	1.7	0.0	0.0	8.5	99.9
1941.7	43661.2	578.2	192.7	10.0	26.1	4.0	0.0	0.0	90.3	38.1	2.0	0.0	0.0	2.0	0.0	0.0	10.0	86.3
1941.8	43663.6	690.4	189.5	2.3	79.0	2.3	0.0	2.3	108.3	24.8	6.8	6.8	0.0	2.3	0.0	0.0	4.5	94.8
1941.9	43666.1	911.7	217.3	10.0	79.9	2.5	0.0	0.0	134.9	20.0	0.0	5.0	0.0	2.5	0.0	0.0	17.5	77.4
1942.0	43668.5	802.2	235.8	3.1	137.8	3.1	0.0	0.0	147.0	39.8	9.2	6.1	0.0	0.0	0.0	0.0	15.3	104.1
1942.1	43670.2	1045.5	253.7	0.0	183.4	0.0	0.0	0.0	122.3	58.1	3.1	3.1	0.0	0.0	0.0	0.0	6.1	119.2
1942.2	43671.8	970.7	267.0	8.3	194.7	0.0	0.0	5.6	164.1	36.2	8.3	5.6	5.6	2.8	0.0	0.0	22.3	122.4
1942.3	43673.5	1068.4	312.8	7.0	274.1	0.0	0.0	0.0	200.3	66.8	14.1	10.5	0.0	7.0	0.0	0.0	28.1	151.1
1942.4	43675.1	888.8	278.9	5.5	191.4	0.0	0.0	2.7	210.6	49.2	10.9	13.7	0.0	2.7	0.0	0.0	27.3	142.2
1942.5	43676.8	627.5	211.1	8.4	109.7	0.0	0.0	0.0	154.8	33.8	11.3	14.1	0.0	0.0	0.0	0.0	25.3	121.0
1942.6	43678.4	710.2	290.6	2.7	134.4	0.0	0.0	2.7	205.6	21.9	24.7	21.9	0.0	2.7	0.0	0.0	16.5	131.6
1942.7	43680.1	823.1	315.6	4.3	153.5	0.0	0.0	0.0	170.6	51.2	34.1	34.1	0.0	0.0	0.0	0.0	21.3	123.7
1942.8	43681.7	932.4	382.8	14.7	186.5	0.0	0.0	0.0	230.6	29.4	14.7	19.6	0.0	0.0	0.0	0.0	14.7	147.2
1942.9	43683.4	923.0	273.9	0.0	238.2	6.0	0.0	6.0	178.6	29.8	23.8	11.9	0.0	0.0	0.0	0.0	17.9	196.5
1943.0	43685.0	672.8	226.0	2.6	181.3	0.0	0.0	2.6	126.2	18.4	7.9	18.4	0.0	5.3	0.0	0.0	26.3	107.8
1943.1	43686.7	580.9	191.2	1.8	156.2	0.0	0.0	0.0	132.3	23.9	7.4	7.4	3.7	0.0	0.0	0.0	14.7	117.6
1943.2	43688.4	558.7	194.3	3.5	138.8	3.5	0.0	3.5	124.9	27.8	3.5	6.9	0.0	0.0	0.0	0.0	24.3	76.3
1943.3	43690.1	693.5	243.1	0.0	114.4	0.0	0.0	3.6	146.6	17.9	3.6	3.6	7.1	3.6	0.0	0.0	14.3	121.5
1943.4	43691.8	607.7	253.7	2.0	69.6	2.0	0.0	0.0	163.7	32.7	2.0	2.0	0.0	2.0	0.0	0.0	16.4	92.1
1943.5	43693.5	384.9	99.2	5.0	21.9	0.0	1.7	1.7	154.6	18.5	8.4	0.0	0.0	1.7	0.0	0.0	8.4	57.2
1943.6	43695.2	535.8	205.2	6.3	17.2	0.0	1.6	1.6	224.0	31.3	0.0	4.7	0.0	3.1	0.0	0.0	11.0	83.0
1943.7	43696.9	644.0	230.7	0.0	12.8	3.2	0.0	0.0	365.2	25.6	0.0	3.2	0.0	3.2	0.0	0.0	9.6	112.1
1943.8	43698.6	1253.4	375.6	0.0	69.9	0.0	0.0	0.0	458.6	56.8	0.0	4.4	4.4	0.0	0.0	0.0	8.7	104.8
1943.9	43700.3	1086.2	335.7	0.0	55.9	0.0	0.0	0.0	438.2	65.3	14.0	9.3	4.7	9.3	0.0	0.0	23.3	144.5
1944.0	43702.0	1164.5	270.7	3.3	65.2	6.5	0.0	0.0	440.3	29.4	19.6	16.3	3.3	6.5	0.0	0.0	13.0	166.4
1944.1	43704.2	1453.3	264.2	0.0	114.9	0.0	0.0	0.0	453.8	28.7	17.2	5.7	0.0	0.0	0.0	0.0	11.5	166.6

Core MD03-2622 Absolute Abundance Data (continued)

Depth (cm)	Age (yBP)	*G.b* #/g	*N.d* #/g	*O.u* #/g	*G.a* #/g	*G.c* #/g	*P.o* #/g	*G.m* #/g	*G.r*(p) #/g	*G.r*(w) #/g	*G.s* #/g	*G.g* #/g	*G.t* #/g	*G.rs* #/g	*N.p*(l) #/g	*N.p*(r) #/g	*G.q* #/g	Other #/g
1944.2	43706.4	787.7	215.6	4.1	66.3	0.0	0.0	0.0	398.0	29.0	8.3	12.4	0.0	0.0	0.0	0.0	4.1	91.2
1944.3	43708.6	770.4	194.1	0.0	55.9	8.8	0.0	0.0	426.4	20.6	5.9	5.9	0.0	0.0	0.0	0.0	11.8	105.9
1944.4	43710.8	578.4	166.9	0.0	31.8	2.0	2.0	0.0	335.9	23.8	6.0	6.0	0.0	0.0	0.0	0.0	6.0	49.7
1944.5	43713.0	1096.5	241.2	0.0	120.6	0.0	0.0	0.0	398.4	43.9	0.0	11.0	0.0	3.7	0.0	0.0	7.3	190.1
1944.6	43715.2	1188.8	329.2	0.0	128.0	12.2	0.0	0.0	432.8	54.9	0.0	0.0	0.0	12.2	0.0	0.0	12.2	176.8
1944.7	43717.4	1505.7	296.4	5.9	272.7	0.0	0.0	0.0	415.0	47.4	17.8	5.9	0.0	35.6	0.0	0.0	5.9	142.3
1944.8	43719.6	1698.5	312.9	0.0	320.3	0.0	0.0	0.0	476.8	44.7	0.0	14.9	0.0	29.8	0.0	0.0	14.9	253.3
1944.9	43721.8	1523.2	288.4	7.4	192.2	0.0	0.0	0.0	340.1	73.9	7.4	7.4	0.0	29.6	0.0	0.0	7.4	214.4
1945.0	43724.0	904.8	171.2	0.0	112.5	0.0	0.0	0.0	215.2	24.5	14.7	9.8	4.9	9.8	0.0	0.0	19.6	107.6
1945.1	43725.4	761.1	169.9	6.5	52.3	6.5	0.0	0.0	117.6	32.7	0.0	3.3	3.3	3.3	0.0	0.0	13.1	62.1
1945.2	43726.8	817.1	249.8	0.0	67.8	0.0	0.0	0.0	110.6	25.0	0.0	7.1	0.0	0.0	0.0	0.0	14.3	67.8
1945.3	43728.2	786.1	217.4	4.2	16.7	0.0	0.0	0.0	129.6	8.4	0.0	4.2	0.0	0.0	0.0	0.0	8.4	83.6
1945.4	43729.6	974.7	308.8	12.0	24.1	0.0	0.0	0.0	124.3	12.0	0.0	8.0	4.0	4.0	0.0	0.0	4.0	108.3
1945.5	43731.0	887.3	272.5	0.0	24.5	0.0	3.5	0.0	111.8	21.0	0.0	0.0	10.5	3.5	0.0	0.0	7.0	164.2
1945.6	43732.4	1010.1	341.0	3.2	29.0	0.0	0.0	0.0	144.8	45.0	0.0	3.2	9.7	0.0	0.0	0.0	9.7	135.1
1945.7	43733.8	672.7	223.5	2.2	26.3	4.4	0.0	0.0	94.2	13.1	4.4	6.6	2.2	0.0	0.0	0.0	4.4	85.5
1945.8	43735.2	230.9	51.8	1.1	11.3	0.0	0.0	0.0	31.5	7.9	0.0	2.3	0.0	0.0	0.0	0.0	4.5	37.2
1945.9	43736.6	287.9	91.2	4.8	11.2	0.0	0.0	0.0	52.8	8.0	0.0	4.8	0.0	0.0	0.0	0.0	4.8	33.6
1946.0	43738.0	282.6	81.2	1.6	20.3	3.1	0.0	0.0	37.5	10.9	1.6	4.7	1.6	1.6	0.0	0.0	1.6	37.5
1946.1	43739.6	1162.9	177.3	3.0	9.0	0.0	0.0	0.0	273.4	27.0	0.0	6.0	12.0	3.0	0.0	0.0	15.0	129.2
1946.2	43741.1	845.3	142.8	0.0	18.8	3.8	0.0	0.0	131.5	30.1	3.8	7.5	7.5	0.0	0.0	0.0	7.5	124.0
1946.3	43742.7	951.5	207.3	0.0	4.7	0.0	0.0	4.7	160.2	14.1	0.0	4.7	0.0	0.0	0.0	0.0	9.4	80.1
1946.4	43744.2	1127.2	236.0	0.0	19.3	0.0	0.0	0.0	245.7	33.7	0.0	0.0	9.6	0.0	0.0	0.0	4.8	72.3
1946.5	43745.8	361.1	83.2	0.0	5.3	0.0	0.0	5.3	109.7	8.9	0.0	3.5	3.5	0.0	0.0	0.0	1.8	51.3
1946.6	43747.3	462.2	114.2	0.0	18.6	0.0	0.0	0.0	143.4	31.9	2.7	0.0	5.3	2.7	0.0	0.0	5.3	74.4
1946.7	43748.9	849.6	147.3	3.1	34.5	0.0	0.0	0.0	213.2	37.6	0.0	3.1	0.0	0.0	0.0	0.0	9.4	131.7
1946.8	43750.4	849.9	157.2	14.6	8.7	0.0	0.0	0.0	183.4	34.9	0.0	5.8	0.0	0.0	0.0	0.0	8.7	101.9
1946.9	43752.0	1174.6	303.7	0.0	20.0	4.0	0.0	4.0	195.8	28.0	0.0	0.0	4.0	0.0	0.0	0.0	12.0	279.7

Core MD03-2622 Absolute Abundance Data (continued)

Depth (cm)	Age (yBP)	*G.b* #/g	*N.d* #/g	*O.u* #/g	*G.a* #/g	*G.c* #/g	*P.o* #/g	*G.m* #/g	*G.r*(p) #/g	*G.r*(w) #/g	*G.s* #/g	*G.g* #/g	*G.t* #/g	*G.rs* #/g	*N.p*(l) #/g	*N.p*(r) #/g	*G.q* #/g	Other #/g
1947.0	43753.5	1033.1	285.5	0.0	13.6	3.4	0.0	0.0	118.9	34.0	3.4	3.4	0.0	3.4	0.0	0.0	17.0	302.5
1947.1	43754.8	1596.7	465.7	0.0	7.4	7.4	0.0	0.0	88.7	59.1	7.4	14.8	0.0	7.4	0.0	0.0	22.2	303.1
1947.2	43756.1	1040.8	282.3	4.2	25.3	0.0	0.0	0.0	172.8	33.7	0.0	8.4	8.4	4.2	0.0	0.0	8.4	227.5
1947.3	43757.4	1038.7	267.1	3.0	20.8	0.0	0.0	0.0	139.5	71.2	5.9	11.9	5.9	17.8	0.0	0.0	20.8	175.1
1947.4	43758.7	1134.0	248.1	0.0	7.9	0.0	0.0	0.0	204.8	78.8	3.9	11.8	0.0	15.8	0.0	0.0	11.8	149.6
1947.5	43760.0	1397.5	472.0	0.0	24.8	0.0	0.0	0.0	161.5	55.9	0.0	18.6	6.2	24.8	0.0	0.0	12.4	254.7
1947.6	43761.3	1344.4	373.8	12.1	6.0	0.0	0.0	0.0	144.7	48.2	6.0	18.1	0.0	0.0	0.0	0.0	12.1	156.8
1947.7	43762.6	726.7	228.6	3.4	37.5	0.0	0.0	0.0	78.5	27.3	10.2	17.1	0.0	0.0	0.0	0.0	3.4	71.7
1947.8	43763.9	540.4	179.5	4.0	14.0	2.0	0.0	0.0	43.9	6.0	0.0	10.0	2.0	0.0	0.0	0.0	4.0	53.8
1947.9	43765.2	374.3	112.3	0.0	7.5	3.7	0.0	0.0	11.2	11.2	1.9	1.9	0.0	1.9	0.0	0.0	3.7	43.0
1948.0	43766.5	192.1	83.7	3.8	10.5	1.9	0.0	0.0	33.3	7.6	0.0	2.9	1.0	0.0	0.0	0.0	1.9	18.1
1948.1	43768.4	298.6	113.1	1.3	21.6	1.3	0.0	0.0	28.0	5.1	1.3	2.5	0.0	0.0	0.0	0.0	3.8	31.8
1948.2	43770.3	585.4	178.7	0.0	47.6	0.0	0.0	0.0	59.0	11.5	1.6	6.6	0.0	0.0	0.0	0.0	4.9	77.1
1948.3	43772.2	681.4	242.3	0.0	22.7	0.0	0.0	0.0	45.4	18.9	0.0	7.6	0.0	0.0	0.0	0.0	7.6	117.3
1948.4	43774.1	816.5	233.3	3.2	50.4	0.0	0.0	3.2	75.7	15.8	0.0	9.5	3.2	0.0	0.0	0.0	12.6	135.6
1948.5	43776.0	521.0	162.3	1.7	13.7	5.1	0.0	0.0	68.3	10.2	1.7	1.7	5.1	0.0	0.0	0.0	1.7	59.8
1948.6	43777.9	498.4	121.9	10.6	30.0	1.8	0.0	3.5	49.5	15.9	7.1	7.1	0.0	0.0	0.0	0.0	8.8	104.3
1948.7	43779.8	485.1	141.9	2.3	27.5	2.3	0.0	2.3	45.8	16.0	9.2	4.6	4.6	2.3	0.0	0.0	4.6	89.2
1948.8	43781.7	357.9	98.5	0.0	11.4	0.0	0.0	0.0	34.1	5.7	1.9	3.8	1.9	0.0	0.0	0.0	5.7	58.7
1948.9	43783.6	344.6	96.3	0.0	9.3	0.0	0.0	0.0	46.3	11.1	5.6	1.9	1.9	0.0	0.0	0.0	1.9	64.8
1949.0	43785.5	262.5	64.7	0.0	9.7	0.0	0.0	0.0	34.7	8.7	3.9	1.9	0.0	0.0	0.0	0.0	1.0	30.9
1949.1	43787.9	253.2	68.0	1.3	10.7	0.0	0.0	1.3	21.3	14.7	2.7	4.0	0.0	0.0	0.0	0.0	0.0	25.3
1949.2	43790.3	133.8	41.8	1.5	4.6	0.8	0.0	0.8	26.3	5.4	3.9	0.8	1.5	0.0	0.0	0.0	0.0	17.0
1949.3	43792.7	148.3	53.7	0.0	3.5	1.4	0.0	0.0	25.4	4.9	2.8	3.5	0.7	0.7	0.0	0.0	2.1	16.2
1949.4	43795.1	189.1	57.4	0.0	8.1	1.6	0.0	0.0	25.9	10.5	1.6	3.2	0.8	0.8	0.0	0.0	3.2	25.9
1949.5	43797.5	375.1	107.7	0.0	25.9	0.0	0.0	2.0	53.9	6.0	0.0	6.0	2.0	8.0	0.0	0.0	4.0	37.9
1949.6	43799.9	717.8	180.4	0.0	41.3	0.0	0.0	0.0	165.4	15.0	11.3	15.0	3.8	26.3	0.0	0.0	3.8	90.2
1949.7	43802.3	899.2	187.5	7.7	26.8	0.0	0.0	0.0	141.6	42.1	7.7	0.0	7.7	38.3	0.0	0.0	11.5	126.3

Core MD03-2622 Absolute Abundance Data (continued)

Depth (cm)	Age (yBP)	*G.b* #/g	*N.d* #/g	*O.u* #/g	*G.a* #/g	*G.c* #/g	*P.o* #/g	*G.m* #/g	*G.r*(p) #/g	*G.r*(w) #/g	*G.s* #/g	*G.g* #/g	*G.t* #/g	*G.rs* #/g	*N.p*(l) #/g	*N.p*(r) #/g	*G.q* #/g	Other #/g
1949.8	43804.7	907.0	238.8	0.0	33.3	0.0	0.0	0.0	160.2	21.2	3.0	6.0	0.0	24.2	0.0	0.0	9.1	145.1
1949.9	43807.1	852.8	242.8	0.0	11.8	5.9	0.0	0.0	136.2	29.6	3.0	17.8	3.0	20.7	0.0	0.0	11.8	82.9
1950.0	43809.5	458.3	160.5	0.0	14.6	1.5	0.0	0.0	56.9	4.4	5.8	2.9	2.9	2.9	0.0	0.0	2.9	55.5
1950.1	43811.6	364.5	156.2	1.6	13.0	0.0	0.0	0.0	61.8	6.5	3.3	3.3	3.3	1.6	0.0	0.0	3.3	60.2
1950.2	43813.7	195.4	63.1	1.7	4.3	0.9	0.0	0.9	26.8	2.6	2.6	3.5	0.0	0.9	0.0	0.0	0.9	25.9
1950.3	43815.8	211.9	72.2	1.4	5.6	0.7	0.0	0.0	22.9	2.8	0.0	1.4	0.0	0.7	0.0	0.0	2.1	34.7
1950.4	43817.9	431.4	123.9	0.0	9.2	0.0	0.0	2.3	55.1	9.2	4.6	0.0	0.0	0.0	0.0	0.0	4.6	62.0
1950.5	43820.0	548.2	175.8	0.0	18.9	1.9	0.0	0.0	47.3	7.6	0.0	5.7	0.0	0.0	0.0	0.0	0.0	73.7
1950.6	43822.1	683.1	189.0	4.3	12.9	2.1	0.0	0.0	90.2	12.9	2.1	6.4	0.0	2.1	0.0	0.0	2.1	81.6
1950.7	43824.2	698.7	223.0	0.0	16.1	0.0	0.0	0.0	110.2	10.7	0.0	2.7	0.0	0.0	0.0	0.0	8.1	94.1
1950.8	43826.3	596.0	208.5	0.0	23.5	1.5	0.0	0.0	79.3	4.4	2.9	2.9	1.5	0.0	0.0	0.0	4.4	79.3
1950.9	43828.4	697.5	191.3	0.0	12.3	4.1	0.0	0.0	90.5	8.2	4.1	6.2	2.1	0.0	0.0	0.0	4.1	100.8
1951.0	43830.5	1243.5	443.6	3.8	22.7	3.8	0.0	0.0	159.2	30.3	0.0	3.8	3.8	0.0	0.0	0.0	15.2	197.1
1951.1	43832.6	673.9	208.6	1.7	5.0	1.7	0.0	0.0	72.9	14.9	8.3	8.3	0.0	0.0	0.0	0.0	11.6	132.5
1951.2	43834.7	717.6	291.4	0.0	16.5	0.0	0.0	0.0	68.7	19.2	0.0	5.5	0.0	0.0	0.0	0.0	11.0	118.2
1951.3	43836.8	807.6	299.3	0.0	10.8	0.0	0.0	0.0	46.9	32.4	7.2	3.6	0.0	0.0	0.0	0.0	7.2	144.2
1951.4	43838.9	1047.7	385.1	5.7	11.3	5.7	0.0	0.0	56.6	51.0	11.3	11.3	0.0	0.0	0.0	0.0	5.7	215.2
1951.5	43841.0	1316.0	342.2	3.5	14.1	3.5	0.0	0.0	84.7	84.7	0.0	7.1	0.0	0.0	0.0	0.0	10.6	208.2
1951.6	43843.1	1400.4	397.1	0.0	13.9	0.0	0.0	0.0	139.3	125.4	0.0	7.0	0.0	7.0	0.0	0.0	7.0	271.7
1951.7	43845.2	1605.2	512.7	0.0	30.5	0.0	0.0	0.0	73.2	158.7	0.0	6.1	6.1	0.0	0.0	0.0	24.4	335.7
1951.8	43847.3	1326.5	348.0	12.3	24.6	0.0	0.0	0.0	106.4	122.8	4.1	8.2	0.0	0.0	0.0	0.0	28.7	208.8
1951.9	43849.4	1203.5	350.6	4.3	13.0	0.0	0.0	0.0	129.9	147.2	0.0	4.3	0.0	0.0	0.0	0.0	17.3	199.1
1952.0	43851.5	1260.6	357.5	0.0	9.4	0.0	0.0	0.0	47.0	84.7	0.0	9.4	0.0	0.0	0.0	0.0	14.1	188.1
1952.1	43853.8	914.3	260.7	0.0	7.3	0.0	0.0	0.0	66.1	44.1	0.0	3.7	0.0	0.0	0.0	0.0	3.7	143.2
1952.2	43856.0	950.9	271.7	3.7	11.0	3.7	0.0	0.0	51.4	40.4	0.0	3.7	3.7	0.0	0.0	0.0	7.3	117.5
1952.3	43858.3	1481.0	478.8	6.4	19.2	0.0	0.0	0.0	76.6	51.1	0.0	6.4	19.2	12.8	0.0	0.0	19.2	172.4
1952.4	43860.5	1091.0	279.3	7.4	7.4	3.7	0.0	0.0	52.1	14.9	3.7	7.4	3.7	7.4	0.0	0.0	7.4	93.1
1952.5	43862.8	1301.7	310.3	7.6	7.6	0.0	0.0	0.0	117.3	22.7	0.0	0.0	18.9	15.1	0.0	0.0	11.4	128.7

Core MD03-2622 Absolute Abundance Data (continued)

Depth (cm)	Age (yBP)	*G.b* #/g	*N.d* #/g	*O.u* #/g	*G.a* #/g	*G.c* #/g	*P.o* #/g	*G.m* #/g	*G.r*(p) #/g	*G.r*(w) #/g	*G.s* #/g	*G.g* #/g	*G.t* #/g	*G.rs* #/g	*N.p*(l) #/g	*N.p*(r) #/g	*G.q* #/g	Other #/g
1952.6	43865.0	1182.9	283.2	0.0	16.7	3.3	0.0	0.0	66.6	33.3	10.0	10.0	0.0	6.7	0.0	0.0	10.0	130.0
1952.7	43867.3	1132.3	282.0	0.0	13.2	0.0	0.0	0.0	127.8	57.3	4.4	8.8	4.4	48.5	0.0	0.0	13.2	141.0
1952.8	43869.5	1223.4	324.6	0.0	20.8	4.2	0.0	0.0	91.5	66.6	0.0	4.2	0.0	0.0	0.0	0.0	8.3	149.8
1952.9	43871.8	1073.4	302.9	4.5	4.5	0.0	0.0	0.0	57.9	24.5	6.7	8.9	6.7	11.1	0.0	0.0	13.4	126.9
1953.0	43874.0	1121.1	302.7	0.0	7.5	0.0	0.0	0.0	71.0	26.2	3.7	7.5	11.2	3.7	0.0	0.0	11.2	100.9
1953.1	43876.4	948.1	244.2	10.8	10.8	3.6	0.0	0.0	43.1	28.7	0.0	14.4	3.6	0.0	0.0	0.0	7.2	129.3
1953.2	43878.7	933.7	300.3	3.3	6.5	0.0	0.0	0.0	68.6	35.9	0.0	6.5	0.0	3.3	0.0	0.0	9.8	160.0
1953.3	43881.1	893.1	376.6	3.6	10.8	3.6	0.0	0.0	64.6	7.2	7.2	7.2	0.0	0.0	0.0	0.0	17.9	150.6
1953.4	43883.4	961.3	315.0	4.0	16.2	0.0	0.0	0.0	32.3	8.1	4.0	8.1	0.0	4.0	0.0	0.0	8.1	137.3
1953.5	43885.8	941.9	293.6	8.2	8.2	4.1	0.0	0.0	40.8	24.5	4.1	4.1	0.0	0.0	0.0	0.0	16.3	159.0
1953.6	43888.1	751.2	268.6	6.1	6.1	4.0	0.0	2.0	40.4	30.3	4.0	2.0	4.0	0.0	0.0	0.0	6.1	96.9
1953.7	43890.5	707.6	276.0	3.2	6.3	0.0	0.0	0.0	34.9	9.5	3.2	9.5	0.0	3.2	0.0	0.0	9.5	123.7
1953.8	43892.8	796.9	279.0	5.8	0.0	0.0	0.0	0.0	69.0	11.5	0.0	5.8	0.0	0.0	0.0	0.0	14.4	161.1
1953.9	43895.2	915.2	360.6	3.4	10.2	0.0	0.0	0.0	51.0	20.4	3.4	0.0	0.0	0.0	0.0	0.0	17.0	180.3
1996.0	44668.0	391.3	31.6	4.9	7.3	0.0	0.0	0.0	34.0	0.0	7.3	2.4	2.4	0.0	4.9	0.0	19.4	330.5
1996.1	44670.2	534.8	76.7	4.8	2.4	4.8	2.4	0.0	48.0	7.2	4.8	7.2	0.0	0.0	2.4	0.0	50.4	515.6
1996.2	44672.3	427.6	75.0	0.0	4.1	0.0	0.0	0.0	56.7	6.1	2.0	10.1	2.0	0.0	0.0	0.0	42.6	407.3
1996.3	44674.5	394.4	82.9	1.7	1.7	0.0	1.7	1.7	59.2	8.5	1.7	3.4	6.8	0.0	0.0	0.0	20.3	370.7
1996.4	44676.6	332.9	85.4	1.7	8.5	1.7	0.0	1.7	27.3	5.1	5.1	10.2	0.0	0.0	0.0	0.0	18.8	332.9
1996.5	44678.8	226.3	58.1	3.7	7.4	0.0	1.2	0.0	28.4	3.7	0.0	8.7	1.2	0.0	2.5	0.0	14.8	206.6
1996.6	44680.9	299.1	91.7	4.0	0.0	0.0	0.0	2.0	39.9	2.0	6.0	2.0	0.0	0.0	2.0	0.0	17.9	277.2
1996.7	44683.1	274.3	79.8	3.9	5.8	1.9	0.0	1.9	44.7	1.9	5.8	7.8	3.9	0.0	0.0	0.0	27.2	177.0
1996.8	44685.2	385.0	56.4	7.4	12.3	0.0	2.5	0.0	31.9	4.9	12.3	4.9	0.0	0.0	0.0	0.0	27.0	321.3
1996.9	44687.4	341.3	112.7	1.7	8.4	1.7	0.0	1.7	45.4	11.8	3.4	8.4	0.0	0.0	3.4	0.0	26.9	346.4
1997.0	44689.5	408.8	105.6	3.8	7.7	1.9	1.9	0.0	49.9	5.8	7.7	7.7	1.9	0.0	0.0	0.0	30.7	284.1

Core MD03-2622 Absolute Abundance Data (continued)

Depth (cm)	Age (yBP)	*G.b* #/g	*N.d* #/g	*O.u* #/g	*G.a* #/g	*G.c* #/g	*P.o* #/g	*G.m* #/g	*G.r*(p) #/g	*G.r*(w) #/g	*G.s* #/g	*G.g* #/g	*G.t* #/g	*G.rs* #/g	*N.p*(l) #/g	*N.p*(r) #/g	*G.q* #/g	Other #/g
1997.1	44691.9	466.5	102.7	2.2	11.2	4.5	0.0	0.0	46.9	8.9	2.2	2.2	2.2	0.0	2.2	0.0	26.8	352.7
1997.2	44694.3	616.0	104.7	0.0	10.0	0.0	2.5	0.0	54.9	2.5	10.0	12.5	0.0	2.5	5.0	0.0	57.4	503.7
1997.3	44696.7	378.8	84.2	3.8	1.9	5.7	0.0	0.0	51.6	1.9	5.7	3.8	1.9	0.0	1.9	0.0	40.2	296.5
1997.4	44699.1	257.7	99.0	1.4	1.4	0.0	0.0	1.4	39.3	2.7	2.7	5.4	1.4	0.0	4.1	0.0	27.1	230.6
1997.5	44701.5	272.1	64.9	1.4	2.8	2.8	0.0	0.0	27.6	5.5	2.8	1.4	1.4	0.0	1.4	0.0	9.7	183.7
1997.6	44703.9	196.3	53.7	1.2	3.5	0.0	0.0	1.2	28.0	2.3	2.3	3.5	0.0	0.0	2.3	0.0	7.0	158.9
1997.7	44706.3	155.2	33.1	0.9	0.9	0.0	0.0	0.0	17.0	2.8	0.9	2.8	1.9	0.0	0.0	0.0	5.7	141.0
1997.8	44708.7	172.7	32.0	1.0	3.0	0.0	0.0	1.0	16.0	5.0	1.0	5.0	3.0	0.0	1.0	0.0	12.0	200.7
1997.9	44711.1	183.0	47.0	0.0	4.1	1.0	0.0	0.0	19.4	1.0	1.0	1.0	3.1	0.0	1.0	0.0	11.2	176.9
1998.0	44713.5	242.7	57.7	3.3	5.4	2.2	1.1	2.2	21.8	2.2	1.1	2.2	1.1	0.0	2.2	0.0	14.1	228.5
1998.1	44715.6	232.1	55.1	6.0	6.0	0.0	0.0	0.0	29.8	3.0	0.0	1.5	3.0	0.0	0.0	0.0	8.9	208.3
1998.2	44717.7	261.6	56.2	3.0	7.4	1.5	0.0	0.0	25.1	4.4	3.0	3.0	3.0	0.0	0.0	0.0	19.2	233.6
1998.3	44719.8	320.2	55.4	1.7	5.2	1.7	0.0	1.7	50.2	3.5	5.2	1.7	0.0	0.0	0.0	0.0	27.7	294.2
1998.4	44721.9	311.5	84.1	5.7	1.9	0.0	1.9	0.0	28.7	3.8	0.0	3.8	1.9	0.0	0.0	0.0	22.9	273.3
1998.5	44724.0	320.3	85.4	7.1	0.0	0.0	2.4	0.0	42.7	2.4	2.4	9.5	0.0	0.0	0.0	0.0	16.6	249.1
1998.6	44726.1	327.9	101.0	1.9	5.7	5.7	3.8	0.0	49.6	5.7	1.9	7.6	5.7	0.0	0.0	0.0	11.4	324.1
1998.7	44728.2	332.8	88.0	4.3	8.6	0.0	6.4	0.0	45.1	2.1	0.0	6.4	2.1	0.0	0.0	0.0	21.5	296.3
1998.8	44730.3	255.2	60.9	1.1	3.4	1.1	0.0	0.0	39.1	2.3	3.4	4.6	3.4	0.0	0.0	0.0	11.5	231.0
1998.9	44732.4	265.2	99.5	5.9	2.0	3.9	0.0	0.0	27.3	9.8	5.9	2.0	0.0	0.0	0.0	0.0	17.6	267.2
1999.0	44734.5	153.6	51.6	2.2	3.3	0.0	0.0	0.0	34.0	2.2	0.0	2.2	3.3	0.0	0.0	0.0	6.6	144.8
1999.1	44736.2	282.0	57.5	0.0	3.7	1.9	0.0	0.0	29.7	0.0	3.7	9.3	3.7	0.0	0.0	0.0	13.0	259.7
1999.2	44737.9	347.2	82.9	0.0	2.6	5.2	0.0	0.0	25.9	2.6	5.2	7.8	0.0	0.0	0.0	0.0	31.1	305.7
1999.3	44739.6	163.4	39.0	0.0	0.0	1.9	0.0	1.0	24.7	2.9	1.9	2.9	2.9	0.0	0.0	0.0	12.4	147.3
1999.4	44741.3	161.5	40.4	2.0	2.0	0.0	1.0	0.0	20.7	1.0	2.0	2.0	0.0	0.0	0.0	0.0	9.8	105.4
1999.5	44743.0	72.5	6.7	0.0	0.0	0.7	0.0	0.0	3.7	0.7	0.0	0.0	0.0	0.0	0.0	0.0	3.7	32.1
1999.6	44744.7	144.5	34.8	3.0	0.8	0.8	0.8	0.0	18.9	2.3	0.8	1.5	0.0	0.0	0.0	0.0	6.8	98.3
1999.7	44746.4	81.3	34.3	0.6	1.7	1.1	0.6	0.0	15.5	1.7	0.6	1.7	0.6	0.0	0.0	0.0	5.5	68.0
1999.8	44748.1	157.1	34.1	3.6	2.7	1.8	0.9	0.0	26.9	3.6	1.8	0.9	0.9	0.0	0.9	0.0	4.5	116.7

Core MD03-2622 Absolute Abundance Data (continued)

Depth (cm)	Age (yBP)	*G.b* #/g	*N.d* #/g	*O.u* #/g	*G.a* #/g	*G.c* #/g	*P.o* #/g	*G.m* #/g	*G.r*(p) #/g	*G.r*(w) #/g	*G.s* #/g	*G.g* #/g	*G.t* #/g	*G.rs* #/g	*N.p*(l) #/g	*N.p*(r) #/g	*G.q* #/g	Other #/g
1999.9	44749.8	413.4	59.6	0.0	5.4	3.6	0.0	3.6	37.9	1.8	0.0	1.8	1.8	0.0	0.0	0.0	25.3	285.2
2000.0	44751.5	808.0	159.7	0.0	9.4	0.0	0.0	0.0	56.4	14.1	0.0	4.7	9.4	0.0	0.0	0.0	32.9	638.9
2000.1	44754.1	624.4	165.8	3.5	0.0	0.0	0.0	0.0	63.5	14.1	0.0	3.5	0.0	0.0	3.5	0.0	52.9	522.1
2000.2	44756.6	798.8	139.4	0.0	3.8	3.8	3.8	0.0	49.0	3.8	3.8	3.8	15.1	0.0	7.5	0.0	22.6	602.8
2000.3	44759.2	1078.1	217.4	4.4	8.9	0.0	4.4	0.0	44.4	8.9	0.0	4.4	0.0	0.0	0.0	0.0	48.8	665.5
2000.4	44761.7	786.1	169.5	0.0	0.0	7.7	0.0	0.0	50.1	3.9	0.0	0.0	0.0	0.0	0.0	0.0	30.8	443.1
2000.5	44764.3	680.9	181.8	0.0	0.0	0.0	0.0	0.0	50.7	4.2	0.0	4.2	0.0	0.0	0.0	0.0	12.7	363.7
2000.6	44766.8	608.2	110.6	0.0	2.8	0.0	0.0	0.0	38.7	2.8	0.0	0.0	0.0	0.0	0.0	0.0	19.4	287.5
2000.7	44769.4	854.9	146.2	0.0	7.5	0.0	3.7	0.0	56.2	7.5	0.0	0.0	0.0	0.0	0.0	0.0	22.5	345.0
2000.8	44771.9	784.1	153.8	0.0	0.0	0.0	0.0	0.0	55.4	3.1	0.0	3.1	3.1	0.0	6.2	0.0	36.9	399.8
2000.9	44774.5	842.4	158.9	0.0	3.0	0.0	0.0	0.0	54.0	6.0	0.0	3.0	0.0	0.0	0.0	0.0	27.0	398.7
2001.0	44777.0	1050.9	167.5	0.0	0.0	4.2	0.0	0.0	75.4	16.7	0.0	0.0	0.0	0.0	0.0	0.0	75.4	510.8
2001.1	44779.1	1144.9	238.3	0.0	0.0	0.0	0.0	0.0	60.7	4.7	4.7	9.3	4.7	0.0	0.0	0.0	37.4	560.7
2001.2	44781.2	1013.5	182.4	0.0	3.5	0.0	0.0	0.0	28.1	14.0	0.0	0.0	3.5	0.0	0.0	0.0	35.1	487.4
2001.3	44783.3	955.5	265.4	7.1	3.5	0.0	0.0	0.0	63.7	0.0	7.1	0.0	3.5	0.0	0.0	0.0	46.0	527.3
2001.4	44785.4	753.7	124.0	3.3	3.3	0.0	3.3	0.0	22.8	3.3	0.0	0.0	3.3	0.0	0.0	0.0	22.8	365.4
2001.5	44787.5	527.8	76.7	0.0	0.0	0.0	2.3	0.0	41.9	7.0	0.0	0.0	4.7	0.0	0.0	0.0	18.6	299.9
2001.6	44789.6	558.6	84.9	0.0	0.0	2.7	2.7	0.0	30.1	2.7	0.0	0.0	0.0	0.0	0.0	0.0	16.4	260.1
2001.7	44791.7	345.0	66.3	0.0	1.7	1.7	0.0	0.0	45.9	1.7	0.0	0.0	0.0	0.0	0.0	0.0	13.6	175.1
2001.8	44793.8	466.0	85.0	3.4	0.0	1.7	0.0	0.0	45.9	1.7	3.4	1.7	3.4	0.0	0.0	0.0	34.0	227.9
2001.9	44795.9	393.7	77.5	6.0	4.0	2.0	0.0	0.0	53.7	4.0	2.0	0.0	0.0	0.0	0.0	0.0	15.9	204.8
2002.0	44798.0	453.0	66.7	6.9	0.0	0.0	0.0	2.3	52.9	6.9	2.3	0.0	6.9	0.0	0.0	0.0	16.1	207.0
2002.1	44800.3	758.7	169.9	0.0	0.0	0.0	0.0	0.0	47.4	4.0	11.9	4.0	0.0	0.0	0.0	0.0	23.7	320.1
2002.2	44802.6	661.0	144.3	3.8	0.0	0.0	3.8	0.0	72.2	11.4	0.0	0.0	7.6	0.0	0.0	0.0	19.0	265.9
2002.3	44804.9	603.4	141.1	0.0	0.0	0.0	0.0	0.0	60.0	3.0	0.0	6.0	3.0	0.0	0.0	0.0	18.0	297.2
2002.4	44807.2	658.9	129.6	0.0	0.0	0.0	0.0	0.0	32.4	3.6	3.6	0.0	7.2	0.0	0.0	0.0	25.2	248.4
2002.5	44809.5	737.6	137.0	0.0	0.0	8.1	4.0	0.0	72.6	12.1	4.0	4.0	8.1	0.0	0.0	0.0	44.3	262.0
2002.6	44811.8	543.2	118.9	0.0	2.0	2.0	0.0	0.0	43.0	6.1	2.0	0.0	0.0	0.0	0.0	0.0	34.8	272.6

Core MD03-2622 Absolute Abundance Data (continued)

Depth (cm)	Age (yBP)	*G.b* #/g	*N.d* #/g	*O.u* #/g	*G.a* #/g	*G.c* #/g	*P.o* #/g	*G.m* #/g	*G.r*(p) #/g	*G.r*(w) #/g	*G.s* #/g	*G.g* #/g	*G.t* #/g	*G.rs* #/g	*N.p*(l) #/g	*N.p*(r) #/g	*G.q* #/g	Other #/g
2002.7	44814.1	427.2	130.3	0.0	0.0	0.0	2.1	0.0	42.7	4.3	2.1	0.0	2.1	0.0	0.0	0.0	21.4	200.8
2002.8	44816.4	606.0	120.5	0.0	0.0	0.0	7.3	0.0	25.6	14.6	3.7	0.0	0.0	0.0	0.0	0.0	32.9	306.7
2002.9	44818.7	567.7	142.6	0.0	5.6	0.0	0.0	0.0	50.3	2.8	0.0	2.8	2.8	0.0	0.0	0.0	36.4	271.3
2003.0	44821.0	642.8	118.4	4.6	9.3	0.0	2.3	0.0	46.4	11.6	2.3	2.3	2.3	0.0	0.0	0.0	20.9	294.7
2003.1	44822.9	955.6	185.4	0.0	0.0	0.0	4.8	0.0	76.1	9.5	9.5	0.0	4.8	0.0	0.0	0.0	57.0	389.8
2003.2	44824.7	1050.5	345.5	0.0	0.0	4.7	4.7	0.0	84.0	18.7	14.0	4.7	4.7	0.0	0.0	0.0	79.4	485.6
2003.3	44826.6	944.4	160.3	0.0	0.0	8.7	8.7	0.0	69.3	4.3	4.3	0.0	4.3	0.0	0.0	0.0	39.0	346.6
2003.4	44828.4	965.3	179.0	3.2	3.2	6.4	6.4	0.0	38.4	16.0	9.6	3.2	0.0	0.0	0.0	0.0	38.4	453.9
2003.5	44830.3	650.7	214.2	0.0	0.0	8.2	0.0	0.0	86.5	8.2	0.0	0.0	4.1	0.0	0.0	0.0	57.7	329.5
2003.6	44832.1	801.5	185.6	4.2	4.2	0.0	0.0	0.0	46.4	4.2	8.4	0.0	0.0	0.0	0.0	0.0	42.2	333.2
2003.7	44834.0	634.0	144.1	4.1	4.1	4.1	4.1	0.0	98.8	8.2	4.1	0.0	4.1	0.0	4.1	0.0	53.5	304.6
2003.8	44835.8	533.2	146.9	0.0	3.2	6.4	0.0	0.0	57.5	9.6	6.4	3.2	0.0	0.0	0.0	0.0	25.5	287.3
2003.9	44837.7	729.1	140.6	3.7	3.7	3.7	0.0	0.0	62.9	3.7	0.0	3.7	7.4	0.0	0.0	0.0	37.0	344.2
2004.0	44839.5	544.5	120.4	2.9	8.6	0.0	0.0	0.0	65.9	5.7	2.9	2.9	5.7	0.0	0.0	0.0	25.8	286.6
2004.1	44841.7	615.7	109.5	0.0	0.0	5.9	3.0	0.0	32.6	3.0	0.0	3.0	0.0	0.0	0.0	0.0	20.7	340.4
2004.2	44843.9	715.1	97.7	0.0	0.0	3.5	3.5	0.0	48.8	3.5	0.0	3.5	3.5	0.0	0.0	0.0	41.9	341.9
2004.3	44846.1	757.5	148.5	3.8	0.0	3.8	0.0	0.0	60.9	3.8	0.0	0.0	7.6	0.0	0.0	0.0	41.9	308.3
2004.4	44848.3	1016.8	151.0	0.0	3.7	7.4	0.0	0.0	47.9	3.7	0.0	3.7	0.0	7.4	0.0	0.0	62.6	445.8
2004.5	44850.5	715.4	90.3	2.4	4.8	2.4	4.8	0.0	42.8	7.1	4.8	7.1	2.4	2.4	4.8	0.0	30.9	297.1
2004.6	44852.7	1235.9	129.3	4.8	0.0	4.8	0.0	0.0	81.4	0.0	4.8	0.0	0.0	0.0	0.0	0.0	47.9	550.9
2004.7	44854.9	1838.9	221.5	6.7	26.8	13.4	0.0	0.0	47.0	6.7	0.0	20.1	0.0	0.0	20.1	0.0	40.3	617.4
2004.8	44857.1	963.9	114.1	0.0	11.8	3.9	0.0	0.0	39.3	11.8	0.0	3.9	0.0	0.0	0.0	0.0	3.9	405.2
2004.9	44859.3	765.9	153.9	3.7	3.7	0.0	0.0	3.7	73.3	3.7	0.0	7.3	0.0	0.0	11.0	0.0	14.7	381.1
2005.0	44861.5	813.6	76.5	0.0	0.0	0.0	3.5	0.0	48.7	3.5	3.5	0.0	0.0	0.0	20.9	0.0	55.6	427.7
2005.1	44863.5	644.5	110.7	2.5	2.5	2.5	4.9	0.0	78.7	4.9	0.0	7.4	0.0	0.0	4.9	0.0	14.8	344.4
2005.2	44865.4	780.9	130.6	0.0	10.7	0.0	0.0	10.7	77.3	16.0	0.0	8.0	2.7	0.0	0.0	0.0	5.3	199.9
2005.3	44867.4	816.6	59.5	0.0	3.3	0.0	6.6	3.3	69.4	9.9	0.0	13.2	6.6	0.0	0.0	0.0	6.6	320.7
2005.4	44869.3	629.8	125.3	3.1	3.1	3.1	0.0	0.0	73.4	21.4	3.1	18.3	0.0	0.0	6.1	0.0	27.5	211.0

Core MD03-2622 Absolute Abundance Data (continued)

Depth (cm)	Age (yBP)	*G.b* #/g	*N.d* #/g	*O.u* #/g	*G.a* #/g	*G.c* #/g	*P.o* #/g	*G.m* #/g	*G.r*(p) #/g	*G.r*(w) #/g	*G.s* #/g	*G.g* #/g	*G.t* #/g	*G.rs* #/g	*N.p*(l) #/g	*N.p*(r) #/g	*G.q* #/g	Other #/g
2005.5	44871.3	809.7	109.9	0.0	4.1	4.1	4.1	0.0	44.8	12.2	0.0	4.1	0.0	0.0	4.1	0.0	20.3	260.4
2005.6	44873.2	635.5	125.2	0.0	2.4	0.0	0.0	0.0	82.7	23.6	2.4	7.1	4.7	0.0	0.0	0.0	9.4	342.5
2005.7	44875.2	586.2	152.1	0.0	0.0	7.4	0.0	0.0	85.3	7.4	0.0	3.7	0.0	0.0	11.1	0.0	33.4	282.0
2005.8	44877.1	1060.2	177.4	4.4	0.0	4.4	0.0	0.0	106.5	22.2	8.9	13.3	4.4	4.4	0.0	0.0	4.4	647.6
2005.9	44879.1	620.7	100.6	0.0	3.5	0.0	0.0	0.0	59.0	0.0	0.0	3.5	3.5	0.0	0.0	0.0	62.4	277.4
2006.0	44881.0	984.8	160.0	12.3	16.4	8.2	0.0	0.0	73.9	16.4	4.1	8.2	0.0	0.0	4.1	0.0	32.8	549.9
2006.1	44882.9	998.9	136.6	0.0	7.8	3.9	0.0	0.0	93.6	7.8	0.0	3.9	3.9	0.0	3.9	0.0	39.0	542.4
2006.2	44884.8	852.1	127.0	8.2	4.1	0.0	0.0	0.0	49.2	16.4	0.0	12.3	4.1	0.0	0.0	0.0	28.7	422.0
2006.3	44886.7	422.2	78.6	0.0	0.0	0.0	0.0	0.0	31.4	11.2	0.0	2.2	2.2	2.2	4.5	0.0	15.7	197.6
2006.4	44888.6	366.3	53.1	0.0	5.5	0.0	0.0	0.0	36.6	9.2	1.8	9.2	1.8	0.0	0.0	0.0	1.8	157.5
2006.5	44890.5	491.1	116.6	4.5	4.5	0.0	2.2	0.0	38.1	9.0	4.5	6.7	0.0	0.0	0.0	0.0	11.2	262.4
2006.6	44892.4	458.4	82.5	0.0	4.9	2.4	0.0	0.0	41.2	7.3	0.0	4.9	0.0	0.0	2.4	0.0	14.6	220.7
2006.7	44894.3	367.8	81.3	1.7	1.7	1.7	0.0	1.7	61.0	15.3	0.0	3.4	0.0	0.0	5.1	0.0	30.5	274.6
2006.8	44896.2	502.3	108.0	1.9	3.8	1.9	0.0	1.9	60.7	7.6	5.7	13.3	1.9	1.9	1.9	0.0	13.3	248.3
2006.9	44898.1	320.2	61.1	5.0	3.3	5.0	0.0	1.7	47.9	5.0	0.0	3.3	0.0	0.0	3.3	0.0	18.2	104.0
2007.0	44900.0	518.6	98.7	0.0	13.5	0.0	0.0	0.0	77.4	3.9	5.8	5.8	1.9	0.0	0.0	0.0	15.5	207.1
2007.1	44902.1	1030.3	143.1	0.0	4.1	0.0	0.0	0.0	171.7	24.5	0.0	12.3	4.1	0.0	8.2	0.0	36.8	731.8
2007.2	44904.1	478.1	69.7	0.0	5.0	7.5	0.0	0.0	82.2	12.5	5.0	5.0	0.0	0.0	2.5	0.0	7.5	420.8
2007.3	44906.2	582.3	85.5	0.0	8.1	0.0	0.0	0.0	85.5	16.3	0.0	0.0	0.0	0.0	0.0	0.0	20.4	435.7
2007.4	44908.2	587.0	132.3	4.6	7.0	0.0	4.6	0.0	67.3	13.9	2.3	4.6	7.0	0.0	9.3	0.0	30.2	494.2
2007.5	44910.3	979.5	117.4	4.5	4.5	4.5	0.0	0.0	40.6	4.5	0.0	4.5	0.0	0.0	4.5	0.0	45.1	600.3
2007.6	44912.3	648.6	148.6	3.6	3.6	0.0	0.0	0.0	61.6	25.4	3.6	7.2	3.6	0.0	10.9	0.0	36.2	605.2
2007.7	44914.4	874.2	211.2	4.2	8.4	0.0	4.2	0.0	63.3	12.7	4.2	8.4	8.4	0.0	8.4	0.0	71.8	743.3
2007.8	44916.4	820.6	113.0	8.4	8.4	0.0	4.2	0.0	113.0	12.6	4.2	8.4	4.2	0.0	4.2	0.0	75.4	711.7
2007.9	44918.5	751.2	150.2	3.8	7.5	3.8	3.8	0.0	60.1	22.5	0.0	7.5	3.8	0.0	7.5	0.0	33.8	612.2
2008.0	44920.5	762.5	131.3	4.2	4.2	4.2	4.2	0.0	114.4	8.5	4.2	4.2	4.2	0.0	12.7	0.0	29.7	648.1
2008.1	44921.9	807.0	116.9	3.7	3.7	3.7	0.0	0.0	124.2	14.6	3.7	3.7	3.7	0.0	11.0	0.0	11.0	664.6
2008.2	44923.2	609.8	107.2	11.1	0.0	7.4	7.4	0.0	70.2	25.9	11.1	7.4	0.0	0.0	7.4	0.0	7.4	650.5

Core MD03-2622 Absolute Abundance Data (continued)

Depth (cm)	Age (yBP)	*G.b* #/g	*N.d* #/g	*O.u* #/g	*G.a* #/g	*G.c* #/g	*P.o* #/g	*G.m* #/g	*G.r*(p) #/g	*G.r*(w) #/g	*G.s* #/g	*G.g* #/g	*G.t* #/g	*G.rs* #/g	*N.p*(l) #/g	*N.p*(r) #/g	*G.q* #/g	Other #/g
2008.3	44924.6	673.7	94.6	3.9	0.0	0.0	3.9	0.0	67.0	15.8	0.0	11.8	3.9	0.0	3.9	0.0	27.6	559.4
2008.4	44925.9	485.2	70.8	3.4	3.4	3.4	0.0	0.0	57.3	6.7	0.0	13.5	0.0	0.0	6.7	0.0	50.5	535.7
2008.5	44927.3	570.3	118.1	0.0	12.2	0.0	4.1	0.0	57.0	12.2	4.1	0.0	4.1	0.0	0.0	0.0	24.4	594.7
2008.6	44928.6	522.8	104.1	2.4	4.7	0.0	2.4	0.0	40.2	4.7	4.7	2.4	0.0	0.0	0.0	0.0	26.0	615.1
2008.7	44930.0	606.7	89.7	0.0	4.3	4.3	4.3	0.0	64.1	4.3	4.3	4.3	0.0	0.0	0.0	0.0	68.4	875.8
2008.8	44931.3	615.6	67.6	0.0	7.5	0.0	0.0	3.8	90.1	3.8	0.0	7.5	3.8	0.0	0.0	0.0	75.1	822.0
2008.9	44932.7	703.5	120.4	3.8	0.0	3.8	0.0	0.0	90.3	3.8	7.5	3.8	7.5	0.0	0.0	0.0	86.5	823.9
2009.0	44934.0	885.3	136.5	0.0	0.0	0.0	0.0	0.0	30.8	0.0	0.0	8.8	13.2	0.0	4.4	0.0	79.3	616.6
2009.1	44935.9	839.5	117.1	0.0	4.9	0.0	0.0	0.0	68.3	4.9	0.0	9.8	0.0	0.0	9.8	0.0	83.0	697.9
2009.2	44937.8	718.8	75.7	0.0	3.8	0.0	7.6	0.0	64.3	7.6	0.0	7.6	11.3	3.8	11.3	0.0	113.5	518.3
2009.3	44939.7	773.0	78.2	0.0	4.3	4.3	0.0	0.0	99.9	4.3	0.0	8.7	17.4	0.0	8.7	0.0	91.2	568.9
2009.4	44941.6	688.2	63.1	9.0	15.0	6.0	0.0	0.0	51.1	3.0	0.0	12.0	12.0	0.0	9.0	0.0	78.1	474.8
2009.5	44943.5	806.9	115.8	0.0	3.9	0.0	0.0	0.0	65.6	3.9	7.7	7.7	11.6	0.0	7.7	0.0	77.2	494.2
2009.6	44945.4	792.8	77.5	0.0	4.6	4.6	0.0	0.0	136.7	4.6	0.0	9.1	9.1	0.0	9.1	0.0	104.8	510.3
2009.7	44947.3	644.2	103.9	0.0	4.2	0.0	0.0	0.0	83.1	8.3	8.3	4.2	0.0	0.0	4.2	0.0	66.5	473.8
2009.8	44949.2	676.3	135.3	4.5	9.0	4.5	0.0	0.0	139.8	13.5	4.5	4.5	0.0	0.0	9.0	0.0	54.1	496.0
2009.9	44951.1	570.8	75.5	0.0	0.0	3.0	3.0	0.0	105.7	12.1	6.0	6.0	3.0	0.0	0.0	0.0	48.3	428.8
2010.0	44953.0	559.1	112.3	0.0	2.6	0.0	5.2	0.0	86.2	2.6	2.6	7.8	2.6	0.0	2.6	0.0	52.3	357.9
2010.1	44955.1	723.8	65.8	8.8	0.0	0.0	0.0	0.0	79.0	4.4	0.0	4.4	0.0	0.0	4.4	0.0	57.0	465.0
2010.2	44957.2	530.5	89.7	2.5	2.5	0.0	0.0	0.0	87.2	7.5	0.0	5.0	2.5	0.0	5.0	0.0	52.3	363.7
2010.3	44959.3	583.4	96.2	9.6	16.0	3.2	0.0	0.0	60.9	6.4	0.0	0.0	0.0	0.0	0.0	0.0	51.3	384.7
2010.4	44961.4	696.8	82.0	10.2	3.4	0.0	0.0	0.0	75.1	6.8	10.2	6.8	3.4	0.0	6.8	0.0	27.3	556.8
2010.5	44963.5	547.5	78.8	6.6	8.8	2.2	4.4	2.2	65.7	11.0	4.4	11.0	4.4	0.0	4.4	0.0	39.4	453.4
2010.6	44965.6	373.3	62.2	3.3	1.6	0.0	0.0	1.6	55.7	11.5	9.8	4.9	1.6	0.0	0.0	0.0	39.3	284.9
2010.7	44967.7	133.3	21.4	3.1	0.8	0.0	0.8	0.0	19.1	1.5	3.1	1.5	0.0	0.0	0.0	0.0	10.0	101.9
2010.8	44969.8	70.4	8.7	0.3	2.0	1.3	0.3	0.0	10.0	2.3	2.0	0.7	0.0	0.0	0.3	0.0	4.3	44.0
2010.9	44971.9	102.3	17.3	0.8	1.6	0.0	0.4	0.4	10.9	1.6	0.8	1.6	0.4	0.0	0.0	0.0	6.0	61.6
2011.0	44974.0	220.0	35.0	4.4	7.3	4.4	0.0	1.5	17.5	2.9	4.4	4.4	1.5	0.0	0.0	0.0	10.2	138.4

Core MD03-2622 Absolute Abundance Data (continued)

Depth (cm)	Age (yBP)	*G.b* #/g	*N.d* #/g	*O.u* #/g	*G.a* #/g	*G.c* #/g	*P.o* #/g	*G.m* #/g	*G.r*(p) #/g	*G.r*(w) #/g	*G.s* #/g	*G.g* #/g	*G.t* #/g	*G.rs* #/g	*N.p*(l) #/g	*N.p*(r) #/g	*G.q* #/g	Other #/g
2011.1	44975.3	321.1	65.0	4.1	0.0	4.1	0.0	2.0	48.8	10.2	4.1	2.0	4.1	0.0	2.0	0.0	36.6	256.0
2011.2	44976.5	513.8	115.6	0.0	2.1	6.4	4.3	2.1	81.3	15.0	8.6	10.7	4.3	0.0	0.0	0.0	49.2	423.9
2011.3	44977.8	586.8	130.8	4.0	0.0	0.0	4.0	0.0	79.3	4.0	11.9	7.9	0.0	0.0	0.0	0.0	47.6	440.1
2011.4	44979.0	555.9	139.9	3.6	7.2	0.0	3.6	0.0	82.5	14.3	3.6	14.3	7.2	0.0	3.6	0.0	43.0	484.2
2011.5	44980.3	515.7	150.6	3.8	3.8	0.0	15.1	0.0	86.6	0.0	3.8	15.1	3.8	0.0	0.0	0.0	33.9	455.5
2011.6	44981.5	436.7	157.9	4.6	2.3	9.3	4.6	0.0	85.9	0.0	2.3	7.0	2.3	0.0	4.6	0.0	25.6	504.0
2011.7	44982.8	449.1	131.0	3.7	3.7	0.0	0.0	0.0	82.3	3.7	3.7	3.7	0.0	0.0	3.7	0.0	44.9	404.2
2011.8	44984.0	429.3	89.3	1.9	0.0	0.0	1.9	0.0	93.2	5.8	0.0	1.9	3.9	0.0	0.0	0.0	17.5	371.0
2011.9	44985.3	451.0	138.8	0.0	0.0	0.0	3.5	0.0	97.1	6.9	3.5	3.5	6.9	0.0	3.5	0.0	27.8	444.0
2012.0	44986.5	424.7	79.5	2.1	0.0	0.0	0.0	2.1	100.4	2.1	4.2	6.3	0.0	0.0	0.0	0.0	33.5	422.6
2012.1	44988.7	452.0	101.8	2.5	5.0	2.5	0.0	0.0	111.8	5.0	0.0	17.4	0.0	0.0	0.0	0.0	67.1	462.0
2012.2	44990.8	450.8	126.5	0.0	2.0	2.0	0.0	0.0	120.4	6.1	6.1	8.2	6.1	0.0	0.0	0.0	42.8	381.5
2012.3	44993.0	481.4	116.4	6.3	6.3	0.0	0.0	0.0	135.3	6.3	3.1	3.1	9.4	0.0	0.0	0.0	28.3	409.0
2012.4	44995.1	505.4	121.2	3.0	0.0	0.0	3.0	0.0	112.3	3.0	3.0	5.9	14.8	0.0	0.0	0.0	47.3	360.5
2012.5	44997.3	516.7	162.9	11.9	4.0	4.0	4.0	0.0	119.2	4.0	0.0	0.0	7.9	0.0	0.0	0.0	51.7	405.4
2012.6	44999.4	456.8	137.4	6.1	4.0	4.0	2.0	0.0	99.0	4.0	2.0	6.1	4.0	0.0	0.0	0.0	52.5	424.4
2012.7	45001.6	564.8	190.7	3.7	7.3	3.7	0.0	0.0	99.0	0.0	0.0	11.0	11.0	0.0	0.0	0.0	55.0	429.1
2012.8	45003.7	554.9	163.2	3.3	6.5	0.0	0.0	6.5	150.2	6.5	0.0	6.5	9.8	0.0	0.0	0.0	71.8	463.5
2012.9	45005.9	511.3	96.5	0.0	0.0	3.6	3.6	0.0	210.9	3.6	0.0	14.3	7.2	0.0	3.6	0.0	107.3	429.1
2013.0	45008.0	445.4	146.2	6.8	0.0	0.0	0.0	0.0	132.6	3.4	0.0	3.4	3.4	0.0	0.0	0.0	51.0	353.6
2013.1	45010.3	411.7	119.2	1.8	0.0	3.6	3.6	0.0	84.9	1.8	0.0	3.6	1.8	0.0	0.0	0.0	32.5	321.4
2013.2	45012.5	373.1	126.1	1.7	1.7	0.0	3.5	0.0	74.3	5.2	1.7	3.5	5.2	0.0	0.0	0.0	22.5	295.4
2013.3	45014.8	451.0	107.9	7.7	1.9	1.9	5.8	1.9	67.5	3.9	3.9	3.9	1.9	0.0	0.0	0.0	40.5	346.9
2013.4	45017.0	362.2	108.8	4.0	0.0	0.0	2.0	0.0	61.3	2.0	5.9	4.0	0.0	2.0	0.0	0.0	19.8	257.3
2013.5	45019.3	325.4	82.8	1.9	1.9	0.0	0.0	1.9	67.4	7.7	1.9	0.0	3.9	0.0	1.9	0.0	28.9	273.4
2013.6	45021.5	413.4	83.1	4.2	4.2	2.1	0.0	4.2	72.7	4.2	4.2	0.0	12.5	0.0	0.0	0.0	14.5	315.7
2013.7	45023.8	430.7	79.8	2.1	2.1	2.1	0.0	0.0	46.2	4.2	2.1	0.0	2.1	0.0	0.0	0.0	35.7	342.5
2013.8	45026.0	483.6	72.4	0.0	3.3	0.0	0.0	0.0	102.0	9.9	0.0	3.3	6.6	0.0	0.0	0.0	49.3	417.8

Core MD03-2622 Absolute Abundance Data (continued)

Depth (cm)	Age (yBP)	*G.b* #/g	*N.d* #/g	*O.u* #/g	*G.a* #/g	*G.c* #/g	*P.o* #/g	*G.m* #/g	*G.r*(p) #/g	*G.r*(w) #/g	*G.s* #/g	*G.g* #/g	*G.t* #/g	*G.rs* #/g	*N.p*(l) #/g	*N.p*(r) #/g	*G.q* #/g	Other #/g
2013.9	45028.3	334.9	42.9	2.9	1.4	1.4	2.9	1.4	54.4	4.3	0.0	2.9	0.0	0.0	1.4	0.0	17.2	247.6
2014.0	45030.5	422.3	53.3	2.0	0.0	2.0	2.0	2.0	39.5	9.9	5.9	7.9	3.9	0.0	2.0	0.0	63.1	331.5
2014.1	45032.5	457.8	48.9	3.6	3.6	3.6	0.0	0.0	61.5	1.8	1.8	5.4	5.4	0.0	1.8	0.0	68.8	347.4
2014.2	45034.5	505.8	46.8	3.7	3.7	1.9	1.9	0.0	35.6	11.2	0.0	1.9	3.7	0.0	3.7	0.0	54.3	444.0
2014.3	45036.5	358.6	32.9	1.6	1.6	0.0	0.0	0.0	25.1	6.3	0.0	0.0	3.1	0.0	1.6	0.0	26.6	270.9
2014.4	45038.5	303.7	59.9	1.5	1.5	2.9	0.0	0.0	42.3	2.9	1.5	2.9	0.0	0.0	0.0	0.0	24.8	255.5
2014.5	45040.5	323.2	25.0	5.8	1.9	0.0	0.0	0.0	30.8	9.6	1.9	7.7	0.0	0.0	3.8	0.0	38.5	296.3
2014.6	45042.5	339.6	30.7	0.0	0.0	0.0	1.7	0.0	27.3	1.7	1.7	3.4	3.4	1.7	0.0	0.0	17.1	250.9
2014.7	45044.5	345.2	28.4	2.0	6.1	0.0	0.0	0.0	28.4	8.1	2.0	0.0	0.0	0.0	0.0	0.0	24.4	241.6
2014.8	45046.5	275.9	26.9	3.4	1.7	1.7	1.7	0.0	28.6	1.7	0.0	1.7	3.4	0.0	0.0	0.0	26.9	188.4
2014.9	45048.5	208.8	32.5	3.1	0.0	2.1	1.0	2.1	32.5	1.0	2.1	3.1	1.0	0.0	2.1	0.0	30.4	173.1
2015.0	45050.5	175.2	21.9	1.8	2.7	0.0	0.9	0.0	15.5	1.8	0.9	1.8	0.0	0.0	0.0	0.0	9.1	131.4
2015.1	45051.7	115.0	11.9	1.0	1.0	0.5	0.0	0.0	15.2	2.4	0.5	0.5	1.4	0.5	0.5	0.0	7.6	86.0
2015.2	45052.8	132.8	17.6	0.0	0.8	0.0	0.0	1.5	18.3	1.5	0.0	0.8	0.8	0.0	0.0	0.0	4.6	81.7
2015.3	45054.0	122.4	8.6	0.0	0.0	0.8	0.8	0.8	15.7	1.6	1.6	1.6	3.1	0.0	0.0	0.0	9.4	78.4
2015.4	45055.1	238.5	19.6	1.1	0.0	0.0	1.1	0.0	25.1	4.4	1.1	0.0	3.3	0.0	0.0	0.0	16.3	205.8
2015.5	45056.3	354.7	59.1	0.0	6.6	0.0	2.2	0.0	21.9	8.8	2.2	4.4	2.2	0.0	0.0	0.0	30.6	328.4
2015.6	45057.4	492.3	74.8	0.0	8.3	0.0	0.0	2.1	33.2	2.1	2.1	2.1	2.1	2.1	2.1	0.0	22.9	405.1
2015.7	45058.6	372.5	64.2	3.1	1.6	0.0	0.0	0.0	31.3	7.8	1.6	3.1	1.6	0.0	4.7	0.0	32.9	314.6
2015.8	45059.7	385.1	75.6	4.1	5.5	1.4	2.8	1.4	50.9	4.1	6.9	4.1	2.8	1.4	1.4	0.0	26.1	240.7
2015.9	45060.9	347.3	56.9	0.0	4.6	0.0	1.5	0.0	29.2	4.6	3.1	4.6	3.1	0.0	1.5	0.0	35.3	307.4
2016.0	45062.0	332.6	49.6	1.7	1.7	0.0	0.0	0.0	41.4	6.6	1.7	5.0	3.3	0.0	1.7	0.0	51.3	359.1
2016.1	45063.9	504.3	42.0	0.0	0.0	1.8	0.0	0.0	42.0	12.3	1.8	1.8	0.0	0.0	0.0	0.0	31.5	304.7
2016.2	45065.7	382.6	50.8	1.7	0.0	1.7	0.0	0.0	47.4	5.1	3.4	1.7	1.7	0.0	1.7	0.0	40.6	326.8
2016.3	45067.6	302.0	61.3	4.7	1.6	0.0	0.0	0.0	51.9	4.7	1.6	1.6	0.0	0.0	0.0	0.0	29.9	250.1
2016.4	45069.4	284.7	35.4	2.8	7.1	1.4	0.0	0.0	52.4	0.0	7.1	1.4	0.0	0.0	1.4	0.0	36.8	247.9
2016.5	45071.3	243.1	36.8	0.0	3.2	1.1	2.1	0.0	25.3	10.5	3.2	1.1	3.2	0.0	2.1	0.0	26.3	223.1
2016.6	45073.1	194.6	30.4	1.5	1.5	1.5	0.0	0.0	31.9	3.0	6.1	4.6	4.6	0.0	3.0	0.0	18.2	187.0

Core MD03-2622 Absolute Abundance Data (continued)

Depth (cm)	Age (yBP)	*G.b* #/g	*N.d* #/g	*O.u* #/g	*G.a* #/g	*G.c* #/g	*P.o* #/g	*G.m* #/g	*G.r*(p) #/g	*G.r*(w) #/g	*G.s* #/g	*G.g* #/g	*G.t* #/g	*G.rs* #/g	*N.p*(l) #/g	*N.p*(r) #/g	*G.q* #/g	Other #/g
2016.7	45075.0	165.6	35.7	3.0	4.0	1.0	0.0	1.0	34.7	4.0	6.0	2.0	4.0	0.0	4.0	0.0	10.9	162.7
2016.8	45076.8	255.7	32.6	0.0	1.8	0.0	0.0	0.0	41.7	3.6	5.4	5.4	3.6	0.0	5.4	0.0	14.5	228.5
2016.9	45078.7	233.0	37.8	4.7	6.3	1.6	0.0	0.0	48.8	6.3	11.0	0.0	1.6	0.0	4.7	0.0	22.0	226.7
2017.0	45080.5	264.6	57.4	6.2	0.0	2.1	2.1	2.1	84.1	4.1	2.1	0.0	4.1	0.0	0.0	0.0	16.4	268.7
2017.1	45082.9	243.3	56.3	0.0	1.8	0.0	0.0	0.0	49.0	3.6	9.1	0.0	1.8	0.0	3.6	0.0	12.7	197.9
2017.2	45085.2	246.0	62.4	3.7	1.2	8.7	0.0	0.0	58.7	6.2	12.5	0.0	1.2	0.0	0.0	0.0	16.2	178.6
2017.3	45087.6	266.5	81.1	3.9	1.9	0.0	0.0	0.0	63.7	1.9	3.9	0.0	1.9	0.0	5.8	0.0	9.7	266.5
2017.4	45089.9	212.4	59.1	4.8	3.2	0.0	1.6	0.0	67.1	3.2	11.2	1.6	3.2	0.0	1.6	0.0	4.8	178.9
2017.5	45092.3	221.8	71.0	0.0	8.9	6.7	0.0	0.0	66.5	8.9	0.0	0.0	4.4	0.0	6.7	0.0	8.9	286.1
2017.6	45094.6	267.3	45.8	0.0	1.9	1.9	0.0	0.0	66.8	7.6	7.6	1.9	5.7	0.0	1.9	0.0	3.8	219.6
2017.7	45097.0	295.8	80.7	4.7	1.6	1.6	0.0	0.0	85.4	4.7	6.3	3.2	3.2	0.0	3.2	0.0	4.7	215.1
2017.8	45099.3	289.9	88.2	0.0	3.4	3.4	1.7	0.0	62.7	8.5	5.1	0.0	1.7	0.0	3.4	0.0	8.5	322.1
2017.9	45101.7	264.3	45.8	0.0	6.2	0.0	0.0	0.0	56.2	4.2	6.2	2.1	2.1	0.0	6.2	0.0	12.5	291.4
2018.0	45104.0	232.3	63.8	3.5	0.0	3.5	3.5	1.8	51.4	5.3	3.5	1.8	0.0	0.0	3.5	0.0	14.2	285.5
2018.1	45106.1	282.6	48.3	4.2	2.1		1.1	0.0	31.5	5.3	1.1	0.0	2.1	0.0	4.2	0.0	5.3	208.0
2018.2	45108.2	352.8	35.1	4.8	4.8		1.6	0.0	49.5	12.8	8.0	0.0	3.2	0.0	1.6	0.0	1.6	223.5
2018.3	45110.3	283.8	57.8	2.6	1.3		3.9	1.3	20.5	1.3	3.9	1.3	2.6	0.0	0.0	0.0	2.6	242.7
2018.4	45112.4	234.3	33.6	4.5	1.1		0.0	0.0	25.8	3.4	10.1	1.1	1.1	0.0	6.7	0.0	0.0	192.8
2018.5	45114.5	140.6	28.1	1.0	1.0		0.0	0.0	19.4	2.9	1.0	1.9	0.0	0.0	1.0	0.0	1.0	119.3
2018.6	45116.6	99.1	19.4	0.7	0.7		0.7	0.7	21.6	3.0	4.5	0.7	1.5	0.0	2.2	0.0	0.0	105.1
2018.7	45118.7	58.7	18.3	0.8	0.4		0.8	0.0	13.7	2.5	1.7	0.0	0.4	0.0	0.4	0.0	0.4	66.2
2018.8	45120.8	55.6	11.2	0.4	0.9		0.0	0.4	10.3	3.6	1.3	0.4	0.4	0.0	0.9	0.0	0.0	59.7
2018.9	45122.9	100.3	27.6	2.4	2.4	1.6	0.0	0.8	20.5	9.5	3.9	0.8	3.2	0.0	1.6	0.0	0.8	88.4
2019.0	45125.0	120.0	19.8	2.8	1.9		1.9	0.9	25.5	5.7	3.8	2.8	1.9	0.0	1.9	0.0	1.9	98.3
2019.1	45126.2	223.6	38.4	2.7	1.4		0.0	1.4	39.8	8.2	4.1	1.4	2.7	0.0	2.7	0.0	1.4	182.5
2019.2	45127.4	139.1	38.9	2.9	1.9		0.0	0.0	38.9	9.7	4.9	1.0	4.9	0.0	4.9	0.0	0.0	150.8
2019.3	45128.6	167.9	42.3	1.2	5.0		1.2	0.0	37.3	5.0	5.0	1.2	6.2	0.0	5.0	0.0	2.5	109.4
2019.4	45129.8	162.3	32.1	4.9	4.9		1.0	1.0	46.6	10.7	4.9	1.9	1.9	0.0	3.9	0.0	0.0	152.5

Core MD03-2622 Absolute Abundance Data (continued)

Depth (cm)	Age (yBP)	*G.b* #/g	*N.d* #/g	*O.u* #/g	*G.a* #/g	*G.c* #/g	*P.o* #/g	*G.m* #/g	*G.r*(p) #/g	*G.r*(w) #/g	*G.s* #/g	*G.g* #/g	*G.t* #/g	*G.rs* #/g	*N.p*(l) #/g	*N.p*(r) #/g	*G.q* #/g	Other #/g
2019.5	45131.0	174.8	34.3	2.4	4.9		2.4	0.8	32.7	7.3	4.1	0.8	5.7	0.0	4.9	0.0	0.0	155.2
2019.6	45132.2	178.6	28.9	2.5	0.8		2.5	0.8	37.2	8.3	3.3	0.8	4.1	0.0	4.1	0.0	0.0	137.2
2019.7	45133.4	170.6	41.6	1.1	1.1		2.1	0.0	48.0	8.5	6.4	1.1	7.5	0.0	5.3	0.0	1.1	174.9
2019.8	45134.6	189.3	38.3	3.9	1.0		0.0	1.0	40.2	11.8	7.8	0.0	2.9	0.0	7.8	0.0	0.0	193.2
2019.9	45135.8	267.4	41.9	1.7	3.5	3.5	1.7	1.7	36.7	12.2	10.5	0.0	1.7	0.0	3.5	0.0	0.0	178.3
2020.0	45137.0	199.2	36.9	3.5	2.6		1.8	0.0	34.2	14.0	4.4	0.9	2.6	0.0	3.5	0.0	0.0	129.9
2020.1	45139.5	213.9	29.2	1.9	1.0		2.9	0.0	27.2	9.7	4.9	1.0	1.0	1.0	5.8	0.0	0.0	149.7
2020.2	45141.9	199.7	40.9	1.9	3.9		1.0	0.0	26.3	5.8	6.8	1.0	1.0	0.0	6.8	0.0	0.0	156.9
2020.3	45144.4	190.7	43.3	1.9	3.9		2.9	0.0	35.6	3.9	8.7	1.9	0.0	0.0	7.7	0.0	0.0	137.7
2020.4	45146.8	162.4	44.4	1.6	2.4		0.0	0.8	31.5	9.7	4.0	0.8	2.4	0.0	6.5	0.0	0.8	139.8
2020.5	45149.3	164.1	60.0	0.9	1.9		2.8	0.0	39.4	10.3	5.6	1.9	3.8	0.0	6.6	0.0	1.9	150.0
2020.6	45151.7	141.3	45.8	0.0	1.9		2.9	0.0	30.5	7.6	3.8	0.0	1.9	0.0	5.7	0.0	0.0	137.5
2020.7	45154.2	211.7	81.3	1.7	1.7		5.1	0.0	28.8	3.4	11.9	0.0	1.7	0.0	3.4	0.0	0.0	199.8
2020.8	45156.6	284.1	65.8	0.0	3.5		0.0	0.0	72.8	6.9	5.2	1.7	5.2	0.0	8.7	0.0	3.5	272.0
2020.9	45159.1	305.6	101.9	1.4	0.0	4.3	0.0	0.0	48.8	1.4	11.5	0.0	5.7	0.0	2.9	0.0	0.0	157.8
2021.0	45161.5	308.6	85.9	0.0	2.7		1.3	1.3	59.0	4.0	1.3	0.0	8.1	0.0	1.3	0.0	0.0	187.9
2021.1	45163.8	317.5	98.1	10.7	0.0		3.6	1.8	42.8	7.1	3.6	1.8	3.6	1.8	7.1	0.0	0.0	281.9
2021.2	45166.0	237.5	70.9	0.0	1.6		0.0	0.0	54.4	8.2	8.2	1.6	4.9	0.0	4.9	0.0	0.0	230.9
2021.3	45168.3	264.3	67.2	4.7	4.7		0.0	0.0	57.9	6.3	4.7	0.0	4.7	0.0	7.8	0.0	1.6	223.6
2021.4	45170.5	244.1	61.4	5.0	3.3		0.0	3.3	46.5	6.6	3.3	3.3	5.0	0.0	8.3	0.0	0.0	262.3
2021.5	45172.8	190.3	64.1	0.9	4.6		0.0	0.0	44.6	3.7	0.9	1.9	4.6	0.0	3.7	0.0	0.0	186.6
2021.6	45175.0	186.0	61.7	1.0	1.0		0.0	1.0	23.3	4.0	7.1	1.0	5.1	0.0	12.1	0.0	0.0	126.4
2021.7	45177.3	208.4	60.6	4.1	3.1		0.0	2.1	52.4	3.1	1.0	0.0	7.2	0.0	10.3	0.0	1.0	128.3
2021.8	45179.5	178.7	57.3	1.4	0.0		0.0	0.0	35.5	4.1	0.0	1.4	2.7	0.0	9.6	0.0	0.0	136.4
2021.9	45181.8	240.0	51.9	9.7	1.6	0.0	0.0	0.0	29.2	3.2	6.5	0.0	3.2	0.0	4.9	0.0	0.0	139.5
2022.0	45184.0	187.2	79.1	1.0	5.0		1.0	1.0	41.0	5.0	3.0	0.0	3.0	0.0	0.0	0.0	0.0	163.1
2022.1	45186.4	215.1	104.9	5.3	4.2		1.1	1.1	45.6	6.4	4.2	0.0	6.4	0.0	1.1	0.0	0.0	113.4
2022.2	45188.7	261.9	114.8	7.2	12.6		0.0	1.8	39.5	7.2	7.2	1.8	3.6	0.0	3.6	0.0	0.0	131.0

Core MD03-2622 Absolute Abundance Data (continued)

Depth (cm)	Age (yBP)	*G.b* #/g	*N.d* #/g	*O.u* #/g	*G.a* #/g	*G.c* #/g	*P.o* #/g	*G.m* #/g	*G.r*(p) #/g	*G.r*(w) #/g	*G.s* #/g	*G.g* #/g	*G.t* #/g	*G.rs* #/g	*N.p*(l) #/g	*N.p*(r) #/g	*G.q* #/g	Other #/g
2022.3	45191.1	313.5	109.2	1.8	3.5		1.8	0.0	35.2	10.6	12.3	3.5	5.3	0.0	1.8	0.0	1.8	144.4
2022.4	45193.4	294.5	121.4	4.1	2.7		1.4	0.0	49.1	8.2	9.5	1.4	15.0	0.0	6.8	0.0	6.8	105.0
2022.5	45195.8	232.9	100.7	0.0	12.0		0.0	1.5	33.1	4.5	3.0	4.5	7.5	0.0	1.5	0.0	6.0	99.2
2022.6	45198.1	172.8	89.8	2.3	2.3		3.1	2.3	23.8	2.3	7.7	2.3	5.4	0.0	3.1	0.0	5.4	60.7
2022.7	45200.5	138.3	70.1	4.7	4.7		1.9	0.0	20.6	8.4	3.7	1.9	4.7	0.0	3.7	0.0	4.7	50.5
2022.8	45202.8	112.9	41.0	2.6	1.9		0.0	1.3	12.2	4.5	1.9	0.0	2.6	0.0	1.3	0.0	1.3	36.5
2022.9	45205.2	142.2	51.6	2.9	1.5	1.5	0.7	0.0	14.7	4.4	2.2	0.7	5.2	0.0	3.7	0.0	2.9	40.5
2023.0	45207.5	165.5	77.1	3.5	5.3		0.9	0.0	16.6	3.5	4.4	0.9	7.0	0.0	1.8	0.0	2.6	39.4
2023.1	45208.6	248.0	100.5	0.0	1.6		3.1	0.0	34.5	7.8	7.8	0.0	4.7	0.0	3.1	0.0	4.7	58.1
2023.2	45209.7	260.7	113.8	1.2	6.1		3.7	2.4	45.3	11.0	3.7	1.2	14.7	0.0	2.4	0.0	6.1	93.0
2023.3	45210.8	281.9	125.7	0.0	10.1		2.0	2.0	46.6	4.1	4.1	4.1	12.2	0.0	4.1	0.0	6.1	113.6
2023.4	45211.9	225.9	125.5	1.1	5.7		0.0	0.0	51.3	6.8	14.8	1.1	5.7	0.0	6.8	0.0	5.7	91.3
2023.5	45213.0	289.6	145.7	6.9	5.2		1.7	1.7	65.9	5.2	24.3	0.0	3.5	0.0	3.5	0.0	10.4	112.7
2023.6	45214.1	308.3	153.2	8.0	8.0		2.0	2.0	57.7	6.0	9.9	0.0	6.0	0.0	4.0	0.0	6.0	89.5
2023.7	45215.2	328.5	147.7	5.8	13.6		0.0	0.0	54.4	19.4	7.8	1.9	5.8	0.0	3.9	0.0	11.7	118.6
2023.8	45216.3	329.4	133.7	1.6	9.8		0.0	0.0	81.5	3.3	1.6	1.6	3.3	0.0	0.0	0.0	16.3	99.5
2023.9	45217.4	279.7	134.0	5.0	10.0	0.0	1.7	0.0	53.6	15.1	6.7	0.0	6.7	0.0	3.3	0.0	11.7	68.7
2024.0	45218.5	365.4	149.8	0.0	12.0		2.0	0.0	45.9	16.0	8.0	0.0	8.0	0.0	2.0	0.0	18.0	91.9
2024.1	45220.9	250.2	96.8	0.0	10.4		3.0	0.0	43.2	14.9	6.0	0.0	20.9	0.0	4.5	0.0	6.0	44.7
2024.2	45223.2	314.4	120.0	2.1	2.1		0.0	0.0	70.3	20.7	10.3	0.0	10.3	0.0	0.0	0.0	12.4	60.0
2024.3	45225.6	274.6	143.4	1.5	10.7		1.5	0.0	47.3	10.7	9.2	0.0	4.6	0.0	1.5	0.0	15.3	50.3
2024.4	45227.9	283.6	117.6	6.9	2.8		1.4	1.4	36.0	15.2	4.1	0.0	12.4	0.0	1.4	0.0	8.3	38.7
2024.5	45230.3	290.5	118.5	8.1	11.4		3.2	1.6	43.8	17.8	3.2	1.6	11.4	1.6	1.6	0.0	11.4	61.7
2024.6	45232.6	306.1	111.7	1.4	1.4		1.4	1.4	31.7	15.2	13.8	1.4	9.7	0.0	4.1	0.0	4.1	59.3
2024.7	45235.0	345.5	165.4	3.3	4.9		0.0	0.0	36.0	6.6	0.0	0.0	6.6	0.0	6.6	0.0	14.7	54.0
2024.8	45237.3	312.0	117.6	2.6	3.8		3.8	0.0	32.0	20.5	2.6	1.3	0.0	0.0	2.6	0.0	7.7	84.4
2024.9	45239.7	396.4	101.1	4.0	2.0	2.0	5.9	0.0	27.8	7.9	4.0	0.0	4.0	0.0	0.0	0.0	13.9	91.2
2025.0	45242.0	470.5	108.6	6.0	8.0		0.0	0.0	40.2	12.1	2.0	6.0	10.1	0.0	8.0	0.0	24.1	60.3

Core MD03-2622 Absolute Abundance Data (continued)

Depth (cm)	Age (yBP)	*G.b* #/g	*N.d* #/g	*O.u* #/g	*G.a* #/g	*G.c* #/g	*P.o* #/g	*G.m* #/g	*G.r*(p) #/g	*G.r*(w) #/g	*G.s* #/g	*G.g* #/g	*G.t* #/g	*G.rs* #/g	*N.p*(l) #/g	*N.p*(r) #/g	*G.q* #/g	Other #/g
2025.1	45244.5	467.7	120.7	5.0	5.0		0.0	2.5	40.2	15.1	15.1	0.0	0.0	0.0	5.0	0.0	50.3	95.5
2025.2	45247.0	532.2	224.1	10.8	10.8		2.2	0.0	43.1	21.5	12.9	2.2	2.2	0.0	10.8	0.0	28.0	101.3
2025.3	45249.5	438.7	152.5	2.3	7.0		0.0	0.0	28.1	21.1	0.0	2.3	2.3	0.0	4.7	0.0	25.8	70.4
2025.4	45252.0	428.6	214.3	1.9	3.7		0.0	0.0	44.7	26.1	5.6	0.0	3.7	0.0	7.5	0.0	50.3	108.1
2025.5	45254.5	467.9	149.0	8.1	13.0		0.0	0.0	34.0	13.0	27.5	4.9	3.2	0.0	6.5	0.0	50.2	123.1
2025.6	45257.0	527.1	133.0	2.4	4.8		2.4	0.0	33.9	9.7	9.7	0.0	2.4	0.0	7.3	0.0	58.0	106.4
2025.7	45259.5	447.5	123.7	1.8	5.5		3.6	0.0	45.5	9.1	14.6	1.8	5.5	0.0	7.3	0.0	65.5	98.2
2025.8	45262.0	490.8	128.7	3.4	1.7		1.7	0.0	34.3	12.0	10.3	0.0	10.3	0.0	8.6	0.0	63.5	109.8
2025.9	45264.5	434.4	134.5	5.5	3.6	1.8	1.8	0.0	38.2	12.7	3.6	0.0	7.3	0.0	7.3	0.0	52.7	105.4
2026.0	45267.0	401.3	115.5	2.0	2.0		0.0	0.0	36.5	8.1	12.2	0.0	2.0	0.0	4.1	0.0	54.7	87.1
2026.1	45269.4	482.7	108.6	1.9	1.9		1.9	0.0	36.8	9.7	15.5	1.9	1.9	0.0	7.8	0.0	44.6	87.2
2026.2	45271.7	614.9	179.5	3.3	19.9		3.3	0.0	26.6	23.3	13.3	0.0	10.0	0.0	6.6	0.0	103.0	103.0
2026.3	45274.1	543.9	159.6	0.0	6.5		9.8	0.0	39.1	19.5	3.3	0.0	3.3	0.0	0.0	0.0	114.0	87.9
2026.4	45276.4	574.5	189.3	3.4	6.8		3.4	0.0	30.4	27.0	0.0	6.8	3.4	0.0	6.8	0.0	148.7	141.9
2026.5	45278.8	439.2	210.4	0.0	12.9		3.7	0.0	22.1	9.2	5.5	1.8	9.2	0.0	1.8	0.0	140.2	131.0
2026.6	45281.1	592.1	211.5	0.0	2.0		2.0	0.0	28.2	12.1	4.0	2.0	8.1	0.0	8.1	0.0	102.7	130.9
2026.7	45283.5	523.1	186.0	0.0	2.7		2.7	0.0	24.3	13.5	8.1	2.7	0.0	0.0	2.7	0.0	83.6	137.5
2026.8	45285.8	369.2	179.8	1.9	3.9		1.9	3.9	23.2	9.7	3.9	1.9	7.7	0.0	3.9	0.0	42.5	114.1
2026.9	45288.2	367.6	211.5	4.0	4.0	5.9	2.0	2.0	23.7	4.0	2.0	2.0	4.0	0.0	2.0	0.0	41.5	128.5
2027.0	45290.5	450.4	156.0	3.9	5.8		0.0	1.9	29.2	7.8	3.9	0.0	5.8	0.0	3.9	0.0	64.3	115.0
2027.1	45292.7	473.4	165.1	4.4	11.0		0.0	2.2	24.2	13.2	11.0	0.0	6.6	0.0	0.0	0.0	46.2	167.3
2027.2	45294.9	265.2	137.2	6.2	6.2		1.0	0.0	21.7	8.3	5.2	1.0	4.1	0.0	0.0	0.0	33.0	79.4
2027.3	45297.1	345.7	205.7	8.6	6.9		0.0	1.7	22.5	6.9	1.7	0.0	3.5	0.0	3.5	0.0	34.6	74.3
2027.4	45299.3	332.1	171.4	7.7	7.7		0.0	1.5	18.4	12.2	6.1	1.5	1.5	0.0	1.5	0.0	23.0	62.8
2027.5	45301.5	289.9	130.1	3.4	4.6		2.3	0.0	24.0	10.3	4.6	1.1	2.3	0.0	1.1	0.0	12.6	51.4
2027.6	45303.7	166.6	182.1	3.4	17.2		1.7	0.0	27.5	10.3	10.3	0.0	3.4	0.0	8.6	0.0	0.0	104.8
2027.7	45305.9	482.6	300.5	6.3	6.3		6.3	2.1	86.8	25.4	29.6	2.1	8.5	0.0	0.0	0.0	0.0	61.4
2027.8	45308.1	264.9	127.6	8.2	4.1		4.1	1.4	38.4	9.6	12.4	0.0	2.7	0.0	0.0	0.0	2.7	46.7

Core MD03-2622 Absolute Abundance Data (continued)

Depth (cm)	Age (yBP)	*G.b* #/g	*N.d* #/g	*O.u* #/g	*G.a* #/g	*G.c* #/g	*P.o* #/g	*G.m* #/g	*G.r*(p) #/g	*G.r*(w) #/g	*G.s* #/g	*G.g* #/g	*G.t* #/g	*G.rs* #/g	*N.p*(l) #/g	*N.p*(r) #/g	*G.q* #/g	Other #/g
2027.9	45310.3	324.3	155.0	5.7	7.2	2.9	8.6	0.0	47.4	17.2	14.4	2.9	11.5	0.0	1.4	0.0	0.0	57.4
2028.0	45312.5	295.7	216.1	9.5	5.7		1.9	0.0	56.9	7.6	3.8	1.9	3.8	0.0	0.0	0.0	0.0	56.9
2028.1	45314.9	277.5	214.3	1.8	5.3		1.8	0.0	47.4	12.3	10.5	1.8	5.3	0.0	3.5	0.0	0.0	86.1
2028.2	45317.3	532.6	413.9	3.8	15.3		0.0	0.0	34.5	30.7	15.3	0.0	0.0	0.0	7.7	0.0	3.8	141.8
2028.3	45319.7	603.2	449.0	10.3	13.7		0.0	0.0	51.4	17.1	6.9	3.4	0.0	0.0	13.7	0.0	3.4	188.5
2028.4	45322.1	606.5	550.4	3.5	24.5		3.5	0.0	38.6	21.0	17.5	0.0	0.0	0.0	14.0	0.0	0.0	220.9
2028.5	45324.5	578.8	526.5	0.0	30.5		0.0	0.0	56.6	13.1	8.7	0.0	8.7	0.0	8.7	0.0	0.0	230.6
2028.6	45326.9	444.4	541.0	2.8	33.1		8.3	0.0	52.4	44.2	11.0	0.0	8.3	2.8	5.5	0.0	2.8	176.6
2028.7	45329.3	598.1	553.4	10.3	34.4		6.9	0.0	75.6	10.3	6.9	3.4	3.4	0.0	3.4	0.0	0.0	220.0
2028.8	45331.7	267.3	336.6	0.0	9.9		3.3	3.3	57.8	8.3	3.3	0.0	5.0	0.0	3.3	0.0	0.0	95.7
2028.9	45334.1	316.9	446.9	0.0	15.8	0.0	3.2	3.2	79.2	19.0	3.2	0.0	3.2	0.0	6.3	0.0	6.3	79.2
2029.0	45336.5	326.8	425.0	6.4	21.4		2.1	0.0	57.7	8.5	2.1	2.1	0.0	0.0	8.5	0.0	0.0	94.0
2029.1	45338.9	322.7	310.3	7.4	24.6		4.9	0.0	73.9	22.2	12.3	2.5	0.0	0.0	4.9	0.0	0.0	105.9
2029.2	45341.3	430.5	718.7	0.0	26.2		7.5	0.0	63.6	18.7	7.5	0.0	3.7	0.0	18.7	0.0	0.0	82.4
2029.3	45343.7	387.8	461.5	0.0	19.2		6.4	0.0	64.1	16.0	6.4	0.0	0.0	0.0	0.0	0.0	12.8	105.8
2029.4	45346.1	392.4	446.6	12.8	3.2		0.0	0.0	47.9	19.1	9.6	3.2	3.2	0.0	12.8	0.0	9.6	121.2
2029.5	45348.5	464.6	531.4	6.4	19.1		9.5	0.0	47.7	19.1	0.0	3.2	0.0	0.0	6.4	0.0	0.0	127.3
2029.6	45350.9	510.1	429.1	7.2	11.9		0.0	0.0	57.2	19.1	2.4	2.4	2.4	0.0	7.2	0.0	0.0	138.3
2029.7	45353.3	429.9	407.5	4.1	2.0		4.1	0.0	53.0	10.2	2.0	0.0	4.1	0.0	6.1	0.0	4.1	77.4
2029.8	45355.7	312.2	306.1	2.0	2.0		2.0	0.0	32.2	18.1	2.0	0.0	2.0	0.0	4.0	0.0	6.0	90.6
2029.9	45358.1	441.2	431.1	10.1	0.0	0.0	6.7	0.0	43.8	23.6	3.4	0.0	0.0	0.0	6.7	0.0	3.4	101.0
2030.0	45360.5	574.8	195.1	2.1	4.2		4.2	4.2	40.3	21.2	8.5	0.0	6.4	2.1	10.6	0.0	0.0	91.2
2030.1	45363.0	462.0	182.0	2.3	4.7		9.3	0.0	60.7	7.0	11.7	4.7	2.3	0.0	2.3	0.0	0.0	123.7
2030.2	45365.4	293.6	110.8	4.3	8.6		0.0	1.1	29.0	10.8	8.6	1.1	3.2	0.0	3.2	0.0	0.0	46.3
2030.3	45367.9	301.6	92.2	1.8	1.8		1.8	0.0	49.7	8.9	7.1	0.0	0.0	1.8	1.8	0.0	0.0	72.7
2030.4	45370.3	307.8	55.2	3.7	3.7		1.2	0.0	45.4	7.4	6.1	0.0	2.5	0.0	4.9	0.0	0.0	88.3
2030.5	45372.8	343.0	59.0	8.0	6.4		1.6	0.0	62.2	11.2	19.1	1.6	0.0	0.0	6.4	0.0	1.6	102.1
2030.6	45375.2	361.7	59.7	8.8	3.5		0.0	0.0	45.7	14.0	10.5	1.8	0.0	0.0	3.5	0.0	0.0	98.3

Core MD03-2622 Absolute Abundance Data (continued)

Depth (cm)	Age (yBP)	*G.b* #/g	*N.d* #/g	*O.u* #/g	*G.a* #/g	*G.c* #/g	*P.o* #/g	*G.m* #/g	*G.r*(p) #/g	*G.r*(w) #/g	*G.s* #/g	*G.g* #/g	*G.t* #/g	*G.rs* #/g	*N.p*(l) #/g	*N.p*(r) #/g	*G.q* #/g	Other #/g
2030.7	45377.7	373.5	46.4	16.9	4.2		6.3	0.0	71.7	23.2	27.4	0.0	0.0	0.0	6.3	0.0	0.0	86.5
2030.8	45380.1	375.0	27.2	10.2	11.9		1.7	1.7	56.0	15.3	18.7	0.0	0.0	0.0	5.1	0.0	0.0	106.9
2030.9	45382.6	490.0	29.8	17.4	7.5	0.0	0.0	0.0	79.6	17.4	37.3	0.0	2.5	0.0	2.5	0.0	0.0	92.0
2031.0	45385.0	391.5	32.1	13.2	9.5		0.0	0.0	94.6	17.0	15.1	0.0	0.0	0.0	1.9	0.0	0.0	87.0
2031.1	45387.3	373.5	31.0	16.4	12.8		0.0	0.0	63.8	18.2	12.8	1.8	0.0	0.0	3.6	0.0	0.0	91.1
2031.2	45389.6	362.3	44.1	7.4	7.4		0.0	0.0	82.8	9.2	11.0	0.0	0.0	0.0	1.8	0.0	0.0	108.5
2031.3	45391.9	370.1	13.8	9.2	7.6		0.0	0.0	59.6	19.9	24.5	0.0	0.0	0.0	3.1	0.0	0.0	67.3
2031.4	45394.2	344.7	36.4	12.1	6.9		0.0	0.0	71.0	12.1	24.3	0.0	5.2	0.0	1.7	0.0	0.0	109.1
2031.5	45396.5	302.5	27.3	14.6	7.3		0.0	0.0	78.4	16.4	20.0	1.8	1.8	0.0	0.0	0.0	0.0	105.7
2031.6	45398.8	305.4	23.9	6.8	13.7		1.7	0.0	61.4	11.9	20.5	0.0	0.0	0.0	3.4	0.0	0.0	85.3
2031.7	45401.1	394.8	29.8	16.8	27.9		0.0	0.0	113.6	11.2	22.3	0.0	0.0	0.0	1.9	0.0	0.0	98.7
2031.8	45403.4	267.4	23.7	11.1	12.5		0.0	0.0	47.3	13.9	18.1	0.0	0.0	0.0	4.2	0.0	0.0	61.3
2031.9	45405.7	301.2	27.7	13.8	3.5	0.0	5.2	0.0	77.9	20.8	13.8	0.0	0.0	1.7	3.5	0.0	1.7	117.7
2032.0	45408.0	343.4	44.3	11.1	12.7		3.2	3.2	102.9	23.7	30.1	0.0	4.7	4.7	3.2	0.0	3.2	115.5
2032.1	45410.4	301.5	30.6	4.8	9.7		1.6	0.0	66.1	11.3	22.6	1.6	0.0	0.0	3.2	0.0	1.6	108.0
2032.2	45412.7	359.4	35.7	23.8	7.9		0.0	0.0	71.5	27.8	25.8	4.0	0.0	2.0	7.9	0.0	0.0	111.2
2032.3	45415.1	309.5	34.2	4.9	8.1		3.3	0.0	104.3	19.5	21.2	0.0	0.0	0.0	6.5	0.0	1.6	94.5
2032.4	45417.4	373.1	43.8	9.7	9.7		1.6	1.6	66.5	27.6	24.3	0.0	0.0	3.2	6.5	0.0	0.0	100.6
2032.5	45419.8	344.8	42.0	21.0	7.0		1.8	5.3	87.5	21.0	15.8	0.0	0.0	0.0	5.3	0.0	1.8	92.8
2032.6	45422.1	354.1	22.0	11.0	6.6		0.0	0.0	101.2	19.8	24.2	0.0	0.0	0.0	4.4	0.0	0.0	118.8
2032.7	45424.5	355.5	29.3	18.3	7.3		0.0	0.0	80.6	25.7	20.2	1.8	1.8	0.0	12.8	0.0	0.0	86.1
2032.8	45426.8	412.8	37.8	18.9	15.8		0.0	0.0	93.0	29.9	29.9	3.2	0.0	1.6	4.7	0.0	0.0	93.0
2032.9	45429.2	369.4	31.6	20.6	16.5	2.7	1.4	1.4	76.9	33.0	26.1	2.7	0.0	2.7	4.1	0.0	2.7	92.0
2033.0	45431.5	351.6	29.9	12.3	14.1		1.8	3.5	68.6	52.7	24.6	1.8	0.0	0.0	7.0	0.0	3.5	100.2
2033.1	45433.9	328.8	36.5	12.8	16.4		1.8	1.8	89.5	16.4	34.7	1.8	0.0	0.0	5.5	0.0	1.8	82.2
2033.2	45436.3	341.6	41.1	28.0	7.5		0.0	1.9	98.9	16.8	29.9	7.5	1.9	0.0	5.6	0.0	0.0	93.3
2033.3	45438.7	468.3	53.8	29.6	18.8		2.7	0.0	105.0	37.7	29.6	8.1	0.0	0.0	10.8	0.0	0.0	142.7
2033.4	45441.1	360.2	40.5	15.4	12.6		0.0	1.4	69.8	29.3	25.1	4.2	1.4	0.0	12.6	0.0	1.4	94.9

Core MD03-2622 Absolute Abundance Data (continued)

Depth (cm)	Age (yBP)	*G.b* #/g	*N.d* #/g	*O.u* #/g	*G.a* #/g	*G.c* #/g	*P.o* #/g	*G.m* #/g	*G.r*(p) #/g	*G.r*(w) #/g	*G.s* #/g	*G.g* #/g	*G.t* #/g	*G.rs* #/g	*N.p*(l) #/g	*N.p*(r) #/g	*G.q* #/g	Other #/g
2033.5	45443.5	447.4	41.4	27.6	19.3		0.0	0.0	110.5	49.7	30.4	0.0	0.0	0.0	13.8	0.0	0.0	99.4
2033.6	45445.9	594.9	62.4	23.0	13.1		0.0	0.0	134.8	32.9	39.4	3.3	3.3	0.0	9.9	0.0	0.0	101.9
2033.7	45448.3	427.9	14.3	36.9	10.2		0.0	2.0	81.9	24.6	24.6	0.0	0.0	0.0	6.1	0.0	0.0	83.9
2033.8	45450.7	497.7	37.5	18.7	13.4		0.0	0.0	101.7	32.1	29.4	0.0	0.0	0.0	5.4	0.0	0.0	77.6
2033.9	45453.1	331.7	25.0	10.7	7.1	1.8	0.0	0.0	69.6	19.6	8.9	3.6	0.0	0.0	7.1	0.0	0.0	64.2
2034.0	45455.5	283.9	14.7	7.4	4.4		0.0	0.0	67.7	25.0	5.9	0.0	0.0	1.5	7.4	0.0	0.0	66.2
2034.1	45457.7	222.7	13.2	7.9	5.3		0.0	0.0	51.7	14.9	10.5	0.0	0.0	0.0	4.4	0.0	0.0	59.6
2034.2	45459.8	318.1	22.2	5.2	7.8		0.0	1.3	63.9	20.9	20.9	0.0	0.0	0.0	5.2	0.0	0.0	73.0
2034.3	45462.0	308.6	21.9	8.8	7.7		1.1	0.0	62.4	20.8	17.5	1.1	1.1	0.0	1.1	0.0	0.0	47.1
2034.4	45464.1	286.8	33.6	9.0	7.8		0.0	1.3	49.1	25.8	16.8	0.0	1.3	0.0	3.9	0.0	0.0	49.1
2034.5	45466.3	250.0	19.2	6.1	8.7		0.0	0.0	54.2	16.6	14.9	1.7	0.0	0.0	5.2	0.0	0.0	49.8
2034.6	45468.4	211.8	17.9	8.9	7.3		0.8	0.0	30.8	12.2	12.2	0.0	0.8	0.0	4.9	0.0	0.0	42.2
2034.7	45470.6	203.3	15.1	9.2	6.7		0.0	0.0	41.2	15.1	8.4	0.0	0.0	0.8	2.5	0.0	0.0	41.2
2034.8	45472.7	366.6	22.3	13.7	12.0		0.0	0.0	72.0	25.7	12.0	0.0	0.0	0.0	3.4	0.0	0.0	83.9
2034.9	45474.9	317.9	12.7	6.4	7.9	0.0	0.0	0.0	62.0	23.8	9.5	1.6	0.0	0.0	0.0	0.0	0.0	68.3
2035.0	45477.0	326.8	17.6	14.7	11.7		0.0	0.0	87.9	19.0	17.6	0.0	2.9	0.0	2.9	0.0	0.0	71.8
2035.1	45479.2	447.6	40.5	16.2	8.1		4.9	0.0	97.3	19.5	24.3	1.6	0.0	0.0	3.2	0.0	0.0	90.8
2035.2	45481.4	402.8	31.6	12.4	12.4		1.4	2.7	77.0	31.6	16.5	0.0	0.0	0.0	5.5	0.0	0.0	97.6
2035.3	45483.6	467.7	26.0	7.6	15.3		0.0	1.5	87.1	26.0	16.8	0.0	0.0	0.0	1.5	0.0	0.0	79.5
2035.4	45485.8	476.2	21.6	13.3	20.0		0.0	0.0	91.6	21.6	21.6	1.7	0.0	0.0	3.3	0.0	0.0	83.3
2035.5	45488.0	426.8	10.2	17.0	11.9		0.0	0.0	110.5	22.1	22.1	1.7	0.0	0.0	17.0	0.0	0.0	119.0
2035.6	45490.2	345.7	17.9	4.0	6.0		0.0	0.0	111.2	27.8	29.8	0.0	0.0	0.0	7.9	0.0	0.0	95.4
2035.7	45492.4	432.8	28.1	8.0	8.0		0.0	0.0	138.2	30.1	30.1	2.0	0.0	0.0	6.0	0.0	0.0	92.2
2035.8	45494.6	382.8	35.4	9.2	7.7		0.0	0.0	96.9	27.7	27.7	3.1	0.0	0.0	6.1	0.0	0.0	76.9
2035.9	45496.8	401.3	14.3	21.5	9.0	3.6	0.0	1.8	152.3	37.6	25.1	0.0	1.8	0.0	3.6	0.0	0.0	89.6
2036.0	45499.0	434.4	15.3	8.7	19.6		0.0	0.0	104.8	32.7	28.4	0.0	0.0	0.0	6.5	0.0	0.0	69.9
2036.1	45500.9	521.0	41.4	3.8	13.2		0.0	1.9	124.1	13.2	35.7	0.0	1.9	0.0	9.4	0.0	0.0	94.0
2036.2	45502.7	398.2	21.8	10.9	8.7		2.2	0.0	124.0	39.2	17.4	0.0	2.2	0.0	6.5	0.0	0.0	91.4

Core MD03-2622 Absolute Abundance Data (continued)

Depth (cm)	Age (yBP)	*G.b* #/g	*N.d* #/g	*O.u* #/g	*G.a* #/g	*G.c* #/g	*P.o* #/g	*G.m* #/g	*G.r*(p) #/g	*G.r*(w) #/g	*G.s* #/g	*G.g* #/g	*G.t* #/g	*G.rs* #/g	*N.p*(l) #/g	*N.p*(r) #/g	*G.q* #/g	Other #/g
2036.3	45504.6	446.7	34.0	13.6	11.9		0.0	3.4	118.9	27.2	40.8	0.0	0.0	0.0	5.1	0.0	0.0	93.4
2036.4	45506.4	481.8	18.6	10.1	13.5		0.0	6.8	104.8	18.6	38.9	0.0	1.7	0.0	0.0	0.0	0.0	84.5
2036.5	45508.3	467.3	23.6	6.7	6.7		0.0	0.0	97.8	33.7	32.1	0.0	3.4	0.0	3.4	0.0	0.0	86.0
2036.6	45510.1	507.6	18.0	12.0	10.5		0.0	0.0	104.8	21.0	18.0	3.0	3.0	1.5	3.0	0.0	0.0	112.3
2036.7	45512.0	509.0	21.1	11.5	11.5		0.0	0.0	88.4	28.8	23.1	0.0	0.0	0.0	5.8	0.0	0.0	92.2
2036.8	45513.8	448.0	31.3	12.5	18.8		0.0	0.0	60.4	14.6	25.0	0.0	0.0	0.0	6.3	0.0	0.0	81.3
2036.9	45515.7	516.8	25.1	15.7	7.9	0.0	0.0	0.0	99.0	20.4	18.8	0.0	3.1	1.6	0.0	0.0	0.0	67.5
2037.0	45517.5	598.3	32.9	8.7	12.1		0.0	5.2	131.8	38.1	22.5	0.0	1.7	0.0	0.0	0.0	0.0	88.4
2037.1	45519.9	725.4	35.8	20.7	9.4		1.9	0.0	103.6	52.8	32.0	1.9	0.0	0.0	9.4	0.0	0.0	96.1
2037.2	45522.3	711.5	15.5	34.0	6.2		0.0	3.1	99.0	49.5	6.2	0.0	0.0	0.0	6.2	0.0	0.0	61.9
2037.3	45524.7	735.9	31.5	15.8	13.1		0.0	2.6	71.0	47.3	10.5	0.0	0.0	0.0	0.0	0.0	0.0	68.3
2037.4	45527.1	770.1	9.9	19.7	13.2		0.0	0.0	158.0	26.3	19.7	3.3	0.0	3.3	6.6	0.0	0.0	95.4
2037.5	45529.5	760.4	16.0	16.0	9.6		0.0	0.0	166.8	41.7	6.4	0.0	0.0	0.0	6.4	0.0	0.0	73.8
2037.6	45531.9	710.7	14.0	33.7	11.2		0.0	0.0	98.3	44.9	14.0	0.0	0.0	0.0	5.6	0.0	0.0	73.0
2037.7	45534.3	752.9	14.8	12.9	22.2		0.0	0.0	77.7	27.7	12.9	1.8	3.7	0.0	3.7	0.0	0.0	88.8
2037.8	45536.7	865.4	24.7	5.5	5.5		0.0	0.0	52.2	19.2	16.5	0.0	0.0	0.0	5.5	0.0	0.0	60.4
2037.9	45539.1	667.6	28.8	11.5	21.1	0.0	0.0	0.0	65.2	32.6	7.7	0.0	1.9	0.0	7.7	0.0	0.0	82.5
2038.0	45541.5	620.5	13.6	11.9	6.8		0.0	0.0	68.0	17.0	15.3	0.0	3.4	0.0	8.5	0.0	0.0	44.2
2038.1	45543.8	722.1	16.2	14.2	8.1		0.0	4.1	79.1	26.4	12.2	4.1	0.0	0.0	4.1	0.0	0.0	62.9
2038.2	45546.1	726.7	25.1	13.4	5.0		1.7	1.7	98.6	33.4	13.4	1.7	1.7	0.0	6.7	0.0	0.0	71.8
2038.3	45548.4	729.4	33.4	13.9	5.6		0.0	0.0	105.8	33.4	25.1	0.0	2.8	0.0	8.4	0.0	0.0	66.8
2038.4	45550.7	672.1	29.7	11.9	4.0		0.0	2.0	85.0	39.5	13.8	0.0	0.0	0.0	4.0	0.0	0.0	49.4
2038.5	45553.0	687.9	25.9	6.0	4.0		2.0	0.0	109.7	35.9	12.0	0.0	2.0	0.0	2.0	0.0	0.0	79.8
2038.6	45555.3	733.0	36.8	3.3	6.7		0.0	0.0	80.3	36.8	13.4	0.0	0.0	0.0	10.0	0.0	0.0	90.4
2038.7	45557.6	642.2	28.2	7.1	17.6		0.0	0.0	109.4	30.0	12.3	1.8	3.5	0.0	3.5	0.0	0.0	72.3
2038.8	45559.9	658.8	19.5	14.0	5.6		0.0	0.0	89.3	27.9	11.2	0.0	2.8	2.8	0.0	0.0	0.0	47.5
2038.9	45562.2	628.6	9.0	21.1	15.0	0.0	0.0	6.0	108.3	36.1	21.1	0.0	0.0	0.0	3.0	0.0	0.0	72.2
2039.0	45564.5	778.8	21.8	3.6	25.5		0.0	0.0	98.3	54.6	14.6	0.0	0.0	0.0	10.9	0.0	0.0	101.9

Core MD03-2622 Absolute Abundance Data (continued)

Depth (cm)	Age (yBP)	*G.b* #/g	*N.d* #/g	*O.u* #/g	*G.a* #/g	*G.c* #/g	*P.o* #/g	*G.m* #/g	*G.r*(p) #/g	*G.r*(w) #/g	*G.s* #/g	*G.g* #/g	*G.t* #/g	*G.rs* #/g	*N.p*(l) #/g	*N.p*(r) #/g	*G.q* #/g	Other #/g
2039.1	45566.6	702.6	29.0	14.5	12.1		4.8	0.0	113.5	31.4	14.5	0.0	0.0	0.0	4.8	0.0	0.0	84.5
2039.2	45568.7	824.5	16.7	20.0	20.0		0.0	3.3	116.8	46.7	16.7	3.3	0.0	0.0	10.0	0.0	0.0	93.5
2039.3	45570.8	808.0	21.7	18.1	3.6		0.0	0.0	141.3	18.1	18.1	0.0	0.0	0.0	7.2	0.0	0.0	54.4
2039.4	45572.9	746.5	37.2	19.6	5.9		0.0	0.0	96.0	58.8	11.8	0.0	0.0	0.0	11.8	0.0	0.0	58.8
2039.5	45575.0	626.7	17.6	13.7	5.9		0.0	2.0	111.6	33.3	9.8	2.0	2.0	0.0	2.0	0.0	0.0	62.7
2039.6	45577.1	613.5	19.8	11.9	5.9		0.0	2.0	128.6	43.5	13.9	0.0	2.0	0.0	5.9	0.0	0.0	71.2
2039.7	45579.2	673.9	43.8	10.1	6.7		0.0	0.0	121.3	64.0	20.2	0.0	0.0	0.0	10.1	0.0	0.0	80.9
2039.8	45581.3	1028.7	27.4	30.9	6.9		0.0	0.0	58.3	27.4	37.7	0.0	0.0	0.0	3.4	0.0	0.0	89.2
2039.9	45583.4	1229.4	30.5	22.9	15.3	0.0	0.0	0.0	57.3	38.2	15.3	0.0	0.0	3.8	7.6	0.0	0.0	76.4
2040.0	45585.5	983.2	32.9	49.3	23.5		0.0	4.7	93.9	44.6	14.1	4.7	0.0	0.0	4.7	0.0	0.0	82.1
2040.1	45587.8	979.1	18.1	27.2	13.6		0.0	2.3	106.5	24.9	6.8	0.0	2.3	2.3	6.8	0.0	0.0	56.7
2040.2	45590.0	1074.6	39.0	17.3	13.0		0.0	0.0	169.0	39.0	8.7	0.0	4.3	0.0	21.7	0.0	0.0	65.0
2040.3	45592.3	1261.6	33.8	16.9	20.3		0.0	0.0	169.1	44.0	16.9	3.4	0.0	6.8	6.8	0.0	0.0	67.6
2040.4	45594.5	1051.8	34.9	26.2	8.7		0.0	0.0	117.8	48.0	8.7	0.0	0.0	0.0	4.4	0.0	0.0	87.3
2040.5	45596.8	1104.6	23.3	21.0	14.0		0.0	0.0	93.2	28.0	14.0	2.3	2.3	4.7	4.7	0.0	0.0	69.9
2040.6	45599.0	1088.3	39.7	18.7	9.3		0.0	0.0	77.1	30.4	11.7	0.0	0.0	0.0	9.3	0.0	0.0	72.4
2040.7	45601.3	1202.6	39.2	19.6	15.7		0.0	0.0	78.3	31.3	19.6	0.0	0.0	0.0	0.0	0.0	0.0	78.3
2040.8	45603.5	981.0	24.9	21.8	12.5		0.0	0.0	71.6	59.2	21.8	0.0	0.0	0.0	3.1	0.0	0.0	62.3
2040.9	45605.8	1078.4	22.2	15.9	9.5	3.2	0.0	0.0	47.6	25.4	12.7	0.0	3.2	0.0	6.3	0.0	0.0	79.3
2041.0	45608.0	1051.5	30.9	8.8	11.0		0.0	0.0	41.9	44.1	19.8	0.0	0.0	4.4	4.4	0.0	0.0	59.5
2041.1	45610.4	1166.2	22.7	26.0	19.5		0.0	0.0	29.2	22.7	19.5	0.0	3.2	3.2	9.7	0.0	0.0	68.2
2041.2	45612.7	1162.1	19.5	16.2	26.0		0.0	0.0	32.5	32.5	16.2	0.0	3.2	0.0	13.0	0.0	0.0	110.4
2041.3	45615.1	1099.4	35.5	10.9	16.4		0.0	2.7	32.7	16.4	19.1	0.0	0.0	0.0	13.6	0.0	0.0	87.3
2041.4	45617.4	941.5	39.4	6.1	15.1		0.0	0.0	27.2	24.2	12.1	6.1	3.0	0.0	9.1	0.0	0.0	109.0
2041.5	45619.8	856.5	33.1	26.5	16.5		0.0	3.3	49.6	26.5	16.5	0.0	0.0	0.0	9.9	0.0	0.0	79.4
2041.6	45622.1	789.2	32.6	16.3	19.9		0.0	1.8	21.7	61.5	18.1	0.0	1.8	0.0	1.8	0.0	0.0	67.0
2041.7	45624.5	881.5	31.3	28.4	17.1		2.8	0.0	45.5	34.1	17.1	5.7	0.0	0.0	2.8	0.0	0.0	71.1
2041.8	45626.8	837.8	42.2	24.6	10.6		0.0	3.5	45.8	38.7	24.6	0.0	0.0	3.5	7.0	0.0	0.0	66.9

Core MD03-2622 Absolute Abundance Data (continued)

Depth (cm)	Age (yBP)	*G.b* #/g	*N.d* #/g	*O.u* #/g	*G.a* #/g	*G.c* #/g	*P.o* #/g	*G.m* #/g	*G.r*(p) #/g	*G.r*(w) #/g	*G.s* #/g	*G.g* #/g	*G.t* #/g	*G.rs* #/g	*N.p*(l) #/g	*N.p*(r) #/g	*G.q* #/g	Other #/g
2041.9	45629.2	668.0	40.6	5.4	13.5	0.0	0.0	0.0	29.7	32.5	32.5	8.1	0.0	0.0	10.8	0.0	0.0	78.4
2042.0	45631.5	889.8	39.8	25.3	21.7		0.0	3.6	47.0	32.6	10.9	0.0	0.0	3.6	14.5	0.0	0.0	76.0
2042.1	45633.7	979.9	40.6	26.3	21.5		0.0	0.0	23.9	38.2	7.2	0.0	0.0	0.0	11.9	0.0	0.0	64.5
2042.2	45635.8	1082.9	30.1	23.4	30.1		0.0	0.0	50.1	50.1	30.1	0.0	0.0	0.0	13.4	0.0	0.0	73.5
2042.3	45638.0	824.9	25.2	10.8	16.2		0.0	1.8	52.2	36.0	21.6	0.0	1.8	1.8	5.4	0.0	0.0	75.6
2042.4	45640.1	834.1	39.2	14.9	16.8		0.0	0.0	61.6	33.6	20.5	1.9	0.0	0.0	9.3	0.0	0.0	82.1
2042.5	45642.3	932.4	41.8	28.9	9.6		0.0	0.0	25.7	32.2	22.5	0.0	0.0	3.2	22.5	0.0	0.0	70.7
2042.6	45644.4	856.4	33.1	15.6	7.8		0.0	1.9	35.0	25.3	38.9	0.0	0.0	0.0	11.7	0.0	0.0	70.1
2042.7	45646.6	738.4	29.1	19.4	3.2		1.6	0.0	17.8	32.3	19.4	3.2	1.6	0.0	4.8	0.0	0.0	82.4
2042.8	45648.7	769.9	36.2	22.4	15.5		0.0	0.0	17.2	37.9	25.8	0.0	1.7	3.4	5.2	0.0	0.0	70.6
2042.9	45650.9	607.2	36.2	16.5	9.9	0.0	0.0	0.0	29.6	29.6	23.0	0.0	0.0	0.0	4.9	0.0	0.0	80.6
2043.0	45653.0	621.8	44.1	13.6	10.2		0.0	0.0	35.6	28.8	40.7	0.0	0.0	0.0	8.5	0.0	0.0	71.2
2043.1	45655.4	513.6	48.6	14.6	11.3		0.0	1.6	37.3	22.7	29.2	1.6	0.0	1.6	4.9	0.0	0.0	64.8
2043.2	45657.7	500.6	43.8	6.3	6.3		0.0	0.0	26.6	31.3	31.3	0.0	1.6	0.0	4.7	0.0	0.0	64.1
2043.3	45660.1	415.1	25.0	19.7	5.4		0.0	1.8	23.3	26.8	30.4	0.0	0.0	0.0	5.4	0.0	0.0	60.8
2043.4	45662.4	455.8	41.6	18.1	3.6		0.0	0.0	18.1	21.7	25.3	0.0	0.0	1.8	3.6	0.0	0.0	77.8
2043.5	45664.8	386.2	29.6	18.5	5.5		0.0	0.0	14.8	20.3	22.2	0.0	0.0	0.0	1.8	0.0	0.0	68.4
2043.6	45667.1	447.4	34.7	19.3	13.5		0.0	0.0	30.9	38.6	27.0	1.9	7.7	0.0	1.9	0.0	0.0	63.6
2043.7	45669.5	447.6	27.6	21.7	7.9		0.0	2.0	25.6	27.6	15.8	0.0	0.0	2.0	9.9	0.0	0.0	69.0
2043.8	45671.8	411.4	23.3	19.0	14.6		0.0	0.0	29.2	27.7	21.9	0.0	0.0	0.0	5.8	0.0	0.0	83.2
2043.9	45674.2	469.1	20.0	18.0	10.0	0.0	0.0	0.0	18.0	31.9	29.9	0.0	0.0	2.0	12.0	0.0	0.0	73.9
2044.0	45676.5	425.1	36.3	19.0	19.0		0.0	1.7	19.0	32.8	31.1	0.0	0.0	1.7	3.5	0.0	0.0	58.7
2044.1	45679.0	503.0	19.2	17.3	13.4		0.0	0.0	26.9	19.2	25.0	0.0	1.9	1.9	1.9	0.0	0.0	80.6
2044.2	45681.4	502.6	34.4	18.9	13.8		0.0	0.0	22.4	41.3	27.5	0.0	1.7	1.7	12.0	0.0	0.0	84.3
2044.3	45683.9	500.2	35.9	12.8	9.0		0.0	0.0	21.8	52.6	19.2	0.0	0.0	1.3	5.1	0.0	0.0	77.0
2044.4	45686.3	503.0	25.4	32.7	14.5		0.0	1.8	23.6	45.4	23.6	1.8	0.0	0.0	10.9	0.0	0.0	72.6
2044.5	45688.8	537.1	31.5	14.2	9.5		0.0	1.6	29.9	34.7	25.2	1.6	1.6	0.0	4.7	0.0	0.0	83.5
2044.6	45691.2	589.2	36.4	24.3	10.4		1.7	0.0	31.2	48.5	10.4	0.0	0.0	0.0	10.4	0.0	0.0	58.9

Core MD03-2622 Absolute Abundance Data (continued)

Depth (cm)	Age (yBP)	*G.b* #/g	*N.d* #/g	*O.u* #/g	*G.a* #/g	*G.c* #/g	*P.o* #/g	*G.m* #/g	*G.r*(p) #/g	*G.r*(w) #/g	*G.s* #/g	*G.g* #/g	*G.t* #/g	*G.rs* #/g	*N.p*(l) #/g	*N.p*(r) #/g	*G.q* #/g	Other #/g
2044.7	45693.7	645.7	57.8	12.0	6.0		0.0	0.0	33.9	59.8	17.9	0.0	0.0	2.0	8.0	0.0	0.0	57.8
2044.8	45696.1	628.8	28.3	8.5	5.7		0.0	0.0	39.7	68.0	28.3	0.0	0.0	0.0	8.5	0.0	0.0	48.2
2044.9	45698.6	703.0	41.7	15.9	15.9	7.9	0.0	0.0	43.7	51.6	15.9	2.0	0.0	0.0	13.9	0.0	0.0	75.5
2045.0	45701.0	682.5	49.7	22.9	11.5		0.0	0.0	38.2	84.1	30.6	0.0	3.8	0.0	15.3	0.0	0.0	65.0
2045.1	45703.3	670.9	32.5	17.1	12.0		0.0	1.7	25.7	44.5	15.4	0.0	0.0	1.7	17.1	0.0	0.0	70.2
2045.2	45705.5	730.9	25.3	25.3	15.6		0.0	0.0	19.4	77.8	33.0	0.0	0.0	0.0	9.7	0.0	0.0	83.6
2045.3	45707.8	854.0	50.2	12.6	15.7		0.0	0.0	34.5	47.1	22.0	0.0	0.0	0.0	9.4	0.0	0.0	56.5
2045.4	45710.0	786.5	20.7	22.5	13.8		0.0	1.7	22.5	55.3	20.7	1.7	0.0	0.0	6.9	0.0	0.0	77.8
2045.5	45712.3	681.0	18.2	34.5	14.5		1.8	0.0	18.2	61.7	18.2	0.0	0.0	0.0	9.1	0.0	0.0	67.2
2045.6	45714.5	615.7	27.4	23.5	17.6		0.0	0.0	25.4	62.5	23.5	2.0	2.0	3.9	11.7	0.0	0.0	68.4
2045.7	45716.8	550.7	31.2	21.4	13.2		0.0	0.0	13.2	51.0	21.4	0.0	0.0	0.0	9.9	0.0	0.0	51.0
2045.8	45719.0	645.3	46.0	23.8	22.1		0.0	0.0	13.6	59.6	13.6	1.7	0.0	0.0	13.6	0.0	0.0	83.4
2045.9	45721.3	765.3	28.2	19.8	16.9	0.0	0.0	2.8	5.6	67.8	25.4	0.0	0.0	0.0	14.1	0.0	0.0	93.2
2046.0	45723.5	690.9	73.2	28.7	6.4		0.0	0.0	22.3	38.2	15.9	0.0	0.0	0.0	6.4	0.0	0.0	89.1
2046.1	45725.6	735.8	23.2	34.9	19.4		0.0	1.9	21.3	77.5	17.4	0.0	0.0	0.0	9.7	0.0	0.0	63.9
2046.2	45727.7	722.6	31.7	20.4	15.9		0.0	2.3	29.4	58.9	6.8	0.0	0.0	0.0	9.1	0.0	0.0	63.4
2046.3	45729.8	886.7	31.5	24.5	7.0		0.0	0.0	17.5	56.1	3.5	0.0	0.0	0.0	3.5	0.0	0.0	63.1
2046.4	45731.9	733.1	27.9	23.0	9.8		1.6	0.0	14.8	57.4	18.0	0.0	0.0	0.0	8.2	0.0	0.0	55.8
2046.5	45734.0	627.2	28.4	16.7	8.4		0.0	0.0	11.7	36.8	20.1	0.0	0.0	0.0	3.3	0.0	0.0	68.6
2046.6	45736.1	465.7	19.9	5.4	14.5		0.0	0.0	16.3	32.6	16.3	0.0	0.0	0.0	7.2	0.0	0.0	48.9
2046.7	45738.2	697.1	16.0	8.9	5.3		1.8	0.0	21.4	55.3	25.0	0.0	0.0	0.0	8.9	0.0	0.0	62.4
2046.8	45740.3	806.3	10.3	27.6	6.9		0.0	0.0	24.1	51.7	24.1	0.0	0.0	0.0	6.9	0.0	0.0	79.3
2046.9	45742.4	780.5	27.3	18.2	3.0	0.0	0.0	0.0	21.3	36.4	24.3	0.0	0.0	0.0	6.1	0.0	0.0	82.0
2047.0	45744.5	833.8	16.4	29.2	7.3		1.8	0.0	10.9	51.1	20.1	0.0	0.0	0.0	9.1	0.0	0.0	56.6
2047.1	45746.8	1055.3	30.5	15.2	26.7		0.0	0.0	15.2	53.3	19.0	0.0	0.0	0.0	11.4	0.0	0.0	83.8
2047.2	45749.1	1053.1	27.5	9.2	15.3		0.0	0.0	9.2	51.9	24.4	0.0	0.0	0.0	21.4	0.0	0.0	82.4
2047.3	45751.4	1071.3	25.4	15.9	15.9		0.0	0.0	19.1	63.6	25.4	0.0	0.0	0.0	9.5	0.0	0.0	66.8
2047.4	45753.7	1235.8	16.3	8.1	28.5		0.0	0.0	12.2	65.0	12.2	0.0	0.0	0.0	16.3	0.0	0.0	56.9

Core MD03-2622 Absolute Abundance Data (continued)

Depth (cm)	Age (yBP)	*G.b* #/g	*N.d* #/g	*O.u* #/g	*G.a* #/g	*G.c* #/g	*P.o* #/g	*G.m* #/g	*G.r*(p) #/g	*G.r*(w) #/g	*G.s* #/g	*G.g* #/g	*G.t* #/g	*G.rs* #/g	*N.p*(l) #/g	*N.p*(r) #/g	*G.q* #/g	Other #/g
2047.5	45756.0	1147.1	32.0	40.0	12.0		0.0	0.0	12.0	67.9	40.0	0.0	0.0	0.0	32.0	0.0	0.0	111.9
2047.6	45758.3	1165.2	36.0	21.6	25.2		0.0	0.0	39.6	57.5	25.2	0.0	0.0	0.0	3.6	0.0	0.0	82.7
2047.7	45760.6	980.4	28.8	25.9	2.9		0.0	0.0	25.9	63.3	23.0	0.0	0.0	0.0	5.8	0.0	0.0	103.5
2047.8	45762.9	870.6	17.2	17.2	17.2		0.0	0.0	25.8	74.5	17.2	0.0	0.0	0.0	8.6	0.0	0.0	63.0
2047.9	45765.2	1114.5	25.6	12.8	19.2	0.0	0.0	0.0	19.2	54.4	19.2	0.0	0.0	0.0	9.6	0.0	0.0	102.5
2048.0	45767.5	1271.3	24.7	42.3	10.6		0.0	0.0	21.1	77.5	21.1	0.0	0.0	0.0	17.6	0.0	0.0	91.6
2048.1	45769.5	1231.7	55.3	15.8	19.7		0.0	0.0	23.7	90.8	31.6	0.0	0.0	0.0	27.6	0.0	0.0	110.5
2048.2	45771.4	1319.9	51.7	23.9	11.9		0.0	0.0	11.9	63.6	19.9	0.0	0.0	0.0	4.0	0.0	0.0	103.4
2048.3	45773.4	1235.7	41.5	38.1	13.8		0.0	0.0	10.4	65.8	24.2	0.0	0.0	0.0	0.0	0.0	0.0	90.0
2048.4	45775.3	1116.8	19.4	19.4	19.4		0.0	0.0	19.4	71.0	32.3	0.0	0.0	0.0	25.8	0.0	0.0	96.8
2048.5	45777.3	967.2	44.0	27.1	10.1		0.0	0.0	27.1	67.6	20.3	0.0	0.0	0.0	23.7	0.0	0.0	77.8
2048.6	45779.2	1525.4	27.9	17.5	10.5		0.0	0.0	24.4	80.3	38.4	0.0	0.0	0.0	31.4	0.0	0.0	55.9
2048.7	45781.2	1148.9	59.2	27.9	31.3		0.0	0.0	20.9	83.6	31.3	0.0	0.0	0.0	38.3	0.0	0.0	107.9
2048.8	45783.1	1219.6	80.8	29.4	47.8		0.0	0.0	11.0	73.5	25.7	0.0	0.0	0.0	11.0	0.0	0.0	128.6
2048.9	45785.1	1205.2	56.3	16.6	16.6	0.0	0.0	0.0	26.5	49.7	16.6	0.0	0.0	0.0	19.9	0.0	0.0	122.5
2049.0	45787.0	1149.7	25.6	4.3	8.5		0.0	0.0	17.1	68.4	25.6	0.0	0.0	0.0	38.5	0.0	0.0	132.5
2049.1	45789.3	1109.1	24.0	8.0	4.0		0.0	0.0	24.0	104.1	36.0	0.0	0.0	0.0	0.0	0.0	0.0	64.1
2049.2	45791.6	683.4	20.5	16.4	6.1		0.0	0.0	20.5	57.3	20.5	0.0	0.0	0.0	8.2	0.0	0.0	57.3
2049.3	45793.9	1074.8	33.5	26.0	18.6		0.0	0.0	18.6	70.7	29.8	0.0	0.0	0.0	11.2	0.0	0.0	59.5
2049.4	45796.2	917.5	32.6	7.3	14.5		0.0	3.6	14.5	54.4	18.1	0.0	0.0	0.0	10.9	0.0	0.0	94.3
2049.5	45798.5	892.1	43.7	18.2	7.3		0.0	0.0	7.3	54.6	18.2	0.0	0.0	0.0	58.3	0.0	0.0	54.6
2049.6	45800.8	669.7	59.0	8.9	5.9		0.0	0.0	35.4	76.7	17.7	0.0	3.0	0.0	23.6	0.0	0.0	67.9
2049.7	45803.1	575.3	32.5	14.4	3.6		0.0	0.0	14.4	66.7	14.4	0.0	0.0	0.0	43.3	0.0	0.0	57.7
2049.8	45805.4	391.9	34.9	13.6	11.6		0.0	0.0	25.2	67.9	17.5	0.0	1.9	0.0	69.8	0.0	0.0	60.1
2049.9	45807.7	503.4	64.5	18.4	16.6	0.0	0.0	0.0	22.1	47.9	9.2	0.0	0.0	0.0	92.2	0.0	0.0	40.6